# Proteomic Analyses of Thyroid Hormone-sensitive Tissues During Frog Tadpole Metamorphosis

by

Dominik Domanski

B.Sc., University of Victoria, 2001

A Dissertation Submitted in Partial Fulfillment of the Requirements

for the Degree of

**DOCTOR OF PHILOSOPHY**

In the Department of Biochemistry and Microbiology

© Dominik Domanski, 2008

University of Victoria

All rights reserved. This dissertation may not be reproduced in whole or in part, by photocopying or other means, without the permission of the author.

# Proteomic Analyses of Thyroid Hormone-sensitive Tissues During Frog Tadpole Metamorphosis

by

Dominik Domanski

B.Sc., University of Victoria, 2001

Supervisory Committee:

Dr. Caren C. Helbing, (Department of Biochemistry and Microbiology)

---

Supervisor

Dr. Terry W. Pearson, (Department of Biochemistry and Microbiology)

---

Departmental Member

Dr. Perry Howard, (Department of Biochemistry and Microbiology, and Biology)

---

Departmental Member

Dr. Ben Koop (Department of Biology)

---

Outside Member

## Supervisory Committee

Dr. Caren C. Helbing

**Supervisor**

Dr. Terry W. Pearson

**Departmental Member**

Dr. Perry Howard

**Departmental Member**

Dr. Ben Koop

**Outside Member**

# ABSTRACT

Thyroid hormones (THs) are vital in the maintenance of homeostasis and in the control of development. One postembryonic developmental process that is principally regulated by THs is amphibian metamorphosis. This process has been intensively studied at the genomic level yet very little information at the proteomic level exists. There is also increasing evidence that changes in the phosphoproteome influence TH action. In addition, the disruption of TH-action by endocrine-disrupting compounds (EDC) is an emerging field and the developmental process of metamorphosis is a target as well as a model system for this research.

This work identifies components of the proteome and phosphoproteome in TH-sensitive tadpole tissues that are altered during the initiation stages of TH-induced metamorphosis prior to the overt remodeling of the tissues. Proteomic analyses included two-dimensional (2D) gel electrophoresis for the assessment of differential protein/phosphoprotein expression, combined with mass spectrometry (MS) protein analysis for protein identification. Initial proteomic approaches in *Xenopus laevis* identified a number of proteins that are differentially expressed in the tadpole tail within 48 h of exposure of premetamorphic tadpoles to 3,5,3'-triiodothyronine ($T_3$). Additionally, a time-course analysis of brain tissue within this 48 h period revealed alterations in phosphoproteins. The importance of phosphoproteome modulation in the process of metamorphosis was further revealed in the TH-induced tail of *Rana catesbeiana* tadpoles, where the inhibition of cyclin-dependent kinase activity which prevents tail regression, altered the tail phosphoproteome profile.

Failure to identify the phosphoproteins involved in these initial studies led me to develop and apply new proteomic approaches. To this end, subcellular and protein fractionation methods were developed and combined with 2D gel electrophoresis and phosphoprotein-specific staining. Altered proteins were identified using MS. Here components of the proteome and phosphoproteome were identified in the tail fin that changed within 48 h of exposure of premetamorphic *R. catesbeiana* tadpoles to 10 nM $T_3$. This approach allowed the identification of and led to the cloning of a novel *Rana* larval type I keratin, RLK I, which is a target for caspase-mediated proteolysis upon exposure to $T_3$. In addition, the RLK I transcript level was reduced during $T_3$-induced and natural metamorphosis, consistent with a larval keratin. Furthermore, GILT, a protein involved in the immune system, was changed in phosphorylation state which is linked to its activation.

Using a complementary MS technique for the analysis of differentially-expressed proteins, isobaric tags for relative and absolute quantitation (iTRAQ) revealed 15 additional proteins whose levels were altered upon $T_3$ treatment. The success in identifying proteins whose levels changed upon $T_3$ treatment with iTRAQ was enhanced through *de novo* sequencing of MS data and homology database searching. These proteins are involved in apoptosis, extracellular matrix structure, immune system, metabolism, mechanical function, and oxygen transport. This study demonstrated the ability to derive proteomics-based information from a model species for postembryonic development for which limited genome information is currently available.

The early appearance of caspase-cleaved RLK I in the TH-induced process led to its investigation as a contributor to apoptosis. Furthermore, the caspase-cleavage product of RLK I was used as a biomarker in the development of an assay for the detection of disruptors of TH-action based on *ex-vivo* multi-well culturing of *R. catesbeiana* tail fin biopsies. This assay was able to detect perturbations in TH-signalling within 48h of exposure demonstrating that it has utility as a novel system for screening of TH disrupting chemicals.

The present study identified proteins whose levels and/or phosphorylation states are altered within 48 h of the induction of tadpole metamorphosis prior to overt tissue remodeling and provided important insight into the molecular mechanisms of this postembryonic development. In particular, I have identified a novel keratin that is a target for $T_3$-mediated changes in the tail that can serve as an indicator of early response to this hormone and can be used for the detection of EDCs of TH-action in an *ex vivo* assay.

# TABLE OF CONTENTS

# List of tables

# List of figures

## Acknowledgements

I would like to thank my supervisor, Dr. Caren C. Helbing for her support and commitment to my project. I would like to thank former and present lab members for their help and knowledge: Dr. Nik Veldhoen, Rachel C. Skirrow, Dr. Mary J. Wagner, Dr. Mark P. Gunderson, Lan Ji, Dr. Fang Zhang, and Carmen Bailey. I would like to thank Ryan Bonfield for providing the data presented in figure 4.1D. I would also like to thank Dr. Robert Olafson, Darryl Hardie, Leanne Ohlund, Derek Smith and Monica Elliott from the University of Victoria - Genome British Columbia Proteomics Centre for assistance in the mass spectrometry analysis and helpful technical advice. This work was supported by NSERC PGS A and PGS D Canada Graduate Scholarships, University of Victoria President's Research Scholarship and a Dr. Julius Schleicher Graduate Scholarship.

I would also like to thank my partner Donna Carrigan for her great support and amazing ability to motivate me in this pursuit and other life goals.

## Dedications

I would like to dedicate this work to my parents Anetta and Wojtek Domanski as they have given up a great deal in their lives so their two children could have more. Their effort has made my schooling possible, culminating in this work, and has opened doors and opportunities that without them would not have been attainable.

# Chapter 1: Introduction

## 1.1 SIGNIFICANCE OF RESEARCH

The thyroid hormones (TH), 3,5,3',5'-tetraiodothyronine (thyroxine; $T_4$) and 3,5,3'-triiodothyronine ($T_3$), are vital signaling molecules used by organisms for the maintenance of homeostasis, and during developmental processes. One developmental process that is largely regulated by the presence of TH is amphibian metamorphosis. This process is especially dramatic in the anuran amphibian, the frog. During anuran metamorphosis the larval, aquatic, herbivorous tadpole changes to an adult, terrestrial, carnivorous frog. This event requires drastic changes in essentially every organ and tissue of the tadpole. This includes three major changes: (i) the death and resorption of organs and tissues of the larval form used only by the tadpole, (ii) remodeling of larval organs to adult form and function, and (iii) *de novo* development of new organs and tissues for adult use (Shi, 2000). Adult frog organs are structurally and functionally similar to those in adult mammals. In addition, at the physiological and molecular level, amphibian metamorphosis shares many similarities with post-embryonic organ development in higher vertebrates, which is also TH- dependent (Tata, 1993; 2006). Like during amphibian metamorphosis, TH is high in humans for several months after birth when extensive organ development and maturation occurs. Changes in hemoglobins, intestine morphology, serum proteins, skin keratinization, induction of urea cycle enzymes in the liver, and development and restructuring of the central and peripheral nervous system all occur in mammals like they occur in amphibians under the influence of TH (Hasebe et al., 1999; Shi, 2000; Helbing and Atkinson, 1994; Yoshizato, 2007; Zoeller and Rovet, 2004). This makes amphibian metamorphosis a perfect model to study the post-embryonic developmental actions of TH.

It is also evident that in these early developmental stages of life, organisms could be especially sensitive to the disruption of hormone signals. We are presently seeing an increase in the appearance of polluting, man-made compounds in our environment capable of disrupting such normal hormone action. These, referred to as endocrine-disrupting compounds (EDCs), can disrupt vital hormonal systems of many organisms at extremely low levels. The frog tadpole is one such affected organism and is used as a model system in our research on EDCs of TH action. Our laboratory has shown that a number of polluting chemicals can disrupt normal TH action by interfering in the TH signal pathways thereby preventing the correct molecular response from occurring, leading to aberrant metamorphic development (Crump et al., 2002; Veldhoen et al., 2006a, 2006b). Many compounds are suspected of being EDCs of TH action but the data is

lacking (Gray et al., 2002). Further research into TH regulated development and into the chemical compounds that can affect it is therefore warranted and its findings could benefit human and animal health. A large body of knowledge exists on TH action in metamorphosis based on genomic methods. However, how proteins and phosphoproteins are involved is poorly understood. My research focuses on using proteomic methods to identify protein and phosphoprotein components involved in metamorphosis and their disruption by EDCs of TH action.

## 1.2 THE ANURAN MODEL AND METAMORPHOSIS

Anuran larvae, or tadpoles, are incapable of reproduction and require the developmental process of metamorphosis to continue their life-cycle. The most striking changes during metamorphosis are the formation of the limbs from undifferentiated mesenchyme cells and the apoptotic death and complete resorption of the tail (Shi, 2000). The initiating stages of the latter process have been the focus for the majority of this thesis. Additionally, other tissues and organs, such as the digestive tract, skin, skeletal muscle and the central nervous system, undergo extensive remodeling which involves the coordinated apoptosis of larval cells with the proliferation and differentiation of adult precursor cells. All of these seemingly disparate processes occur due to a single hormonal signal, TH. How TH is able to orchestrate such a complex developmental process as metamorphosis remains a fascinating area of research. In addition to being used as models for the study of TH regulated development, anurans can be used as sentinel species because of their wide global distribution, their proximity to potentially contaminated water, and their sensitivity to pollutants. Two frog species whose tadpoles were used in the research for this thesis were the African clawed-frog, *Xenopus laevis* and the North American bullfrog, *Rana catesbeiana*. *X. laevis* is a genetically well-characterized organism that has been extensively used in the laboratory for developmental biology and on which most of the research concerning metamorphosis has been performed. *R. catesbeiana* has also been used in studies of metamorphosis. Although it is a genetically less characterized species, it has the advantages of being physically larger, providing higher protein amounts for proteomic studies, and being present in the North American environment.

The post-embryonic development of anurans can be separated into three specific periods: premetamorphosis, prometamorphosis and metamorphic climax (Figure 1.1) (Shi, 2000). Staging systems, based on morphology, are used to define specific points in the development. In this manuscript, the Nieuwkoop and Faber (NF) staging system is used for *X. laevis* (Nieuwkoop and

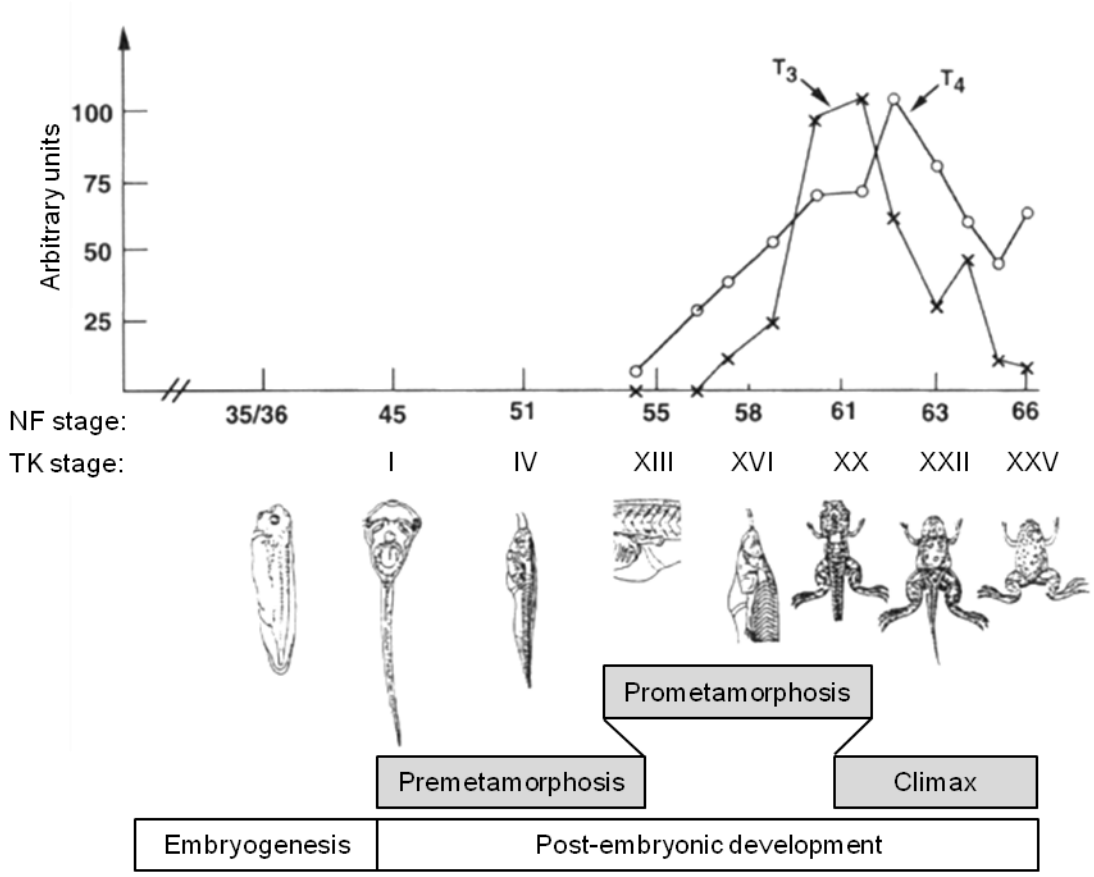


**Figure 1.1. Anuran development and correlation with plasma TH levels.** Progression of *X. laevis* development during metamorphosis as TH levels rise through prometamorphosis, peak during metamorphic climax, and decrease as tadpoles complete metamorphosis into juvenile frogs. Developmental stages are based on Nieuwkoop and Faber (1994) (NF) and on Taylor and Kollros (1946) (TK). TH levels are based on *X. laevis* (Leloup and Buscaglia, 1977). Peak concentrations at metamorphic climax are about 10 and 8 nM for $T_4$ and $T_3$, respectively. (Adapted from Shi, 2000).

Faber, 1994) and the Taylor and Kollros (TK) system is used for staging *R. catesbeiana* (Taylor and Kollros, 1946). The first period, premetamorphosis (NF stages 45-54 or TK I-XII), is primarily a period of tadpole growth. These events occur in the absence of TH, due to an immature thyroid gland (Dodd and Dodd, 1976). This is followed by prometamorphosis (NF stages 55-59 or TK XIII-XIX), when the thyroid gland matures and TH increases in the circulating plasma (Leloup and Buscaglia, 1977). This stage is characterized by overt changes in limb morphology. The last stage is metamorphic climax (NF stages 60-64 or TK XX-XXV), when TH is at its highest levels, and rapid and dramatic morphological changes such as resorption of the tail occur. In *X. laevis*, at metamorphic climax, the peak concentrations for $T_4$ and $T_3$ in the plasma are about 10 nM and 8 nM, respectively (Leloup and Buscaglia, 1977). Similarly, the peak

plasma levels of $T_4$ and $T_3$ in the *R. catesbeiana* tadpoles have been measured at around 7-13 nM and 9 nM, respectively (White and Nicoll, 1981). Upon completion of metamorphosis TH is reduced. The occurrence of metamorphosis can be completely controlled through the control of TH levels. Premetamorphic tadpoles, which are functionally athyroid, are capable of responding to exogenous TH and can be induced to undergo precocious metamorphosis by exposure to TH either via rearing water or by injection (Tata, 1968). Conversely, inhibitors of TH synthesis or removal of the thyroid gland can prevent metamorphosis (Dodd and Dodd, 1976). In addition, the effects of TH are organ-autonomous, in that organs such as the tail, intestine and hind limb will undergo their normal morphological changes when cultured *in vitro* in the presence of TH (Tata et al., 1991). This ability to tightly control the process of metamorphosis by simple hormonal manipulation is what makes it an ideal system and has contributed greatly to our understanding of this post-embryonic developmental process.

TH controls metamorphosis but it is also under complex neuroendocrine control and it itself influences neuroendocrine function in the hypothalamus-pituitary-thyroid (HPT) axis (Figure 1.2) (Denver, 1996). In tadpoles, environmental cues act on the central nervous system, which acts on the hypothalamus causing it to release corticotropin releasing factor (CRF). CRF then acts positively on the pituitary thyrotropes and pituitary corticotropes to cause the release of thyroid stimulating hormone (thyrotropin or TSH) and adrenocorticotropin (ACTH), respectively. Mammals differ from anurans in that the hypothalamus thyrotropin-releasing hormone (TRH) released from the hypothalamus stimulates TSH release from the pituitary instead of CRF. In both cases TSH then stimulates the thyroid gland to release TH. TH forms a negative feedback loop to the pituitary and hypothalamus. TSH mRNA expression in tadpoles has been shown to rise and fall a step before the rise and fall of TH (Okada et al., 2000).

Although TH is the only obligatory hormone that regulates metamorphosis, other hormones modulate this process (Kaltenbach, 1996). CRF in addition to causing the release of TSH also induces ACTH release, which then causes the interrenal glands to produce corticoids such as corticosterone and aldosterone (Figure 1.2). The corticoids rise in synchrony with TH, and furthermore they antagonize metamorphosis at low TH concentrations, but accelerate metamorphosis at high TH concentrations (Krain and Denver, 2004; Kikuyama et al., 1993; Hayes et al., 1993). Corticoids function through their nuclear receptor, the glucocorticoid receptor (GR), which is TH-inducible in the tail and repressed in the brain, but presently, the mechanism of modulation is not well understood (Krain and Denver, 2004). Gonadal steroids such as testosterone and estradiol have been generally shown to inhibit metamorphosis, probably by

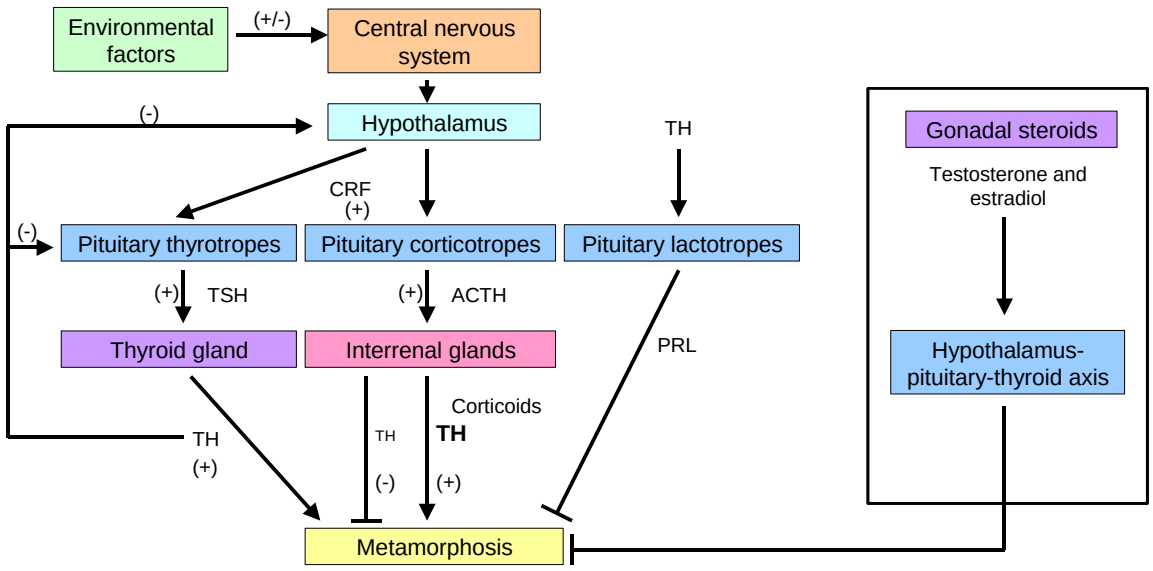


**Figure 1.2. The effects of the hypothalamus-pituitary-thyroid axis on amphibian metamorphosis.** CRF: corticotropin releasing factor. TSH: thyroid stimulating hormone. ACTH: adrenocorticotropin. TH: thyroid hormones. PRL: prolactin. (+): positive effect. (-): negative effect. Lines with bar-ends indicate inhibition of metamorphosis. TH (small font): indicates corticoids with low levels of TH are antagonistic. TH (large font): indicates corticoids with high TH levels are agonistic. Note: Mammals differ from anurans in that the hypothalamus releases thyrotropin releasing hormone (TRH), instead of CRF, which acts on the pituitary causing it to release TSH. (Adapted from Shi, 2000).

influencing the hypothalamus-pituitary-thyroid axis, since this response was only observed in whole tadpoles and not in organ culture, however, these observations were made at μM concentrations (Gray and Janssens, 1990). In anurans, TH has been shown indirectly to cause the pituitary lactotropes to release prolactin (PRL), which in turn has been shown to have a growth promoting effect in tadpoles but an inhibitory effect on metamorphosis that was organ autonomous (Tata et al., 1991; Kikuyama et al., 1993). In the tadpole tail, the PRL receptor was found to increase in expression at climax and exogenous PRL was observed to prevent TH-induced expression of the TH receptors with the concomitant inhibition in regression (Hasunuma et al., 2004; Baker and Tata, 1992; Tata et al., 1991). Using a transgenic *X. laevis* overexpressing PRL, this protection from regression was shown to be tissue specific, protecting the tail fin but not the tail muscle (Huang and Brown, 2000).

The roles of these additional hormones are thought to be in coordinating metamorphosis of different organs and tissues, which occur at different TH concentrations during specific stages of the developmental process, as well as in the control of the timing of metamorphosis which is

dependent on environmental stresses. For example, a hormone at a certain TH level will act on individual organs/tissues, inhibiting some tissues but not others, resulting in coordinated metamorphosis. This may explain why the hind limbs undergo metamorphic changes in prometamorphosis (low TH) but the tail remains intact until metamorphic climax (high TH) and then begins to resorb (Shi, 2000). The difference in organ/tissue response to these hormones will depend on the presence and level of receptors and downstream effectors. The ability of additional hormones besides TH in acting on metamorphosis indicates at the possibility that EDCs with hormonal capabilities other than TH-mimetic could affect metamorphosis. Furthermore, it points to the importance of determining what types of molecular mechanisms exist in the different organs and tissues that could be influenced.

## 1.3 TH METABOLISM

The thyroid gland produces two thyroid hormones. The predominant form is 3,5,3',5'-tetraiodothyronine ($T_4$ or thyroxine) and the minor form is 3,5,3'-triiodothyronine ($T_3$) (Figure 1.3) (Norris, 1996; Fort et al., 2007). TH is produced in the follicles of the thyroid gland. The follicles consist of thyrocytes surrounding a lumen which contains the colloid, the precursor of TH. The base of the thyrocytes is exposed to the circulating plasma and sodium iodide symporters pump inorganic iodide ($I^-$) into the thyrocytes which then diffuses across the apical side into the lumen. The thyrocytes also produce the extracellular glycoprotein thyroglobulin, which contains many tyrosine residues, and present it on the apical side facing the lumen. In the same location, the integral membrane enzyme, thyroid peroxidase, through an unknown mechanism converts $I^-$ into active iodide which then iodinates the tyrosine residues on thyroglobulin, forming 3-monoiodinated (MIT) and 3-5-diiodinated (DIT) tyrosine residues. The same enzyme is then responsible for coupling of the MITs and DITs, resulting in thyroid hormones, which remain linked to the thyroglobulin protein forming the colloid. TSH then stimulates the pinocytosis of the iodinated thyroglobulin protein from the colloid, inclusion, and fusing with lysosomes. Hydrolysis then results in the cleavage of the thyroglobulin and release of $T_3$ and $T_4$ which diffuse into the plasma. TSH also up-regulates the sodium iodide symporter and the thyroglobulin protein within the thyrocytes, and its own expression is negatively regulated by TH at the pituitary (Levy et al., 1997; Fort et al., 2007; Denver, 1996). The mechanisms involved in the synthesis of TH appear to be highly conserved between mammals and anurans, with the anuran mechanisms often being more closely related to mammals than to lower vertebrates such as fish (Fort et al., 2007).

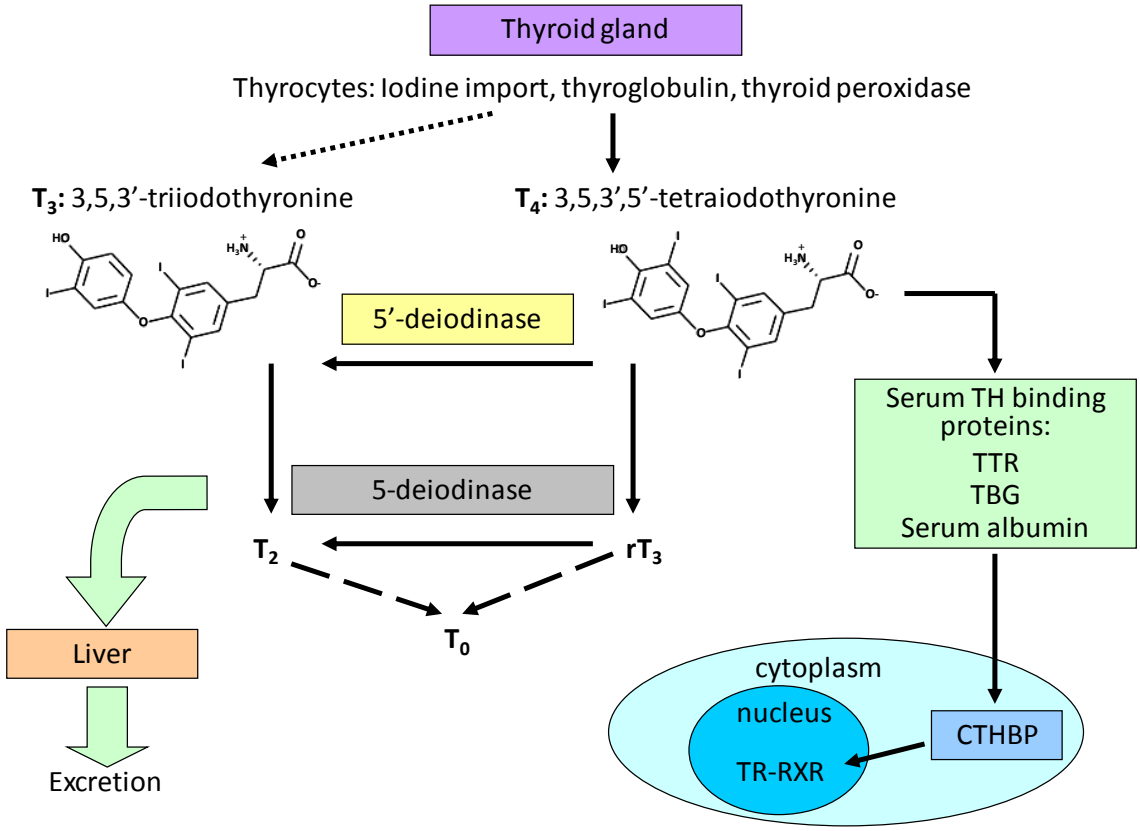


**Figure 1.3. Thyroid hormone metabolism.** An overview of the steps involved in TH synthesis, metabolism and transport. Refer to text for details. TTR: transthyretin; TBG: thyronine-binding globulin; CTHBP: cytoplasmic TH binding proteins; TR: thyroid hormone receptor; RXR: 9-cis-retinoic acid receptor; $rT_3$: reverse-$T_3$; $T_2$: diiodothyronine; $T_0$: thyronine. Deiodinases are located within the cells of the thyroid gland and peripheral tissues.

$T_4$ can be converted into the biologically more active form, $T_3$, by the action of 5'-deiodinases (type II; D2), which remove an iodine from the outside ring (Figure 1.3) (Davey et al., 1995; St Germain and Galton, 1997). This occurs in the thyrocytes, as well as in the peripheral tissues. In addition, $T_4$ and $T_3$ can be deactivated by the action of 5-deiodinases (type III; D3), which remove iodide from the inside ring, producing the inactive reverse-$T_3$ ($rT_3$) and $T_2$, respectively (St Germain et al., 1994). These can be further sequentially deiodinated by 5'- and 5-deiodinases in the end producing thyronine ($T_0$), which is then excreted. As discussed later, these deiodinases are regulated in a tissue- and stage-specific manner to control the sequence of events in metamorphosis (Becker et al., 1997). TH can also be removed from the serum by the action of uridine disphosphate glucuronyltransferase (UDP-GT), present in the liver, which glucurodinates THs, causing them to be eliminated in the bile (DeVito et al., 1999; Fort et al., 2007). In *X. laevis*, at metamorphic climax, the peak concentrations for $T_4$ and $T_3$ in the plasma are about 10 nM and

8 nM, respectively (Leloup and Buscaglia, 1977). The peak tissue concentrations based on whole-body measurements, however, have been observed to be 7 and 18 nM for $T_4$ and $T_3$, respectively (Krain and Denver, 2004). In *R. catesbeiana* the peak plasma levels of $T_4$ and $T_3$ at climax have been measured to be around 7-13 nM and 9 nM, respectively (White and Nicoll, 1981).

Most of the TH in the plasma is bound by serum TH binding proteins leaving little free TH. These carrier proteins include serum albumin, thyronine-binding globulin (TBG), transthyretin (TTR) and lipoproteins (Shi, 2000; Fort et al., 2007). There are some species differences in regards to these proteins. TBG is the main carrier in humans and carries $T_3$ and $T_4$, while rodents possess only albumin and TTR which only carries $T_4$. TTR is the major binding and transport protein of THs in metamorphosing tadpoles, and in contrast to mammals, has been found to bind $T_3$ with higher affinity then $T_4$ (Yamauchi et al., 1993). These proteins carry the lipophilic TH, increasing its life-time in the serum, act as a buffer for TH levels, and function as a reserve for TH (Shi, 2000). TH is thought to enter cells by diffusion of free TH across the plasma membrane, as a complex with serum binding proteins or possibly *via* active import. Recent evidence has shown that active transport may be the most likely mode and may involve amino acid transporters such as the System L amino acid transporter (Ritchie et al., 2003) and monocarboxylate transporter 8 (MCT8) (Friesema et al., 2003), as shown in transfected *X. laevis* oocytes, and the aromatic amino acid transporter (System T)-linked transporter as found in *R. catesbeiana* red blood cells (Shimada and Yamauchi, 2004).

Once in the cytoplasm TH is bound by cytoplasmic TH binding proteins (CTHBP). These are multifunctional proteins that bind TH with low affinities ranging from $K_d$ of 1-100 nM (Shi, 2000). An example is xCTHBP, a *Xenopus* homolog of human M2 pyruvate kinase. As monomers, these proteins bind TH, possibly acting as chelators of free intracellular TH and/or act as transport proteins to the nucleus. As tetramers, these proteins act as enzymes, such as pyruvate kinase. Similarly as with the deiodinases, xCTHBP levels have been shown to be tissue- and stage-specific, and have thus been suggested to modulate the metamorphic process (Shi et al., 1994).

All of the above steps in the TH metabolism path are potential targets of endocrine disruption. The effects of EDCs of TH action have been clearly documented on the thyroid gland, liver excretion, and serum transport proteins (Brucker-Davis 1998; Leatherland, 2000; DeVito et al., 1999; Cheek et al., 1999b; Meerts et al., 2000). However, the effects on deiodinases, membrane

transporters, intracelleular TH-binding proteins, receptors and down-stream effectors are less well known and an area to be explored (Shimada and Yamauchi, 2004; Boas et al., 2006).

## 1.4 THYROID HORMONE RECEPTORS

The TH signal is largely mediated through the nuclear thyroid hormone receptors (TRs), which belong to the nuclear hormone receptor superfamily and impart changes in gene expression (Yen et al., 2006; Buchholz et al., 2006). Some of the effects of TH on cells are known to occur via non-genomic action, where the hormone binds membrane or cytosolic proteins causing a change without first affecting transcription (Davis et al., 2005; Bassett et al., 2003). The majority of the effects of TH and the largely studied mechanisms, however, are known to be mediated through the nuclear receptors (Buchholz et al., 2004; Furlow and Neff, 2006; Tata, 2006). TRs localize to the nucleus and are associated with chromatin in the presence and absence of TH (Shi, 2000). TRs bind $T_3$ with a 5-10 fold higher affinity then $T_4$, with a $K_d$ below 1 nM (Griffin and Ojeda, 2000). $T_4$ is thought to only alter gene expression after conversion to $T_3$ by 5'-deiodinases, as inhibitors of this deiodinase inhibit biological effects of $T_4$.

Higher vertebrates, including *R. catesbeiana*, have two TR genes: TRα and TRβ (Bassett et al., 2003; Davey et al., 1994). There are four TR genes in the tetraploid *X. laevis*: TRαA, TRαB, TRβA and TRβB (Shi, 2000). Additionally, some of the genes produce multiple isoforms. In *X. laevis*, the TRβ genes produce two isoforms each through alternative splicing. In mammals, each gene produces four isoforms by alternative splicing or alternative promoter use. Out of these, all of the TRβ isoforms bind TH, but only three bind DNA, wheras only one TRα, TRα1, binds TH indicating that some receptors can act as TR inhibitors. In *R. catesbeiana* only one isoform for each gene has been defined thus far (Schneider et al., 1993; Davey et al., 1994). In anurans, TRα protein appears during embryogenesis and is present throughout post-embryonic development and metamorphosis (Eliceiri and Brown, 1994). In contrast, the levels of TRβ protein, follow those of endogenous TH, being completely undetectable during embryogenesis and premetamorphosis and then increasing in concentration during metamorphosis to a peak at metamorphic climax.

There is a high degree of conservation with TRs and members of the steroid/TH receptor superfamily, with divergence in the hormone binding domain (Bassett et al., 2003). Most of the TR isoforms share a similar domain organization composed of five domains: A/B, C, D, E and F, sequentially from the N- to the C-terminal (reviewed in Zhang and Lazar, 2000; Bassett et al., 2003). The A/B domain, at the N-terminal side, varies in length between the different TRβ

isoforms and in sequence when compared to the TRα isoforms. Also known as the activation function 1 (AF-1) domain, it has $T_3$-independent coactivator recruitment abilities. The C domain is the DNA binding domain (DBD), and it serves as the dimerization domain. It contains two zinc-fingers, and binds to the TH response elements (TRE) in the promoter or enhancer regions of TH responsive genes. The most common TREs consist of two direct repeats of the consensus sequence AGGTCA, separated by four nucleotides, although other combinations such as palindromes and inverted palindromes have also been observed (Buchholz et al., 2006; Yen, 2001). The D domain contains the nuclear localization signal, and has transactivation and DNA binding functions. The E and F regions make up the ligand binding domain (LBD). The E region contains the majority of the hormone binding domain and it also functions in dimerization, and transcriptional repression and activation (Yen, 2001). The F region, also known as the AF-2 domain, binds coactivators with LXXLL motifs, and has transcriptional regulation functions. The LBD composed of 12 α-helices and 4 β-strands, has low homology to other nuclear receptors (Wagner et al., 1995). It buries TH inside, with the C-terminal α-helix 12, located in the F region, folding inward upon binding, changing co-regulator associations with TR (Eckey et al., 2003).

TRs heterodimerize with 9-*cis*-retinoic acid receptors (RXRs). Although TRs can form homodimers, the TR-RXR heterodimer form is the most stable and is believed to be the true *in vivo* mediator of the effects of TH (Wong and Shi, 1995). TH bound to TRs can either activate or repress transcription (Yen et al., 2006). Most TH responsive genes are up-regulated by TH, and these have been most commonly studied (Buchholz et al., 2006; Wang and Brown, 1993; Helbing et al., 2003, 2007a,b). These possess a positive TRE (pTRE) and the gene is repressed by unliganded TR-RXR heterodimer through recruitment of corepressors, and activated in the presence of ligand by coactivator recruitment (Bassett et al., 2003; Buchholz et al., 2006). Unliganded TR-RXR participates with corepressors such as silencing mediators of receptors of thyroid hormone (SMRT) and nuclear receptor co-repressor (N-Cor), which interact with α-helices 1 to 11 within the LBD of TR and with RXR (Sachs et al., 2002; Eckey et al., 2003; Tomita et al., 2004). SMRT and N-Cor in turn bind to transcriptional repressor complex Sin3A which interacts with histone deacetylases (HDACs). HDACs activity leads to a more compact chromatin state and gene repression. Evidence also exists that the corepressors act by affecting basal transcription factors (Eckey et al., 2003). In addition, unliganded TRs have been shown to prevent the formation of the preinitiation complex by binding to basal transcription factors (Yen, 2001).

The binding of TH to TR causes a conformational change, which causes the dissociation of corepressors and association with coactivators (Paul and Shi, 2003). These bind through their LXXLL motifs to the now folded in α-helix 12 in the LBD of the TR (Wagner et al., 1995). The identified coactivators with intrinsic histone acetyltransferase (HAT) activity include CBP/p300 (cAMP-response element-binding protein), SRC/p160 (steroid receptor co-activators), and P/CAF (p300/CBP-associated factor) (Paul and Shi, 2003; Yen, 2001; Bassett et al., 2003). These exist as multimeric complexes of different coactivators and lead to chromatin disruption, increasing gene transcription. SRC/p160 has been shown to bind TRs and recruit CBP/p300 which directly binds RNA polymerase II, forming a link to the basal transcriptional machinery (Huang et al., 2003). Other coactivator complexes which lack HAT activity, such as TRAPs or DRIPs (thyroid receptor associated proteins or Vitamin D receptor interacting proteins) also associate and are thought to play a role subsequent to HAT activity and chromatin remodeling (Bassett et al., 2003). An example is TRAP220 that anchors a TRAP/DRIP complex to TRs and mediates RNA polymerase II binding (Bassett et al., 2003).

The mechanism of gene down-regulation by TH is not as well understood, but is thought to depend on the position of the TRE creating a negative TRE (nTRE) and different co-regulator binding (Eckey et al., 2003). nTREs are usually located close to the transcription start site or downstream of the TATA box. These have been found in the TH-down-regulated genes for TSH and TRH (Shibusawa et al., 2003). The absence of TH causes a different conformation of TR on a nTRE than on a pTRE and still causes recruitment of corepressors such as SMRT and N-Cor. But in this case, the gene is activated (Eckey et al., 2003). TH binding then facilitates HDAC recruitment causing gene silencing. As indicated above, a great deal is known about the molecular mechanisms of TR-mediated gene regulation based on *in vitro* studies, however, relatively little is known about how TR functions in an *in vivo* developmental system (Buchholz et al., 2006).

TR binding and cofactor recruitment are mechanisms that are susceptible to endocrine disruption by environmental contaminants which will be discussed further later in the chapter. It is possible that EDCs may alter coregulator associations thereby altering TH action. Such effects have been shown for compounds like the drug amiodarone, whose metabolite disrupted co-activator binding to TRβ (van Beeren et al., 2000). Additionally, EDCs can exert their action without directly affecting ligand binding or receptor activation (Tabb and Blumberg, 2006). This can occur by increasing expression levels of co-activators, as was observed for the EDC bisphenol A which increased TRAP220 and estrogen receptor (ER) β levels in the mouse uterus (Inoshita et al., 2003). EDCs can also limit co-activator availability to one receptor type through competition by

stimulating a different set of receptors. For example, a xenobiotic that activated the constitutive androstane receptor (CAR) led to the reduction in ER activity which was returned to normal by antagonizing CAR or increasing co-activator levels (Min et al., 2002). EDCs can also modulate receptor stability by altering proteasome-mediated degradation, as was observed for bisphenol A which slowed ERβ degradation, possibly increasing an EDCs effect (Masuyama and Hiramatsu, 2004). Finally, certain compounds, such as xenobiotic short-chain fatty acids, can inhibit HDAC activity and thus increase receptor (ERα, ERβ, androgen receptor, progesterone receptor and TRβ) activity thereby potentiating a hormone's effect (Jansen et al., 2004).

## 1.5 CONTROL OF THE MORPHOGENIC PROGRAM

During metamorphosis, different organs develop or regress at distinct developmental stages to allow for a proper tadpole to frog transition. This timing is critical for the animal's survival. For example, the growth and differentiation of the hind- and forelimbs must be complete before the tail is lost, and the lungs must become fully functional before the gills are resorbed (Shi, 2000). Thus, the limbs begin to grow and differentiate when the levels of circulating TH are still low (around NF stage 54 for *X. laevis*) while the tail does not begin to resorb until after NF stage 60 once TH levels are maximal.

TR levels control amphibian development in the absence and presence of TH. TRs and RXRs are absent during embryogenesis allowing transcription of TRE containing genes (Wong and Shi, 1995; Eliceiri and Brown, 1994). TRα and RXRs then become up-regulated in early premetamorphosis, repressing those genes in the absence of TH allowing for growth of the tadpole and at the same time giving the tadpole competence to respond to TH in metamorphosis (Sato et al., 2007; Puzianowska-Kuznicka et al., 1997). A constitutively expressed, dominant negative mutant of TRα (TRDN) prevents TH-induced metamorphosis in the entire transgenic tadpole (Schreiber et al., 2001), and in contrast, transgenic tadpoles expressing a dominant positive TRα undergo precocious metamorphosis (Buchholz et al., 2004). Furthermore, intracellular receptor and $T_3$ levels appear to control the timing of the different morphogenic programs of different tissues which occur at distinct developmental stages (Figure 1.4). This mechanism can be exemplified by looking at the *de novo* development of the hindlimb and resorption of the tadpole tail. Hindlimb morphogenesis is the earliest event in metamorphosis and begins when circulating $T_4$ is only 1-2 nM, and $T_3$ is not yet detectable (Leloup and Buscaglia, 1977). The xCTHBP protein, thought to bind up cellular TH, as well as the TH deactivating enzyme, 5-deiodinase, are known to be repressed in this tissue during this period (Shi et al., 1994;

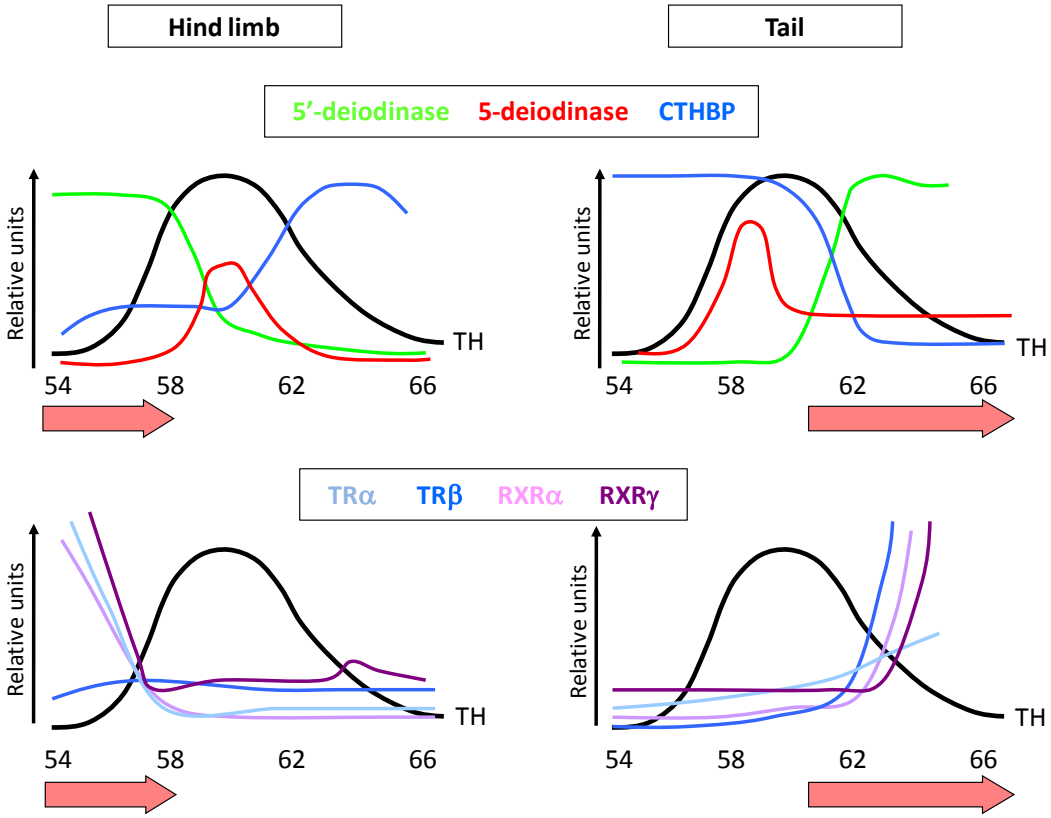


**Figure 1.4. Temporal regulation of metamorphosis.** Red arrows indicate developmental stages at which morphological changes occur in the respective organs. Black lines indicate relative serum TH levels during metamorphosis based on *X. laevis* (Leloup and Buscaglia, 1977). Other colors correspond to the indicated enzymes/genes in the respective tissues. Levels indicated are relative. Deiodinase levels are base on enzyme activity in *R. catesbeiana* (Becker et al., 1997). Other levels represent relative mRNA levels (Shi et al., 1994; Wong and Shi, 1995). Developmental stages are based on NF staging (Nieuwkoop and Faber, 1994).

Becker et al., 1997). At the same time, activating 5'-deiodinase activity is high. In addition, the receptors TRα, RXRα, and RXRγ are highly expressed and are subsequently reduced (Wong and Shi, 1995). Although the plasma TH concentrations are low, the $K_d$ of the TR-TH complex is even lower at 0.1 nM or less, and it is therefore speculated that enough intracellular $T_3$ can be accumulated to interact with the high levels of receptors to activate the limb morphogenic program.

In contrast, tail resorption begins late in metamorphosis, just after maximal levels of TH are reached (around 10 nM). In this tissue, xCTHBP and 5-deiodinase are high and then drop after climax as the tail resorbs (Shi et al., 1994; Becker et al., 1997; St. Germain et al., 1994). In turn, the levels of 5'-deiodinase activity rise after climax (Figure 1.4). In addition, the levels of the

receptors TRβ, RXRα, RXRγ, but not TRα, rise dramatically (Wong and Shi, 1995). All of the above events ensure that the metamorphic program in the tail is initiated after climax. TRα is therefore thought to provide the competence to respond to TH and is associated with proliferating tissues during metamorphosis, while TRβ is considered to be involved in regressing tissues (Tata, 2006). The hindlimbs have similar tissues and cell types as the resorbing tail that undergoes apoptotic death, yet TH causes these to develop. The tail has an increase in lysosome proliferation and the activation of lytic enzymes such as collagenase, nucleases, phosphatases, and matrix metalloproteinases (Shi, 2000). In contrast, the limb bud involves *de novo* formation of bone, skin, muscle, and nerves through cell proliferation, differentiation and chondrogenesis. The temporal regulation of the different morphogenic programs is understood, but what controls cell fate is poorly understood.

## 1.6 TAIL METAMORPHIC PROGRAM

In response to TH the tail degenerates completely with every cell type eventually undergoing apoptotic cell death (Shi et al., 2001). This hormone-controlled, developmental apoptotic process has been the focus of the research for this thesis. Genomic studies have revealed some mechanisms of the tail metamorphic program. A commitment point has been discovered which is set between 24 and 48 h of TH exposure, where the complete genetic program required for tail resorption is established, after which, removal of TH or exposure to protein synthesis inhibitors can not prevent regression (Wang and Brown, 1993). In *X. laevis*, based on a polymerase chain reaction (PCR) subtractive hybridization method that could detect changes in gene expression of at least 6-fold at a sensitivity of at least 10 copies/cell of an mRNA, it was estimated that this program would contain 25 up-regulated genes within the first 24 hours and another 10 genes by 48 h, with less then 10 down-regulated genes (Wang and Brown, 1993; Brown et al., 1996). This screen isolated 17 up-regulated and 4 down-regulated genes. Two phases of gene up-regulation were observed. Early direct response genes, which did not require the synthesis of new proteins, were up-regulated within 4-8 h, and delayed response genes were up-regulated after 24 h. Most of the early direct response genes code for transcription factors such as BTEB (Basic transcription element binding protein), FRA-2 (bZIP), TH/bZip (basic leucine-zipper motif-containing transcription factor) and TRβ (Brown et al., 1996). Two additional early direct response genes were stromelysin-3, an extracellular matrix (ECM) metalloprotease, and 5-deiodinase. The delayed genes consisted mainly of proteolytic enzymes, ECM metalloproteases, and ECM

components such as fibronectin and integrin α-1. The down-regulated genes, named gene 17, 18, 19 and 20, were all inhibited within 16 h, and code for putative extracellular proteins.

*In situ* hybridization has shown that the different TRs and the TH responsive genes are expressed differentially in different cell types (Figure 1.5) (Berry et al., 1998a). The tail consists of several major tissues such as epidermal cells, fibroblast cells, connective tissue, fast and slow muscle cells, notochord fibroblasts, notochord, nerve cells, and blood vessels (Figure 1.5A). TRs and their RXR partners were expressed in all cells of the tail (Figure 1.5B). Of importance was the fact that TRα was expressed highly in the epidermis, muscle and connective tissue between muscle, while TRβ was expressed highly in fibroblast cells of the subepidermal layer, the notochord sheath and surrounding the notochord. These fibroblasts expressed the delayed genes coding for proteases, ECM metalloproteases and the ECM components. Furthermore, they were observed to invade and dissolve their respective collagen lamellaes. The expression of the transcription factor genes BTEB, FRA-2, and TH/bZip, was low in these fibroblasts, and was in turn high in the proliferating cells of the epidermis and connective tissue. These genes have also been shown to be up-regulated in growing tissues of head and body structures, such as cartilage, nervous tissue, adult epidermis and adult muscle during metamorphosis (Berry et al., 1998b). Therefore, a metamorphic model has been proposed where these genes, under the control of TRα, are associated with proliferating tissues (Figure 1.5C).

In addition, the proteolytic and ECM delayed genes were expressed by fibroblasts in resorbing tissues of head and body structures. Therefore, TRβ is thought to up-regulate the delayed response genes, leading to resorption of larval tissues, such as cartilage, lamellae, and larval muscle. The only early response ECM modifying gene, stromelysin-3, was only expressed by the fibroblasts cells of the fins, which are the first tissue in the tail to resorb. In the head-body, stromelysin-3 colocalized with resorbing epithelial and connective tissues and therefore, under the control of TRα, it is believed to be responsible for the death of these tissues. The down-regulated genes were only expressed in the single apical cell layer of the larval epidermis that is lost to apoptosis upon metamorphosis, and probably under TRα control, they are responsible for its death. 5-deiodinase was highly expressed in fibroblasts and observed to first increase and then decrease as the rest of the TH-responsive gene transcripts increased. Therefore, 5-deiodinase is thought to prevent premature tail regression.

Additional genes involved in tail metamorphosis have been discovered by the use of cDNA gene arrays (Helbing et al., 2003; Veldhoen et al., 2002). Fourty-five and 53 new TH-responsive genes

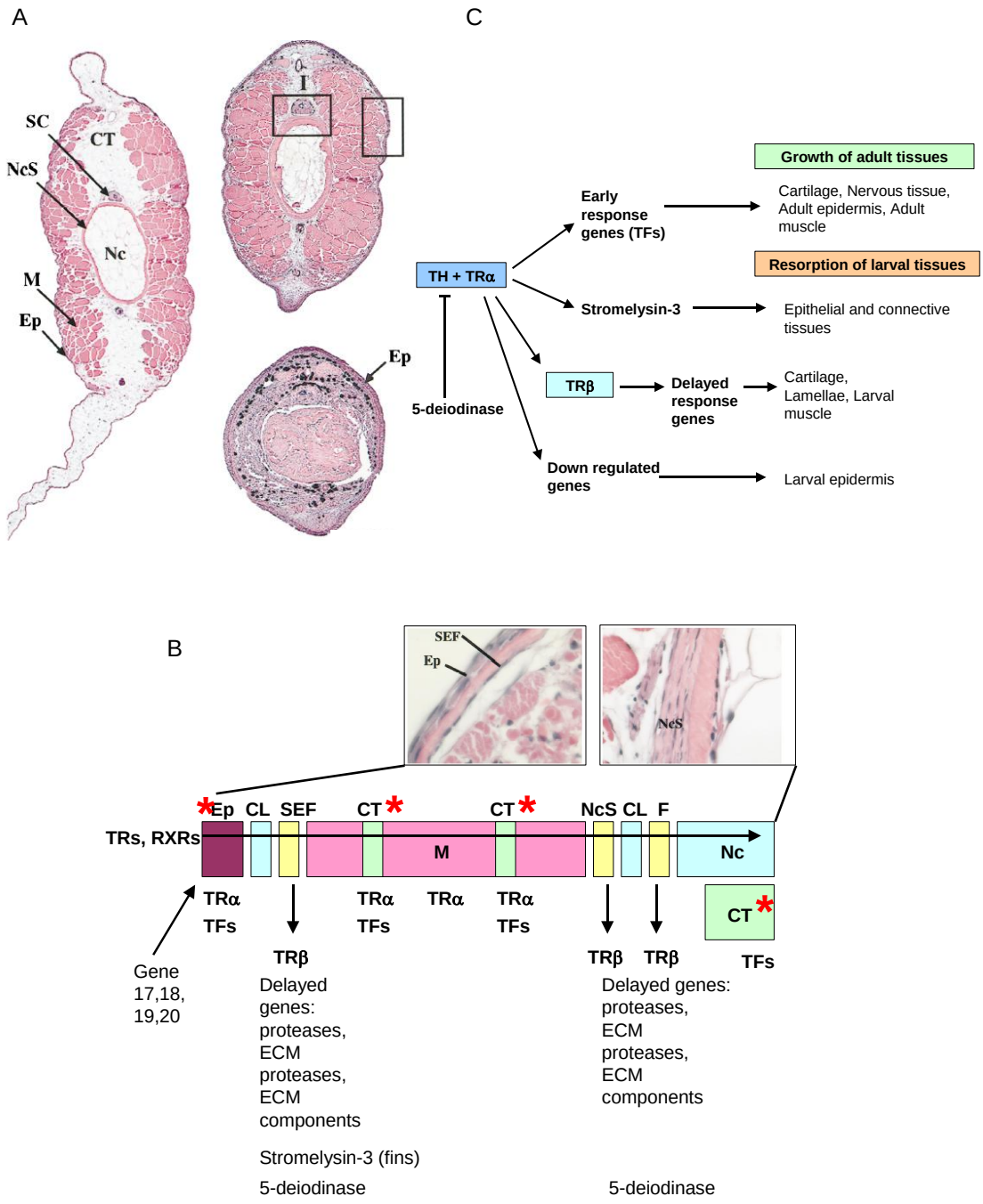


**Figure 1.5. Tail metamorphic program.** (A) Cross section of *X. laevis* tadpole tail undergoing resorption. Dorsal and ventral tail fins die first, followed by larval epidermis and muscle cell death, and finally ending with the collapse of the notochord. The tail consists of several major tissues (A and B): Ep, epidermal cells; Fibroblast cells (yellow boxes): SEF, subepidermal fibroblasts. NcS, notochord sheath fibroblasts. F, notochord fibroblasts. Nc, notochord. CT, connective tissue. M, muscle. CL, collagen lamellae. (B) Differential tissue expression of the early and delayed genes. TFs, transcription factors. Red asterisk indicates proliferating cells. (C) Model of metamorphosis. (Partly adapted from Berry et al., 1998a, 1998b).

were identified in natural and TH-induced *X. laevis* metamorphosis, respectively. These genes could be clustered into several groups according to their kinetics. Additionally, multiple functional groups of genes were differentially regulated, with transcription factors showing a gradual increase through metamorphosis, structural proteins decreasing in premetamorphosis and up in prometamorphosis, and metabolism, signaling and cell-growth control proteins increasing in prometamorphosis. In TH-induced metamorphosis most functional groups, which include proteins involved in transcription, signal transduction, chromatin structure, hormone regulation, metabolism, cell growth control, apoptosis/degradation and structural proteins, all go up incrementally towards 48 h and are then repressed by 72 h. More intricate gene responses were also observed that have not been reported before, which included transient down-regulation of most genes at metamorphic climax and a transient decrease at 6 h in TH-induced metamorphosis. A similar analysis on *R. catesbeiana* TH-induced tadpole tails revealed 92 genes exhibiting a two-fold or greater change in steady-state levels after 24 and 48 h (Veldhoen et al., 2006). Fifty-seven of these were not previously identified as TH-responsive in amphibians or mammals. The majority of these were up-regulated maximally at 48 h and are involved in a variety of cellular functions which include regulation of gene transcription and modulation of chromatin structure, mediation of extracellular stimuli and intracellular signaling cascades, biosynthesis and processing of cell components, and determination of cell fate. These new genes have to be further characterized to reveal their exact role in metamorphosis. As well, accordance of most of these genomic findings to protein data is yet to be verified.

Expression of the dominant negative TRα directed to muscle cells revealed that fast muscle in the tail, which makes up the majority of the muscle, is acted on by TH directly and dies cell autonomously early on in the regression process (Nakajima and Yaoita, 2003; Das et al., 2002). While slow tail muscle, which makes up structures called cords that contract the tail towards the body as the tail resorbs, is not affected by TH directly. However, both types of muscle die by an apoptotic process later on in the regression process due to extensive disruption of the ECM. Therefore, as the ECM is degraded by the release of proteolytic enzymes from the surrounding fibroblast cells, muscle begins to die by TH-direct as well as by indirect, yet unknown, processes (Nakajima and Yaoita, 2003). The apoptotic mechanism in metamorphosis seems to be conserved with that of higher vertebrates. Apoptotic members of the mitochondrial pathway such as pro-apoptotic Bax, and anti-apoptotic Bcl-$X_L$, have been shown to be involved in TH-dependent tail muscle cell death (Sachs et al., 1997, 2004; Rowe et al., 2002). A number of effector caspases, such as caspase 3, 6 and 7, increase in expression and activity during metamorphosis in the tail

(Rowe et al., 2005; Nakajima et al., 2000; Veldhoen et al., 2006). It has been shown that the regulatory caspase 9 is required for muscle cell death implicating the mitochondrial/apoptosome apoptotic pathway in this cell type (Rowe et al., 2005). Recently, observations have been made that the BH3-Interacting Death agonist (BID) protein and caspase-8 may be involved in TH-induced tail muscle death, also implicating a surface receptor activated apoptotic pathway (Du Pasquier et al., 2006). In addition to muscle tissue, the larval epidermal skin cells within the tail express caspase 3 and undergo TH-induced cell autonomous death (Schreiber and Brown, 2003; Nakajima and Yaoita, 2003). What is unknown are the steps between TR-TH gene activation and initiation of the apoptotic pathway, as well as the steps between ECM modification and cell death.

## 1.7 PROTEIN STUDIES

Metamorphosis has been largely studied by looking at gene transcript levels with some work on gene targets. In contrast, very little work has been done at the protein level. The objective of the research for this thesis was to find proteins involved in metamorphosis using proteomic techniques. Two-dimensional sodium dodecyl sulfate-polyacrylamide gel electrophoresis (2D-SDS-PAGE; 2D gel) resolves a complex protein sample within a two-dimensional gel matrix based on the proteins isoelectric point (pI) in one dimension and molecular mass in the second dimension (O'Farrell, 1975). The combination of two separation parameters has allowed the technique to achieve high resolving power capable of separating up to 10,000 individual protein species in a single gel, with a sensitivity that can detect a protein which constitutes $10^{-4}$ to $10^{-5}$ % of the total protein sample (Klose and Kobalz, 1995; O'Farrell, 1975). The research presented in this thesis extensively employed 2D gel analysis for the separation of protein samples, combined with mass spectrometry for accurate protein identification. Differential expression of proteins was assessed by comparing the intensity of stained protein spots from 2D gels resolving a control protein sample and a sample from a TH-induced tissue. This approach of 2D gel protein separation and mass spectrometry identification has been used extensively for the discovery of new proteins involved in a myriad of biological processes (Van den Bergh and Arckens, 2005).

Research in metamorphosis on a proteomic scale has been scarce. Ray and Dent (1986) examined $^{35}$S-methionine labelled protein extracts from *R. catesbeiana* tail fin in natural and induced metamorphosis and using 2D gel analysis observed several changing spots. Kobayashi et al. (1996) used 2D gel electrophoresis to analyze changes in protein expression in the back and tail skin of *X. laevis* during metamorphosis. From the 2D protein spot patterns they could classify the back skin into larval or adult type and observe the transition. Attempts were made in these studies

to identify the altered protein spots; this however, involved identifying the spots based on position, co-migration or immunological detection methods. In addition, the lack of any sample fractionation led to the identification of only abundant proteins.

One tissue that has been extensively studied at the protein level is the *R. catesbeiana* liver (Atkinson et al., 1996). The liver is the source of serum proteins and is the site of urea biosynthesis for excretion of nitrogenous waste as tadpoles switch from ammonotelism to ureotelism during metamorphosis. During spontaneous and precocious metamorphosis, albumin and other serum proteins, as well as the ornithine-urea cycle enzymes increase in level and activity, respectively, in addition to their transcripts (Atkinson et al., 1996; Helbing et al., 1992, Helbing and Atkinson, 1994).

During metamorphosis, proteome function may also include changes in protein phosphorylation. Protein phosphorylation is a post-translational, reversible modification. It changes protein activity and/or interaction by changing the three-dimensional protein structure or affinity for other proteins (Gomperts et al., 2002). Phosphorylation is the key mode of signal transduction and signal amplification inside a cell. It is modulated by kinases and phosphatases. There are about 500 kinases and about 100 phosphatases in humans, coding 2% of the genome (Manning et al., 2002). A third of all proteins are believed to be phosphorylated at any one time. In eukaryotes phosphorylation mainly occurs on serine, threonine and tyrosine residues. The ratio of phosphorylated Serine (pSer) to pThr to pTyr is 1800:200:1 (Hunter and Sefton, 1980). Immunodetection of phosphorylated proteins on electroblotted 2D gels can be used to create maps of proteins phosphorylated on tyrosine, serine or threonine, revealing the phosphoproteome. This approach with subsequent protein identification by mass spectrometry has been successfully used in the identification of components of signal transduction pathways (Soskic et al., 1999; Birkelund et al., 1997). Antibodies that are specific for phosphorylated Tyr, Thr and Ser residues without any sequence specificity have been produced, and the method of detecting phosphoproteins separated by 2D gel electrophoresis by immunodetection is very sensitive, capable of detecting as little as a few fmol of epitope (Kaufmann et al., 2001). Signal transduction and cell cycle regulation events involve alterations in the phosphorylation state of proteins and this thesis, therefore also, focused on identifying changes that occur in the phosphoproteome during metamorphosis.

Likewise, very little research has been done on the phosphoproteome during anuran metamorphosis. Research in our laboratory has shown that the cyclin-dependent kinase (Cdk)

inhibitor, roscovitine, can prevent TH-induced tail regression (Skirrow, 2003). This inhibition was found to be due to roscovitine acting on a Cdk or Cdk-like kinase, distinct from those Cdks known to regulate the cell cycle and required in tail proliferation. This kinase activity phosphorylates a protein or proteins, required for tail regression, at the onset of the commitment point between 24 and 48 h (Skirrow, 2003; Skirrow and Helbing, 2007). Other research from our laboratory has indicated that tyrosine kinase signaling is important in the tail regression process of *R. catesbeiana*, and may be through phosphorylation of TRs (Ji, 2005). TH action has also been implicated in the activation of a number of kinases and kinase pathways through non-genomic action in mammalian cell cultures (Lin et al., 1999a; Kavok et al., 2001). This was usually observed with $T_4$, which has been recently shown to bind a cell-surface integrin receptor leading to the activation of the mitogen-activated protein kinase (MAPK) pathway (Bergh et al., 2005). This $T_4$-induced MAPK activation has been found to be central in all these observations. This activation was found to potentiate the effects of EGF (epidermal growth factor) and IFNγ (interferon-γ) through STAT (signal transducer and activator of transcription) phosphorylation (Lin et al., 1999a, 1999b). It increased activation of estrogen responsive genes through estrogen receptor phosphorylation (Zhao et al., 2005). And it activated TRβ by its phosphorylation, leading to SMRT dissociation, implying that $T_4$ may have non-genomic potentiating effects on genomic TH action (Lin et al., 1999a; Davis et al., 2000). How the phosphoproteome is modulated *in vivo* in a TH-dependent developmental process is unknown. Changes in phosphorylation and their implications in tadpole metamorphosis are just beginning to be investigated (Ji et al., 2007; Skirrow and Helbing, 2007).

## 1.8 ENDOCRINE DISRUPTION OF TH ACTION

Disruption of TH function could occur at any of the steps in TH metabolism. Disruption of iodine uptake into thyrocytes and disruption of tyrosine iodination and coupling by thyroid peroxidase is known to occur by many compounds (Brucker-Davis 1998; Leatherland, 2000). By looking at the structure of TH it is evident that some polluting polyhalogenated aromatic hydrocarbon (PHAH) compounds, such as polychlorinated biphenyls (PCBs) and brominated flame retardants (BFRs), resemble it in structure. This structural similarity implies that these compounds could act as EDCs of TH action through binding to TH-carrier proteins in the blood, CTHBPs, or TRs. If such disruptions were to occur during an organism's developmental stage they could potentially have life lasting consequences. Although the use of PCBs has been largely banned, they are persistent organic pollutants and these compounds have alerted us to the possibility of endocrine disruption

in the TH path (Zoeller, 2005). A correlation has been observed between PCB exposure and decreased serum $T_4$ levels, increased TSH, and increased $T_4$ excretion (Brucker-Davis 1998; Leatherland, 2000; Zoeller, 2005; Boas et al., 2006). This has been observed in a number of wildlife species, rats and humans. It is thought to be due to the displacement of bound $T_4$ from such carrier proteins as TTR and TBG, allowing the free $T_4$ to be excreted (Boas et al., 2006). Jelaso et al. (2005) have found that PCBs delayed *X. laevis* metamorphosis while altering expression of a neurotrophic factor and a neuro-hormone. A correlation between PCB exposure and reduced mental development in humans has also been found (Schantz et al., 2003). These findings and the know fact that TH action is important in brain development indicate that PHAH exposure during development could have serious effects on an organism's health (Zoeller and Rovet, 2004; Boas et al., 2006).

BFRs are compounds, which are added into plastics and circuitboards to act as flame retarding agents (Alaee et al., 2003). BFRs such as tetrabromobishpenol A (TBBPA) and polybrominated diphenyl ethers (PBDEs) are contained in numerous consumer goods and leach out into the environment. A general trend that has been observed between the 1970s and 2000 is that contaminant PCB concentrations are dropping in the environment while the levels of contaminating BFRs are on the rise (Watanabe and Sakai, 2003). Between 1990 and 2000, the worldwide use of BFRs has doubled, mainly consisting of TBBPA (Law et al., 2006). In North America, BFR contamination in the environment and in humans is rising exponentially (Hale et al., 2003). Like PCBs, PBDEs lower total $T_4$ concentrations in rat serum, possibly by increasing UDP-GT activity, which leads to increased glucuronidation of $T_4$ and its removal (Legler and Brouwer, 2003). Their metabolites were shown to bind TTR and they have caused neuronal development problems in fetuses which led to behavioural defects. TBBPA is considered to be mostly non-toxic, with only possible concerns of it being an EDC of TH action (Darnerud, 2003). *In vitro* it has been shown to bind to human TTR with a 10 times higher potency than $T_4$ (Meerts et al., 2000). TBBPA competed with TH for human TRs in an *in vitro* assay, acted as an antagonist, preventing $T_3$-induced transcription of a TRE-driven reporter gene, and it inhibited TH-induced tail shortening and limb development in a Ranid species (Kitamura et al., 2005b). One obvious disruption on TH action is by lowering serum TH levels; the other intracellular disruption of molecular mechanisms is not well understood and needs to be studied further.

Additional chemicals, such as acetochlor and triclosan, have shown potential of being EDCs of TH action in research from our laboratory. Triclosan, an antimicrobial agent used in personal care products, with structural similarity to TH, has recently been shown to affect *R. catesbeiana*

tadpole development and alter TH-induced gene expression (Veldhoen et al., 2006a). At environmentally relevant concentrations, triclosan accelerated $T_3$-induced metamorphic hindlimb development and altered $T_3$-induced gene expression in an antagonistic manner for the TRβ receptor in the tail fin and in a potentiating fashion for proliferating cell nuclear antigen (PCNA) in the brain. Additionally, triclosan had a potentiating effect on the $T_3$-induced gene expression for TRα, TRβ and BTEB in a *X. laevis*-derived cell line.

Acetochlor, a pre-emergent herbicide, although having no structural similarity to TH, has been shown to be an EDC of TH action. At an environmentally relevant concentration, it was shown to accelerate $T_3$-induced metamorphosis, which was associated with increased TRβ levels in both *X. laevis* and *R. catesbeiana* tadpole tails (Crump et al., 2002; Veldhoen and Helbing, 2001). To observe the expression of downstream genes, a 420-gene cDNA amphibian array was used on *X. laevis*. Acetochlor enhanced the $T_3$-induction of some genes, which included the direct and delayed response genes previously identified. It affected the expression of some genes that were not TH responsive with $T_3$-induction. It also attenuated the response of some TH-responsive genes, which are normally down-regulated, like genes 17, 18 and 19. In the brain of *R. catesbeiana* tadpoles, acetochlor alone and in combination with $T_3$ increased the levels of TRα and TRβ, and by itself it increased the levels of both receptors in prometamorphic tadpole tail fin (Helbing et al., 2006). The mechanisms of how acetochlor causes these effects need to be investigated. Acetochlor was found not to bind to TRβ, however it was shown to bind to estrogen receptors (Cheek et al., 1999b; Rollerova et al., 2000). Considering that there is cross-talk between the TH and estrogen paths, the involvement of both pathways could be a possible mechanism (Zhao et al., 2005; Vasudevan et al., 2001).

## 1.9 MASS SPECTROMETRY AND PROTEOMICS

Mass spectrometry (MS) is the production, differentiation and detection of ions in the gas phase. Mass spectrometers are capable of the accurate determination of masses of ions, which depending on the type of instrument, can be accurate to within hundreds to thousands of a single atomic mass unit (Aebersold and Mann, 2003; Kinter and Sherman, 2000). A major breakthrough in the field of mass spectrometry was the development of soft ionization techniques such as electrospray ionization (ESI) and matrix-assisted laser desorption/ionization (MALDI), which allowed the ionization, and therefore detection and differentiation of large biomolecules such as proteins and peptides, without the previously observed fragmentation (Fenn et al., 1989; Karas and Hillenkamp, 1988). This ability to analyze intact ions of peptides and proteins lead to the ability

to quickly and accurately identify large numbers of proteins within complex biological mixtures and created the field of MS-based proteomics. MS analysis of proteins can lead to protein identification based on primary sequence or peptide mass determination, it can reveal post-translational modifications and protein-protein interactions, and it can precisely quantify protein expression within complex samples (Aebersold and Mann, 2003).

A mass spectrometer consists of an ion source (ESI or MALDI), a mass analyzer that measures the mass-to-charge-ratio (m/z) of the ionized analytes, and a detector that registers the number of ions at each m/z value (Kinter and Sherman, 2000) (Figure 1.6A). ESI ionizes the analytes out of an acidic solution and it is commonly coupled to liquid chromatography separation (Figure 1.6C). MALDI ionizes samples out of a dry acidic UV-absorbing crystalline matrix by a laser pulse (Figure 1.6B). Due to the acidic conditions and a large positive potential applied at the source, positively charged peptide or protein ions are produced and injected into the mass analyzer. The mass analyzer is central to the mass spectrometer, and it determines the sensitivity, resolution and mass accuracy of the instrument. Two types of mass analyzers that were used in the research for this thesis were the time-of-flight (TOF) and quadrupole (Q) analyzers.

The TOF analyzer measures the mass of an ion based on the time it takes for the ion to travel through a flight tube to the detector once it is accelerated by an applied voltage at the source (Kovtoun et al., 2002). The time will depend on the mass as well as the charge of the ion, with ions of low m/z travelling faster then ions of high m/z. In the quadrupole analyzer electric fields between four rods, which are positioned parallel to the path of the ions, are varied over time permitting the passing of ions of a particular m/z (Morris et al., 1996). The disadvantage of such an analyzer is that it spends a short time at each m/z, while purposefully defocusing and therefore losing other ions leading to lower sensitivity and mass accuracy which ranges between 100 and 200 ppm (Kinter and Sherman, 2000). The advantage of the quadrupole is that it can be used for selecting ions of a specific m/z for further analysis within the mass spectrometer. The TOF analyzer, because it collects all of the ions that pass through the flight tube, has a higher sensitivity and mass accuracy which ranges between 5 and 20 ppm. The higher mass accuracy in TOF analyzers is also obtained from the use of a reflectron or ion mirror (reflector) which increases the flight path and focuses ions of the same m/z (Kovtoun et al., 2002). Depending on the instrument, these mass analyzers can be put together in tandem in different combinations to take advantage of the strengths of each (Morris et al., 1996). In combination with the ion source, the three instruments that were used in this research were the MALDI-TOF, ESI-Qq-TOF and the MALDI-TOF-TOF (Figure 1.6D).

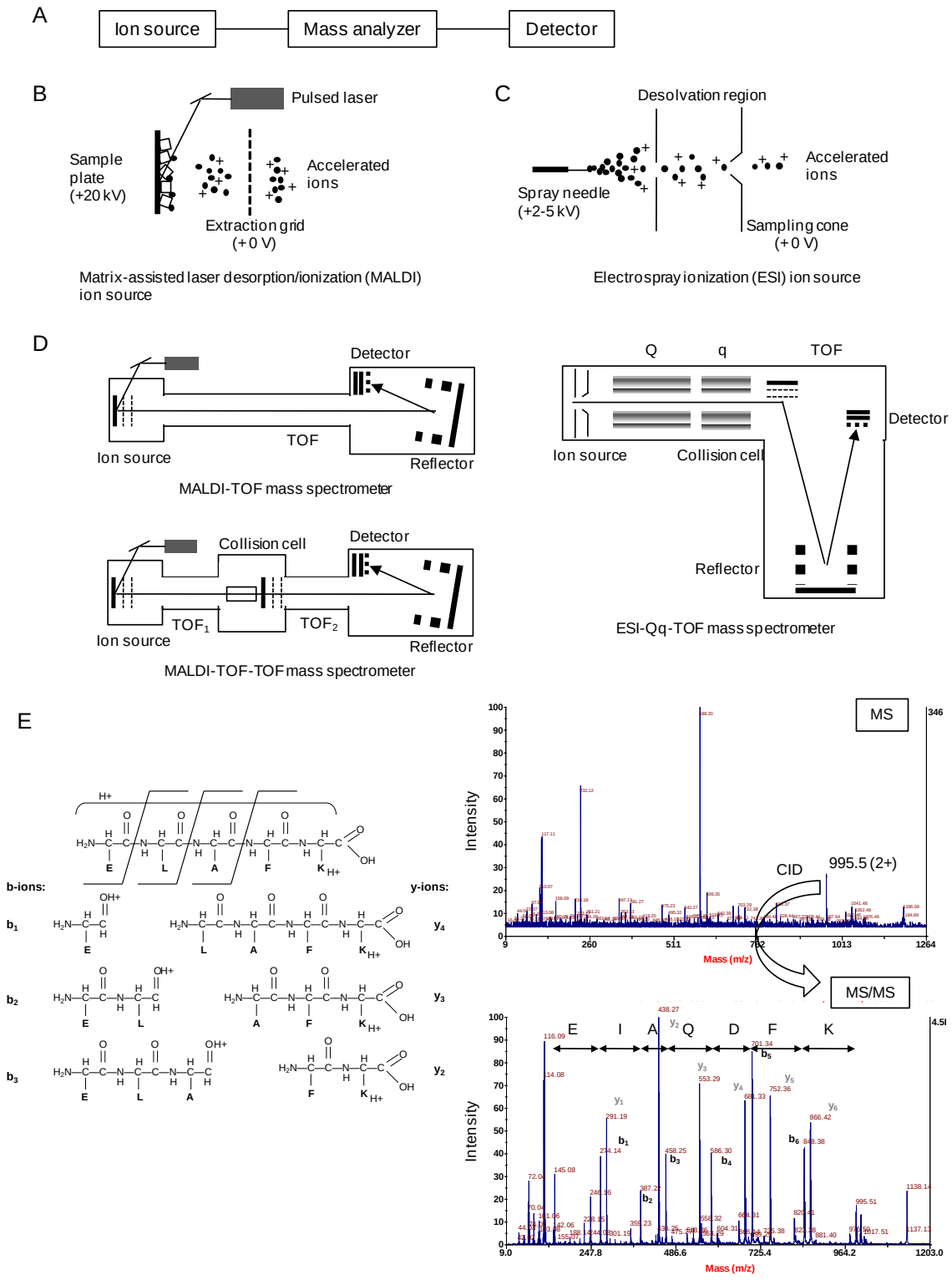


**Figure 1.6. Mass spectrometry of peptides.** (A) Basic configuration of a mass spectrometer. (B) MALDI ion source depicting the ionization and introduction of sample. Sample co-crystallized with the matrix compound is protonated and desorbed from a charged sample plate by a pulse

from a UV laser. Packets of positively charged peptides are then accelerated by an applied electric field into the flight tube. (C) ESI ion source depicting the ionization and introduction of sample. Charged droplets are sputtered from a needle and reduced in size through a desolvation process that ultimately produces protonated ions that enter the mass analyzer. (D) The different instrumental configurations shown with their typical ion source. In the MALDI-TOF instrument, ions are accelerated and separated along a flight tube as a result of their different velocities. The reflector compensates for slight differences in kinetic energy for ions of the same m/z. Ions then hit the detector which counts the ions and amplifies the signal. In the MALDI-TOF-TOF instrument, a collision cell is incorporated between the two TOF mass analyzers. Ions of a specific m/z are selected by the first TOF analyzer, fragmented in the collision cell and the resulting fragments are separated by the second TOF analyzer. In the ESI-Qq-TOF instrument, the quadrupole (Q) analyzer selects the specific ion to be fragmented in the collision cell (q) and the fragments are analyzed by the TOF analyzer. (E) A simplified fragmentation pattern that would occur within a collision cell to a doubly charged peptide derived from trypsin cleavage and ionized in an ESI source producing the predominant b- and y-ion series. Instruments with tandem mass analyzers first produce a normal mass spectrum (MS) revealing all the charged peptides in the sample being analyzed using the last mass analyzer (i.e. TOF). A peptide of interest (e.g. 995.5 m/z) can then be gated by the first mass analyzer ($TOF_1$ or Q) and fragmented in the collision cell. The resulting fragments are again analyzed by the last TOF analyzer revealing the product ion scan (MS/MS). The spectrum is then analyzed to determine the amino acid sequence of the gated peptide (e.g. EIAQDFK).

---

MS analysis of whole proteins is less sensitive and insufficient for identification when compared to MS analysis of peptides (Aebersold and Mann, 2003). Therefore, proteins to be analyzed by MS are most commonly digested with trypsin and the analysis is performed on the derived peptides. Due to the specificity of trypsin, all of the peptides, except possibly for the C-terminal peptide of the protein, will all carry a lysine or arginine on the C-terminal ends. Due to the acidic conditions used and ion source-specific gas phase chemistry, the majority of the peptide ions from a MALDI source will possess a 1+ charge from a proton residing on the C-terminal lysine or arginine, while peptide ions from an ESI source will possess a 2+ charge, one from the protonated C-terminal lysine or arginine and another from a proton residing on the N-terminus (Fenn et al., 1989; Karas and Hillenkamp, 1988). An additional charge may also be present due to an internal histidine and due to any missed-cleavages at lysine and arginine. Although an m/z value does not directly indicate mass, the charge on the peptide and therefore its mass can easily be determined by measuring the separation of peaks within the isotope cluster for that peptide. MALDI coupled to a TOF analyzer (MALDI-TOF) is commonly used to measure the mass of peptides resulting from the digestion of a purified protein such as one obtained from a single spot on a 2D gel (Figure 1.6D).

Protein identification can then be achieved by what is known as peptide-mass mapping or peptide-mass fingerprinting (PMF) (Jensen et al., 1996). In this method, proteins are identified by matching the list of the observed peptide masses to a list of peptide masses generated *in silico* based on information for a specific entry contained in a protein database. Protein databases are largely composed of predicted amino acid sequence information based on data in gene and genome sequence databases. For PMF-based identification to be successful a few observed peptide masses have to match the database peptide masses exactly (i.e. possess identical amino acids), making this method less successful in matching homologous proteins from organisms that are not well represented in gene sequence databases (Aebersold and Mann, 2003).

The success in identifying a protein is greatly increased if amino acid sequence information is obtained from the specific peptides being analyzed. This information can be obtained by instruments configured with two mass analyzers in tandem, namely the ESI-Qq-TOF and MALDI-TOF-TOF (Figure 1.6D). In the ESI-Qq-TOF mass spectrometer ions are first analyzed by the TOF analyzer revealing the spectrum of peptides present in the sample (Morris et al., 1996). This analysis is referred to as a MS experiment or $MS_1$ which reveals the mass spectrum (Figure 1.6E). To obtain amino acid sequence from a peptide of interest within this MS mass spectrum, the first quadrupole (Q) analyzer is used to gate the peptide at a specific m/z allowing only that peptide, also known as a precursor ion, to pass into a collision cell (q). Within this collision cell the peptide is fragmented by collision-induced dissociation (CID) and the newly generated fragment ions are analyzed by the second TOF analyzer, producing what is known as a tandem MS (MS/MS) spectrum or product ion spectrum (Figure 1.6E). This type of analysis is also referred to as a MS/MS or $MS_2$ experiment. A MALDI-TOF-TOF instrument works in a similar manner with a CID cell between the two TOF analyzers (Medzihradszky et al., 2000). The MS/MS spectrum is then interpreted to obtain amino acid sequence information for the fragmented peptide leading to protein inference. As with PMF, peak lists from MS/MS spectra can be queried against protein databases to find a protein match, or MS/MS spectra can be interpreted manually to derive the peptide sequence in a process referred to as *de novo* sequencing. For a positive identification, the automated analysis of a mass list requires a perfect match with an existing entry in the database while submission of primary sequence derived from *de novo* sequencing allows similarity alignments (Grossmann et al., 2007).

The ability to determine primary peptide sequence from MS/MS spectra stems from the fragmentation characteristics of a peptide under CID. Figure 1.6E shows a simplified fragmentation pattern that would occur within a CID collision cell with a doubly charged peptide

derived from trypsin cleavage and ionized in an ESI source. Although the peptide can fragment in three different possible locations along its backbone once energetically excited by CID, the majority of the breaks occur at the amide bond (Kinter and Sherman, 2000). This is thought to occur according to the mobile proton hypothesis, where the proton on the C-terminal lysine or arginine remains fixed while the N-terminal proton travels along the peptide amide bonds, causing fragmentation at its present location when CID is induced (McCormack et al., 1993). The prevailing reaction in the gas phase produces an N-terminal fragment which retains one proton, and is referred to as a b-ion, and a C-terminal fragment protonated at the terminal lysine or arginine, referred to as the y-ion. The nomenclature further uses a numerical subscript to indicate the number of residues present in the fragment (e.g. $b_2$ contains two residues). Depending on the sequence composition and any post-translational modifications, the peptide will fragment at multiple amide bonds with unequal efficiency and the resulting MS/MS spectrum will show an overlapping pattern of b-ion and y-ion series. In *de novo* sequencing the b-ion and y-ion series are distinguished and are used in a complementary fashion to deduce the amino acid sequence of the peptide with additional fragmentation ions due to other reactions helping in the confirmation of the analysis (Kinter and Sherman, 2000).

### *1.9.1 Quantitation of proteins using mass spectrometry*

In addition to being able to identify proteins, mass spectrometry can also be used to quantify proteins through the use of additional techniques. This ability is due to the use of stable-isotope labeling of the peptides being analyzed and the fact that pairs of chemically identical analytes of different stable-isotope composition can be differentiated in a mass spectrometer. The ratio of signal intensities from the two differentially-labeled analytes accurately indicates the abundance ratio for the two analytes (Goshe and Smith, 2003). Stable-isotope tags can be introduced to proteins via metabolic labelling using isotopically enriched amino acids (Ong et al., 2002), enzymatically via transfer of $^{18}O$ from water during the trypsin digestion (Heller et al., 2003), or via chemical reactions using isotope-coded affinity tags targeting specific functional groups within proteins. The latter method has been employed in the isotope-coded affinity tagging (ICAT) technique (Gygi et al., 1999) and the isobaric tags for relative and absolute quantitation (iTRAQ) (Ross et al., 2004) technique. In the ICAT method, two, chemically identical tags, differentiated only isotopically, are used to separately label peptides through cysteine residues in two protein samples to be compared. After tagging, the two peptide samples are mixed and concurrently analyzed by MS. Peptides of identical sequence from the two samples will produce doublet peaks separated by the difference in mass imposed by the stable-isotope. The difference

in intensity between the two peaks will reflect the relative abundance of the peptide and therefore its protein in the two original samples. One of the peaks within this doublet can then undergo MS/MS analysis to reveal the peptide sequence. In iTRAQ, the approach is similar except four different tags can be used to compare four samples and the tags label primary amines. Additionally, the tags are initially isobaric, producing a single peak for a specific peptide for all four samples during MS analysis. The quantitation step occurs after CID in the MS/MS analysis where the isotope-coded tags fragment, each producing a distinct ion in the low mass region of the spectrum and whose intensity reflects the abundance of the peptide in the original sample. The iTRAQ approach allows greater proteome coverage through the primary amine tagging and the isobaric tags allow for higher sensitivity in the MS analysis and better peptide fragmentation characteristics in MS/MS analysis.

### *1.9.2 Detection of phosphorylation by mass spectrometry*

Mass spectrometry can also be used for the analysis of posttranslational modifications (PTMs). The PTM of interest in the research for this thesis was protein phosphorylation. Mass spectrometry can be used to find or verify the presence of phosphorylated serine, threonine and tyrosine residues on peptides (Gafken and Lampe, 2006). This can be done by comparing masses of peptides to those treated with alkaline phosphatase and looking for mass losses of 80 Da per phosphorylation (Larsen et al., 2001). Another approach is to look for specific fragments from the phosphorylated peptides generated after CID. This is done by performing what is called a precursor ion scan. This is the opposite of a product ion scan, where all the peptides in the sample are scanned for the production of the negative ions of $PO_2^-$ and $PO_3^-$ in negative ion mode, and subsequently the phosphopeptide producing the ion can be identified in positive mode (Zhou et al., 2001). Finally, phosphorylation can be identified by observing neutral losses from metastable precursor ions of phosphopeptides. Here, doublets are observed differing by 98 Da or 80 Da for a loss of $H_3PO_4$ from a phosphorylated serine/threonine or for a loss of $HPO_3$ from a phosphorylated tyrosine, respectively (Kinter and Sherman, 2000). Mass spectrometry can therefore identify the exact location of the phosphate group on a peptide and identify the amino acid sequence context. Therefore, this can lead not only to the identification of the phosphoprotein but can also infer a possible kinase or kinase family responsible for the phosphorylation.

## 1.10 RESEARCH OBJECTIVES AND THESIS OUTLINE

The anuran metamorphic process has been extensively studied. From gene expression studies it is known that TH acts via nuclear receptors to form tissue-specific genetic programs. Protein studies on the metamorphic process have been scarce however, and how changes in the proteome, or its subset, the phosphoproteome, contribute to this process is poorly understood. The molecular mechanisms required in the tissue-specific programs are established early within 24 to 48 hours of TH exposure before any morphological changes are observed. Subsequent to this the different tissues carry out their determined fate, with larval tissue proceeding through apoptosis and regression, and tissues for adult use developing and differentiating. The first objective of the research for this thesis was to identify proteome components that are involved in the early stages of TH signaling where these mechanisms are being established. The goal was to identify proteins and phosphoproteins that are differentially expressed or regulated upon exposure to $T_3$ in the tadpole tail that is destined to undergo apoptotic death, and in the brain which undergoes development. The second objective was to further characterize some of these identified components and reveal their contribution to the metamorphic process. Finally, the final objective was to evaluate the effects of known endocrine disrupting compounds (EDCs) on a potential protein biomarker within the context of a novel organ culture assay.

Chapter 2 of this thesis reveals the initial proteomic approaches that were attempted on the tadpole tail and brain tissue and reveals the successes and hurdles associated with such analysis. Chapter 3 presents the development, improvement and use of novel proteomic methods to analyze tail tissue which led to the identification of a number of proteome components, one of which, a *R. catesbeiana* larval-type keratin (RLKI), was identified as a novel component and cloned. Chapter 4 examines the involvement of RLKI in the mechanisms of apoptosis. Finally, chapter 5 presents the development of a novel tail fin biopsy assay for the assessment of chemicals which might be potential EDCs of TH action using the RLKI protein as a biomarker.

# Chapter 2: Initial proteomic approaches in the study of *X. laevis* and *R. catesbeiana* tadpole metamorphosis

Published in part in: Helbing CC, Werry K, Crump D, Domanski D, Veldhoen N, Bailey CM. Expression profiles of novel thyroid hormone-responsive genes and proteins in the tail of *Xenopus laevis* tadpoles undergoing precocious metamorphosis. Molecular Endocrinology. 2003 Jul;17(7):1395-409.

Ji L, Domanski D, Skirrow RC, Helbing CC. Genistein prevents thyroid hormone-dependent tail regression of *Rana catesbeiana* tadpoles by targetting protein kinase C and thyroid hormone receptor alpha. Developmental Dynamics. 2007, Mar;236(3):777-90.

Skirrow RC, Veldhoen N, Domanski D, Helbing CC. Roscovitine inhibits thyroid hormone-induced tail regression of the frog tadpole and reveals a role for cyclin C/Cdk8 in the establishment of the gene expression program (submitted).

## 2.1 INTRODUCTION

Most of the information currently published focuses on the changes in transcript levels during TH-induced metamorphosis with little information concerning the status of the corresponding encoded proteins. The presence of a transcript may not necessarily reflect the protein levels and it does not address critical issues regarding protein functionality. An important case in point is the relationship between TRα transcripts and protein where during metamorphosis the former is up-regulated but the latter remains constant (Eliceiri and Brown, 1994). The current study identifies some of the components of the proteome that are potentially involved in the process of tadpole tail metamorphosis and defines their relationship with the transcriptome, accentuating the need to examine both components to unravel TH mechanisms of action during development. This was performed through the use of 2D gel electrophoresis for the assessment of differential protein expression in conjunction with mass spectrometry for protein identification, and was compared with results obtained for changes in steady-state transcript levels from real-time quantitative PCR (QPCR) analysis.

The postembryonic development of the brain is thought to be one of the critical targets for EDCs of TH action (Zoeller and Rovet, 2004). The morphological changes in brain include remodeling, axon guidance, axon growth, cell proliferation and death that require the biochemical processes of cell division, apoptosis and new protein synthesis (Tata, 2006). Using PCR-based subtractive hybridization, Denver et al. (1997) isolated 34 cDNAs for TH-regulated genes in the diencephalon of *X. laevis* tadpoles. Most of these genes were up-regulated by TH within 4-8 h and 13 were regulated by TH only in the brain. These include five transcription factors (including BTEB), 5-deiodinase, two metabolic enzymes, a protein disulfide isomerase, a neural-specific β-tubulin, and two hypophysiotropic neuropeptides. During metamorphosis, proteome function may also include changes in protein phosphorylation which occur in processes such as signal transduction and cell cycle regulation events. The current study therefore also focused on identifying changes that occur in the phosphoproteome of the tadpole brain during TH-induced metamorphosis. This was performed through the use 2D gel electrophoresis for protein separation in conjunction with immunoblotting and the use of antibodies directed at phosphorylated amino acid residues of threonine and tyrosine.

Phosphorylation of proteins or peptides can also be detected by the use of mass spectrometry. A mass spectrometry-based method that is capable of quantitating differential phosphoprotein expression between two samples in conjunction with phosphoprotein identification and with an enrichment for the usually low abundance phosphopeptides was developed by Goshe et al. (2001). The current study assessed the method using a model phosphoprotein β-casein.

Evidence from our laboratory has shown that changes in the phosphoproteome do occur and are required during tadpole tail metamorphosis (Ji et al., 2007; Skirrow and Helbing, 2007). More specifically, recent findings suggest that cyclin-dependent kinase (Cdk) activity is required for $T_3$-induced tadpole tail regression in *Rana catesbeiana* tadpoles (Skirrow et al., 2008). The Cdk inhibitor, roscovitine, prevented $T_3$-induced tail regression in organ culture with a concomitant prevention of $T_3$-induced increases in TRβ transcript and Cyclin C protein and transcript levels. The mechanism was further deduced to occur through the inhibition of the transcription modulatory Cdk-8/Cyclin C activity, possibly through negative effects on RNA Polymerase II (RNA Pol II). The effect of roscovitine was found to occur at the level of initiation rather than maintenance of tail regression where it prevented the establishment of the genetic program at the commitment point (i.e. 24-48 h of $T_3$ treatment) required for tail regression. However, other Cdk-like kinases and other Cdk-8 targets beside RNA Pol II may also be involved. These kinase targets are evidently crucial for tail regression, and it was therefore interesting to identify these

additional targets, possibly revealing pivotal phosphoproteins required in the establishment of the regression program. *R. catesbeiana* tail tips were organ cultured in the presence of $T_3$ and/or roscovitine, and compared to a control. Phosphoproteins were extracted using a phosphoprotein-specific purification column in hope of enriching the sample for these low abundance proteins. Differences in phosphorylation, due to the effects of roscovitine on TH-induced regression, were then determined by 2D gel analysis and mass spectrometry.

## 2.2 MATERIALS AND METHODS

### *2.2.1 Experimental animals*

The care and treatment of animals used in this study were in accordance with the guidelines of the Animal Care Committee, University of Victoria. Premetamorphic *X. laevis* tadpoles (NF stage 46; Nieuwkoop and Faber, 1956) were purchased from *Xenopus* I, Inc. (Dexter MN USA) and maintained under natural lighting conditions in a 360L all-glass flow-through aquarium containing charcoal-filtered municipal water at 22±1ºC. Tadpoles were fed Nutrafin flakes (Rolf C. Hagen Inc., Montreal PQ Canada) daily. For the thyroid hormone-induction analysis, 14-15 animals (NF stages 52-54) were collected from the stock population for each of the treatment time periods (0, 2, 6, 12, 24 and 48 h). *Rana catesbeiana* tadpoles were either caught locally or purchased (Wm A Lemberger Co, Oshkosh WI USA) and maintained as indicated above except water was kept at 15±1ºC. Taylor and Kollros (TK) (Taylor and Kollros, 1946) stage VI-X tadpoles were used in the tail organ culture experiments as described below.

### *2.2.2 Thyroid hormone exposure*

Before $T_3$ (Sigma-Aldrich, St. Louis MO USA) exposure, *X. laevis* tadpoles were acclimatized to laboratory conditions at 22±1ºC for 48 h. During the acclimatization and $T_3$ exposure periods, animals were not fed. 14-15 NF stage 52-54 tadpoles were exposed to $T_3$ dissolved in 2.5 mM NaOH (ACP Chemicals Inc., Montreal PQ Canada)) or a 2.5 mM NaOH solvent control by immersion for 0, 2, 6, 12, 24 and 48 h in 1 liter of pre-aerated water maintained at 22±1ºC in glass dishes. $T_3$ was administered at a nominal concentration of 100 nM and the ratio of chemical applicant to water was 1:10,000 (vol/vol). Chemical applications were not renewed during the test period. After the exposures, tadpoles were euthanized in 0.1% tricaine methanesulfonate (MS-222; Syndel Laboratories Ltd., Vancouver BC Canada) and tail and brain tissue were collected.

### *2.2.3 Total protein extraction*

*X. laevis* tadpole tails were obtained as described above and each gram of tail tissue was homogenized by two 10-sec pulses at 9500 rpm in a Heidolph DIAX 600 homogenizer (Heidolph Elektro GmbH & Co. KG, Kelheim Germany) on ice in 3 ml of homogenization buffer. The homogenization buffer consisted of 25 mM 4-(2-Hydroxyethyl)piperazine-1-ethanesulfonic acid (HEPES; pH 7.0); 10 mM ethylenediaminetetraacetic acid (EDTA), 10 mM β-glycerophosphate, 0.1 mM sodium orthovanadate, 1 mM sodium fluoride, 1 mM dithiothreitol (DTT), 100 μM phenylmethylsulfonyl fluoride (PMSF), 4 μg/ml aprotinin, 1 μg/ml leupeptin, 2 μg/ml antipain, and 300 μg/ml benzamidine. All reagents were from Sigma-Aldrich Canada Ltd. (Oakville ON Canada). The homogenate was clarified by centrifugation at 12,000 x g for 10 min. at 4ºC, and the protein concentration was determined using the protein assay from Bio-Rad Laboratories, Inc. (Hercules CA USA) according to the manufacturer's instructions. The protein samples were aliquoted and stored at -70ºC.

### *2.2.4 Subcellular fractionation*

Ventral tail fin and brain tissue were obtained once *X. laevis* tadpoles were euthanized as described above. Cytoplasmic and nuclear fractions were obtained by using a modified version of the differential detergent fractionation method described by Ramsby and Makowski (1999). Changes included the addition of protease and phosphatase inhibitors to the digitonin/EDTA, Triton X-100/EDTA and Tween/deoxycholate extraction buffers to a final concentration of 10 mM β-glycerophosphate, 0.1 mM sodium orthovanadate, 1 mM sodium fluoride, 100 μM PMSF, 4 μg/ml aprotinin, 1 μg/ml leupeptin, 2 μg/ml antipain, and 300 μg/ml benzamidine (All from Sigma-Aldrich). Additionally, the tail fin and brain tissue was homogenized using a 2 ml glass/teflon pestle driven by a Cole Parmer Model 4555C homogenizer at speed 5. Protein concentration was determined as indicated above and samples were stored at -70ºC.

### *2.2.5 Two-Dimensional (2D) polyacrylamide gel electrophoresis*

The first dimension for protein separation used isoelectric focusing (IEF) tube gels (2.5 mm x 12 cm) that consisted of 9.5 M urea (SigmaUltra urea; Sigma-Aldrich), 4% (wt/vol) total acrylamide (3.78% acrylamide; EM Science, Darmstadt Germany, 0.22% bis-acrylamide; Sigma-Aldrich), 4.2% (vol/vol) Pharmalyte 3-10 ampholytes (Amersham Pharmacia Biotech AB, Uppsala Sweden), 2% (vol/vol) Pharmalyte 5-8 ampholytes (Amersham Pharmacia Biotech AB), 2% (vol/vol) Igepal CA-630 (Sigma-Aldrich), 0.05% (wt/vol) ammonium persulphate (ACP

Chemicals Inc.), and 0.07% (vol/vol) *N,N,N',N'*-tetramethylethylenediamine (TEMED; Sigma-Aldrich). The IEF gels were prefocused at 200 V for 15 min., 300 V for 30 min., and 400 V for 30 min. In the IEF running apparatus, the catholyte was 50 mM NaOH (EM Science), and the anolyte was 0.8% (vol/vol) phosphoric acid (ACP Chemicals Inc.). The protein samples were adjusted to 9.5 M urea, 2% (vol/vol) Igepal CA-630, 2% (vol/vol) Pharmalyte 3-10, 2% (wt/vol) DTT, and incubated at room temperature for 2 h. Sixty μg for silver stained 2D gels and 300 μg for Coomassie stained 2D gels of protein were loaded onto each IEF gel in a 100 μl volume. Samples were electrophoresed for 16 h at 350 V (5600 Vh), then hyperfocused at 800 V for 1 h. The IEF gels were then rinsed in deionized distilled $H_2O$ ($ddH_2O$) for 30 sec. and equilibrated twice for 15 min. in 5 ml of 125 mM Tris-HCl (EM Science) (pH 6.8), 2.5% sodium dodecyl sulfate (SDS; Fisher Scientific, Fair Lawn NJ USA), 5 mM DTT, 10% (vol/vol) glycerol (EM Science), 0.05% (wt/vol) bromophenol blue (Sigma-Aldrich).

The second dimension separation used SDS-PAGE (15 cm x 14 cm x 1.5 mm) composed of a 12% separating gel and a 5% stacking gel. The IEF gels were overlayed with 0.5% (wt/vol) agarose (EM Science) in 125 mM Tris-HCl (pH 6.8), with 0.05% (wt/vol) bromophenol blue, and 2% (wt/vol) SDS. Full Range Rainbow RPN 800 (Amersham Pharmacia Biotech AB) molecular weight markers were used. The gels were electrophoresed at 100 V for 1 h at constant voltage and then at 30 mA per gel at constant current for 4 h. For colloidal Coomassie staining the gels were then fixed in 50% (vol/vol) ethanol (EM Science), 3% (vol/vol) phosphoric acid at room temperature with shaking overnight, rinsed three times for 30 min. in $ddH_2O$, equilibrated in 16% (wt/vol) ammonium sulfate (EM Science), 25% (vol/vol) methanol (EM Science), 5% (vol/vol) phosphoric acid for 1 h, and subsequently stained by adding Coomassie brilliant blue G250 (Bio-Rad Laboratories, Inc.) to 0.01% (wt/vol) and shaking at room temperature for 3 days. Gels were then stored in 20% ammonium sulfate. For silver staining the 2D gels were fixed in 50% methanol, 5% acetic acid (EM Science) overnight. Then washed in 50% methanol for 10 min. and $ddH_2O$ for 10 min. The gels were then sensitized in 0.02% sodium thiosulfate (EM Science) for 3 min., rinsed in $ddH_2O$ twice for 1 min. and submerged in 0.1% silver nitrate for 30 min. at 4ºC. The gels were rinsed once in $ddH_2O$ and developed in 0.04% formaldehyde, 2% sodium carbonate (EM Science) for about 3 min. The reaction was terminated with 5% acetic acid and the gels were stored in 1% acetic acid. Gel images were obtained using a DVC digital camera and analyzed using Northern Eclipse software (Empix Imaging Inc., Mississauga ON Canada).

*2.2.6 Mass spectrometry analysis*

Spots of interest were excised and the proteins within were reduced, alkylated, and digested with trypsin according to an in-gel digestion protocol (Kinter and Sherman, 2000) with a few modifications. The following sequence was used: the gel pieces were destained in 50% (vol/vol) methanol, 5% (vol/vol) acetic acid (ACP Chemicals Inc.), dehydrated with acetonitrile (EM Science), dried, reduced with 50 mM DTT in 100 mM ammonium bicarbonate (Sigma-Aldrich) at 56ºC for 30 min., alkylated with 100 mM iodoacetamide (Sigma-Aldrich) in 100 mM ammonium bicarbonate at 45ºC for 30 min. in the dark, dehydrated with acetonitrile, hydrated with 100 mM ammonium bicarbonate, dehydrated with acetonitrile, dried, and digested with 20 ng/µl of Sequencing Grade Modified Trypsin (Promega Corp., Madison WI USA) in 50 mM ammonium bicarbonate at 37ºC overnight. The resulting peptides were extracted out of the gel pieces by incubation in 100 mM sodium carbonate (EM Science), pH 10, for 1 h at 37ºC. The peptides were desalted using ZipTip pipette tips containing $C_{18}$ reversed-phase media (Millipore Corp., Bedford MA USA) by washing with 0.1% (vol/vol) formic acid (ACP Chemicals Inc.) and eluting with 50% (vol/vol) acetonitrile, 0.1% (vol/vol) formic acid. The eluted peptide sample was applied to the target plate with an equal volume of matrix solution (1% (wt/vol) α-cyano-4-hydroxycynnamic acid (Sigma-Aldrich) in 50% (vol/vol) acetonitrile, 0.3% (vol/vol) formic acid) and allowed to dry. Adrenocorticotropic hormone fragment 1-17 (FW 2093.4), bradykinin fragment 2-9 (FW 904.0) and angiotensin 1 (FW 1296.5) (Sigma-Aldrich) in 30% acetonitrile, 0.01% formic acid were mixed with an equal volume of matrix solution and placed next to every sample spot on the target plate as external calibrants.

Spectra were obtained using a Voyager-DE STR Biospectrometry Workstation matrix-assisted laser desorption-ionization time-of-flight (MALDI-TOF) mass spectrometer (PE Applied Biosystems, Foster City CA USA) operating in positive reflector mode with delayed extraction. Data were manipulated using the Voyager Version 5.1 software with Data Explorer (PE Applied Biosystems). The sample spectra were further internally calibrated using autolytic trypsin peptide peaks. To identify the protein spots from the 2D gels, the measured masses of the tryptic peptides were searched against the *X. laevis* entries from the NCBInr03/26/2002 protein database (nonredundant database compiled from a combination of several publicly available protein databases at the National Center for Biotechnology Information, Washington DC USA) using the MS-Fit program (University of California, San Francisco; prospector.ucsf.edu). MS-Fit searches were performed with the following parameters: protein molecular mass range of 1,000-100,000 Da, only *X. laevis* species allowed, one missed cleavage allowed for trypsin digests, cysteines

modified by carbamidomethylation, oxidized methionines, and acrylamide modified cysteines as considered modifications, and peptide mass tolerance of ±50 ppm.

### *2.2.7 Immunoblotting*

For immunoblot analysis, 150 μg of protein obtained from the different subcellular fractions were resolved by 2D gel electrophoresis as described above. Proteins were then electrophoretically transferred onto a 0.2-μm nitrocellulose membrane (Bio-Rad) at 0.5 Amps for 2 h using a tank-blotter (Amersham Pharmacia) and transfer buffer consisting of 20 mM Tris-base and 150 mM glycine (EM Science). Protein transfer was verified by membrane staining with 0.1% Ponceau S (Sigma-Aldrich) in 5% acetic acid. Membranes were blocked with 5% nonfat milk in 20 mM Tris-base pH 7.6, 140 mM NaCl, 0.1% Tween (TBST), for 1 hour, then probed with an anti-phospho-threonine rabbit polyclonal antibody (#9381; Cell Signaling Technology, Danvers MA USA) diluted at 1/1000 in 5% bovine serum albumin (BSA; Sigma-Aldrich) in TBST with gentle agitation overnight at 4ºC. The blots were washed with TBST for 1 hour with the solution changed every 10 min. The membranes were then incubated with secondary antibody, HRP-conjugated goat anti-rabbit IgG diluted at 1/2000 in 5% nonfat milk/TBST for 1 hour at room temperature. The blots were again washed with TBST for 1 hour. Blots were then processed using the enhanced chemiluminescence (ECL) method, as described by the manufacturer (Amersham Pharmacia), and exposed to Kodak Biomax film.

To determine tyrosine phosphorylation the probed blots were first stripped by washing in 0.2 M glycine, 0.5 M NaCl, pH 2.4 with shaking at room temperature for 20 min. The blots were then blocked and reprobed as indicated above but with the primary anti-phospho-tyrosine mouse monoclonal IgG1 antibody (#9416; Cell Signaling Technology) diluted at 1/2000 and HRP-conjugated goat anti-mouse IgG as secondary antibody. The blots were subsequently stained with Amido Black to verify equal protein transfer: stained for 2 min. in 0.1% amido black (Sigma-Aldrich), 25% isopropanol (EM Science) and 10% acetic acid (EM Science), destained for 10 min. in 25% isopropanol and 10% acetic acid, and rinsed in $dH_2O$.

### *2.2.8 Phosphoprotein isotope-coded affinity tag (PhIAT) method*

The procedure was carried out as described by Goshe et al. (2001) with minor modifications. The PhIAT method was tested using β-casein (C6905; Sigma-Aldrich). Briefly, β-casein denatured in guanidine HCl (GdnHCl; Sigma-Aldrich) was reduced with tris-(2-carboxyethyl)-phosphine (TCEP) (Pierce, Rockford IL USA) and cysteines were blocked using iodoacetamide. After

desalting on Sephadex G-25 medium (Amersham Biosciences), the phosphate groups present on serine and threonine were removed by β-elimination under basic conditions, and concurrently reacted with 1,2-ethanedithiol (EDT), which attacked the modified β-casein. Two samples of β-casein were used. One was reacted with normal EDT (EDT-$D_0$; Sigma-Aldrich) and the other with deuterated EDT (EDT-$D_4$; C/D/N Isotopes, Point-Claire PQ Canada). The reaction was neutralized in the presence of 4 M GdnHCl and 15 mM TCEP to prevent precipitate formation. After neutralization of the reactions, the two β-casein samples were mixed, desalted, reduced with TCEP, and reacted with iodoacetyl-PEO-biotin (Pierce), which attached the biotin tag onto the EDT in each modified phosphoprotein. Samples were then desalted and digested with sequencing grade trypsin. The modified phosphopeptides were then obtained by avidin affinity chromatography (ICAT kit; Applied Biosystems). Samples were analyzed by MALDI-TOF MS as described earlier and by ESI-MS/MS as described in chapter 3.

### *2.2.9 Tail organ culture*

Premetamorphic tadpoles of *Rana catesbeiana* at TK stages VI-X were euthanized as described previously and then immersed in sterile distilled water for 10 sec., followed by 5 sec. in 70% ethanol and two 10 sec. rinses in sterile distilled water. Tail tips (2 cm) were removed and placed into tadpole Minimal Essential Medium (TMEM) comprising a 55% strength solution of MEM (Invitrogen, Burlington ON Canada) adjusted to pH 7.1 and supplemented with 25 mM HEPES, 3 mM $NaHCO_3$, 1.2 mM $Na_2HPO_4$, 1.2 mM $NaH_2PO_4$, 20 mM NaCl, 2 mM L-glutamine, 50 U/ml penicillin, 50 μg/ml streptomycin, and 50 μg/ml neomycin, at a density of one tip per 5 ml media. Tips were incubated for 24 h at 25°C and then treated with equal volumes of dimethyl sulfoxide (DMSO) vehicle control, 100 nM $T_3$, 60 μM roscovitine (Sigma-Aldrich) or 100 nM $T_3$ in combination with 60 μM roscovitine. Media and chemicals were replenished daily for the duration of the experiment. Four tadpole tails per treatment were used for the tail measurements and 8 tails per treatment were used for the phosphoproteome analysis.

### *2.2.10 Tail measurements*

Photographs were taken of cultured tails every 24 h for 96 h by using a digital camera (DVC Company, Austin TX USA), and the tail area was measured by using Northern Eclipse v5.0 (Empix Imaging, Mississauga ON Canada).

*2.2.11 Phosphoprotein enrichment of protein samples from organ cultured tails*

The PhosphoProtein Purification kit (QIAGEN, Mississauga ON Canada) was used according to the manufacturer's protocol with minor modifications. After 48 h of exposure, *R. catesbeiana* organ cultured tail tips were washed in cold saline consisting of 7.5 mM Tris-HCl pH 7.6, 88 mM NaCl, 1 mM KCl, 2.4 mM $NaHCO_3$, and were then homogenized in cold lysis buffer at 8 tail tips per 5 ml of buffer using two 10-sec pulses at 9500 rpm in a Heidolph DIAX 600 homogenizer. Samples were then incubated for 30 min. at 4ºC and subsequently centrifuged at 13,000 x g for 30 min. at 4ºC. 2.5 mg of total protein per sample was then processed through the column according to the manufacturer's protocol. The obtained phosphoprotein fraction was stored at -70ºC.

*2.2.12 2D gel analysis of phosphoprotein fractions from organ cultured tails*

Forty µg of protein from the phosphoprotein fraction for each treatment were resuspended in 450 µl rehydration buffer (8 M Urea, 2% CHAPS, 0.5% carrier ampholytes (Amersham Biosciences), 0.2% DTT) and separated in the first dimension by isoelectric focusing on a 24 cm pH 3-10 immobilized pH gradient (IPG) strip (Amersham Biosciences) for 60 000 Vh using an IPGphor Isoelectric Focusing apparatus (Amersham Biosciences) according to the manufacturers protocol. The IPG strips were then incubated for 15 min. in a reducing solution (50 mM Tris HCl pH 8.8, 6 M urea, 30% glycerol, 2% SDS, 1% DTT) and for a further 15 min. in an alkylating solution (50 mM Tris HCl pH 8.8, 6 M urea, 30% glycerol, 2% SDS, 4.8% iodoacetamide). Proteins within the IPG strips were then separated in the second dimension. The IPG strips were sealed on top of 9-16% 26 cm x 20 cm polyacrylamide gels using agarose sealing solution (25mM Tris, 192 mM glycine, 0.1% SDS, 0.5% agarose, bromophenol blue) and the gels were run at a 30 mA per gel in a Ettan DALTtwelve (Amersham Biosciences) gel system at 9ºC until the dye front ran off the bottom of the gels. Protein spots were visualized by SYPRO Ruby fluorescent gel stain (Molecular Probes, Burlington ON Canada) according to the manufacturer's protocol and scanned using the ProExpress Proteomic Imaging System (Perkin Elmer, Waltham MA USA). Protein spots of interest were excised and analyzed using mass spectrometry as indicated above.

*2.2.13 Statistics*

Statistical analyses were performed using SPSS Ver. 12.0 (Chicago IL USA) software using the Mann-Whitney U non-parametric two-tailed test.

## 2.3 RESULTS AND DISCUSSION

### *2.3.1 Changes in the tail tissue proteome of X. laevis tadpoles undergoing precocious metamorphosis*

The process of tail regression during metamorphosis requires active protein synthesis (Wang and Brown, 1993). To determine what components of the proteome might be involved in this developmental program the current study set out to identify some of the proteins whose steady-state levels are altered by $T_3$. Premetamorphic (NF stage 52-54) *X. laevis* tadpoles were exposed by immersion to 100 nM $T_3$ for 0, 12, 24 and 48 h. Cytoplasmic protein extracts were subsequently isolated from the tail fin and resolved by 2D gel electrophoresis. Changes in protein expression were observed as early as 24 h and were more numerous by 48 h (Figure 2.1). A number of protein spots increased in expression level starting at 24 h of $T_3$ treatment and increased further with additional new spots appearing at 48 h (red boxes). A smaller number of protein spots decreased in expression due to $T_3$ treatment (green boxes). These proteins are observed at 0 h and 12 h, but not at 24 or 48 h of treatment. These observations are in accordance with changes in gene expression observed by cDNA array analysis in the tail of *X. laevis* tadpoles undergoing precocious metamorphosis where the majority of changes were increases in expression at 48 h (Helbing et al., 2003). These observations support the existence of the commitment point established at 24 to 48 h of TH treatment, where the complete genetic program required for tail resorption is set, after which, removal of TH or exposure to protein synthesis inhibitors can not prevent regression (Wang and Brown, 1993). Additional protein spots (blue boxes) shift position towards the more alkaline side of the 2D gel at 24 and 48 h of $T_3$ treatment, implying a possible dephosphorylation event (Figure 2.1). No protein spots could be identified due to the low abundance of protein within the protein spots of these silver stained 2D gels.

To identify some of these altered proteins total protein homogenates were isolated from whole tails of control and $T_3$-treated tadpoles after 48 h and a larger 300 μg protein amount was resolved by 2D gel electrophoresis. Comparison of Coomassie blue-stained gels revealed 7 protein spots that were reduced and 30 that were increased at 48 h of hormone treatment (Figure 2.2). Several protein spots that were in sufficient quantity were isolated for peptide mass fingerprinting of their tryptic fragments using MALDI-TOF mass spectrometry and their identities are shown in Table 2.1. Of particular note is the identification of two spots corresponding to the zinc finger protein XLCGF3.1, originally identified in *Xenopus* gastrula-stage embryos, that increase to levels greater than 4-fold in the presence of $T_3$ compared with the control. Other identified proteins that

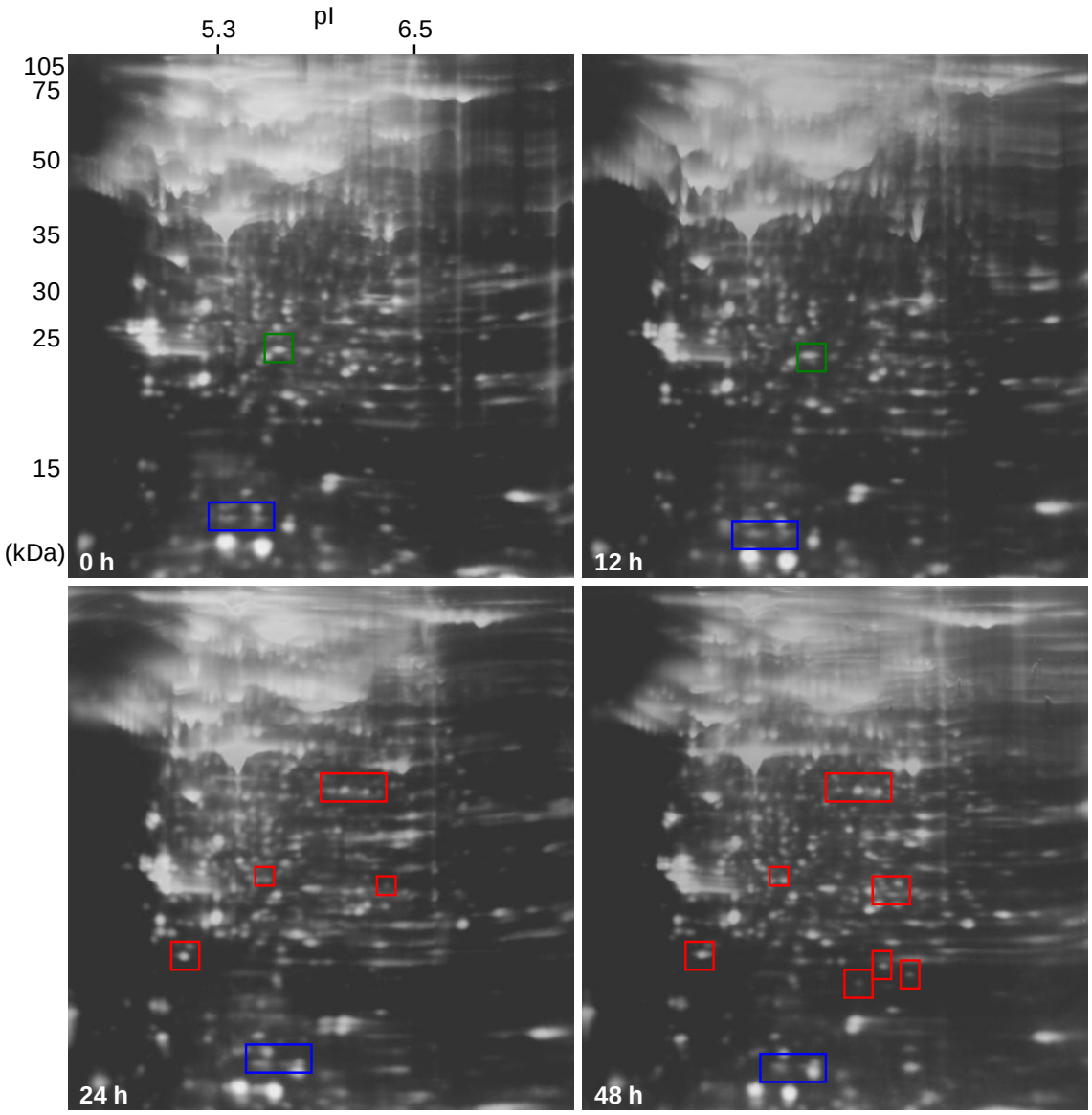


**Figure 2.1. TH-induced changes in the *X. laevis* tadpole tail proteome observed over time.** Premetamorphic tadpoles were exposed to 100 nM $T_3$ for the indicated time periods, tail fin cytoplasm proteins were extracted, 60 μg amounts were resolved by 2D gel electrophoresis and visualized by silver staining. Red boxes indicate protein spots that increase in expression as a result of treatment, green boxes indicate a decrease in expression, and blue boxes indicate a shift in protein spot position, indicating a possible dephosphorylation event. Relative molecular weights of protein standards are indicated in kDa and isoelectric point reference markers are indicated by pI.

increased in expression include a number of tubulin isoforms and the ribonucleotide reductase protein R1. The latter binds to γ- and α/β tubulin *in vitro* and promotes microtubule nucleation on the centrosome at the onset of mitosis in *Xenopus* egg mitotic extracts (Takada et al., 2000). In

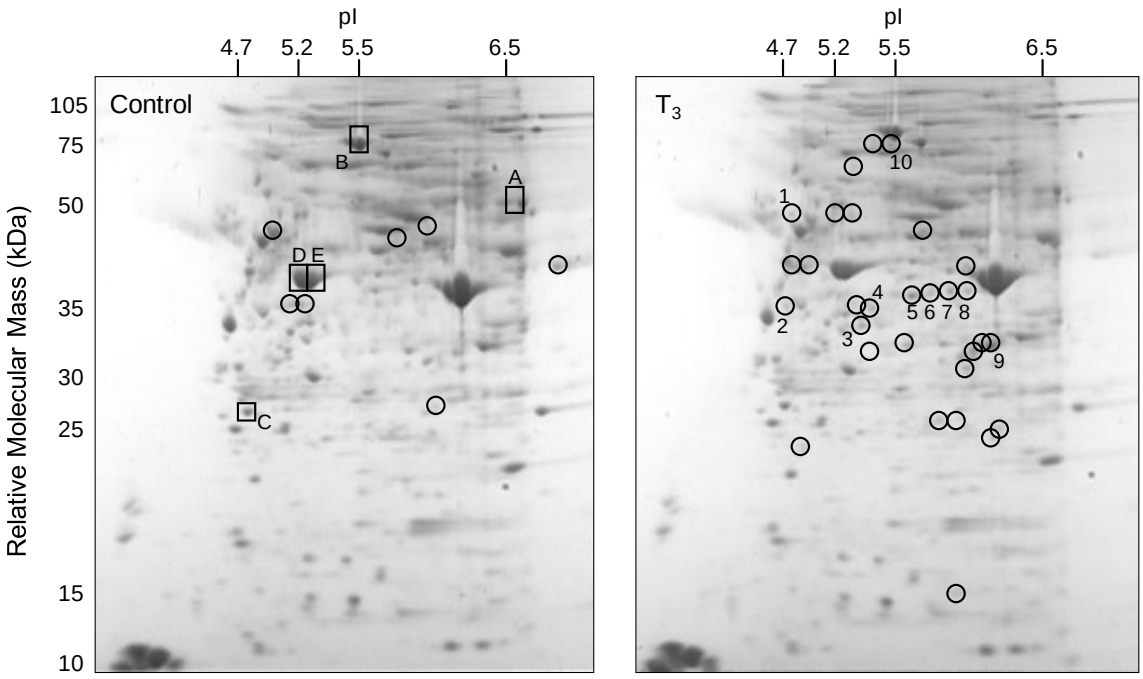


**Figure 2.2. Changes in the tail tissue proteome of *X. laevis* tadpoles undergoing precocious metamorphosis.** 2D polyacrylamide gels of total protein (300 μg) extracted from tail tissue of tadpoles treated for 48 h with 100 nM $T_3$ or vehicle control are shown that are representative of two independent experiments. Colloidal Coomassie brilliant blue G250 was used to stain the proteins. Protein spots that increase in intensity due to $T_3$ treatment are circled on the $T_3$ gel, whereas those that decrease in intensity are circled on the control gel. Proteins used as isoelectric point reference markers are boxed. Spot identities and characteristics are shown in Table 2.1.

addition to mitotic spindle activation, the ribonucleotide reductase protein R1 is part of the ribonucleotide reductase complex which functions in DNA replication and repair. Two protein spots that appeared below a reference spot that was identified as 74 kDa serum albumin also matched this serum albumin. These could also represent the 68 kDa form of serum albumin whose mRNA has been found to be $T_3$-responsive and increase at the onset of metamorphosis in *X. laevis* (Moskaitis et al., 1989). These findings show that the albumin protein is increased as well and confirm its TH responsiveness. Other proteins that increased as a result of $T_3$ treatment included the muscle specific proteins desmin, an intermediate filament protein whose mRNA has been found to increase during *X. laevis* embryogenesis (Herrmann et al., 1989), and creatine kinase, an enzyme important in energy metabolism. A number of *Xenopus* creatine kinase isozymes have been found to be tissue and developmental stage specific (Robert et al., 1990, 1991).

**Table 2.1. Identification of proteins and related transcripts in the *X. laevis* tadpole tail**

| Protein Spot[a] | Protein Identification | NCBI Protein Accession No. | Peptide Match[b] | Percent Protein Coverage | Fold Change | |
|---|---|---|---|---|---|---|
| | | | | | Protein[c] | mRNA[d] |
| | *Isoelectric point markers* | | | | | |
| A | Cytosolic thyroid hormone binding protein, (CTHBP)/pyruvate kinase, muscle isozyme | 2497536 | 18/68 | 45 | 1.0 | 1.0 |
| B | 74-kDa Serum albumin | 213931 | 22/72 | 48 | 1.1 | ND |
| C | 14-3-3 Protein ε | 2895518 | 7/45 | 22 | 1.1 | 1.5 |
| D | α-Skeletal actin | 64509 | 13/90 | 50 | 1.0 | 0.6 |
| E | Cytoplasmic β actin | 3348131 | 8/31 | 37 | 1.0 | 0.6 |
| | *Thyroid hormone responsive* | | | | | |
| 1 | Ribonucleotide reductase subunit R1 | 12002837 | 5/43 | 16 | 2.0 | 1.8 |
| 2 | Desmin | 64653 | 8/64 | 27 | 2.0 | 1.2 |
| 3 | β-2 Tubulin | 135463 | 6/57 | 21 | 5.3 | 1.8 |
| 4 | α-Tubulin | 135441 | 8/55 | 30 | 2.4 | 3.0 |
| 5 | β-5 Tubulin | 567053 | 6/35 | 22 | 4.1 | - |
| 6 | δ-Tubulin | 16612089 | 6/97 | 11 | 2.2 | 3.6 |
| 7 | Gastrula zinc finger protein XLCGF3.1 | 141645 | 6/39 | 30 | 4.1 | - |
| 8 | Gastrula zinc finger protein XLCGF3.1 | 141645 | 5/54 | 19 | 7.6 | - |
| 9 | Creatine kinase | 539482 | 9/47 | 36 | 2.3 | - |
| 10 | 74-kDa Serum albumin | 213931 | 10/92 | 22 | 1.8 | ND |

[a] Protein spot *number* and *letter* designations correspond to those shown in Fig. 2.2. [b] Comparison of matched peptide masses to total peptides analyzed. [c] Fold change represents the ratio of normalized spot intensities on the $T_3$ gel compared to the control gel. Spot intensities between the two gels were normalized using α skeletal actin (spot D) and cytoplasmic β actin (spot E). [d] The ratio of normalized mRNA copy number determined for $T_3$ treatment compared with that for vehicle control generated by QPCR analyses. Copy numbers between the two treatments were normalized using ribosomal L8 transcript levels. ND, Not detectable. –, Not assessed due to lack of available genetic data. Adapted from Helbing et al., (2003). QPCR analysis was performed by Helbing et al., and not D. Domanski.

To examine the relationship between the identified proteins in this study and their gene transcript levels, Helbing et al. (2003) performed QPCR analyses and found that the difference in detected fold changes were within approximately 2-fold for most proteins and their respective transcripts (Table 2.1). Some notable discrepancies were found with serum albumin and β-2 tubulin. Increases in α- and β-tubulin gene expression have also been observed in $T_3$-induced *X. laevis* tadpole tails by cDNA array analysis (Helbing et al., 2003, 2007b). Serum albumin gene transcripts were not detected in tail tissue as expected because it is a protein synthesized in the liver and released into the blood (Moskaitis et al., 1989). This underlines the usefulness of examining proteins in addition to the transcriptome in the study of metamorphosis as some critical components might not be produced in the tissue being investigated.

This study also identified cytosolic TH binding protein (CTHBP)-pyruvate kinase-muscle isozyme, a protein that is directly involved in thyroid hormone action. In its tetrameric form, this enzyme acts as pyruvate kinase and, as a monomer, it interacts with intracellular TH, thereby modulating intracellular TH concentration. In this manner, CTHBP is thought to be involved in

modulating the metamorphic process in different tissues by controlling the level of intracellular thyroid hormones. CTHBP mRNA has been detected in the tail of premetamorphic tadpoles and its level drastically decreases in the resorbing tail (Shi et al., 1994). The current study did not observe an alteration in the transcript or the protein spot intensity under the conditions used.

### *2.3.2 Changes in protein phosphorylation in the brain of X. laevis tadpoles undergoing precocious metamorphosis*

Premetamorphic (NF stage 52-54) *X. laevis* tadpoles were exposed by immersion to 100 nM $T_3$ for 0, 2, 6, 12, 24 and 48 h or vehicle control for 48 h. To improve the chance of observing changes in low abundance proteins such as phosphoproteins, a fractionation method was used that provided nuclear and cytoplasmic fractions of the tadpole brain tissue. These protein fractions were resolved by 2D gel electrophoresis and changes in the phosphorylation state of threonine and tyrosine residues were assessed by immunoblot analysis. The time course of $T_3$ treatment revealed that phosphorylation and dephosphorylation events occur on threonine residues as early as 2 h after treatment and different events occurred in the cytoplasm compared to the nucleus (white boxes; Figure 2.3). In the cytoplasmic fraction, a cluster of threonine phosphorylated protein spots was observed to appear at 6 h of $T_3$ treatment and persisted till 48 h. This phosphorylation was not observed at time 0 h and at 2 h of $T_3$ treatment or in the 48 h control (C 48 h), suggesting a phosphorylation event due to $T_3$ treatment. In the nuclear fraction, four threonine phosphorylated protein spots (~60 kDa, pI ~5.5) decreased in intensity at 2 h of $T_3$ treatment, and at the same time, a cluster of spots (~35 kDa, pI ~6) becomes more phosphorylated. Comparing the 48 h control (C 48 h) to the 24 and 48 h $T_3$ treatments in the nuclear fraction, a group of proteins at ~30-35 kDa, pI ~6-6.5, and a row of proteins at 75 kDa, pI ~6-6.5, become dephosphorylated due to $T_3$ treatment. The group of spots at ~30-35 kDa, pI ~6-6.5 is also observed in the cytoplasmic brain fraction, but remains constant during $T_3$ treatment, suggesting a possible shuttling of these phosphorylated proteins out of the nucleus or nucleus specific dephosphorylation due to $T_3$.

Fewer changes were observed in tyrosine phosphorylation (black boxes; Figure 2.4). In the cytoplasmic fraction a row of proteins becomes maximally phosphorylated on tyrosine residues at 12 h of $T_3$ treatment. In the nuclear fraction one tyrosine phosphorylated protein spot shifts towards the more alkaline side of the gel after 48 h of $T_3$ treatment. The protein spot is in alignment with another protein spot above it in all the other treatments, as well as the 48 h control (C 48 h). This shift might indicate a dephosphorylation event due to $T_3$ treatment, which causes

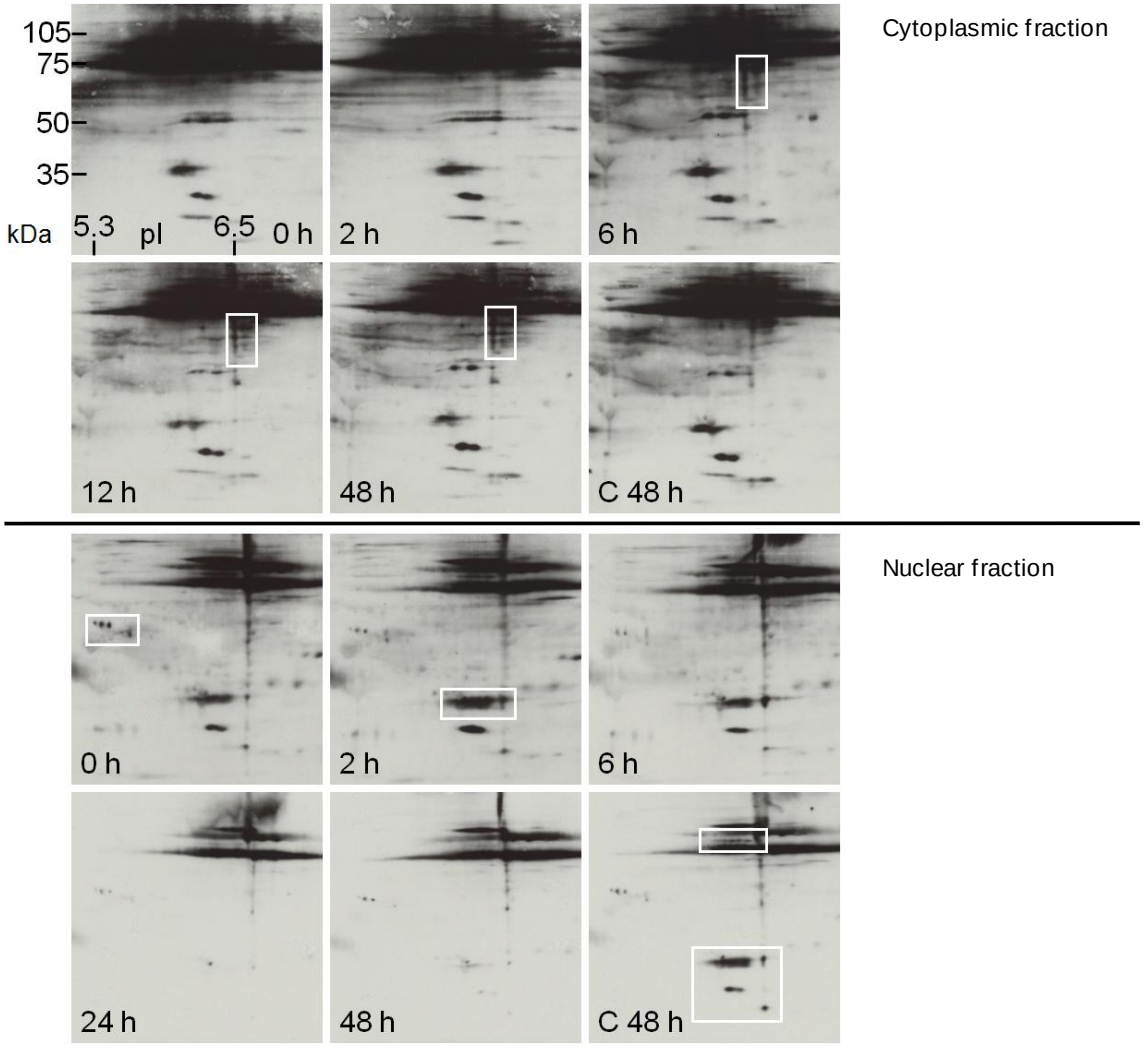


**Figure 2.3. Changes in protein phosphorylation on threonine residues in the cytoplasmic and nuclear brain fractions of *X. laevis* tadpoles undergoing precocious metamorphosis.** Tadpoles were exposed to 100 nM $T_3$ for the indicated time periods, cytoplasmic and nuclear protein fractions were extracted from the brain, resolved by 2D gel electrophoresis and an immunoblot was performed to indicate proteins phosphorylated on threonine residues. Changes in phosphorylation are marked with white boxes. Relative molecular weights of protein standards are indicated in kDa and isoelectric point reference markers are indicated by pI.

the protein to become less acidic. Due to the high sensitivity of immunoblotting in comparison to the amount of protein required for MS analysis, none of the phosphoproteins could be identified.

In the mammalian system thyroid hormones have been shown to be critical in brain function and development (Zoeller and Rovet, 2004), and some evidence exists showing that thyroid hormones can activate signal transduction pathways such as the phosphatidylinositol 3-kinase (PI3K)/Akt signaling pathway and its downstream targets in the brain (Sui et al., 2007). Thus far, no such

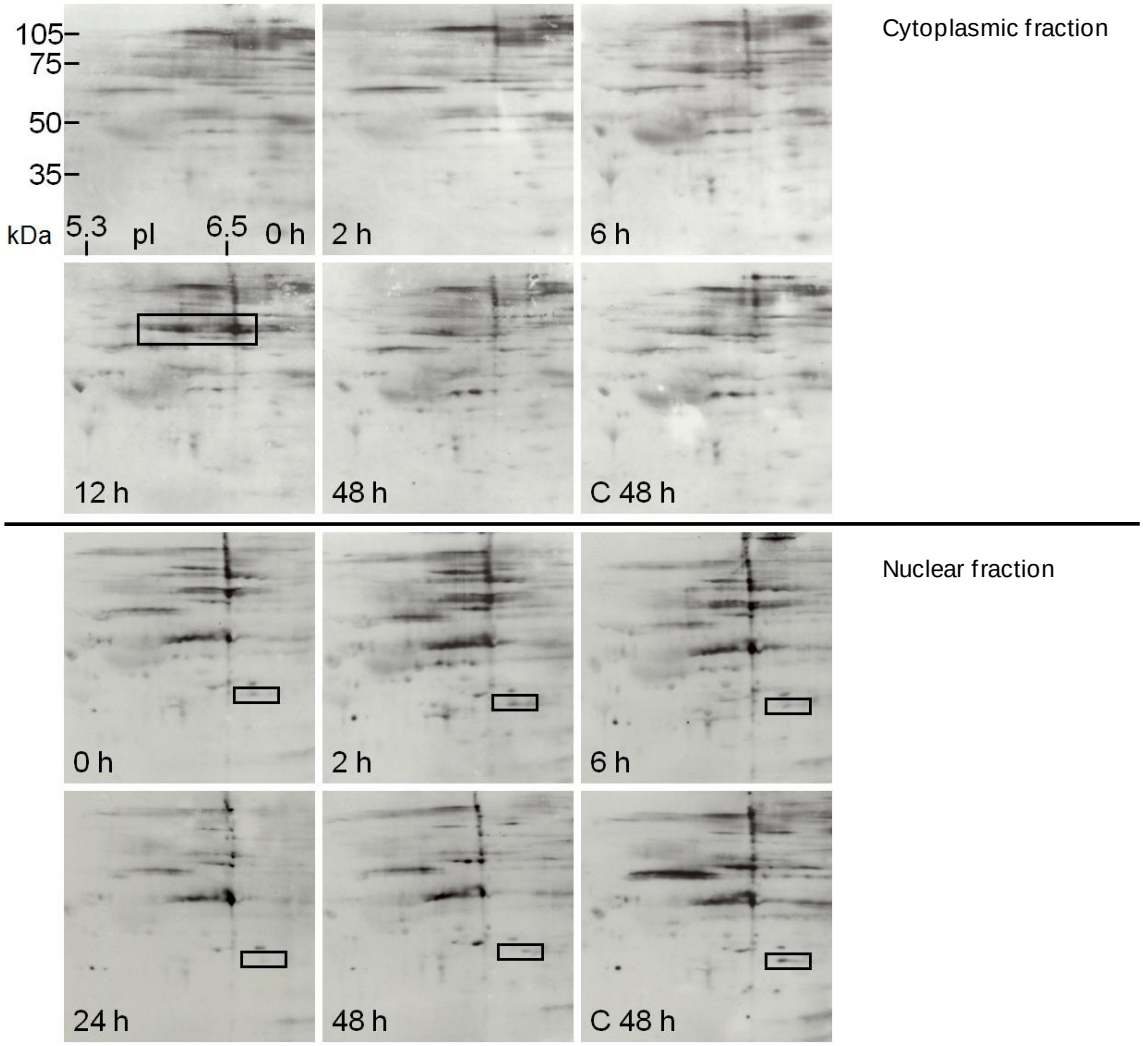


**Figure 2.4. Changes in protein phosphorylation on tyrosine residues in the cytoplasmic and nuclear brain fractions of *X. laevis* tadpoles undergoing precocious metamorphosis.** Tadpoles were exposed to 100 nM $T_3$ for the indicated time periods, cytoplasmic and nuclear protein fractions were extracted from the brain, separated by 2D gel electrophoresis and an immunoblot was performed to indicate proteins phosphorylated on tyrosine residues. Changes in phosphorylation are marked with black boxes. Relative molecular weights of protein standards are indicated in kDa and isoelectric point reference markers are indicated by pI.

evidence has been presented for the metamorphosing anuran brain. However, using the model of tadpole tail regression, we recently demonstrated that this TH-dependent process is dependent upon phosphorylation through targeting protein kinase C (PKC) and TRα (Ji et al., 2007) thereby linking PKC with the promotion of tail regression. Our laboratory has also reported that decreased cyclin A and cyclin-dependent kinase 2 (Cdk2) activity, rather than mitogen associated protein kinase (MAPK) or PI3K pathways, promotes tail regression (Skirrow and Helbing, 2007).

Therefore, a complex role for distinctive phosphorylation events appears to contribute to TH-dependent processes.

*2.3.3 Phosphoprotein isotope-coded affinity tag (PhIAT) method*

Due to the inability of identifying phosphoproteins in the previous 2D gel analysis, a newly developed mass spectrometric method termed PhIAT (Goshe et al., 2001) was assessed for its ability to determine differential phosphoprotein expression and concurrent identification. This method employed a phosphoprotein enrichment step, and without the need for 2D gel protein separation and instead with a direct analysis and quantitation by mass spectrometry, it thus promised a higher success in the discovery of modulated phosphoproteins. The method relies on hydroxide ion-mediated β-elimination of the O-phosphate moiety from phosphorylated threonine and serine residues (Figure 2.5A). After this, 1,2-ethanedithiol (EDT) containing either four alkyl hydrogens or four alkyl deuteriums is added onto the newly formed double bond, forming a nucleophilic sulfhydryl in place of the phosphate. This nucleophilic sulfhydryl then attacks the biotin tag, iodoacetyl-PEO-biotin (R; figure 2.5A), forming a biotinylated peptide that is stable-isotope tagged. The two resulting protein samples to be compared, one containing heavy-EDT and the other light-EDT, are then pooled and after proteolytic digestion the mixture is enriched for tagged phosphopeptides by avidin affinity chromatography. The enriched sample is then analyzed by mass spectrometry where tagged phosphopeptides are observed as doublets separated by 4 Da for every tagged residue on the peptide, due to the isotope tagging. The intensity of the peaks indicates the relative abundance of the phosphoprotein within the two samples, and phosphoprotein identification is achieved by performing tandem MS analysis on one of the peptide peaks within the doublet.

The PhIAT method was tested using a model phosphoprotein, β-casein that contains phosphorylated serine residues. Two samples of β-casein were used. One was reacted with normal EDT (EDT-$D_0$) and the other with deuterated EDT (EDT-$D_4$). The two samples were mixed in equal amounts and the modified phosphopeptides obtained at the end of the procedure were analyzed by MALDI-TOF MS. Several modified β-casein peptides were observed showing peak separations of 4 Da as expected for the two EDT-$D_0$/EDT-$D_4$ modified phosphopeptides containing one phosphorylated serine (Figure 2.5B). The peaks were of equal intensities reflecting the 1:1 ratio of the two samples of β-casein that were used. However, except for one peak, the masses of most of the peptides were not as expected, even after taking into account incomplete additions of EDT and/or iodoacetyl-PEO-biotin and different combinations of

A

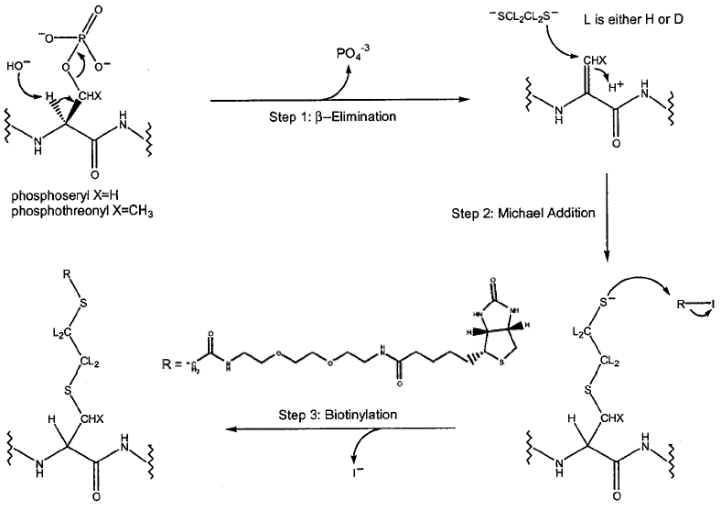
L is either H or D
Step 1: β--Elimination
Step 2: Michael Addition
Step 3: Biotinylation
phosphoseryl X=H
phosphothreonyl X=CH3

B

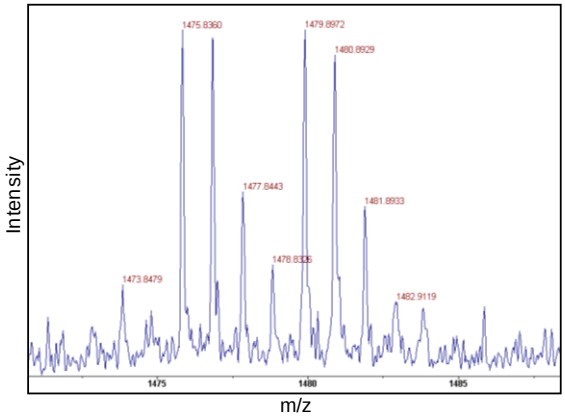
Intensity
m/z
1475.8360
1479.8972
1480.8929
1477.8443
1481.8933
1478.8336
1473.8479
1482.9119

C

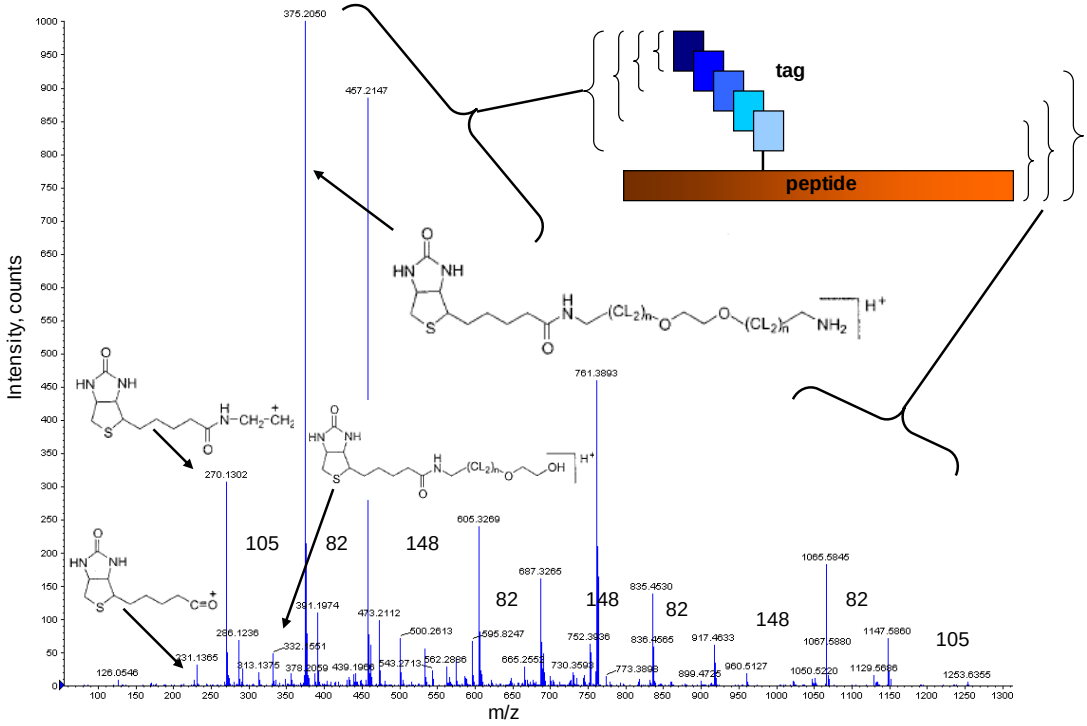
tag
peptide
Intensity, counts
m/z
375.2050
457.2147
761.3893
270.1302
605.3269
687.3265
835.4530
1065.5845
105
82
148
82
148
82
148
105

**Figure 2.5. Investigation of the PhIAT method for the analysis of the phosphoproteome.** (A) Modification and tagging of phospho amino acid residues within a peptide by the PhIAT method. (B) Mass spectrum showing successful labeling of two β-casein samples mixed in equal amounts, labeled using the two PhIAT tags, which are isotopically differentiated by 4 Da, indicating the labeling of a single phosphoserine containing peptide. (C) MS/MS analysis of a PhIAT tagged peptide indicating excessive fragmentation of the tag instead of the peptide. Numbers between peaks indicate mass differences that do not match any amino acid residue masses.

phosphorylation. A possible explanation for the unexpected peptide masses could be that β-casein undergoes base hydrolysis during the phosphate elimination reaction. Goshe at al. (2002) expressed concern about the use of highly basic conditions in the procedure but claims not to have observed excessive degradation of the protein. Further analysis of the peptides was carried out using ESI-MS/MS to obtain peptide sequence information. A product ion spectrum is shown for one of the peptides in Figure 2.5C. Amino acid sequence information could not be obtained from the MS/MS spectra. It appeared that all the peaks observed in the spectra are due to biotin tag fragmentation and possibly due to the EDT fragments as well. Fragmentation of the peptide was not observed at all.

Biotin tag fragments in MS/MS spectra have been documented in the PhIAT and other biotin tag-using procedures as ICAT (Goshe et al., 2002; Borisov et al., 2002). Tag fragmentation has been shown to use up much of the energy induced within the collision cell (CID) of the mass spectrometer, preventing efficient peptide fragmentation (Borisov et al., 2002). Due to the inability of being able to acquire peptide amino acid sequence information further research on this procedure was abandoned. In any future approaches this method could be improved through the use of a cleavable tag instead of the iodoacetyl-PEO-biotin tag. This improvement has recently been introduced into the ICAT method, allowing removal of the biotin fragment before MS/MS analysis increasing fragmentation efficiency upon CID (Goshe et al., 2003). The procedure could also be completely modified by using normal and isotope labeled ($d_{10}$) dithiothreitol (DTT) instead of EDT and iodoacetyl-PEO-biotin. DTT adds onto the modified phosphopeptide as in the PhIAT method, but the peptides are then purified by using a thiol-Sepharose column instead of biotin-avidin affinity chromatography. The procedure has been used by Wells et al. (2002) to study O-GlcNAc modifications of serine and threonine. The group observed that the method worked better then a biotin based tag, giving much better peptide fragmentation in MS/MS spectra.

### *2.3.4 Effects of the Cdk-inhibitor, roscovitine, on the phosphoproteome of $T_3$-induced tadpole tails*

The purine analogue, roscovitine (2-(1-Ethyl-2-hydroxyethylamino)-6-benzylamino-9-isopropylpurine) is a reversible specific competitive inhibitor of Cdks. At 60 μM, roscovitine, was able to prevent 100 nM $T_3$-induced *R. catesbeiana* tadpole tail regression in an organ culture setting (Figure 2.6A and B). This and other evidence suggest that a pivotal phosphoprotein(s) acted upon by a Cdk(s) is/are required in the initiation of tadpole tail regression (Skirrow and Helbing, 2007; Skirrow, 2003; Skirrow et al., 2008).

To reveal these phosphoproteins, the current study examined the phosphoproteome of premetamorphic *R. catesbeiana* tail tips cultured for 48 h in organ culture in the presence of 100 nM $T_3$, 60 μM roscovitine, or a combination of 100 nM $T_3$ and 60 μM roscovitine, and compared to a control. Phosphoproteins were obtained using a phosphoprotein purification column, resolved by 2D gel electrophoresis and visualized using SYPRO Ruby stain to maximize the sensitivity of detection. The 2D gels revealed numerous potential changes in the phosphoproteome as shown in Figure 2.6C. Whether all of these changing spots are actual phosphoproteins remains to be confirmed, nonetheless interesting observations were made. Of special interest are proteins that increase due to $T_3$ treatment and whose increase is inhibited by roscovitine (marked with purple boxes). Similarly, a couple of protein spots (white boxes) indicate a possible increase in phosphorylation level, which results in a shift of the protein spots towards the acidic end of the gel due to $T_3$ with roscovitine preventing this process. Furthermore, proteins indicated by green boxes indicate a strong increase due to $T_3$ treatment which is inhibited strongly by the combination with roscovitine and still seen slightly in the control and roscovitine alone treatment. The above proteins could indicate Cdk targets whose phosphorylation is prevented by roscovitine in turn inhibiting $T_3$-induced tail regression. In contrast, a number of proteins (blue boxes) are decreased due to $T_3$ treatment, but this event is prevented by the combination of roscovitine. These could indicate targets later in the signaling path that become dephosphorylated instead in the regression process. Of course this study also reveals potential phosphoproteins that are altered as a result of TH action. Interestingly, all of the potential phosphorylation changes that occurred due to $T_3$ when compared to control were inhibited by roscovitine, supporting the notion that roscovitine's actions occur early in the establishment of the regression program rather than later on its maintenance. Although an attempt was made at identifying all of these potential phosphoproteins by mass spectrometry, no identifications could be made due to the very low abundance of the proteins obtained with this methodology.

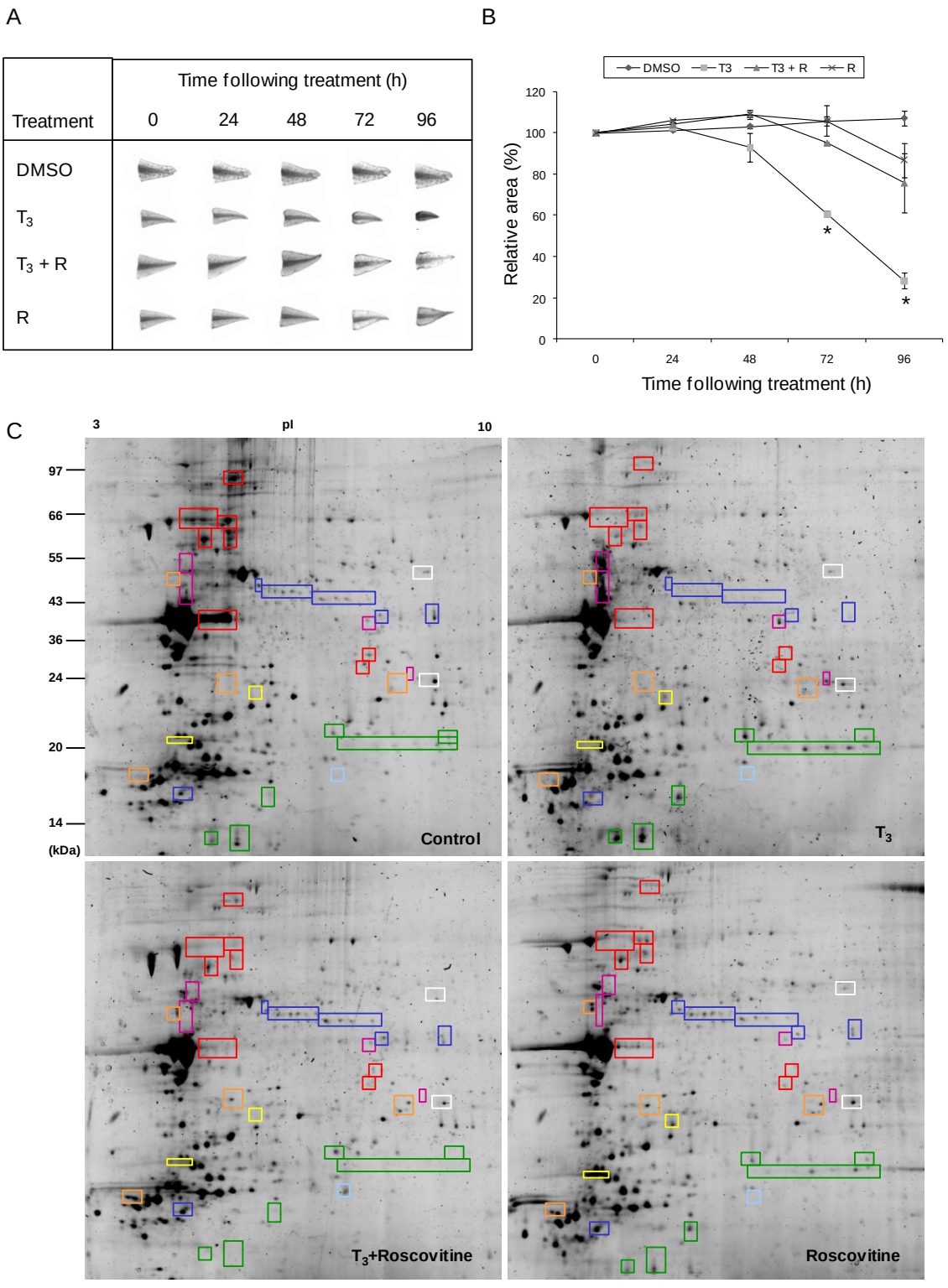


**Figure 2.6. Roscovitine inhibits $T_3$-induced regression of *Rana catesbeiana* cultured tail tips and 2D gel phosphoproteome analysis reveals the potential targets of this kinase inhibition.** Two centimetre tail tips were removed from TK stage VI-X tadpoles and cultured in TMEM for

96 hours. Tail tips were treated with DMSO vehicle control (DMSO), 100 nM $T_3$, 60 μM roscovitine (R) or $T_3$ with roscovitine ($T_3$ + R). (A) Representative example of cultured tail tip response to the above treatments. (B) The tail tip area was measured at each time point and plotted relative to the 0 hour time point (n=3-4 per time point). The error bars represent the standard error of the mean. The asterisk indicates significant difference in tail area between tails treated with $T_3$ and those treated with DMSO or $T_3$ and roscovitine together ($p<0.05$). (C) 2D gels showing potential changes in the *R. catesbeiana* tail phosphoproteome due to $T_3$ and roscovitine treatment. Tail tips were treated as indicated above. Phosphoproteins were then extracted using a phosphoprotein purification column, separated by 2D gel electrophoresis and visualized using SYPRO Ruby stain. Purple boxes indicate proteins increased due to $T_3$ treatment and whose increase is inhibited by roscovitine. Blue boxes indicate proteins decreased due to $T_3$ treatment. This event is also prevented by roscovitine. Orange boxes indicate proteins that are increased due to roscovitine treatment. Red boxes indicate proteins which are decreased in all of the treatments compared to control. White boxes indicate a possible increase in phosphorylation which results in a shift of the protein spot due to $T_3$. Green boxes indicate a strong increase due to $T_3$ treatment which is inhibited strongly by roscovitine and still seen slightly in the control and roscovitine alone treatment. Yellow boxes indicate an increase due to roscovitine alone. Light blue boxes indicate an increase due to roscovitine + $T_3$ treatment. Relative molecular weights of protein standards are indicated in kDa and the span of the isoelectric point separation is indicated by pI.

---

Many Cdks are linked to the control of the cell cycle, however, some Cdks are involved in the regulation of cell differentiation, such as Cdk5 (Lee et al., 1997), and transcription such as Cdks 7-9 (Bregman et al., 2000). Roscovitine is a specific inhibitor of Cdks 1, 2, and 5 and there is some evidence that roscovitine can also inhibit the transcription regulating Cdks7-9 (Hajduch et al., 1999; Wang et al., 2001). Research from our lab has identified Cdk8 as the likely candidate for the roscovitine-sensitive proapoptotic kinase activity, tentatively excluding other Cdks such as 1,2,7 or 9 (Skirrow and Helbing, 2007; Skirrow et al., 2008). Additionally, roscovitine has the potential to inhibit the activation of the MAPKs, ERK1 and ERK2, at the concentration used in these studies (Shchemelinin et al., 2006), although the activities of these have been shown not to be candidates for the proapoptotic signal in tail regression (Skirrow and Helbing, 2007). The large number of protein changes observed in the current study suggests that RNA Pol II might not be the only biological target for Cdk8 action in the context of tail regression. It is possible that other transcription factors may be targets of Cdk8 activity and that other Cdks and kinases might also be affected by roscovitine. This could include phosphorylation of TRs themselves since phosphorylation can lead to protein stabilization and signal potentiation as we have observed in tail tissues (Ji et al., 2007) and others have observed in mammalian cells (Davis et al., 2000). The focus of future research should be on the identification of the potential phosphoproteins observed to be altered by roscovitine in this study. The findings may reveal a link between cell cycle regulators and TH-induced cell death.

## 2.4 CONCLUSIONS

I was able to identify several $T_3$-responsive proteins in the *X. laevis* tadpole tail altered in the early stages of precocious metamorphosis. These included a number of structural proteins, metabolic enzymes, transcription factors and proteins non-native to the tail tissue such as serum proteins. The relationship of these proteins to the transcriptome was also compared, revealing that the two were not always in agreement. Taken together these results underline the importance of examining the proteome in addition to the transcriptome in the study of anuran metamorphosis.

Proteome function was also shown to include changes in the phosphoproteome. Immunoblot analysis of the tadpole brain showed that specific changes in protein phosphorylation occur early and differentially between the cell nucleus and cytoplasm as a result of $T_3$ treatment. This was the first report of phosphorylation changes occurring in the tadpole brain after TH-induction.

The inability to identify any of the phosphoproteins led to the investigation of novel mass spectrometry methods. The PhIAT method, although showing initial promise for the investigation of the phosphoproteome, was unable to provide amino acid sequence information essential for the identification of the measured phosphoprotein, and was abandoned for other phosphoproteome analysis methods. The subsequent experiment on the effects of roscovitine on $T_3$-induced tadpole tail regression employed a phosphoprotein-specific purification column. The study revealed many potential changes within the phosphoproteome that occur as a result of $T_3$ treatment and revealed that these are all targets for the Cdk inhibitor roscovitine which affects the establishment of the genetic program. None of the phosphoproteins could be identified, however, and these warrant future research.

# Chapter 3: Analysis of the *Rana catesbeiana* tadpole tail fin proteome and phosphoproteome during $T_3$-induced metamorphosis: Identification of a novel type I keratin

Published in: Domanski D and Helbing CC. Analysis of the *Rana catesbeiana* tadpole tail fin proteome and phosphoproteome during $T_3$-induced apoptosis: identification of a novel type I keratin. BMC Developmental Biology. 2007 Aug 6;7:94.

## 3.1 INTRODUCTION

In the previous chapter we identified a number of proteins whose expression was altered in the *X. laevis* tadpole tail during TH-induced metamorphosis (Chapter 2; Helbing et al., 2003). The method used a single 2D gel to reveal the tail proteome and thus the majority of these proteins were high abundance proteins. Additional work with phosphoprotein-specific immunoblot detection revealed that fractionation of the cell compartments and separate subsequent analysis can provide an additional level of information in regards to protein localization. The goal of the current study was to observe changes in protein expression and phosphorylation of lower abundance proteins such as signaling proteins, and to determine their cellular localization. To this end, we optimized a subcellular fractionation method for the separation of tadpole tail fin cells, developed a liquid-chromatography protein fractionation method, and analyzed the resulting fractions using multiple 2D gels. This approach increased the chances of observing lower abundance proteins while providing information on protein cellular localization, which might additionally reveal protein translocation events in the absence of expressional change. The previous chapter also revealed the challenges of phosphoprotein identification using immunoblots. In the current study, alterations in phosphorylation were revealed using a phosphoprotein-specific stain. Total proteins and phosphoproteins were detected in the same 2D gel, simplifying the connection between an observation of a change in phosphorylation and subsequent protein spot picking and MS analysis. For this study we focused on the analysis of the tail fin proteome of *R. catesbeiana*, a much larger tadpole than that of *X. laevis*, which provided the large amounts of protein required for such extensive fractionation. This species lacks the extensive genome coverage that is available for *X. laevis* and therefore protein identification

relied on *de novo* sequencing of peptides with tandem-MS analysis. Proteome coverage was further enhanced through the use of the novel MS technique, isobaric tags for relative and absolute quantitation (iTRAQ).

The present study identifies proteins whose levels and/or phosphorylation states are altered within 48 h of the induction of tadpole tail regression prior to overt remodeling of the tail. In particular, we have identified a novel keratin that is a target for $T_3$-mediated changes in the tail that can serve as an indicator of early response to this hormone. iTRAQ revealed 15 additional proteins whose levels were altered upon $T_3$ treatment. These proteins are involved in apoptosis, extracellular matrix structure, immune system, metabolism, mechanical function, and oxygen transport. Through this we have demonstrated the ability to derive proteomics-based information from a model species for postembryonic development for which no genome information is currently available.

## 3.2 MATERIALS AND METHODS

### *3.2.1 Experimental animals*

The care and treatment of animals used in this study were in accordance with the guidelines of the Animal Care Committee, University of Victoria, under the Canadian Council of Animal Care. *Rana catesbeiana* tadpoles were locally caught (Victoria, BC) or purchased (Ward's Natural Science Ltd., St, Catharines, ON). Animals were housed in the University of Victoria aquatics facility and maintained in 360 L all-glass flow-through aquaria containing recirculated water at 15°C with exposure to natural daylight. Tadpoles were fed daily with spirulina (Aquatic ELO-Systems, Inc., FL). *R. catesbeiana* tadpoles, TK stage VI-VIII (Taylor and Kollros, 1946), were exposed to 10 nM $T_3$ (80 µl of $10^{-3}$ M $T_3$ in 2.5 mM NaOH) (Sigma-Aldrich, St. Louis MO USA) or vehicle control (80 µl 2.5 mM NaOH) in the rearing water (8 L per 6 tadpoles) for 24 or 48 h. Tadpoles were acclimatized for 24 h prior to exposures at 24°C, and were not fed during this period or during exposures. For the 2D gel analysis, each treatment or control group consisted of 18 pooled tadpoles. The 48 hour 2D analyses consisted of three, completely independent, control and $T_3$ treatment groups, while the 24 hour analyses were from a single control and $T_3$ treatment group. The 24 hour analyses were only done to further characterize absence or presence of proteins observed to be altered at the 48 hour time point. For the iTRAQ analysis, two independent $T_3$-treatment groups and two independent control groups consisting of six pooled tadpoles per group were used. Tadpoles were euthanized in 0.1% tricaine methanesulfonate

(Syndel Laboratories, Vancouver, BC, Canada) in 25 mM sodium bicarbonate, dorsal and ventral tail fins were removed on ice, and proteins extracted as described below. For QPCR analysis, premetamorphic tadpoles (stage VI-VIII) were exposed to 100 nM $T_3$ or vehicle control in the rearing water for 24, 48 and 72 h and euthanized as above. Tadpoles at the indicated stages were also collected to determine gene expression in tail tissue during natural metamorphosis.

### *3.2.2 Subcellular fractionation*

Two separate procedures were used for the isolation of nuclei and for the cytosolic-mitochondrial-microsomal fractions. All extraction procedures were performed on ice or at 4°C. Tail fin tissue was rinsed with extraction buffer lacking detergents or inhibitors (see below for composition). Three ml of buffer were used per gram of tissue, which was homogenized in a teflon-glass Dounce homogenizer (Wheaton, USA). For the nuclear isolation tissue was homogenized in 20 mM N-[2-Hydroxyethyl]piperazine-N'-[2-ethanosulfonic acid] (HEPES) pH 7.5, 0.25 M sucrose (ACP Chemicals Inc., Montreal Canada), 25 mM KCl, 5 mM $MgCl_2$ (both from BDH chemicals, Toronto Canada), 0.5% Triton X-100, 1mM dithiothreitol (DTT), 2 mM vanadyl ribonucleoside complexes (VRCs), 100 μM phenylmethylsulfonyl fluoride (PMSF), 4 μg/ml aprotinin, 1 μg/ml leupeptin, 2 μg/ml antipain, 300 μg/ml benzamidine, 10 mM β-glycerophosphate, 0.2 mM $Na_3VO_4$, and 1 mM NaF (all remaining from Sigma-Aldrich).

Homogenization efficiency and integrity of nuclei was checked with microscopy and 4'-6-Diamidino-2-phenylindole (DAPI) staining for nuclei. The homogenate was incubated on ice with shaking for 30 min then passed through 100 μm nylon mesh cell-strainer. The homogenate was centrifuged at 1000 x g for 10 min. The nuclei were resuspended in the above extraction buffer (3 ml per g of initial tissue), layered onto a 0.88 M sucrose cushion, which contained everything the extraction buffer did except for Triton X-100 and VRCs, and centrifuged at 2000 x g for 30 min. The resulting nuclear pellet was washed in extraction buffer, without Triton X-100 and RVCs, and centrifuged at 2000 x g for 10 min. The nuclear pellet was stored at -70°C.

To obtain the cytosolic, mitochondrial and microsomal fractions, tail fin tissue was homogenized in 20 mM HEPES pH 7.5, 0.25 M sucrose, 5 mM Ethylenedinitrilo-tetraacetic acid (EDTA) (EM Science, Gibbstown NJ USA), 1mM DTT, 100 μM PMSF, 4 μg/ml aprotinin, 1 μg/ml leupeptin, 2 μg/ml antipain, 300 μg/ml benzamidine, 10 mM β-glycerophosphate, 0.2 mM $Na_3VO_4$, 1 mM NaF. The homogenate was centrifuged at 800 x g for 10 min. The supernatant was then centrifuged at 12,200 x g for 15 min. The pellet was washed twice in extraction buffer and

centrifuged at 12,200 x g for 15 min. This mitochondrial pellet was stored at -70°C. The supernatant was centrifuged at 100,000 x g for 1 hour to obtain the microsomal pellet and cytosolic fractions which were then stored at -70°C.

### *3.2.3 Anion-exchange HPLC fractionation of cytosolic fraction*

The cytosolic fraction was first desalted using size-exclusion chromatography with Sephadex G-25-M beads (Sigma-Aldrich). Sample was kept at 4-8°C throughout the procedure. Six ml of sample was loaded onto a 27 ml column with 60 mM ammonium bicarbonate (EM Science) as buffer. The eluted protein fractions in the first 7.5 ml were kept, frozen at -70°C, and lyophilized for 48 h. The sample was reconstituted in 40 mM ammonium bicarbonate to a concentration of 10 mg/ml. Fractionation of the desalted cytosolic sample was performed using a Waters HPLC setup with a Waters 600S controller, 626 pump and 486 tunable absorbance detector (Waters, Milford MA USA). The column used consisted of 2 ml Accell Plus QMA 300Å anion-exchange media packed into a AP Minicolumn assembly (5 x 100 mm) (Waters). Five mg of total cytosolic sample was loaded onto the column in 40 mM ammonium bicarbonate (pH 8.3), the unbound proteins were captured as the 40 mM fraction. The remaining sample was fractionated using a step-gradient of 190, 260, 340 mM and 1 M ammonium bicarbonate. The flow rate was set at 1ml/minute and each step was 13 min. The detector was set at 280 nm. The fractions were collected on ice, frozen at -70°C, and lyophilized for 48 h.

### *3.2.4 2D polyacrylamide gel electrophoresis*

Proteins from the nuclear pellet were initially extracted in an isoelectric focusing (IEF) buffer lacking ampholytes consisting of 9.5 M urea (SigmaUltra), 4% 3-[(3-cholamidopropyl)dimethylammonio]-1-propanesulfonate (CHAPS), 1% DTT, 40 mM tris(hydroxymethyl)aminomethane (Tris-base) pH 8.5, 5 mM EDTA, 100 μM PMSF, 4 μg/ml aprotinin, 1 μg/ml leupeptin, 2 μg/ml antipain, 300 μg/ml benzamidine, 10 mM β-glycerophosphate, 0.2 mM $Na_3VO_4$, 1 mM NaF (all from Sigma-Aldrich) for 15 min at room temperature. DNA was then precipitated by adding 2% ampholytes (Pharmalyte 3–10 and 5-8 in a 2/3 and 1/3 ratio, respectively; Amersham Pharmacia Biotech AB, Uppsala Sweden), incubating for 15 min at room temperature, and pelleting the DNA at 12,000 x g for 10 min. Ampholytes were then replaced in the supernatent to 2% as indicated above. The mitochondrial and microsomal pellets and the lyophilized HPLC cytosolic fractions were all dissolved in the IEF buffer with the inclusion of 2% ampholytes as described above. Protein concentrations were

assayed using the Bio-Rad Protein Assay (Hercules, CA USA) with protein standards dissolved in the IEF buffer. The amount of pellet to IEF buffer used yielded a protein extract with a protein concentration of 2-6 mg/ml.

Three hundred μg of protein for each fraction (except for the 40 mM cytosolic fraction where 100 μg of protein was used) were aliquoted, made up to 100 μl with IEF buffer, solubilized for seven hours at room temperature, centrifuged at 12,000 x g for 10 min, and loaded onto IEF tube gels used for the first dimension. The IEF tube gels (2.5 mm x 13 cm) consisted of 9.5 M urea, 3.897% acrylamide and 0.104% piperazine diacrylamide (wt/vol) (Bio-Rad), 2% CHAPS, 3.875% Pharmalyte 3–10 ampholytes, 2.375% Pharmalyte 5–8 ampholytes, and 0.05% ammonium persulphate (APS) (ACP Chemicals Inc.) and 0.07% *N*,*N*,*N*',*N*'-tetramethylethylenediamine (TEMED; Sigma-Aldrich) for polymerization.

The IEF gels were prefocused and run as described in (See chapter 2; Helbing et al., 2003) with the following modifications. Samples were electrophoresed for 16 h at 450 V, then hyperfocused at 800 V for 2 h (8800 Vh total). The IEF gels were then equilibrated using the same equilibration buffer as in (chapter 2; Helbing et al., 2003) except the buffer contained 65 mM DTT for 15 min, and then for 15 min in 5 ml of IEF-equilibration buffer with 136 mM iodoacetamide (Sigma-Aldrich).

The IEF gels were then transferred onto the second dimension SDS-polyacrylamide gels (15 cm x 14 cm x 1.5 mm) comprised of an 11% separating gel (37.5:1 acrylamide to bis-acrylamide (Bio-Rad), 375 mM Tris-base pH 8.8, 0.1% SDS, 0.05% APS, 0.05% TEMED) and a 4% stacking gel (125 mM Tris-base pH 6.8, 0.1% SDS, 0.05% APS, 0.1% TEMED). The IEF gels were overlayed with 0.5% agarose (EM Science) in 125 mM Tris-HCl pH 6.8 with 0.05% bromophenol blue/2% SDS. Precision Plus Dual Color (Bio-Rad) molecular weight markers were used. The gels were electrophoresed at 30 mA per gel at constant current in SDS running buffer (25 mM Tris-base, 192 mM glycine (EM Science), 0.1% SDS) until the bromophenol blue ran out of the bottom of the gel,.

The 2D gels were then stained with a fluorescent phosphoprotein stain, ProQ Diamond, according to the manufacturer's instructions (Invitrogen-Molecular Probes, Burlington, Ontario, Canada). Fluorescence was detected with UV light using a ChemiImager 4000 imaging system (Alpha Innotech Corporation, San Leandro CA USA). The gels were then stained for total protein by washing in 50% ethanol (EM Science) and 3% phosphoric acid with shaking overnight, rinsing

three times for 30 min in water, equilibrating in 16% ammonium sulfate (EM Science), 25% methanol (EM Science), 5% phosphoric acid for 1 hour, and subsequently staining by adding Coomassie brilliant blue G250 (Sigma-Aldrich) to 0.01% and shaking for 4 days. Images were obtained by scanning the gels with a Li-Cor Odyssey scanner (Li-Cor, Lincoln NE USA) at 700 nm. Protein spot density was analyzed using Li-Cor Odyssey Ver. 2.0.5 software (Li-Cor). Gel images were analyzed using Adobe PhotoShop Ver. 5.0 (Adobe Systems Inc., San Jose CA USA).

### *3.2.5 Mass spectrometry analysis*

Protein spots of interest were excised from the 2D gels and the proteins within were reduced, alkylated, and digested with trypsin according to an in-gel digestion protocol (Kinter and Sherman 2000) with a few modifications. The gel pieces were destained in 50% methanol/5% acetic acid (ACP Chemicals Inc.), dehydrated with acetonitrile (EM Science), dried, reduced with 50 mM DTT in 100 mM ammonium bicarbonate at 56°C for 30 min, alkylated with 100 mM iodoacetamide in 100 mM ammonium bicarbonate at 45°C for 30 min, dehydrated with acetonitrile, hydrated with 100 mM ammonium bicarbonate, dehydrated with acetonitrile, dried, and digested with 20 ng/μl of sequencing grade modified trypsin (Promega Corp., Madison WI USA) in 50 mM ammonium bicarbonate at 37°C overnight. The resulting peptides were extracted out of the gel pieces by successive incubation in 50 mM ammonium bicarbonate for 1 hour at 37°C and twice in 0.1% formic acid (ACP Chemicals Inc.) for 30 min at 37°C. The peptides were desalted using ZipTip pipette tips containing C18 reversed-phase media (Millipore Corp., Bedford, MA USA) by washing with 0.1% formic acid and eluting with 75% acetonitrile/0.1% formic acid. Peptides were either analyzed by MALDI-TOF MS as follows or by ESI-QqTOF or MALDI-TOF-TOF MS analysis as described in the iTRAQ section. Peptide samples were applied to the target plate with an equal volume of matrix solution (1% α-cyano-4-hydroxycynnamic acid (Sigma-Aldrich) in 50% acetonitrile/0.3% formic acid) and allowed to dry. Adrenocorticotropic hormone fragment 1–17 (FW 2093.4), bradykinin fragment 2–9 (FW 904.0) and angiotensin 1 (FW 1296.5) (Sigma-Aldrich) were used as external calibrants.

Spectra were obtained using a Voyager-DE STR Biospectrometry Workstation MALDI-TOF mass spectrometer (PE Applied Biosystems, Foster City, CA USA) operating in positive reflector mode with delayed extraction. Data were manipulated using the Voyager Version 5.1 software with Data Explorer (PE Applied Biosystems). The sample spectra were further internally calibrated using autolytic trypsin peptide peaks. The masses of the tryptic peptides were used to

search a local protein database using MASCOT Peptide Mass Fingerprint software (Matrix Science Inc., Boston MA USA) using the following settings: all entries, 1 missed cleavage, cysteines modified by carbamidomethylation, oxidized methionines, deamidation of asparagine and glutamine, peptide mass tolerance of ±50 ppm. If the tryptic peptides were analyzed by ESI-QqTOF generating MS/MS spectra, manual *de novo* sequencing was performed viewing the spectra on AnalystQS Ver. 1.1 software (Applied Biosystems, Foster City, CA USA) or automatically using PEAKS Studio Ver.3.0 software (Bioinformatics Solutions Inc., Waterloo ON Canada) as explained in the data analyses section for iTRAQ. The group of peptide spectra that were obtained from the RLK I spot were analyzed using SPIDER software (Han et al., 2005).

### *3.2.6 Immunoblotting*

Protein samples from the total extract and subcellular fractions were analyzed for lamin B1+B2 and for cytochrome c. Protein samples of the 48 hour control and treatment microsomal fraction were analyzed for cytokeratin in duplicate. Thirty μg of protein per sample were boiled for 3 min in 25 μl of 60 mM Tris-base pH 6.8, 2% SDS, 10% glycerol, 100 mM DTT, 0.03% bromophenol blue and loaded onto a 12% SDS-PAGE gel (see '2D gel electrophoresis' above for gel and buffer compositions). Proteins were then electrophoretically transferred onto a nitrocellulose membrane (Bio-Rad). Membranes were blocked with 5% nonfat milk in 140 mM NaCl/20 mM Tris-base pH 7.6 (TBS), for 1 hour, then probed with a pan-cytokeratin rabbit polyclonal IgG antibody (H-240; Santa Cruz Biotechnology Inc., Santa Cruz CA USA) diluted at 1/500 or an anti-lamin B1+B2 mouse monoclonal IgG1 antibody (ab4825; Cedarlane, Hornby ON Canada) diluted at 1/50 or anti-cytochrome c rabbit polyclonal antibody (H-104; Santa Cruz Biotechnology Inc.) diluted at 1/200 in 5% nonfat milk/TBS and 0.1% Tween (TBST) with gentle agitation for 1 hour at room temperature. The blots were washed with TBST for 1 hour. The membranes were then incubated with secondary antibody, IRDye-800 conjugated anti-rabbit IgG or IRDye-800 conjugated anti-mouse IgG (Rockland Inc., Gilbertsville PA USA) diluted at 1/2000 in 5% nonfat milk/TBST for 1 hour at room temperature. The blots were washed with TBST for 1 hour. The prepared blots were scanned by a Li-Cor Odyssey scanner at 800 nm.

### *3.2.7 Isolation of RNA, generation of cDNA, degenerate-primer PCR and 5'-/3'-RACE*

RNA was isolated and cDNA generated from premetamorphic tadpole tail fin tissue as described in Veldhoen et al (2006). The resulting cDNA was used for PCR using degenerate primers: forward: 5'-GAA/G GCA/C GCC AAT/C ACT/C GAA/G CT-3' and reverse: 5'-AC C/TTG

T/AAG C/TTC CTC T/CTC G/ATG-3' (32 fold degeneracy each) with an initial 94°C for 10 min then 40 cycles at 94°C for 30 sec, 52°C for 30 sec, and 72°C for 30 sec, followed by 10 min at 72 °C. This generated a single product at 380 bp. The PCR product was cloned using the TOPO TA Cloning Kit System with pCR2.1 TOPO vector and TOP10 cells (Invitrogen) as described previously (Wagner and Helbing, 2005). The insert was then sequenced in both directions using the TOPO kit M13 forward and reverse primers at the University of Victoria sequencing facility. Based on this sequence two gene specific primers (GSP) were designed: GSP1 for 5'-RACE: 5'-TGTCTCCACCGCTAACACCAACGCCAAC-3' and GSP2 for 3'-RACE: 5'-GTTGGCGTTGGTGTTAGCGGTGGAGACA-3'. RACE-ready cDNA libraries were made from total RNA using the Smart RACE cDNA kit (BD Biosciences, Burlington ON Canada). The RACE reactions used the universal primers supplied with the kit paired with the GSP1 and GSP2. Touchdown PCR was performed on the RACE-ready libraries: 94 °C for 2 min; five cycles at 94°C for 30 sec, and 72°C for 3 min; five cycles at 94°C for 30 sec, 70°C for 30 sec, and 72°C for 3 min; and 25 cycles at 94°C for 30 sec, 68°C for 30 sec, and 72°C for 3 min. The 5'-RACE produced a single product of ~600 bp and the 3' RACE produced three products between ~1400 and ~1500 bp. The PCR products were cloned as above and the longest clones from each RACE reaction were sequenced as above, giving two overlapping sequences that encoded the complete open reading frame. The sequence reported in this manuscript is accessible in GenBank [GenBank: EF156435].

### *3.2.8 Quantitation of gene expression*

The expression of RLK I gene transcript was quantified in tails of individual animals ($n \geq 4$ for all treatments and/or time points). Tail tissue treatment, RNA isolation and cDNA generation was performed as indicated above and expression data were collected using a real-time quantitative PCR assay on a MX4000 system (Stratagene, La Jolla, CA, USA) as described previously (Veldhoen et al., 2006) using the following primers for RLK I: 5'-GTTGGCGTTGGTGTTAGCGG-3' and 5'-GGCACTGCTTCTTGCAACTTG-3'. The QPCR product from the keratin transcript was analyzed on a gel and sequenced ensuring that only this specific keratin transcript was being analyzed. The invariant L8 ribosomal protein transcript was used as a normalizer (Veldhoen et al., 2006).

### *3.2.9 Differential expression analysis using iTRAQ*

***Peptide preparation, iTRAQ labeling, two-dimensional liquid chromatography separation and MS analysis***

Proteins from tadpole tail fin tissue were extracted by homogenization in 6 M urea, 0.2% SDS, 20 mM HEPES pH 7.5 (3 ml/g tissue). The homogenate was centrifuged at 12,000 x g for 15 min at 4°C. The supernatant was adjusted to 4 M urea, 0.05% SDS, 2 mM $MgCl_2$ and 20 mM HEPES pH 8.0, and DNA was digested with 10U/ml of benzonase for 30 min at 8°C. The iTRAQ reagents were used according to the manufacturer's protocol with minor modifications as follows (Applied Biosystems).

Two independent control and two independent treatment protein samples were quantified using the bicinchoninic acid assay (BCA) (Sigma-Aldrich, St Louis, MO USA). One hundred μg of each sample (~55 μl) was precipitated in 1 ml cold acetone, overnight at –20°C. Proteins were then reduced in 3.3 mM tris-(2-carboxyethyl) phosphine, alkylated with 6.7 mM methyl methane thiosulfonate (MMTS) and digested overnight with 10 μg of sequencing grade modified trypsin (Promega, Madison, WI USA) at 37°C. The resulting peptides from the two control samples were labeled with iTRAQ reagents 114 and 116, while peptides from the two $T_3$ treatment samples were labeled with iTRAQ reagents 115 and 117.

The labeled peptide samples were then pooled, adjusted to pH 2.5-3.0 with concentrated phosphoric acid (ACP Chemicals Inc., Montreal, QC Canada), and separated by strong cation-exchange chromatography (SCX) using a PolySULFOETHYL A SCX column (100x4.6 mm, 5μm, 300 Å - PolyLC Inc., Columbia, MD USA) on the VISION Workstation (Applied Biosystems, Foster City, CA USA). Mobile phases used were: Buffer A: 10 mM monobasic potassium phosphate (Sigma-Aldrich, St Louis, MO, USA), 25% acetonitrile (ACN) (EMD Chemicals, Gibbstown, NJ, USA), pH 2.7 and Buffer B: same as A with the addition of 0.5 M potassium chloride (Sigma-Aldrich St Louis, MO, USA). Fractions of 500 μL were collected over an 80 minute gradient: 0-30 min, 5% to 35% Buffer B; 30-80 min, 35% to 100% Buffer B. Sixteen SCX fractions were reduced to 150 μL using a SpeedVac and subjected to reverse-phase chromatography using an integrated system consisting of a Famos autosampler, Switchos switching pump, UltiMate micro pump and a Probot microfraction collector (LC Packings, Amsterdam, Netherlands). The SCX fractions were first desalted on a C18 PepMap guard column (300 μm i.d. x 5 mm 5 μm, 100 Å, LC Packings, Amsterdam) at 50 μl/minute flow rate for 15 min. Peptides were separated over a manually packed 75 μm x 15cm C18 column (Magic C18Aq,

5µm, 100 Å, Michrom Bioresources Inc., Auburn CA, USA) using a 85 min gradient of 5%-75% ACN in 0.1% formic acid flowing at 250 nL/min.

The eluant was either sprayed directly into an Applied Biosystems QSTAR Pulsar i (Applied Biosystems/MDS SCIEX Concord, ON Canada) (ESI-QqTOF) mass spectrometer or spotted onto a MALDI target plate by the Probot for LC-MALDI analysis. The QSTAR operating software Analyst QS v1.1 employed an information dependent acquisition (IDA) method for optimized MSMS spectra acquisition over a 6 sec cycle which was repeated over the duration of the gradient. The MS-TOF survey scan lasted for 1 sec over a range of 400-1200 m/z targeting precursor ions of charge state 2-5+ that exceeded a threshold of 20 counts. Former target ions within 100 ppm were excluded for the next 180 sec. The two most intense ions that met the IDA criteria were gated and fragmented with optimized collision energy. Each product ion scan lasted for 2.5 sec over a range of 100-1500 m/z. 'Enhance-all' was turned on for the product ion scans. LC-MALDI data was acquired on an Applied Biosystems 4800 MALDI TOF/TOF Analyzer (Applied Biosystems/MDS Sciex Foster City, CA USA). Sample spots were overlaid with 3mg/mL α-cyano-4-hydroxycinnamic acid (CHCA) (Sigma-Aldrich, St Louis, MO USA) matrix in 50% ACN and 0.1% TFA. MS data was automatically acquired over a mass range of 800-4000 Da using fixed laser intensity for 500 shots with a uniformly random spot search pattern. In each spot, the 30 strongest peaks by MS (determined by cluster area) were selected for MS/MS using a job-wide interpretation method which excludes ions with a signal-to-noise of less than 60 and filters identical peaks detected in multiple spots. A 1 KV positive MS/MS operating mode was used with the relative precursor mass window set at 150 and collision induced dissociation turned on. MALDI-TOF-TOF data analysis was performed using GPS Explorer Ver. 3.0 (Applied Biosystems) software using the MASCOT (Matrix Science) search engine for protein database searching.

***iTRAQ data analysis***

All of the MS data in ProQUANT (Applied Biosystems) resulting from the ESI-QqTOF analysis was transferred to Excel (Microsoft Corporation, Redmond WA) where the data was filtered to reveal only those MS spectra where a change of 1.5 fold or higher was observed between the treatment and the control for both duplicates. An additional requirement was that the ratio of the iTRAQ tags between the two controls had to be between 0.67 and 1.5. The resulting MS spectra were then manually inspected in AnalystQS 1.1 (Applied Biosystems) software to ensure good quality of the iTRAQ tags and fragmentation information.

High quality spectra where then used for *de novo* peptide sequencing. Peptide sequence was obtained by either manually interpreting spectra and/or through the use of PEAKS Studio Ver.3.0 (Bioinformatics Solutions Inc.) software capable of auto *de novo* sequencing. The parameters were set as follows: parent mass error tolerance of 0.1 Da, fragment mass error tolerance of 0.1 Da, enzyme used was trypsin, fixed posttranslational modifications (PTMs) were MMTS on cysteines, iTRAQ tags on N-terminal and lysine, and variable PTMs were iTRAQ tag on tyrosine and oxidation of methionine histidine and tryptophan. All of the results were manually inspected to ensure correctness. The resulting peptide sequences were then queried against the Entrez Protein (NCBInr) database (Oct. 15, 2006) using BLASTp (Altschul et al., 1997) to allow for short, nearly exact matches: no compositional adjustments, a low complexity filter, expect threshold of 20000, word size of 2, using matrix PAM 30, with gap costs of 9 for existence, and 1 for extension, searching all metazoan sequences.

### *3.2.10 Statistical analyses*

Statistical analyses were performed using SPSS Ver. 12.0. (Chicago IL USA). For the 48 hour 2D gel analysis data P-values were determined using a one-way ANOVA with a test for homogeneity of variance and a Shapiro-Wilk test of normality. For the QPCR analyses P-values were determined using the Mann–Whitney U non-parametric two-tailed test.

## 3.3 RESULTS AND DISCUSSION

### *3.3.1 Fractionation of the tail fin proteome and 2D gel analyses*

The subcellular fractionation method was optimized to provide highly enriched fractions of cytosolic, mitochondrial, nuclear and microsomal samples from the *R. catesbeiana* tail fin. The goals of the method were to limit sample complexity with effective cell fractionation with minimal cross-contamination and reasonable yields. The fractions also had to be salt and buffer-compatible with subsequent proteomic analysis.

We developed two separate procedures based on differential centrifugation to generate nuclear and cytosolic/mitochondrial/microsomal fractions (Figure 3.1A). The nuclear extraction procedure was developed to minimize nuclear clumping and increase nuclei stability through the inclusion of KCl and $MgCl_2$ ions and vanadyl ribonucleoside complexes (VRCs). VRCs have also been shown to minimize cytoskeletal contamination (Gerner et al., 1998). In addition, cytoplasmic/organelle contamination was minimized with Triton X-100, a non-ionic detergent,

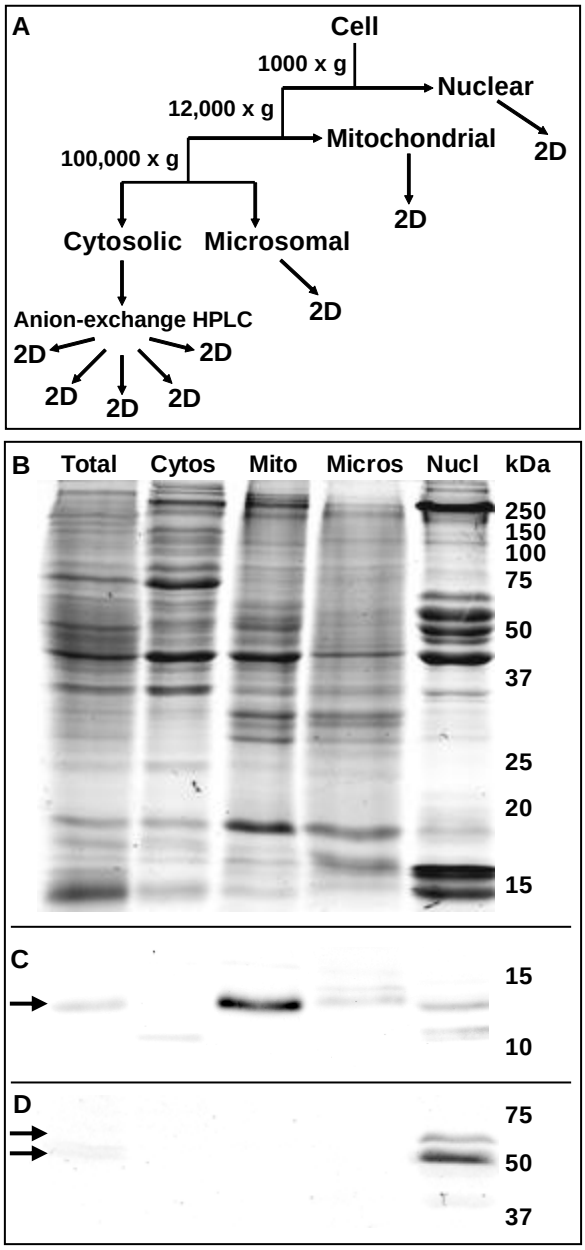


**Figure 3.1. Subcellular fractionation of the tail fin proteome.** (A) Fractionation of tail fin cells into subcellular compartments and subsequent treatments of those fractions. Two different extraction procedures, based on differential centrifugation, were developed to generate the nuclear and the cytoplasmic/ mitochondrial/microsomal fractions. (B) SDS-PAGE shows the successful fractionation of the total tail fin proteome into the cytosolic (Cytos), mitochondrial (Mito), microsomal (Micros), and nuclear (Nucl) fractions. Colloidal Coomassie brilliant blue G250 was used to stain the proteins. Relative molecular weights of protein standards are indicated in kDa. (C) Immunoblot of the gel in (B) for the mitochondrial marker, cytochrome c (arrow) showing the enrichment of mitochondria in the expected fraction. (D) Immunoblot of the gel in (B) for the nuclear markers, lamin B1 and B2 (double arrow) showing the enrichment of nuclei in the expected fraction.

that dissolves membranous organelles and not nuclear membranes, and a subsequent sucrose cushion purification. DNA was finally precipitated with polyamines leaving the nuclear proteins in a final 2D-denaturing buffer.

The cytosolic/mitochondrial/microsomal extraction procedure was developed to increase the disruption of tail fin cell membrane and increase mitochondrial stability and purity. The inclusion of EDTA (to remove divalent and monovalent cations) improved the disruption of the plasma membrane, prevented clumping of organelles and mitochondrial swelling, and inhibited metalloproteases. Additional protease and phosphatase inhibitors were included throughout the procedures. The mitochondria-enriched fraction was obtained with a 12,000 x g centrifugation and it likely also contained lysosomes, peroxisomes, Golgi and endoplasmic reticulum (ER). Centrifugation at 100,000 x g removed the vesicles of the plasma membrane, endosomes, Golgi and ER into the microsomal pellet leaving the cytosolic supernatant with its soluble molecules (cytosolic fraction; Figure 3.1B). Nuclear integrity was monitored by microscopy (data not shown) and fractionation efficiency was determined using immunoblot analysis for subcellular markers. An immunoblot for cytochrome c (a mitochondrial marker) shows substantial enrichment for that organelle in the mitochondrial fraction (Figure 3.1C) while an immunoblot for the nuclear markers, lamins B1 and B2, shows enrichment of nuclei in the nuclear fraction (Figure 3.1D).

The cytosolic fraction is a complex mixture of many proteins and was therefore further fractionated using anion-exchange high performance liquid chromatography (HPLC) (Figure 3.2A). A step-gradient anion-exchange HPLC procedure was developed that used ammonium bicarbonate as a volatile buffer in place of commonly used salt and non-volatile buffer to provide salt-free fractions after lyophilization to render the samples compatible with the subsequent 2D gel analysis. The cytosolic fraction was thus further fractionated into five fractions: 40 mM (unbound proteins), 190 mM, 260 mM, 340 mM and 1 M ammonium bicarbonate with each fraction (except 40 mM) yielding roughly equal amounts of protein as shown by SDS-PAGE (Figure 3.2B). Proteins within each of the resulting fractions were then separated by 2D polyacrylamide gel electrophoresis which separates proteins based on their molecular weight and isoelectric point (pI). Therefore, the entire fractionation protocol divided the tail fin proteome over eight 2D gels: nuclear, mitochondrial, microsomal (Figure 3.3) and five cytosolic fractions (Figure 3.4). This fractionation method increases the ability to observe expression changes in low abundance proteins and provides information on subcellular localization of proteins which cannot be achieved by examining a whole cell homogenate on a single 2D gel. From our results, it is

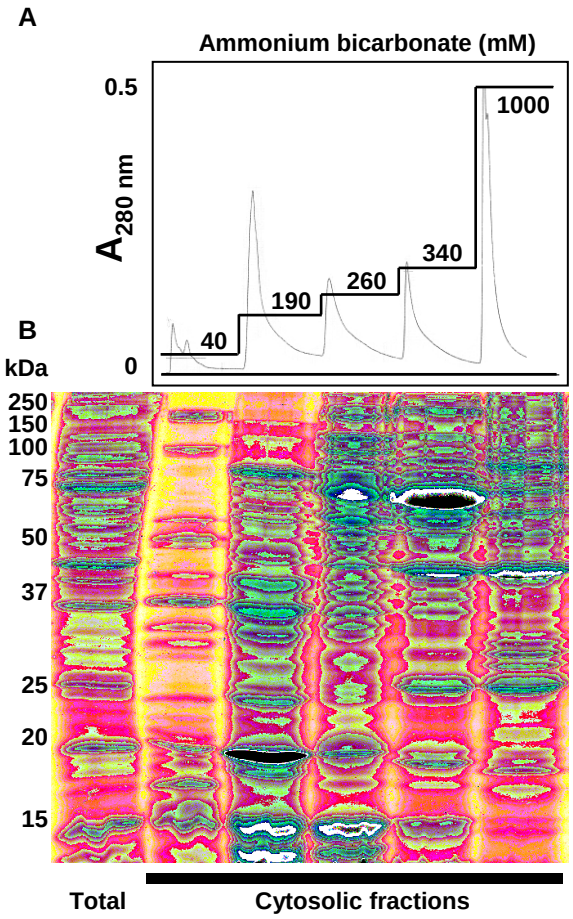


**Figure 3.2. Anion-exchange HPLC fractionation of the cytosolic fraction**. (A) The cytosolic fraction was further fractionated using an anion-exchange column (Accell QMA) with a step-gradient of increasing concentrations of ammonium bicarbonate (straight lines). The concentrations are indicated on each step while absorbance was measured at 280 nm indicating the protein yield of each fraction. (B) The Coomassie blue-stained SDS-PAGE gel shows the fractionation of the cytosolic sample (total) with the lanes corresponding to the cytosolic fractions below the peaks of the HPLC chromatogram. Note the resulting enrichment of certain protein bands. Relative molecular weights of protein standards are indicated in kDa.

evident that each of the fractions shows a distinctive pattern of spots with many unique spots per fraction analyzed (Figures 3.3 and 3.4). There is some overlap with the more abundant protein spots between the neighboring fractions of the HPLC separation and between the microsomal and mitochondrial fractions, which probably share many cellular membrane compartments (e.g. Golgi, ER, and lysosomes). Phosphoproteins were detected on the 2D gels with a phosphoprotein-specific fluorescent stain (Pro-Q Diamond) which detects phosphorylation on Ser, Thr and Tyr residues (Steinberg et al., 2003) (Figures 3.3 and 3.4). Total proteins and phosphoproteins were

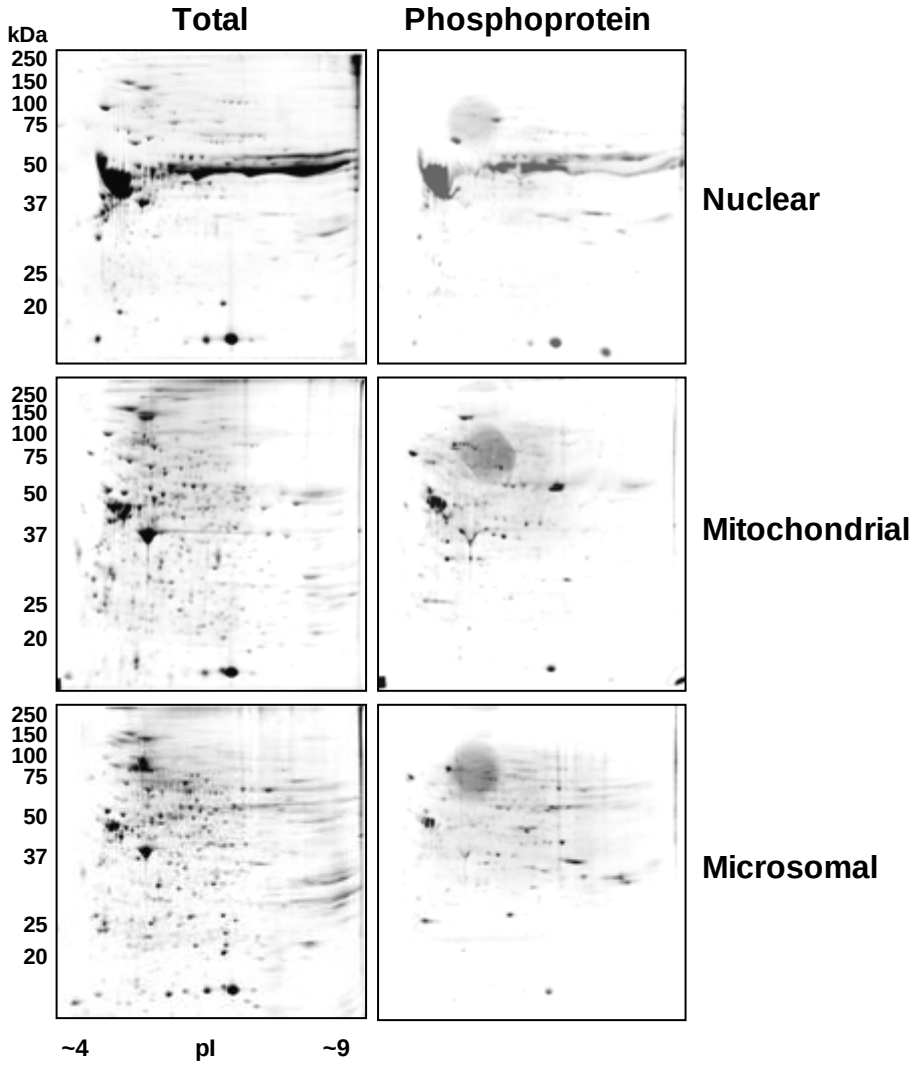


**Figure 3.3. 2D gel analyses of the nuclear, mitochondrial and microsomal fractions.** Proteins from the nuclear, mitochondrial and microsomal fractions were separated by 2D-PAGE according to molecular weight and pI point. Total proteins were detected by colloidal Coomassie stain while phosphoproteins were detected in the same gel using the ProQ Diamond phosphoprotein-specific stain. Relative molecular weights of protein standards are indicated in kDa.

detected in the same 2D gel allowing for easy identification of phosphoprotein location and subsequent isolation for MS analysis. These 2D gels can be seen in greater detail in Appendix 3.1, with the phosphoprotein images overlayed over the total spot images.

The above methods were used to analyze the proteome and phosphoproteome of the premetamorphic *R. catesbeiana* tail fin undergoing precocious metamorphosis at 24 and 48 h induced with 10 nM $T_3$. A minimum of three independent replicates allowed for the verification

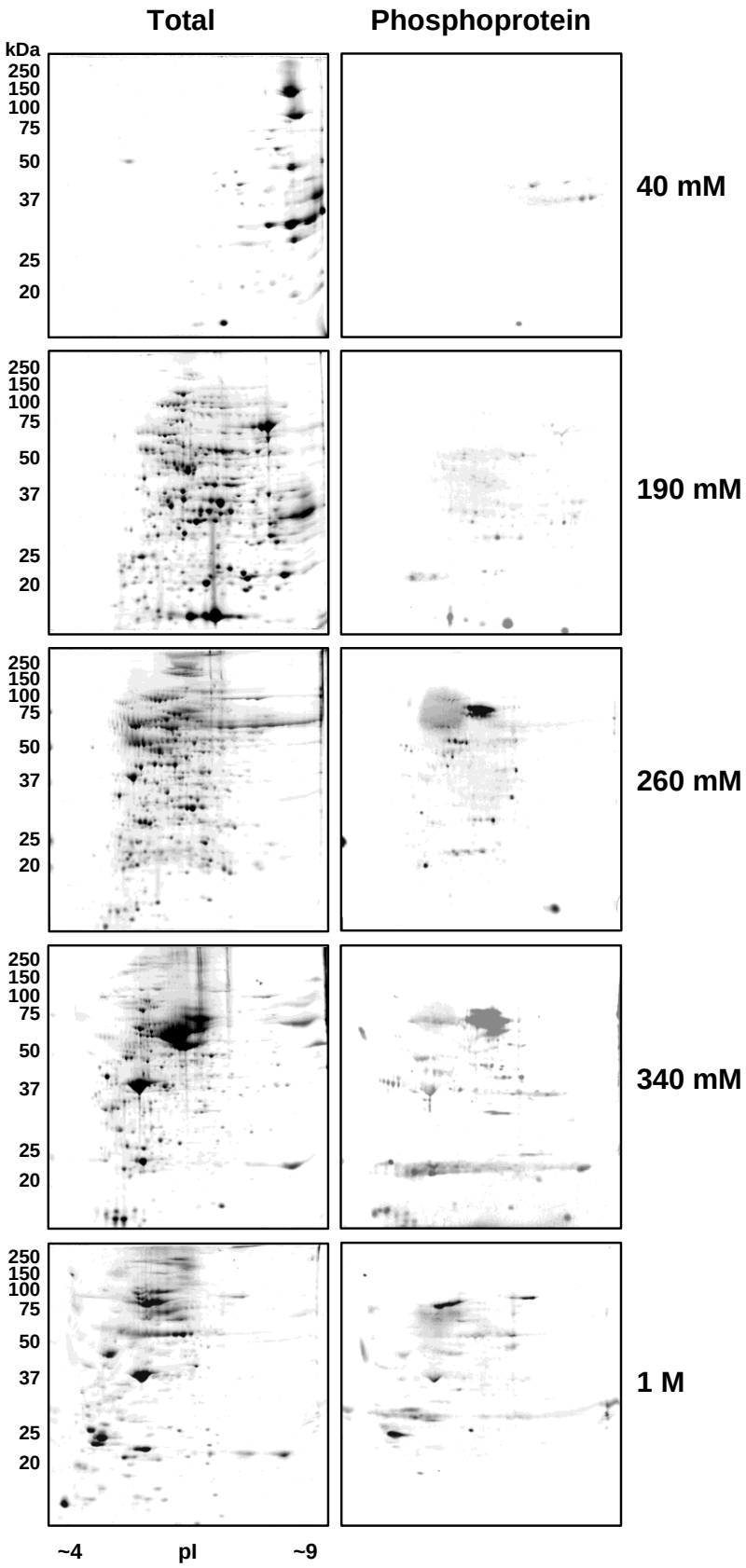
Total
Phosphoprotein
kDa
250
150
100
75
50
37
25
20
40 mM
190 mM
260 mM
340 mM
1 M
~4
pI
~9

**Figure 3.4. 2D gel analysis of the anion-exchange HPLC cytosolic fractions.** Proteins from each of the fractions resulting from the anion-exchange HPLC of the cytosolic sample were separated by 2D-PAGE according to molecular weight and pI point. The 40 mM fraction is the unbound protein fraction, while the subsequent fractions are proteins eluted by the increasing ammonium bicarbonate concentration step-gradients. Total proteins were detected by colloidal Coomassie stain while phosphoproteins were detected in the same gel using the ProQ Diamond phosphoprotein-specific stain. Relative molecular weights of protein standards are indicated in kDa.

of changes in protein and phosphoprotein expression, and MS analysis was used for protein identification.

The sensitivity of this method is presented in Appendix 3.1 (190 mM cytosolic fraction), where mass spectrometric analysis of random protein spots on the 2D gels was able of identifying the low abundance signaling phosphoprotein, Mitogen-activated protein kinase kinase (MAPKK; *Xenopus tropicalis* NCBI#Q66JE6_XENTR), from a low abundance protein spot, with a 100% confidence level. The analysis revealed that this phosphoprotein was not altered in expression level or phosphorylation state under the conditions tested.

### *3.3.2 Identification of a unique R. catesbeiana keratin fragment*

A prominent protein spot at ~24 kDa and pI ~5 was increased upon $T_3$ treatment on the 2D gels of several fractions (Figure 3.5A). It was observed in the 340 mM cytoplasmic fraction as well as in the microsomal, mitochondrial and nuclear fractions. This protein spot was increased by 2-3 fold as early as 24 h (data not shown), but was more intensely expressed at 48 h (2.6 to 5.1 fold increase depending on the fraction) (Figure 3.5B). The greatest increase was observed in the microsomal fraction. The protein spots from each of the fractions were separately analyzed by mass spectrometry proving that each fraction represented the same protein. A combination of electrospray-ionization quadrupole time-of-flight (ESI-QqTOF) and matrix-assisted laser desorption ionization TOF-TOF (MALDI-TOF-TOF) tandem-MS (MS/MS) analyses allowed for peptide sequence information to be obtained for 11 different peptides from this protein (Table 3.1). Protein database searches with these peptides gave the highest homology match to the *X. laevis* type I keratin 47 kDa protein [NCBI: P05781] also known as *X. laevis* keratin B2 [NCBI: 1304283B) from the XK81 gene family (Miyatani et al., 1986).

Parts of the amino acid sequence from two peptides (ALEAANTELELK and NHEEELQVAR) flanking the majority of the peptide sequence identified were used to generate degenerate primers. Degeneracy was limited by taking into account codon usage bias for *R. catesbeiana* and other

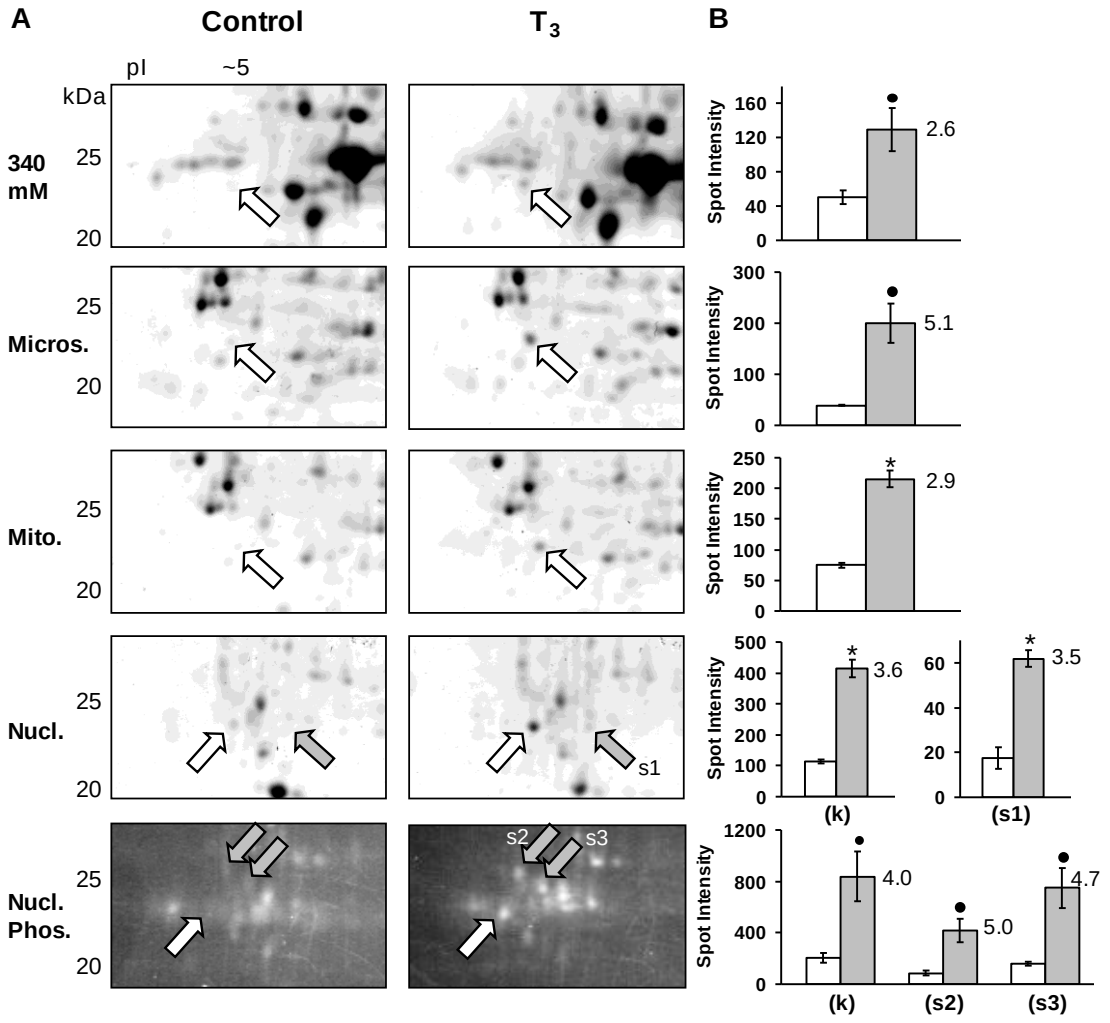


**Figure 3.5. Identification of a novel *R. catesbeiana* type I (RLK I) keratin fragment by 2D gel analysis**. (A) 2D gel regions of the 340 mM cytosolic, microsomal, mitochondrial, and nuclear fractions show the increase of a protein spot at ~24 kDa and pI ~5 due to $T_3$ treatment at 48 h. The corresponding gel region, stained with a phosphoprotein stain, is shown for the nuclear fraction revealing additional changes in the phosphoproteome. The white arrows indicate the spot identified as a novel type I keratin RLK I fragment in the $T_3$ samples (see Table 3.1). In the phosphoprotein gel, the white arrow indicates a possible phosphorylated form of the keratin fragment. The gray arrows indicate an additional unidentified protein and phosphoproteins that are altered upon $T_3$ treatment. Relative molecular weights of protein standards are indicated in kDa. (B) Spot density measurements (in arbitrary values) are graphed for the corresponding 2D gels on the left. The white bar represents the control while the gray bar represents the $T_3$ treatment. Error bars represent the standard error of the mean from three independent controls and three independent $T_3$ samples. Significance is indicated by an asterisk for $p < 0.01$ and by a black dot for $p < 0.04$ (ANOVA). The values adjacent to the gray bars represent the fold increase due to $T_3$. In the nuclear fraction (k) represents the keratin spot, while (s1) represents an additional protein spot observed to be increased, and (s2) and (s3) represent two phosphoproteins that were

increased due to $T_3$ treatment. Spot density measurements were normalized between the gels with the β-actin protein spot.

**Table 3.1. MS analysis of protein spot identified to be a type I keratin fragment**

| Observed peptide mass (Da, $[M+H]^+$)[1] | Peptide sequence from MS/MS[2] | Identified by MALDI-TOF-TOF[3] | % confidence[4] (MS/MS / MALDI) | Matched database sequence[5] |
|---|---|---|---|---|
| 807.4 | LAADDFR | Yes | 84 / 89 | LAADDFR |
| 809.4 | LASYLDK | Yes | 100 / na | LASYL**E**K |
| 991.5 | FENELALR | Yes | 100 / 98 | FENELALR |
| 1041.6 | LVLQIDNAR | Yes | 100 / 100 | **V**VLQIDNA**K** |
| 1073.6 | ILAATIDNSR | Yes | 100 / 100 | IL**S**ATIDNSR |
| 1079.5 | VLDELTMSR | Yes | 100 / 74 | VLDELT**LA**R |
| 1184.6 | YYDIINDLR | - | 96 / - | Y**FE**II**S**DLR |
| 1202.6 | QSVEADINGLR | - | 43 / - | QSVE**T**DINGLR |
| 1224.6 | NHEEELQVAR | - | 73 / - | NHEEE**MSI**A**K** |
| 1232.7 | - | Yes | - / 100 | LKFENELALR |
| 1301.6 | ALEAANTELELK | - | 93 / - | ALEAAN**AD**LELK |

[1]Observed peptide masses resulting from the tryptic digestion of the protein spot, reported as singly charged. [2]Peptide sequence information deduced from MS/MS spectra of the corresponding peptides from ESI-QqTOF analysis. The masses of isoleucine are indistinguishable from leucine in MS and therefore L can be I and *vice versa*. [3]Indicates which peptides were additionally observed with MALDI-TOF-TOF analysis. [4]Percent confidence for the peptide sequences as reported by PEAKS software for the ESI-QqTOF spectra and by MASCOT for MALDI-TOF-TOF data. [5]Highest homology match from protein database searching with the observed peptide sequences to *X. laevis* type I keratin 47kD using SPIDER software. Bold lettering indicates differences between the observed and database sequences.

identified type I keratin cDNA sequences. Two primers with 32 fold degeneracy each, generated a single 380 bp PCR product from *R. catesbeiana* tail cDNA. Based on this sequence two gene specific primers (GSP) were designed to perform 5'- and 3'-rapid amplification of cDNA ends (RACE). Two overlapping clones were obtained from the 5'- and 3'-RACE containing the entire open reading frame of this keratin gene (Figure 3.6). The cloned sequence was 1728 bp long, with a 109 bp 3'-untranslated region, and a polyadenylation signal, AATAAA, at 17 nucleotides upstream of the poly(A) tract. The deduced amino acid sequence coded for a 481 amino acid protein (predicted size of 52 kDa and pI 5.0) and matched exactly all of the observed peptides from the MS analysis indicating that the correct corresponding cDNA sequence was cloned.

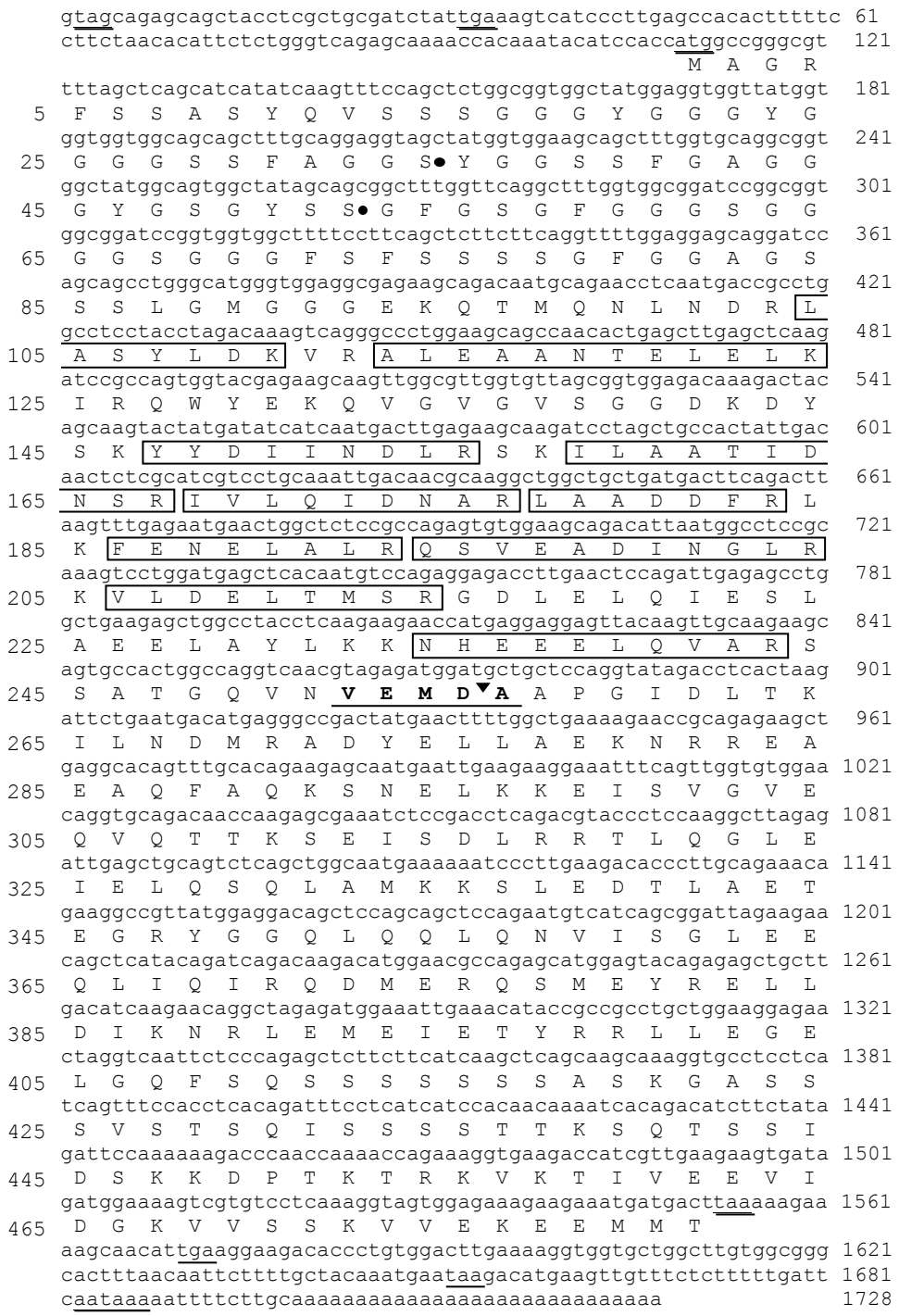


**Figure 3.6. RLK I cDNA and derived amino acid sequence and location of MS/MS peptide fragments.** The complete nucleotide sequence (lower case) of RLK I cDNA is shown. Underlined nucleotide sequences indicate all the in-frame stop codons, the first methionine codon, and a consensus AATAAA polyadenylation signal. Numbers on the right indicate nucleotide position. Upper case letters indicate the deduced amino acid sequence (single letter code). Boxed sequences indicate tryptic peptides observed in the MS analyses of the RLK I

protein spot from the 2D analysis. The underlined VEMDA sequence indicates a consensus caspase cleavage site identified in human type I keratins with the black inverted-triangle indicating the cleavage site. Black dots adjacent to two serine residues indicate possible phosphorylation sites based on those found in human K18 at Ser33 and Ser52 (here Ser34 and Ser52). Numbers on the left indicate amino acid position.

---

BLASTp (Altschul et al., 1997) analysis and ClustalW (Thompson et al., 1994) alignment with this 481 amino acid sequence revealed the highest identity and similarity (80 and 90%, respectively) with the *X. laevis* type I keratin 47 kDa protein [NCBI: P05781] (Figure 3.7). About a dozen keratin proteins have been identified for *X. laevis* (Watanabe et al., 2001; Watanabe et al., 2002). In *R. catesbeiana* only four keratin proteins have been defined so far. These include the adult and larval keratins, RAK and RLK, respectively, and a keratin K8 and inner-ear cytokeratin (Suzuki et al., 2002; Ishida et al., 2003). RAK is the only acidic type I keratin while the remaining three are basic-neutral type II keratins. The sequence we identified is 73% identical (84% similar) to RAK [NCBI: BAB47394.1] and 32-33% identical to the type II keratins: RLK, *Rana* keratin K8 and inner-ear cytokeratin (Figure 3.7 and data not shown). Our sequence also showed 67% identity (81% similarity) to the human type I keratin 19 (K19) protein [NCBI: NP_002267.2]. The sequence was typical of a type I keratin, containing a conserved middle rod domain with highly divergent head and tail domains. Based upon this evidence and that presented below, the isolated sequence constitutes a novel *Rana* type I keratin which we will refer to as RLK I. The previous type II larval RLK will be referred to as RLK II.

Keratins are part of the intermediate filament (IF) protein family and are encoded by over 20 genes (Marceau et al., 2001). They are grouped into two types based on sequence homology: the type I acidic keratins (K9 to K22) and the type II basic-neutral keratins (K1 to K8). The type I and type II keratins are co-expressed as specific pairs, which first form obligate heterodimers, then assemble into tetramers and finally associate into higher order structures leading to IFs with a 1:1 ratio of the two proteins. Keratins are expressed by epithelial cells where they impart a mechanical function. In recent years, they have also been shown to be posttranslationally modified during cell stress, apoptosis, and cell signaling (Marceau et al., 2001; Oshima 2002). Keratins have been extensively studied in anurans during skin differentiation and metamorphosis. The skin in *R. catesbeiana* transitions from a larval type into a pre-adult type, and finally into an adult type with the onset of metamorphosis (Suzuki et al., 2002; Ishida et al., 2003). These changes are associated with the differentiation and apoptosis of specific epidermal cells and changes in connective tissue (Kawai et al., 1994; Suzuki et al., 2002). Each of these changes have been associated with alterations in keratin type expression in specific cells (Suzuki et al., 2001;

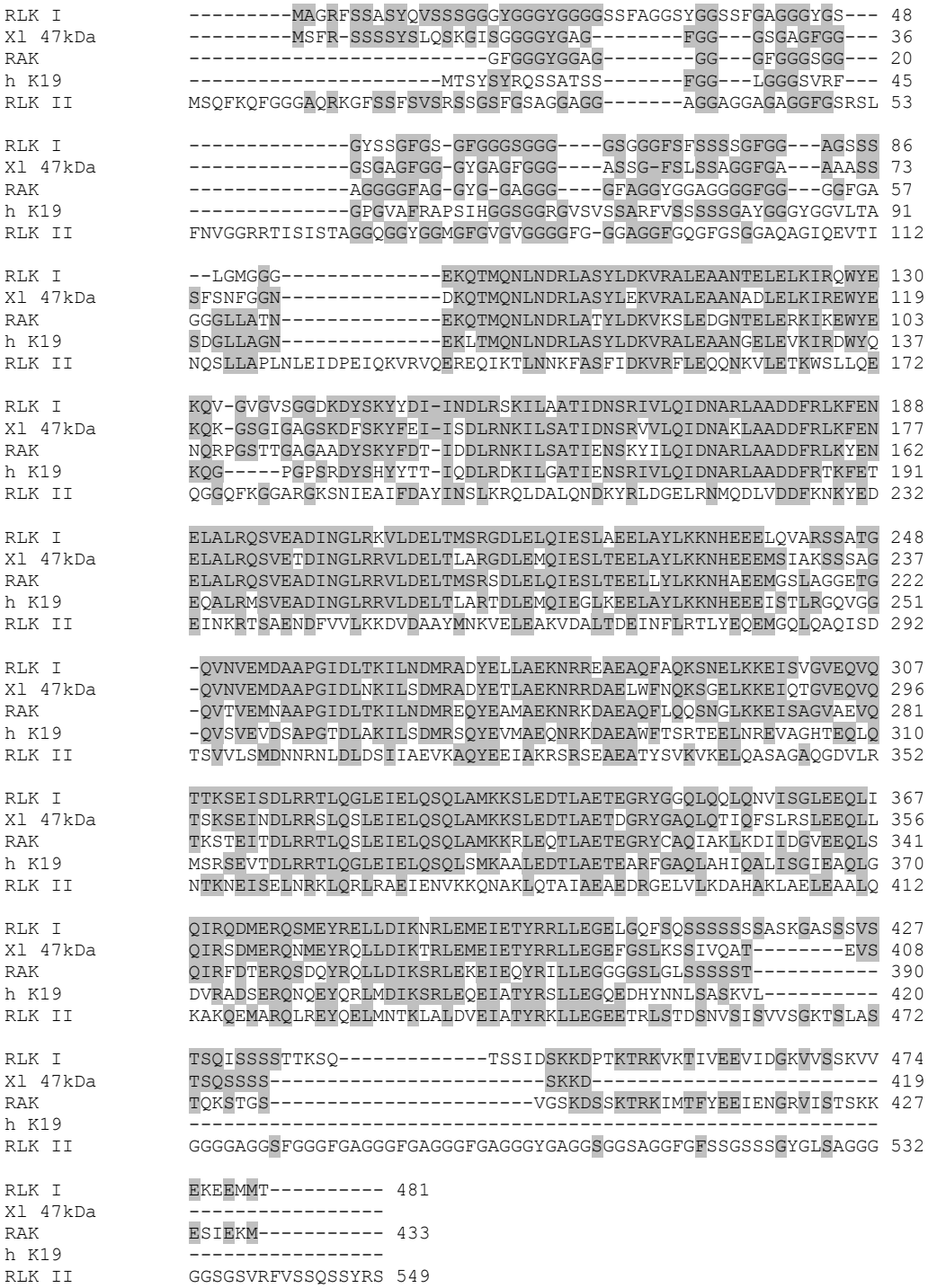


**Figure 3.7. Multiple sequence alignment of the derived amino acid sequence of RLK I**. The derived amino acid sequence of RLK I [GenBank: EF156435] was aligned with the *X. laevis* type I keratin 47 kDa protein [GenBank: P05781] (Xl 47kDa), a partial *R. catesbeiana* adult type I keratin RAK [GenBank: BAB47394.1] (RAK), the human type I keratin K19 [GenBank: NP_002267.2] (h K19), and the *R. catesbeiana* larval type II keratin RLK [GenBank: BAB47395] (RLK II) sequences. Gaps that were inserted for optimal alignment are indicated by a dash.

Identical amino acids are shaded. Numbers indicate amino acid position for each sequence. The alignment was done using ClustalW software (Thompson et al., 1994).

Watanabe et al., 2001). RLK II expression was reduced in tadpole tail and body skin with the onset of metamorphosis while RAK expression increased (Suzuki et al., 2001). These changes are precociously induced by $T_3$ and similar changes have been observed in *X. laevis* with its corresponding larval and adult keratin genes (Watanabe et al., 2001; Watanabe et al., 2002).

RLK I had the highest homology to the *X. laevis* type I keratin 47 kDa which is expressed during embryonic and larval stages, reduced during metamorphosis, and expressed at very low levels in the adult skin (Miyatani et al., 1986). In order to determine the transcript levels of RLK I, we performed quantitative real-time polymerase chain reaction (QPCR) analysis on tail samples from premetamorphic *R. catesbeiana* tadpoles exposed to $T_3$ and during normal tadpole development. Exposure of premetamorphic tadpoles to $T_3$ significantly reduced the steady-state levels of the RLK I transcript by 1.9 and 5.2 fold at 48 and 72 h, respectively, relative to time-matched controls (Figure 3.8A). The same trend was observed during natural metamorphosis. The steady-state level of the keratin transcript remained unchanged from premetamorphosis [Taylor and Kollros (TK) stage VI-VIII (Taylor and Kollros 1946)], through prometamorphosis (TK stage XII-XIX) and then decreased by 3.1 fold upon reaching metamorphic climax (TK stage XX-XXII) when TH levels are maximal and the tail begins to regress (Figure 3.8B) (Gilbert et al., 1996).

Keratins range in size from 40 to 67 kDa. The keratin spot corresponding to RLK I runs at ~24 kDa and all of the peptides that we detected in the MS analysis from the protein spot mapped to the N-terminal end of the complete cloned sequence (Figure 3.6). Immunoblot analyses of the 48 hour microsomal fraction using a pan-cytokeratin antibody revealed the appearance of a similarly migrating fragment in the $T_3$ sample with a concomitant reduction of protein intensity at around 50 kDa compared to the control sample (Figure 3.8C). Interestingly, the identified peptides lie just upstream of what is known as a consensus caspase cleavage site (VEMDA) identified in type I human keratins (Ku and Omary, 2001) suggesting that our observed protein spot is a caspase cleavage product of RLK I (Figure 3.6). No caspase cleavage of any keratins has previously been reported in anurans during metamorphosis. However, a number of effector caspases, such as caspase 3 and 7, increase in expression and activity during metamorphosis in the tail (Sachs et al., 1997; Rowe et al., 2002; Sachs et al., 2004). Caspase 3 is the most markedly up-regulated in the tail. It is expressed in larval skin epidermal cells that undergo TH-induced cell autonomous death

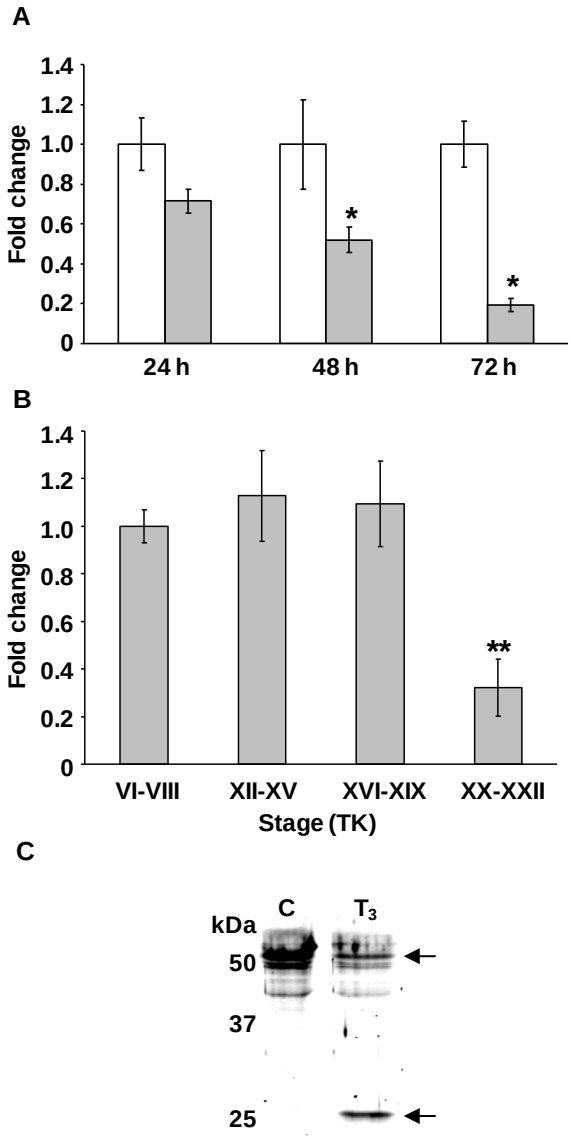


**Figure 3.8. Changes in transcript and protein fragment levels of RLK I in the tail fin**. (A) Fold change in steady-state levels of the keratin transcript relative to time-matched controls after 100 nM $T_3$ exposure for 24, 48 and 72 h. White bars represent controls and gray bars represent $T_3$ treatments. Error bars represent the standard error of the mean ($n \geq 4$ for all treatments). Significance is indicated by an asterisk for $p < 0.03$ (Mann-Whitney U). (B) Fold change in steady-state levels of the keratin transcript at different stages of natural metamorphosis relative to premetamorphic TK stage VI-VIII (Taylor and Kollros, 1946). Error bars represent the standard error of the mean ($n \geq 4$ for all treatments). Significance is indicated by a double asterisk for $p < 0.002$ (Mann-Whitney U). (C) Immunobloting microsomal fraction samples using anti-pan-cytokeratin antibody reveals the appearance of the keratin fragment (25 kDa) and a concomitant loss of keratin at 50 kDa due to 10 nM $T_3$ treatment. Relative molecular weights of protein standards are indicated in kDa. Shown is a representative of two independent experiments.

and is known to act on type I keratins in humans (Ku and Omary 2001; Schreiber and Brown 2003).

RLK I was also highly similar to human K19 protein. This type I keratin and the related K18 protein form heterodimers with the type II keratin K8 in simple-type epithelia and are a prevalent and extensively-studied group of keratins (Omary et al., 1998; Marceau et al., 2001; Oshima 2002). Both K18 and K19 are known caspase 3 substrates (Ku and Omary 2001). Type I keratin caspase cleavage occurs very early in apoptosis before the detection of DNA fragmentation. Type II keratins are not caspase substrates since they lack the caspase cleavage sequence (Ku and Omary 2001). In addition, the onset of apoptosis is associated with rapid phosphorylation of both type I and type II keratins on their head and tail domains. For K18, Ser52 phosphorylation controls its caspase cleavage and Ser33 phosphorylation regulates binding to 14-3-3 protein (Ku and Omary 2001; Marceau et al., 2001). From our results it is possible that our keratin fragment is also phosphorylated. Like K18, it contains Ser residues at positions 34 and 52. Also, the phosphoprotein stain revealed an increased phosphoprotein spot in the nuclear fraction positioned just slightly towards the more acidic end of the gel relative to the RLK I fragment. This phosphoprotein was increased at 24 and 48 h by 1.6 and 4.0 fold respectively which matches the increase of the total-protein keratin spot (Figure 3.5A and B). Although this phosphoprotein could not be identified by MS, its more acidic position adjacent to the RLK I fragment suggests it could be a phosphorylated form of the same fragment.

The reasons for keratin cleavage and phosphorylation are not well understood and are speculated to function as phosphate sinks, for filament re-organization during apoptosis, or mechanisms that protect cells from apoptotic damage allowing a graded sequence of events. In human cancer therapy, the appearance of the caspase cleavage products of K18 and K19 in patient serum are used as indicators of cancer prognosis and apoptotic death of tumor cells undergoing chemotherapy (Linder et al., 2004; Ueno et al., 2005). The ease with which this fragment was detected in our immunoblot using a pan-cytokeratin-specific antibody suggests that it could be used as a protein marker for the induction of a TH response in tadpoles which may be perturbed upon exposure to disruptors of TH action. The very early appearance of this fragment during precocious tail metamorphosis before the detection of any overt apoptotic events (Veldhoen et al., 2006) is very intriguing. It is currently unclear whether the appearance of this keratin fragment is a product of initiation of the apoptotic event or is required for tail regression to occur.

### *3.3.3 Phosphorylation changes in γ-interferon-inducible lysosomal thiol reductase*

Three phosphoprotein spots located at 25 kDa and pI ~5 increased in abundance due to $T_3$ at 48 h in the mitochondrial and microsomal protein fractions (Figure 3.9A). These spots formed a train indicating that this could be a single protein with different posttranslational modifications. The phosphoprotein spots increased ~5 fold, while the only corresponding protein spot that could be detected on the total-protein gels did not change in abundance (Figure 3.9B). This indicates that $T_3$ caused a change in the posttranslational state of the protein while its expression level remained the same. MS analysis of the protein spot from the microsomal and mitochondrial, control and treatment samples indicated that this is the same protein spot (data not shown). ESI-QqTOF MS/MS analysis of the tryptic fragments of the protein spot provided two high quality peptide sequences (Table 3.2). A homology search of the protein database with the two sequences gave the highest match to the *Xenopus tropicalis* γ-interferon-inducible protein 30 (IP30) [NCBI: NP_001017196.1], more commonly known as gamma-interferon-inducible lysosomal thiol reductase (GILT) (Arunachalam et al., 2000). This protein also matched the observed molecular weight and pI point.

GILT is the specific lysosomal enzyme responsible for thiol reduction of proteins in the endocytic pathway for antigen presentation (Arunachalam et al., 2000). Gamma interferon (IFNγ) released by activated T cells, increases antigen presentation on antigen presenting cells (APCs) such as macrophages, dendritic cells, and B cells through the induction of major histocompatability complex II (MHCII) molecules and related proteins. In addition, IFNγ increases the constitutive expression of GILT in APCs and even induces GILT expression in non-hematopoietic cells such as fibroblasts, keratinocytes and endothelial cells (Luster et al., 1988). GILT is transported in its proform (30-35 kDa) from the ER and Golgi complex into the early endosomes of the endocytic pathway where it is combined with MHCII-invariant chain containing vesicles and converted into its mature form (25-30 kDa) by the removal of N- and C-terminal prosequences in the late endosomes and lysosomes (Arunachalam et al., 2000; Phan et al., 2000). It is likely that the GILT protein we identified is the mature form of the protein due to its localization in the microsomal and mitochondrial fractions (which contain vesicles from the ER, Golgi and lysosomes), the size on the 2D gels, and scope of coverage of identified peptides.

Further analyses of the phosphoprotein spots using 2D immunoblots and antibodies specific for the three common phospho-amino acids, phosphoserine, phosphothreonine, and phosphotyrosine did not give any indication that the GILT protein is differentially phosphorylated on any of those

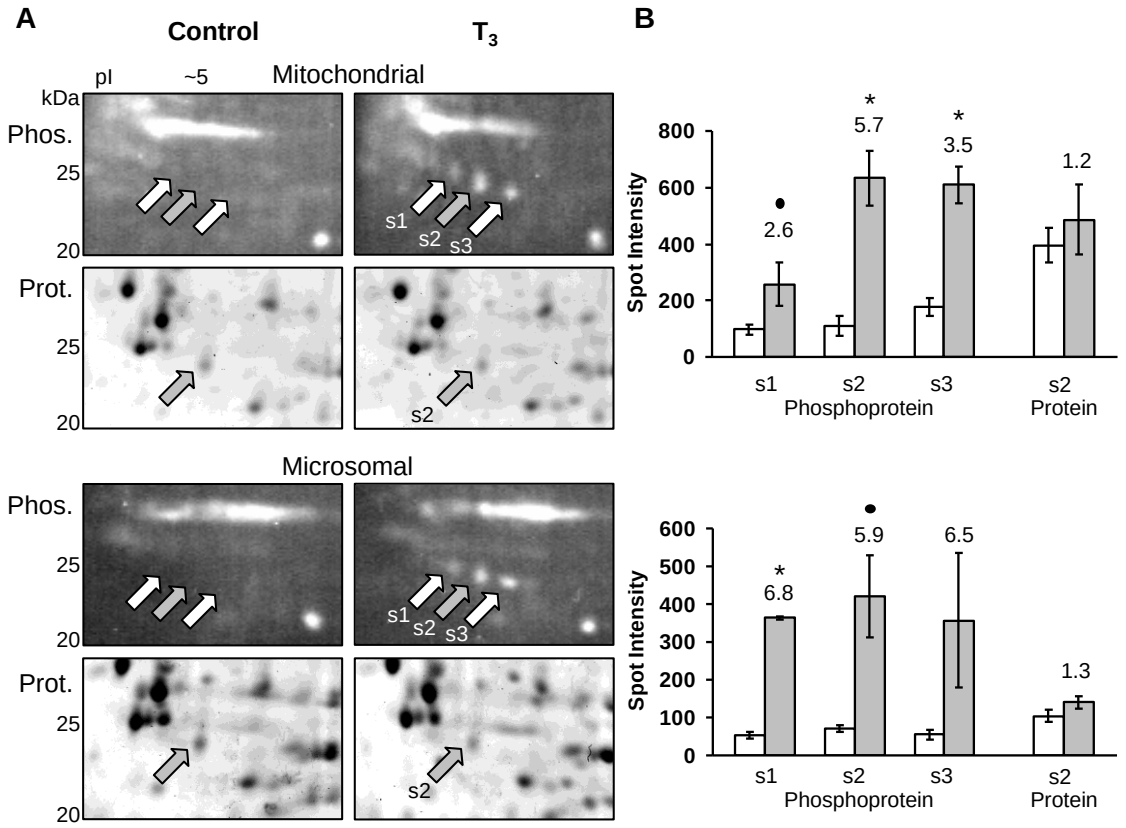


**Figure 3.9. Phosphorylation changes in γ-interferon-inducible lysosomal thiol reductase (GILT)**. (A) Phosphoprotein 2D gel regions of the mitochondrial and microsomal fractions showing the increase in a row of phosphoprotein spots (s1, s2, s3) due to $T_3$ treatment at 48 h, while a corresponding total-protein stained 2D region shows no change in the only detectable protein spot s2 (gray arrows). Relative molecular weights of protein standards are indicated in kDa. (B) Spot density measurements (in arbitrary values) are graphed for the corresponding 2D gels on the left. The white bar represents the control while the gray bar represents the $T_3$ treatment. Error bars represent the standard error of the mean from three independent controls and three independent $T_3$ samples. Significance is indicated by an asterisk for $p < 0.01$ and by black dot for $p<0.1$ (ANOVA). The values adjacent to the gray bars represent the fold increase due to $T_3$. Phosphoprotein spots s1, s2, and s3 increase while the corresponding protein spot s2 does not change. MS analysis of the only detectable protein spot s2 (gray arrow) is indicated in table 3.2. Spot density measurements were normalized between the gels with the β-actin protein spot.

residues (data not shown), while the ProQ Diamond phosphoprotein stain reproducibly detected a change in phosphorylation. As with many lysosomal enzymes, GILT is a glycoprotein with three potential N-linked glycosylation sites. Furthermore, mature GILT contains mannose-6-phosphate (M6P) on one or more of the glycan chains (Arunachalam et al., 2000). Phosphorylation of mannose within the N-linked glycan chain is a signal recognized in the Golgi complex by the

**Table 3.2. MS analysis of protein spot identified as GILT**

| Observed peptide mass (Da, $[M+H]^+$)[1] | Peptide sequence from MS/MS[2] | % confidence[3] | Matched database sequence[4] | E value[5] |
|---|---|---|---|---|
| 1399.8 | (CL)FNLVTELYK | 100 (98) | Observed 1 CLFNLVTELYK 11<br>LFNLV + YK<br>Database 223 SLFNLVCDTYK 233 | 1877 |
| 1405.7 | (TV)LDCVDGDLGNK | 100 (90) | Observed 1 TVLDCVDGDLGNK 13<br>TVL+CV+GDLGNK<br>Database 172 TVLECVNGDLGNK 184 | 0.001 |

MS analysis of the only detectable protein spot s2 (gray arrows in Fig. 3.9). [1]Observed peptide masses resulting from the tryptic digestion of the protein spot s2, reported as singly charged. [2]Peptide sequence information deduced from MS/MS spectra of the corresponding peptides from ESI-QqTOF analysis. The masses of isoleucine are indistinguishable from leucine in MS and therefore L can be I and *vice versa*. [3]Percent confidence for the peptide sequences, as reported by PEAKS software for the ESI-QqTOF spectra. [4]Highest homology match from protein database searching with the observed peptide sequences to *X. tropicalis* GILT. Indicates the sequence alignment of the observed peptide to the identified protein (Database) as aligned by BLASTp. The sequence in between indicates the matching and similar (+) amino acids between the two sequences. [5]From BLASTp alignments.

M6P receptor that targets lysosomal enzymes to the endocytic pathway (Kornfeld and Mellman 1989). Therefore, it is possible that the ProQ Diamond phosphoprotein stain is detecting a phosphate in M6P and that our observed increase in phosphorylation of GILT indicates an increased amount of M6P-containing GILT being directed into the endocytic pathway due to $T_3$. In accordance with this idea of increased endocytic pathway activity, the lysosomal endoprotease, cathepsin D, increases in expression due to $T_3$ in our iTRAQ experiment (see below). Cathepsin D, with other lysosomal cathepsin proteases (B, L and S) also converts the proform of GILT into its mature form by cleaving off the N- and C-terminal prosequences (Phan et al., 2000; Honey et al., 2001). A GILT knock-out study in mice, showed that GILT is required for the presentation of disulfide-containing antigens and the resulting T cell activation (Maric et al., 2001). These ideas, and the additional observation of increased immunoglobulin (Ig) heavy chains from our iTRAQ experiment (see below), indicate that $T_3$ must be stimulating antigen presentation and possibly in turn activating T cell and finally Ig-producing/possessing B cell lymphocytes.

### *3.3.4 Additional changes observed in the 2D gel analysis*

Within the region of the keratin spot, additional proteins and phosphoproteins were increased in the nuclear fraction (Figure 3.5A). A protein spot that could not be identified increased by 2 (data not shown) and 3.5 fold at 24 and 48 h, respectively (Figure 3.5B). And two unidentified phosphoproteins were increased only at 48 h by ~5 fold (Figure 3.5A and B). A protein spot located at 30 kDa and pI ~5.5 in the microsomal fraction was increased by 2.4 fold at 48 h upon $T_3$ exposure (Figure 3.10A). Amino acid sequence was obtained with high confidence for three peptides from this spot but no significant homology match could be made (Table 3.3). A protein spot located at 18 kDa and pI ~5 in the 190 mM cytosolic fraction was observed to appear at 48 h in the $T_3$ treatment for two independent replicates, but could not be replicated in the third experiment (Figure 3.10B). MS/MS analysis produced a high confidence sequence for a single peptide (Table 3.4). Searching of the *Xenopus* databse with the peptide sequence and MS/MS spectra identified this protein as *X. laevis* Survivin [NCBI:BAE02678.1], which also matched the observed molecular weight and pI point. Survivin is a novel inhibitor of apoptosis and is known to interact with RXRα in the absence of ligand (Pennati et al., 2007; Song et al., 2003). The fact that at its appearance was not observed in each experiment might indicate a tadpole population variation as different sources were used in some experiments.

### *3.3.5 Differential expression analysis using iTRAQ*

2D gel analysis has the advantage of identifying specific protein isoforms and posttranslational modifications of whole proteins. This whole-protein analysis approach is limited by the inability to observe hydrophobic proteins and proteins with extremes in size or pI (Patton et al., 2002). In contrast, MS analysis techniques circumvent this limit by analyzing peptides derived from trypsin-cleaved protein samples. However MS peptide analysis has limitations in distinguishing between protein isoforms that potentially share identical peptides (Nesvizhskii and Aebersold 2005). Consequently, 2D gel analysis and MS analysis techniques are complementary methods that can be combined to study differential protein expression. Therefore, to increase the number of observed altered proteins, changes in protein expression in the *R. catesbeiana* tadpole tail fin were additionally assessed using the novel MS technique, iTRAQ (Ross et al., 2004).

The iTRAQ labeling reagents are four unique chemical tags (114, 115, 116 and 117) that label peptides on primary amines allowing for the quantitation of relative protein abundance in four samples simultaneously during a single analysis (Figure 3.11). Each sample is labeled with a

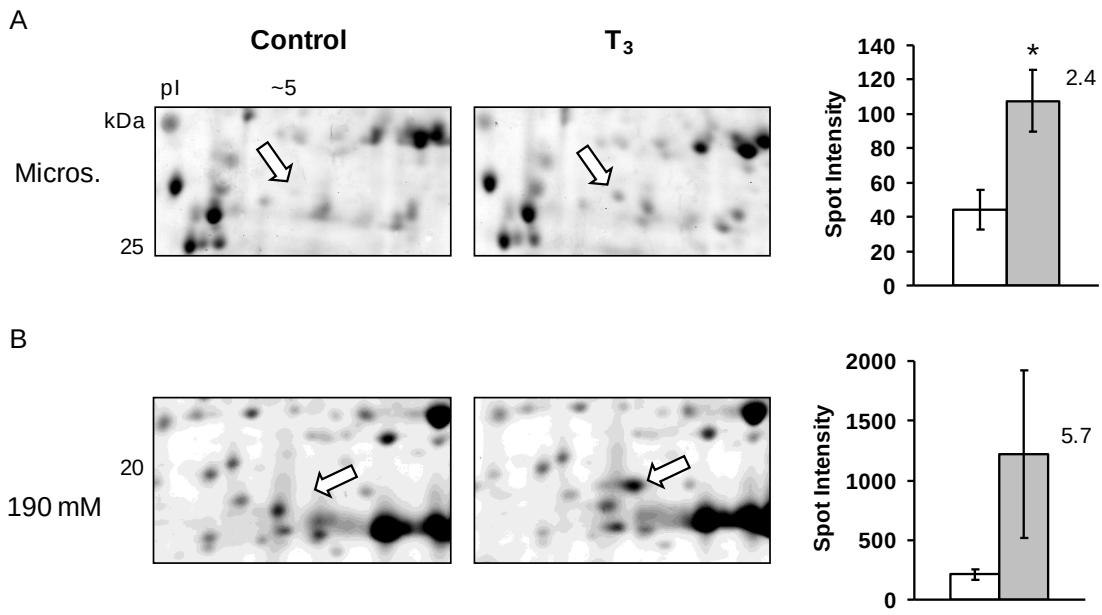


**Figure 3.10. Additional changes identified in 2D analyses of the microsomal and 190 mM cytosolic fractions.** (A) 2D gel regions of the microsomal fraction showing the increase of a protein spot at ~30 kDa and pI ~5 due to $T_3$ treatment at 48 h. (B) 2D gel regions of the 190 mM cytosolic fraction showing the increase of a protein spot identified as *X. laevis* Survivin, at ~18 kDa and pI ~5 due to $T_3$ treatment at 48 h. Relative molecular weights of protein standards are indicated in kDa. Spot density measurements (in arbitrary values) are graphed for the corresponding 2D gels on the left. The white bar represents the control while the gray bar represents the $T_3$ treatment. Error bars represent the standard error of the mean from three independent controls and three independent $T_3$ samples for the microsomal fraction. Data for two independent experiments is presented for the 190 mM cytosolic fraction. Significance is indicated by an asterisk for $p < 0.05$ (ANOVA). Values adjacent to the gray bar represent the fold increase due to $T_3$. Spot density measurements were normalized between the gels with the β-actin protein spot. ESI-QqTOF MS analysis of the protein spots is shown in Tables 3.3 and 3.4.

different tag. The tags are isobaric, meaning that identical peptides from four different samples will be observed in the MS analysis as a single peptide. Peptide fragmentation and tandem-MS (MS/MS) analysis of that peptide then allows peptide sequence information to be acquired leading to a protein inference. In addition, different reporter ions are generated from the tags after peptide fragmentation at 114, 115, 116 and 117 m/z in the MS/MS spectra, representing each of the four samples, indicating the proteins' relative abundance. Relative abundance is obtained by measuring the area underneath the reporter peaks and is reported as a ratio between the samples. In our case, the data is reported as the average ratio of the $T_3$ treatment *versus* the control from two duplicate experiments. A ratio above 1 indicates the fold increase in expression due to $T_3$ exposure, while a ratio below 1 indicates a reciprocal fold decrease in expression.

**Table 3.3. MS analysis of protein spot changing in the microsomal fraction**

| Observed peptide mass (Da, $[M+H]^+$)[1] | Peptide sequence from MS/MS[2] | % confidence[4] |
|---|---|---|
| 1150.6 | YELELD(N)VR | 100 (86) |
| 1422.7 | (GGT)VETFTLENVR | 100 (58) |
| 1719.7 | (E)LELAGLSR (frag.)[3] | 100 (72) |

MS analysis of protein spot in Figure 3.10A. [1]Observed peptide masses resulting from the tryptic digestion of the protein spot, reported as singly charged. [2]Peptide sequence information deduced from MS/MS spectra of the corresponding peptides. [3]Indicates that sequence could only be obtained for a fraction of the observed peptide. The masses of isoleucine are indistinguishable from leucine in MS and therefore L can be I and *vice versa*. [4]Percent confidence for the peptide sequences as reported by PEAKS software.

**Table 3.4. MS analysis of protein spot identified as *X. laevis* Survivin**

| Observed peptide mass (Da, $[M+H]^+$)[1] | Peptide sequence from MS/MS[2] | % confidence[3] | Matched database sequence[4] | E value[5] |
|---|---|---|---|---|
| 615.3 | MYSAK | 100 | Observed 1 MYSAK 5<br>MYSAK<br>Database 1 MYSAK 5 | 30 |

MS analysis of protein spot in Figure 3.10B. [1]Observed peptide masses resulting from the tryptic digestion of the protein spot, reported as singly charged. [2]Peptide sequence information deduced from MS/MS spectra of the corresponding peptide from ESI-QqTOF analysis. [3]Percent confidence for the peptide sequences, as reported by PEAKS software for the ESI-QqTOF spectra. [4]Highest homology match from protein database searching with the observed peptide sequences to *X. laevis* Survivin. Indicates the sequence alignment of the observed peptide to the identified protein (Database) as aligned by BLASTp. The sequence in between indicates the matching amino acids between the two sequences. [5]From BLASTp alignments.

Traditionally, iTRAQ data analysis is performed automatically with software, which greatly reduces the analysis by the end-user. The success of obtaining valid data in this manner, however, is first dependent on the protein identification obtained using software, such as MASCOT, where an identification is reliant on a perfect match of ion peaks in a MS/MS spectrum to an existing protein in the protein sequence database (Perkins et al., 1999). This method works well for the analysis of organisms with extensive entries in gene and protein databases but results in many unidentified spectra when less well-defined species, such as *R. catesbeiana*, are analyzed. Additionally, when a high quality partial MS/MS spectrum is obtained (yielding partial peptide sequence information) software limitations do not permit identification when using ion peaks database searching.

To remedy these problems, we first analyzed the raw iTRAQ data using Excel spreadsheets to find all the MS/MS spectra that showed significant changes in expression due to the $T_3$ treatment. The resulting MS/MS spectra were *de novo* sequenced manually and/or using additional software (PEAKS) (Ma et al., 2003). The resulting peptide sequences were then used to query protein databases using BLASTp. This resulted in substantially higher identification of proteins due to homologous matches or identical matches originally missed by MASCOT.

To increase the proteome coverage and quantitation accuracy, the iTRAQ samples were analyzed three times on an ESI-QqTOF mass spectrometer (Figure 3.11) (Chong et al., 2006). As shown in Table 3.5, many of the peptides that showed changes in abundance due to $T_3$ treatment overlapped between the runs. The mass spectrometer collected 6249 to 7682 unique MS/MS spectra per run. Out of those, ~ 0.3% of the spectra with high quality iTRAQ reporter tags represented peptides that changed according to our criteria of 1.5 fold or higher. In total, 41 unique spectra showed an increase or decrease of 1.5 fold or higher due to the $T_3$ treatment. Successful *de novo* peptide sequence information was obtained for 34 (83%) of those spectra. Nineteen (56%) of those amino acid sequences were identified with homology protein database searching. Only three of the 19 peptides were identified using the standard database matching method that requires a perfect match to a protein database using MASCOT software. These 19 peptides represent at least 11 different proteins, 5 of which increased and 6 of which decreased in abundance due to $T_3$ exposure. Appendix 3.2 presents an example of a *de novo* sequenced MS/MS spectrum. Additional *de novo* sequenced peptides that showed altered abundance, but could not be identified are presented in Appendix 3.3.

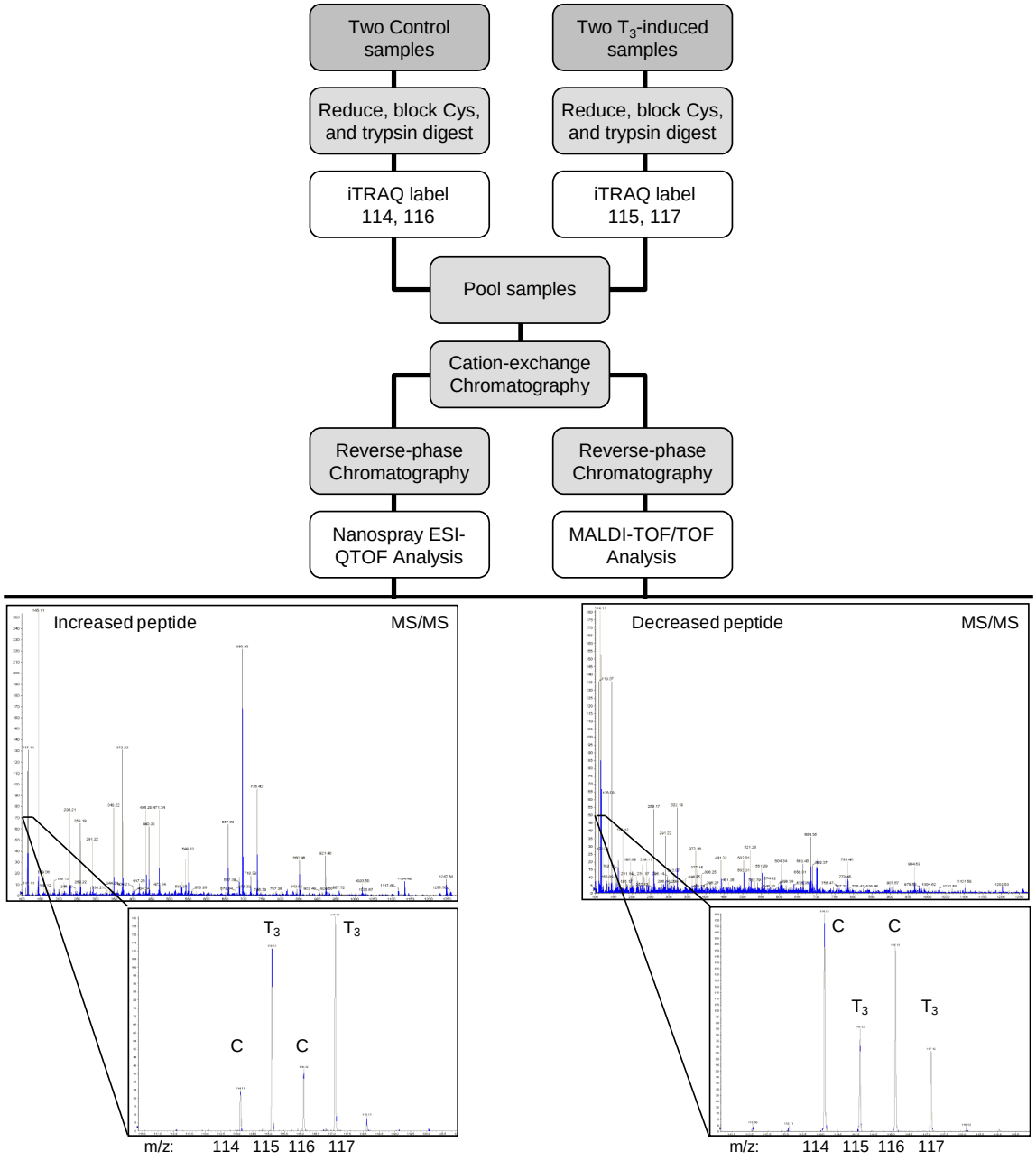


**Figure 3.11. iTRAQ analysis.** Two control and two treatment samples were each labeled with one of the four iTRAQ tags as shown. The peptide samples were pooled, fractionated by two dimensions of liquid chromatography (cation-exchange and reverse-phase), and analyzed by MS. The iTRAQ sample was analyzed three times on an ESI-QqTOF mass spectrometer and once on a MALDI-TOF-TOF mass spectrometer. The image shows two sample MS/MS spectra of two different peptides from which the amino acid sequence is deduced, and in addition, it reveals the four reporter ions (enlarged region) from the iTRAQ tags, in the low-mass region, whose intensity indicates the relative abundance of those two peptides in the four samples. The two controls are labeled with tags 114 and 116, and show reporter ions at that m/z, while the two $T_3$

treatment samples are labeled with tags 115 and 117, showing reporters at those m/z. The spectrum on the left reveals an increase in that peptide due to $T_3$. The spectrum on the right reveals a decrease in that peptide due to $T_3$.

The same iTRAQ samples were also analyzed using a MALDI-TOF-TOF mass spectrometer (Figure 3.11) to obtain additional proteome coverage because the peptide ionization characteristics are different from the ESI-QqTOF. Due to software limitations no *de novo* sequencing of raw MS/MS spectra was performed and the data was analyzed using the standard method of database searching using the observed MS/MS spectra ion peaks using MASCOT. The MALDI-TOF-TOF analysis identified 3352 peptides with over 95% confidence. These peptides represented 729 unique proteins, of which 50% were identified through a single peptide. Four proteins showed altered abundance >1.5 fold due to the $T_3$ treatment. One of these proteins had an increased abundance while three had a decreased abundance. Details of the iTRAQ results are presented in Table 3.6. Interestingly, some of these proteins have established functional connections that may be important during tail regression. In addition, some of the proteins have connections to those identified in the previous 2D gel analyses. The identified proteins are involved in apoptotic events, modulation of the extracellular matrix, immune system, metabolism, mechanical function, and oxygen transport and are discussed in detail below.

***Immune system components***

$T_3$ induces the activation of the immune system as is evident with the increased maturation of GILT as revealed in the 2D analysis. In addition, this is apparent from an increase in immunoglobulin chains and cathepsin D and is possibly related to the decrease of a coatomer protein.

Six peptides that increased 1.5-4.6 fold matched a type of immunoglobulin heavy chain (Table 3.6). The peptides matched sequences from *X. laevis* as well as from other species. The peptides were derived from constant and variable regions of the heavy chain, and one matched the IgM heavy chain isotype.

The immune system plays a major role during the metamorphic process. Macrophages increase in the regressing tadpole tail in number and phagocytic activity removing apoptotic bodies of dying muscle cells (Nishikawa et al., 1998). Larval lymphocyte populations rise in the growing tadpole, decrease sharply at climax of metamorphosis, and expand again with adult lymphocytes (Rollins-Smith 1998). The exchange in lymphocyte populations appears to be required for the tolerance of

**Table 3.5. Summary of results for iTRAQ analysis by ESI-QqTOF**

| | Run 1 | Run 2 | Run 3 | Unique[1] |
|---|---|---|---|---|
| **Unique spectra[2]** | 7682 | 6249 | 6361 | n/a |
| **Changing peptides[3]** | 17 | 17 | 21 | **41** |
| ***de novo* sequenced[4]** | 13 | 16 | 18 | **34** |
| **Homology matched[5]** | 8 | 7 | 11 | **19** |
| **MASCOT ID[6]** | 1 | 1 | 2 | **3** |
| **Total proteins ID[7]** | **11 change:** | **5 up** | **6 down** | |

The iTRAQ samples were analyzed three times on an ESI-QqTOF mass spectrometer. [1]Indicates number of unique spectra shared between the replicate runs. [2]Total number of unique spectra recorded per MS analysis run. These overlap by unknown amount: n/a. [3]Number of spectra that change by $\geq 1.5$ fold due to $T_3$, have good quality reporter tags, and a ratio of the two controls between 0.67 and 1.5. [4]Number of spectra for which amino acid sequence could be obtained through manual sequencing. [5]Number of spectra for which a protein inference was made with BLASTp. [6]Indicates how many spectra were identified using the standard iTRAQ analysis with MASCOT software. [7]Number of different proteins identified from the resulting peptides and their change in abundance.

new adult antigens and for the removal of larval tissues that are seen as 'non-self' in the metamorphosing animal. *X. laevis* tail cells possess larval antigens that stimulate the immune system of a syngeneic adult or a metamorphosing animal (Izutsu et al., 2000). Izutsu and coworkers have shown that a 59 kDa larval antigen expressed specifically by tail epidermal cells only during metamorphosis, causes increased proliferation of newly arising adult-type T lymphocytes, eventually leading to the destruction of tail fin tissue by cytotoxic T lymphocytes (CTL) and natural killer cells (NK) (Izutsu et al., 2002; Watanabe et al., 2003). Collaboration between T- and B-cell types must occur for NK cell activation and may explain our observation of increased immunoglobulin heavy chains which can only come from B cell activation. A reported peptide sequence from the 59 kDa antigen is homologous to keratin $\alpha$, and points at the possibility that the increased keratin fragment observed in the 2D gel analyses may be a larval antigen produced to direct the involvement of the immune system.

A peptide that increased by 1.7 fold was identified in the MALDI-TOF-TOF analysis corresponding to a putative *Xenopus* cathepsin D protein (Table 3.6). Cathepsin D is a lysosomal aspartyl protease that has been previously implicated in tadpole tail regression (Seshimo et al., 1977; Mukai et al., 1995). Its expression was shown to be highly and quickly induced within the tadpole tail at metamorphic climax and with exogenous TH administration (Mukai et al., 1995).

**Table 3.6. Differentially expressed proteins in the *Rana catesbeiana* tail fin due to $T_3$-induction as analyzed by iTRAQ**

| Protein name [accession # / Species][1] | Fold change[2] | Observed peptide mass (Da, iTRAQ [M+H]+)[3] | Observed peptide sequence[4] | % Confidence[5] | Matched database sequence[6] | E value[7] |
|---|---|---|---|---|---|---|
| **INCREASED** | | | | | | |
| MGC80395 protein (Sterol regulatory element-binding transcription factor 2) [AAH72922 / *Xenopus laevis*] | 1.6 | 2949.6 | LTPATVET (frag.) | manual | Query 1 LTPATVET 8<br>LTPATV+T<br>Sbjct 184 LTPATVQT 191 | 136 |
| Inter-α inhibitor H4 [XP_848765 / *Canis familiaris*] | 2.1 | 1789.1 | V(TFE)LVYEEMLK | 90-100 (53) | Query 1 VTFELVYEEMLK 12<br>VTFELVYEE+LK<br>Sbjct 140 VTFELVYEELLK 151 | 0.004 |
| Hemoglobin α-III chain, larval [P02011 / *Rana catesbeiana*] | 1.5 | 1224.7 | FLSFPQTK (frag.) | manual | Query 1 FLSFPQTK 8<br>FLSFPQTK<br>Sbjct 33 FLSFPQTK 40 | 5.4 |
| Hemoglobin α-III chain, larval [P02011 / *Rana catesbeiana*] | 1.5 | 1250.8 | FLSFPQTK (frag.) | 100 | Query 1 FLSFPQTK 8<br>FLSFPQTK<br>Sbjct 33 FLSFPQTK 40 | 5.4 |
| Hemoglobin α-III chain, larval [P02011 / *Rana catesbeiana*] | 1.5 | 2067.0 | YVPHFDLTPGSADLNK | 99 | Query 1 YVPHFDLTPGSADLN 15<br>Y PHFDLTPGSADLN<br>Sbjct 42 YFPHFDLTPGSADLN 56 | 9 e-05 |
| MGC80107 protein (Biliverdin reductase B) [AAH72790 / *Xenopus laevis*] | 1.5 | 1904.3 | VISTPDLSHFFLR | 100 | Query 1 VISTPDLSHFFLR 13<br>VIST DLS FFLR<br>Sbjct 174 VISTHDLSLFFLR 186 | 0.26 |
| Immunoglobulin heavy chain [AAC12909 / *Hydrolagus colliei*] | 1.6 | 1237.8 | VVLLPPSPK | 99 | Query 1 VVLLPPSP 8<br>V+LLPPSP<br>Sbjct 133 VILLPPSP 140 | 63 |
| Immunoglobulin heavy prechain [CAA33212 / *Xenopus laevis*] | 2.0 | 1817.9 | SDPDQGFDGTYTVK | manual | Query 1 SDPDQGFDGTYTVK 14<br>S P++ +DGT+TVK<br>Sbjct 393 SAPEKAYDGTFTVK 406 | 52 |
| Immunoglobulin heavy chain constant region [AAC12914 / *Hydrolagus colliei*] | 4.6 | 1391.7 | LNVADWNSGK | 99 | Query 1 LNVA--DWNSGK 10<br>LNV+ DW SGK<br>Sbjct 69 LNVSTEDWKSGK 80 | 170 |
| Immunoglobulin M heavy chain [AAO37747 / *Ornithorhynchus anatinus*] | 1.5 | 2065.0 | FTCTVSHSDLPAPVEK | 95 | Query 1 FTCTVSHSDLPAP 13<br>FTCTVSH+DLPAP<br>Sbjct 446 FTCTVSHADLPAP 458 | 7 e-04 |
| Immunoglobulin heavy chain variable region [AAP41191 / *Lepus granatensis*] | 1.6 | 1930.3 | (RKQ)VVEEAGGALIK | 100 (92-96) | Query 3 QVVEEAGGALIK 14<br>Q VEE+GG LIK<br>Sbjct 1 QSVEESGGGLIK 12 | 22 |
| Immunoglobulin heavy prechain [CAA33212 / *Xenopus laevis*] | 1.6 | 1471.8 | DQGFDGTYTVK | manual | Query 4 FDGTYTVK 11<br>+DGT+TVK<br>Sbjct 399 YDGTFTVK 406 | 9.2 |
| LOC443721 protein (cathepsin D) [AAH94178 / *Xenopus laevis*] | 1.7 | 980.5 | AYWQIR | 98 (MALDI) | Query 1 AYWQIR 6<br>AYWQIR<br>Sbjct 257 AYWQIR 262 | 42 |
| **DECREASED** | | | | | | |
| α-2-macroglobulin [AAY98517 / *Xenopus laevis*] | 0.67 | 2195.2 | AYVTV(LGD)IMGTALENLDR | 97-100 (41) | Query 1 AYVTVLGDIMGTALENLDR 19<br>AYVTVLGDIMGTA++NLDR<br>Sbjct 958 AYVTVLGDIMGTAMQNLDR 976 | 1 e-08 |
| Calcium-binding protein p26olf [BAA34388 / *Rana catesbeiana*] | 0.47 | 1312.7 | GNTTSMNFK | manual | Query 1 GNTTSMNFK 9<br>GNTTSMNFK<br>Sbjct 31 GNTTSMNFK 39 | 0.57 |
| α 1 type I collagen [BAA29028 / *Rana catesbeiana*] | 0.52 | 2111.2 | TGPAGAPGQDGRPGPPGPPGAR | manual | Query 1 TGPAGAPGQDGRPGPPGPPGAR 22<br>TGPAGAPGQDGRPGPPGPPGAR<br>Sbjct 538 TGPAGAPGQDGRPGPPGPPGAR 559 | 6 e-12 |
| α 1 type I collagen [BAA29028 / *Rana catesbeiana*] | 0.62 | 2418.2 | PPGPSGEK (frag.) | 97 | Query 1 PPGPSGEK 8<br>PPGPSGEK<br>Sbjct 912 PPGPSGEK 919 | 17 |
| Caridac α actin 2 [AAX85445 / *Rana catesbeiana*] | 0.38 | 2244.3 | VAPEEH(PT)LLTEAPLNPK | 93-100 (66) | Query 1 VAPEEHPTLLTEAPLNPK 18<br>VAPEEHPTLLTEAPLNPK<br>Sbjct 98 VAPEEHPTLLTEAPLNPK 115 | 3 e-09 |

**Table 3.6 (continued)**

| Protein name [accession # / Species][1] | Fold change[2] | Observed peptide mass (Da, iTRAQ [M+H]+)[3] | Observed peptide sequence[4] | % Confidence[5] | Matched database sequence[6] | E value[7] |
|---|---|---|---|---|---|---|
| myosin heavy chain (skeletal muscle MHC-3) [AAD13771 / *Rana catesbeiana*] | 0.39 | 2491.9 | FQAALEEAEASLEHEEAK | manual | Query 1 FQAALEEAEASLEHEEAK 18<br>FQAALEEAEASLEHEEAK<br>Sbjct 320 FQAALEEAEASLEHEEAK 337 | 8 e-09 |
| Mylpf-prov protein (myosin light chain 2) [AAH41503 / *Xenopus laevis*] | 0.38 | 2098.2 | NICYVITHGED (frag.) | 100 | Query 1 NICYVITHGED 11<br>NICYVITHGED<br>Sbjct 156 NICYVITHGED 166 | 0.002 |
| MGC68533 protein (coatomer protein complex, subunit γ) [AAH61661 / *Xenopus laevis*] | 0.61 | 1491.6 | NAHSLYLAGVFR | 99 (MALDI) | Query 1 NAHSLYLAGVFR 12<br>NAHSLYLAGVFR<br>Sbjct 824 NAHSLYLAGVFR 835 | 0.002 |
| Cortactin [NP_005222 / *Homo sapiens*] | 0.65 | 1585.9 | YGLFPANYVELR | 98 (MALDI) | Query 1 YGLFPANYVELR 12<br>YGLFPANYVELR<br>Sbjct 538 YGLFPANYVELR 549 | 4 e-04 |
| Triose phosphate isomerase [NP_788764 / *Drosophila melanogaster*] | 0.64 | 1711.8 | DIGADWVILGHSER | 100 (MALDI) | Query 1 DIGADWVILGHSER 14<br>DIGADWVILGHSER<br>Sbjct 185 DIGADWVILGHSER 198 | 7 e-06 |

[1]Name of protein for the highest scoring match that resulted with the observed peptide sequence using BLASTp (2.2.15) and the NCBI protein database (Oct. 15, 2006) searching all metazoans. The NCBI accession number and the species name for the identified protein are shown. [2]Fold change ratios greater then 1.0 indicate a fold increase, and those below 1.0 indicate the reciprocal of fold decrease. The number is the average fold change of two replicate experiments, which consisted of two treatment samples and two control samples. [3]Observed mass of the peptide in the MS analysis, modified with the iTRAQ reagent, reported as singly charged. [4]Amino acid sequence determined for the observed peptide by manual *de novo* or automatic *de novo* by PEAKS software sequencing, or a MASCOT software match. (frag.) indicates that only a partial peptide sequence could be determined. The masses of isoleucine are indistinguishable from leucine in MS and therefore L can be I and *vice versa*. [5]Percent confidence for the peptide sequence as reported by the PEAKS or MASCOT (MALDI) software. (MALDI) indicates that the peptide was identified in the MALDI-TOF-TOF analysis of iTRAQ samples. "manual" indicates that the peptide sequence was obtained manually and no percent confidence can be reported. [6]Indicates the sequence alignment of the observed peptide (Query) to the identified protein (Sbjct) as aligned by BLASTp. The sequence in between indicates the matching and similar (+) amino acids between the two sequences. [7]From BLASTp alignments.

The increase in cathepsin D may be related to GILT maturation inside the lysosomes and a resulting increase in antigen presentation as discussed above.

A subunit γ protein of the coatomer protein complex (COPI) corresponding to the *X. laevis* MGC68533 protein decreased by 1.6 fold in the MALDI-TOF-TOF analysis (Table 3.6). Protein transport between the ER and Golgi compartment is mediated by these non-clathrin-coated vesicular coat protein complexes (Bethune et al., 2006). COPI is composed of seven unique subunits and coats the vesicles on the cytoplasmic side as they are transported from one organelle to another. COPI is mainly associated with retrograde transport of vesicles from the Golgi back to the ER to retrieve escaped ER-resident proteins and vesicle machinery. The γ subunit binds

double lysine motifs in the transmembrane proteins targeted for return to the ER. Interestingly, GILT and other lysosomal zymogens have dilysine motifs which are used as cleavage sites during enzyme maturation. There have not been any previous associations of COPI with TH or metamorphosis, but it is possible that $T_3$ causes a specific change in vesicle trafficking to accomodate tail regression. This change may contribute to an increase in mature GILT in the lysosomes as is observed on the 2Ds of the microsomal and mitochondrial fractions.

***Extracellular matrix components and modifier proteins***

Changes in the extracellular matrix (ECM) of the regressing tadpole tail have been well documented (Shi, 2000). Four proteins involved in ECM structure and modification were identified by iTRAQ (Table 3.6).

The plasma proteinase inhibitor, α-2-macroglobulin (A2M), was decreased 1.5 fold upon $T_3$ treatment (Table 3.6). A2M is synthesized by several cell types such as hepatocytes, lung fibroblasts and monocyte-macrophages, and functions to trap and facilitate clearing of proteases such as trypsin, thrombin and collagenases (Borth 1992; Dodds and Law, 1998). Tissue-specific A2M synthesis is independent of plasma A2M and serves a compartmentalized function such as the regulation of tissue proteinases such as matrix metalloproteinases. Since there is an increase in matrix metalloprotease activity in the tadpole tail in TH-induced and natural metamorphosis (Shi, 2000), the observed decrease in the A2M levels could be a result of an organized downregulation to allow for ECM remodeling or A2M and metalloprotease covalent linkage and subsequent removal and degradation of the proteins. Recently, Lin *et al.* observed a $T_3$-dependent decrease in A2M transcripts in a human hepatocellular carcinoma cell line (Lin et al., 2003).

A peptide matching inter-α inhibitor H4 protein increased by 2.1 fold (Table 3.6). The H4 polypeptide is a less described component of the trimeric plasma serine protease inhibitor, inter-α inhibitor (IaI), more commonly composed of the H1, H2 and bikunin polypeptides (Fries and Kaczmarczyk, 2003; Josic et al., 2006). IaI proteins are linked to inflammation processes and ECM structure. Serine protease inhibitor activity of bikunin regulates plasmin which is a known activator of matrix metalloproteases (Fries and Kaczmarczyk, 2003). The H4 polypeptide is also a serum marker for the acute-phase response in infected animals and humans resulting from the nonspecific immune response (Pineiro et al., 1999; Pineiro et al., 2004; Harraghy and Mitchell 2005) and may be an additional link to our observation of the immune system activation.

Additionally, the H polypeptides stabilize and protect the ECM through covalent links to ECM components and possibly through collagen binding domains (Fries and Kaczmarczyk, 2003).

α 1 type I collagen (α1(I) chain) was identified by two peptides that decreased by 1.6-1.9 fold (Table 3.6). Type I collagen is the most abundant member of the collagen family and is the main constituent of the ECM (Ricard-Blum and Ruggiero, 2005). It is a major substrate of matrix metalloproteinase 1 (MMP1) which is upregulated in *R. catesbeiana* tail and back skin during natural and $T_3$-induced metamorphosis (Oofusa et al., 1994; Sawada et al., 2001). Collagen (α1(I) and α2(I)) gene expression also decreased under these conditions in the tail and intestine (Asahina et al., 1997, 1999; Utoh et al., 2000). It is possible that the α1(I) collagen gene is negatively regulated by a TRE-like site as in rat cardiac fibroblasts (Chen et al., 2000). Here we show that this change also occurs at the protein level.

The last peptide associated with ECM remodeling proteins corresponds with cortactin (Table 3.6). A 1.5 fold decrease in this Src homology 3 (SH3) domain-containing protein suggests altered tyrosine kinase signaling of actin cytoskeleton rearrangements (Daly, 2004). Cortactin is a filamentous-actin binding protein that stabilizes actin networks and promotes actin polymerization. Since cortactin interacts with various proteins involved in actin polymerization, endocytosis (recall an overlap with GILT and cathepsin D proteins) and cell-cell interactions, modification of any or all of these processes could contribute to tail regression.

***Cell metabolism proteins***

Two proteins involved in cell metabolic homeostasis were altered in abundance by $T_3$ treatment (Table 3.6). The first peptide was increased by 1.6 fold matched with a sterol regulatory element binding protein-2 (SREBP-2). This membrane-bound transcription factor regulates lipid homeostasis through the control of genes encoding key enzymes important in cholesterol synthesis (Eberle et al., 2004). The SREBP transcription factors have not been implicated in anuran metamorphosis before, however, they are involved with TH in the mammalian context (Shin and Osborne, 2003; Zhang et al., 2003; Hashimoto et al., 2006). Recently Shin and Osborne (2003) observed that $T_3$ regulates both SREBP-2 mRNA and nuclear protein levels, as well as SREBP-2-controlled genes such as the low density lipoprotein (LDL) receptor in mice. The SREBP-2 promoter contains at least one TR-binding site and is activated directly by TR in a ligand-dependent manner (Shin and Osborne, 2003). It is therefore possible that the increased

level of SREBP-2 observed in our experiments may be a direct response to $T_3$. This remains to be determined.

The second peptide was reduced by 1.6 fold and corresponds to triose phosphate isomerase (TIM; Table 3.6). This enzyme is involved in glycolysis (Sullivan et al., 2003) and its decrease is compatible with a shift from glycolysis to oxidative phosphorylation observed during metamorphosis (Smith-Gill and Carver, 1981).

In addition, two proteins involved in oxygen transport were increased upon $T_3$ treatment. Three peptides corresponding to larval hemoglobin α-III chain increased by 1.5 fold (Table 3.6). This protein is only found in tadpole red blood cells (RBCs) and not adult RBCs (Maruyama et al., 1980; Smith et al., 1993). In *R. catesbeiana* there is a change in erythropoiesis sites and hemoglobin types during tadpole growth and metamorphosis that is influenced by THs (Just and Atkinson, 1972; Maruyama et al., 1980; Watt et al., 1980; Forman and Just, 1981; Hasebe et al., 1999). Young tadpoles produce hemoglobin components I and II in the kidneys, older tadpoles produce components III and IV in the liver, and after metamorphosis, only adult hemoglobins are produced in the bone marrow. This sequential change produces hemoglobins with lower oxygen affinities. Our observation of an increase in hemoglobin α-III is indicative of an accelerated progression of hemoglobin switching due to $T_3$ exposure.

Consistent with a switch in hemoglobin is an 1.5 fold increase in a peptide matching biliverdin reductase B (BVR-B; Table 3.6). This enzyme is important in hemoglobin metabolism and is predominantly found in human fetal liver (Yamaguchi et al., 1994). There, it produces bilirubin IXβ from biliverdin derived from heme. Bilirubin IXβ is the major heme catabolite during human fetal development (Yamaguchi and Nakajima, 1995). In adult human liver biliverdin reductase A (BVR-A) is the major form and it produces bilirubin IXα. The switch in this heme degradation pathway seems to be related to the switch in hemoglobins from fetal to adult forms. BVR-B is also very abundant in RBCs, where it is referred to as flavin reductase, and is known to catalyze the reduction of a number of substrates, including flavins (Pereira et al., 2001). Interestingly, hypothyroidism leads to lowered levels of flavin cofactors and flavoproteins in human RBCs similar to a riboflavin deficiency (Cimino et al., 1987).

***Mechanical function and calcium modulated proteins***

The abundance of peptides from muscle α-actin, myosin heavy chain (MHC) and myosin light chain (MLC) was reduced by exactly the same amount (2.6 fold; Table 3.6). These proteins are the fundamental components of the molecular machinery used in muscle contraction. The peptide for muscle α-actin is distinguished from the β and γ forms of cytoplasmic actins by a T residue instead of V in the HPTLL sequence within this peptide. The peptide sequence matches the *R. catesbeiana* cardiac α-actin 2 sequence perfectly as well as other muscle α actins in other species. The MHC peptide matches the *R. catesbeiana* skeletal muscle MHC-3 and is distinguishable from the other isoforms, MHCs –1, 2, 4, and 5, by three residues in this species (Hu et al., 1999). The MLC peptide matches the *X. laevis* MLC-2 (Mylpf-prov protein) as well as MLC-2 proteins from other species.

An embryonic/larval α-3 skeletal-actin gene has been found in *Xenopus borealis* (Boardman et al., 1992). This gene was expressed in the skeletal muscle of embryos and tadpoles, but not in adults. However, the corresponding gene in *X. laevis* is highly expressed in both adult muscle and at earlier stages. The human skeletal muscle α-actin gene is a direct TH response gene in cardiocytes (Collie and Muscat, 1992; Muscat et al., 1993). The cardiac α-actin gene of rats is also inducible with $T_3$ in heart myocytes (Gustafson et al., 1987).

Five skeletal muscle MHC isoforms have been cloned in *R. catesbeiana* (Hu et al., 1999). No specific larval forms have been found and all five isoforms are expressed in the tail and limb muscle of both tadpoles and adults. In the tadpole tail muscle, $T_3$ increases the mRNA for MHCs –1, 3, 4, and 5 by two to three-fold within 48 h (Hu et al., 1999). However, in contrast, the rate of total MHC protein synthesis was reduced by 40% at 48 h (Hu et al., 1999) consistent with our observations for MHC-3. In fast twitch muscle fibers, MHC-3 is associated with MLC-2 (Lutz and Lieber, 2000). MLCs are $Ca^{2+}$-signaling dependent regulators of muscle contraction and have been investigated in *X. laevis* and *R. pipiens* but their responses to TH are not well understood (Lutz and Lieber, 2000). Our data suggest that MHC and MLC expression are co-regulated.

A peptide that was decreased by 2.1 fold matched the p26olf protein of *R. catesbeiana* (Table 3.6). The p26olf protein is a S100-like $Ca^{2+}$-binding protein with the very unique feature of having two S100-like regions (Miwa and Kawamura, 2003). Thus far p26olf has only been found in the anurans *R. catesbeiana, X. tropicalis* and *X. laevis*, and appears not to have any homologues in other vertebrates. Immunohistochemical studies on *R. catesbeiana* frogs showed

that p26olf primarily localizes in the cilia of olfactory and lung respiratory epithelia. p26olf may be involved in olfactory signal transduction and a related protein, S100/A11 (calgizzarin), is a key mediator of high $Ca^{2+}$-induced growth arrest and differentiation in human keratinocytes (Sakaguchi et al., 2003). In addition, Makino et al. (2004) have shown that introducing an N-terminal peptide of S100/A11 into human carcinoma cell lines induced apoptosis. Thus, it may be possible that p26olf is involved in the control of apoptotic events in the tadpole tail.

## 3.4 CONCLUSIONS

The first 48 h after $T_3$ exposure is a time when the genetic and proteomic program is established leading to the eventual apoptotic death of the tail tissues. Genomic studies on tadpole tail regression have revealed a number of modulated transcripts (Wang and Brown, 1993; Veldhoen et al., 2002; Helbing et al., 2003; Das et al., 2006; Veldhoen et al., 2006). In comparison, our extensive proteomic analyses showed relatively few changes within the first 48 h of $T_3$ treatment. Nonetheless, in the present study we advance the knowledge of the molecular mechanism of the regressing tadpole tail at the proteome level. Furthermore, the few changes in the (phospho)proteome during this time may be critical, as has been demonstrated by changes which support the transcriptome transition, as observed in a study with the tyrosine kinase inhibitor, genistein, which prevents $T_3$-dependent tail regression likely through inhibition of protein kinase C activity and TR$\alpha$ phosphorylation (Ji et al., 2007).

Our proteomic analyses may be limited in their sensitivity to reveal phosphorylation of low-abundance signaling phosphoproteins since no enrichment was performed. Nevertheless our data suggest that RLK I is posttranslationally modified due to a $T_3$ signal most likely through the early action of caspases thereby indicating an early apoptotic event. Our findings with GILT maturation, Ig heavy chains and cathepsin D increases show that the involvement of the immune system in the regressing tadpole tail may be greater than what has been generally considered. Furthermore, a large proportion of the transcripts identified by genomic studies encode transcription factors (Wang and Brown 1993; Veldhoen et al., 2002; Helbing et al., 2003; Das et al., 2006; Veldhoen et al., 2006) whose protein products are most likely below the detection limits of our 2D PAGE and iTRAQ analyses. An improved fractionation strategy for the iTRAQ analysis may reveal these.

The present study provides important insights into the molecular mechanism of $T_3$-dependent tadpole tail regression during postembryonic development which includes novel components at the proteome level.

# Chapter 4: The involvement of RLKI in apoptosis and caspase cleavage

Published in part in: Veldhoen N, Skirrow RC, Ji L, Domanski D, Bonfield RE, Bailey CM, Helbing CC. Use of heterologous cDNA arrays and organ culture in the detection of thyroid hormone-dependent responses in a sentinel frog, *Rana catesbeiana*. Comparative Biochemistry and Physiology, 2006, Part D 1 187-199.

## 4.1 INTRODUCTION

Previous work has shown that the N-terminal fragment of RLK I (N-term RLKI) was observed in the tail fin of *R. catesbeiana* tadpoles as early as 24 h after $T_3$ exposure (Chapter 3; Domanski and Helbing, 2007). Further experiments with tail fin tissues exposed to 10 nM $T_3$ in an organ-culture setting revealed that N-term RLKI can be produced as early as 12 h after exposure (Figure 4.1A). The appearance of N-term RLKI precedes the appearance of overt morphological changes in the *R. catesbeiana* tail which have been observed to begin after 48 to 72 h with 10 nM $T_3$ (Veldhoen et al., 2006 and figure 4.1 B and C). And although N-term RLKI appears to be a result of caspase mediated cleavage, its appearance is earlier than the reported apoptotic hallmarks in anuran tail metamorphosis such as caspase activity or DNA cleavage, which have been reported to occur no earlier then 24 h after TH treatment (Pasquier et al., 2006; Hanada et al., 2003; Kashiwagi et al., 1999). This includes our report of increased caspase-3-like activity at 72 h and reduced cell proliferation at 48 h in TH-induced *R. catesbeiana* tadpole tail (See figure 4.1 D and E) (Veldhoen et al., 2006). Additionally, the timing of the appearance of N-term RLKI seems to be more in line with the response of early direct response genes such as TRβ, TH/bZip and BTEB whose mRNA expression is detected within 12 h in *X. laevis* tadpole tail (Opitz et al., 2006a; Shi, 1999) and is sooner than the earliest detection of TRβ protein reported to be observed at 20 h (Eliceiri and Brown, 1994). These findings suggest that the presence of N-term RLKI might be more than just an end result of apoptosis and that in turn N-term RLKI may in some way modify the apoptotic process. There is some support in the literature for such modifying actions by intermediate filament proteins. Inada et al. (2001) have shown that keratins K18 and K14, through residues 77-128 in the N-terminus, attenuate apoptosis induced by tumour necrosis factor (TNF) through the binding of the C-terminal end of TNF receptor 1-associated death domain (TRADD) and preventing caspase-8 activation. More interestingly, Byun et al. (2001) have shown that the N-terminal caspase-cleavage product of vimentin, a type III intermediate filament, when

A

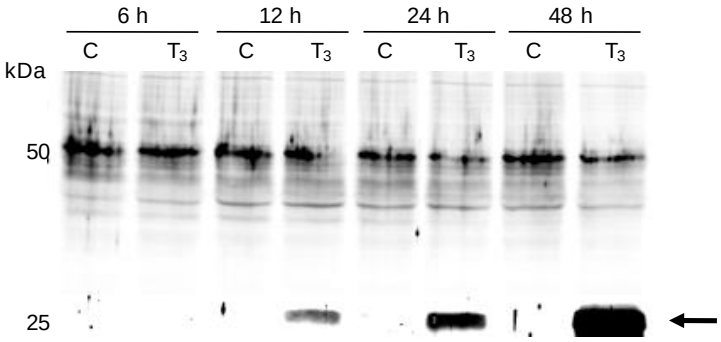
6 h
12 h
24 h
48 h
C
T3
C
T3
C
T3
C
T3
kDa
50
25

B

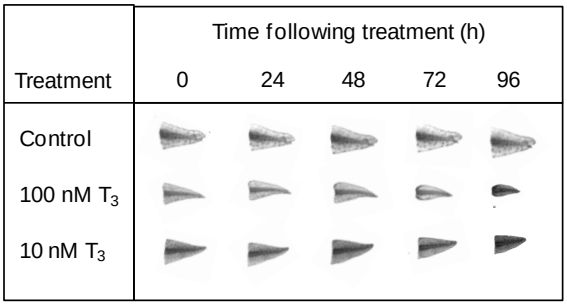
Time following treatment (h)
Treatment
0
24
48
72
96
Control
100 nM T3
10 nM T3

C

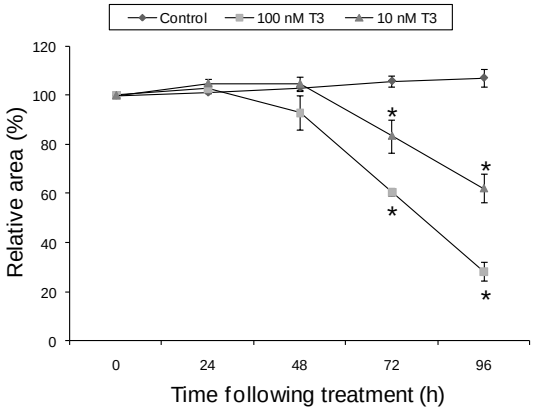
Control
100 nM T3
10 nM T3
Relative area (%)
120
100
80
60
40
20
0
0
24
48
72
96
Time following treatment (h)

D

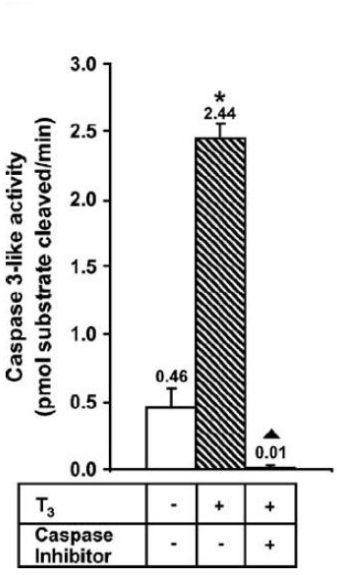
Caspase 3-like activity
(pmol substrate cleaved/min)
3.0
2.5
2.0
1.5
1.0
0.5
0.0
2.44
0.46
0.01
T3
Caspase Inhibitor

E

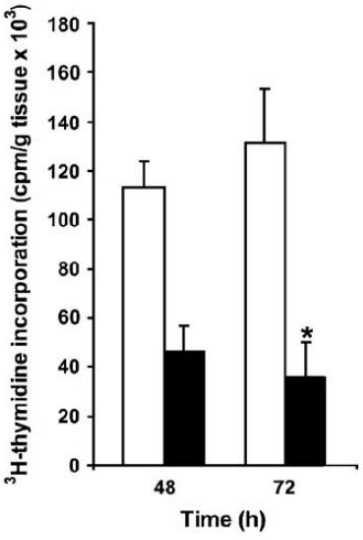
3H-thymidine incorporation (cpm/g tissue x 10^3)
180
160
140
120
100
80
60
40
20
0
48
72
Time (h)

**Figure 4.1. The appearance of N-term RLKI in the tail fin of *R. catesbeiana* occurs before any overt morphological changes or previously reported apoptotic hallmarks.** (A) Time-course expression of N-term RLKI. Premetamorphic *R. catesbeiana* tadpole tail fin tissue (6 mm biopsies) was kept in organ-culture in a serum-free setting for the indicated amount of time in combination with vehicle control (C) or 10 nM $T_3$ ($T_3$). Protein extracts were then analyzed by immunobloting using a pan-cytokeratin antibody. The N-term RLKI fragment is indicated by arrow. Relative molecular weights of protein standards are indicated in kDa. (B and C) $T_3$-induced regression of *R. catesbeiana* cultured tail tips. Two centimeter tail tips were removed from TK stage VI-X tadpoles and cultured in TMEM for 96 hours. Tail tips were treated with vehicle control, 100 nM $T_3$, or 10 nM $T_3$. (B) Representative example of cultured tail tip response to the above treatments. (C) The tail tip area was measured at each time point and plotted relative to the 0 hour time point (n=3-4 per time point). The error bars represent the standard error of the mean. The asterisk indicates significant difference in tail area between tails treated with $T_3$ and those treated with vehicle control ($p<0.05$). (D and E) Changes in cell proliferation and apoptotic activity in premetamorphic *R. catesbeiana* tadpole tails exposed to exogenous $T_3$. (D) Caspase-3-like activity was determined in cultured tail tips treated with either 100 nM $T_3$ or DMSO vehicle for 72 h. Mean caspase-3-like activity in pmol substrate cleaved per minute is shown above each bar. Error bars represent standard error of the mean with n=5 for $T_3$ treatment and n=3 for the DMSO control. A significant increase in activity relative to the DMSO control is indicated by a single asterisk ($p <0.05$) while significant inhibition of this caspase-3-like activity present in the $T_3$-treated samples is identified by a triangle ($p <0.01$). (E) Active DNA replication was examined by pulse labelling with $^3$H-thymidine of cultured tail fin tissue isolated from tadpoles treated with either DMSO vehicle (white bars) or 100 nM $T_3$ (black bars) for 48 h or 72 h. Error bars represent standard error of the mean (n =3 for all $T_3$ treatments and the 48 h DMSO control and n=4 for the 72 h DMSO control) and statistical significant reduction in nascent DNA replication relative to the control at 72 h is denoted by an asterisk ($p <0.05$). Parts D and E have been reproduced from Veldhoen et al. (2006), and part D was performed by Ryan E. Bonfield (Co-op student) under the supervision of D. Domanski.

expressed as a GFP fusion protein induced caspase dependent apoptosis in a transfected cell line. The fact that the N-terminal globular domain of keratins is preferentially phosphorylated during apoptosis (Oshima et al., 2002; Marceau et al., 2001; Ku et al., 2001) additionally suggests that this part of the intermediate filament proteins may play additional roles in the cell than just structural. We therefore hypothesize that the production of the N-terminal fragment of RLKI as a result of the TH signal amplifies or modulates apoptosis in the tail fin tissue. Additionally, further research into how and if RLKI is cleaved by caspase activity is still warranted. For instance, in light of such diseases as epidermolysis bullosa simplex, a genetic blistering skin disease caused by a mutation within the caspase cleavage site VEMDA in keratin K14, that prevents normal caspase cleavage (Ku et al., 2001). This caspase cleavage site is identical to that found in RLKI and it would be of interest to characterize its cleavage. To this end, we studied the effects of N-term RLKI on apoptosis in comparison to the full length protein in the context of TH in a *X.*

*laevis* cell line derived from tadpole tail. Additionally, we investigated whether RLKI is cleaved by a purified caspase and caspase activity in apoptotic cells.

## 4.2 MATERIALS AND METHODS

### *4.2.1 Animal treatment, exposures, tail organ culture and tail measurements*

As discussed in the material and methods section of chapter 2.

### *4.2.2 Organ culture and exposure of tail biopsies*

As discussed in the material and methods section of chapter 5.

### *4.2.3 Caspase-3-like activity assay*

The presence of active caspase-3-like proteases in tail protein extract was determined using the Caspase Colorimetric Substrate/Inhibitor QuantiPak (BIOMOL Research Laboratories Inc, Plymouth Meeting PA USA) based upon *p*-nitroaniline (*p*-NA) release from a caspase-specific substrate according to the manufacturer's protocol. For each 100 µl assay reaction 10 µl (18-24 µg) of protein extract was added to 80 µl of assay buffer (50 mM HEPES, pH 7.4, 100 mM NaCl, 0.1% CHAPS, 10 mM DTT, 1 mM EDTA, and 10% glycerol) and 10 µl of 2 mM Ac–DEVD–*p*-NA colorimetric substrate prepared in assay buffer. To demonstrate that the caspase-3-like activity observed was specific, parallel reactions were performed that included addition of the caspase-3 inhibitor Ac–DEVD–CHO. Inhibitor reactions contained 10 µl protein extract, 70 µl assay buffer, 10 µl of 2 mM Ac–DEVD–*p*-NA substrate, and 10 µl of 0.2 mM Ac–DEVD–CHO inhibitor prepared in assay buffer. To account for background absorbance a third set of parallel null reactions was included that contained 90 µl of assay buffer and 10 µl of protein extract. The absorbance was read at 405 nm with ELx808 Ultramicroplate reader (BIO-TEK Instruments Inc, Winooski VT USA). Measurements were taken every 10 min for 2.5 h and every 0.5 h for an additional 2.25 h. Caspase-3-like specific activity for each reaction was calculated as described in the manufacturer's protocol by plotting the linear relationship between absorbance vs. time. A conversion factor relating the spectrophotometric absorbance of free *p*-NA to molar concentration was also obtained by the average of five $A_{405\ nm}$ readings of 50 µM *p*-NA in assay buffer.

### *4.2.4 $^{3}$H-Thymidine incorporation assay*

To determine the effect of TH on cell division in tadpole tail fin tissue, the extent of incorporation of radioactive [*methyl*-$^{3}$H]thymidine into newly synthesized DNA was measured.

Premetamorphic (TK stage VI-VIII) *R. catesbeiana* tadpoles were exposed to 100 nM $T_3$ or vehicle control DMSO at a dilution of 10,000-fold for 48 or 72 h with the treatments replenished every 24 h. Following exposure tadpoles were euthanized in 0.1% tricaine methanesulfonate and briefly sterilized in 70% ethanol. Dorsal and ventral fin tissue was collected from each 2-cm tail tip region and the four samples from a given treatment and time point were cultured together at 25ºC in air for 6 h in 10 ml TMEM media supplemented with 30 μCi of [*methyl*-$^3$H]thymidine (6.7 Ci/ mmol, 1 μCi/ μl) (PerkinElmer Life Sciences Inc, Boston MA USA). Medium was then removed and the tail fins were washed three times with 10 ml amphibian PBS (128 mM NaCl, 10 mM $Na_2HPO_4$, and 10 mM $NaH_2PO_4$ pH 7.2) pre-cooled on ice. Excess liquid was removed and individual tail fins were weighed and placed into 700 μl of 5% trichloroacetic acid (w/v) pre-cooled on ice. Samples were homogenized using a polypropylene micropestle (Fisher Scientific) and incubated at 4ºC for 30 min. The tissue suspension was centrifuged at 12,000 x g for 5 min and the pellet was washed with cold amphibian PBS and re-centrifuged at 12,000 x g for 5 min. The pellet was then resuspended in 500 μl of 0.5 M NaOH/0.5% SDS and transferred to 10 mL of ScintiVerse scintillation fluid (Fisher Scientific). Samples were measured for incorporation of radioactive thymidine using a Beckman Coulter LS 6000TA liquid scintillation counter (Beckman, Fullerton CA USA). Results were reported as counts per min of incorporated thymidine per g of wet mass of tissue.

### *4.2.5 Construction of expression vectors*

Gene fragments for Full RLKI and N-term RLKI were produced by performing PCR on a premetamorphic (TK stage VI-VIII) *R. catesbeiana* tadpole tail fin cDNA library. Primers used were: ATAGTTGCTAGCCATGGCCGGGCGTTTTAG (P1) and ATTAATGAATTCTTAATCCATCTCTA CGTTGACCTGG (P2) for N-term RLKI, and P1 and ATTAATGAATTCCACAAGCCAGCACCACCT (P3) for Full RLKI. The primers introduced *Nhe* I and *Eco*R I restriction sites and a stop codon as indicated in Figure 2A. The 50 μl PCR reaction consisted of 20 mM Tris-HCl (pH 8.8), 10 mM $(NH_4)_2SO_4$, 10 mM KCl, 0.1% (v/v) Triton X-100, 0.1 mg/ml BSA and 2 mM $MgSO_4$, 200 μM deoxynucleotidylphosphates (dNTPs), 1.6 U of *Pfu* DNA polymerase (all from Fermentas, Burlington ON Canada), 5 pmol of each respective primer (Integrated DNA Technologies, Coralville IA USA), and 4.7 ng of cDNA. The following cycling parameters were used: 94ºC for 1 min, 40 cycles of 94ºC for 30 sec, 55ºC for 30 sec, 72ºC for 30 sec, and 10 min at 74ºC. The expected PCR products of 790 bp and 1530 bp for N-term RLKI and Full RLKI, respectively, were gel purified and extracted using the QIAquick Gel Purification kit (Qiagen, Mississauga ON Canada), and then digested with *Nhe* I

and *Eco*R I restriction endonucleases according to the manufacturer's protocol (New England Biolabs, Beverly MA USA). The pIRES2-EGFP expression vector (BD Biosciences, Burlington ON Canada) was also digested with the *Nhe* I and *Eco*R I restriction endonucleases and subsequently dephosphorylated by calf-intestinal phosphatase according to the manufacturer's protocol (New England Biolabs). The digests were then cleaned using the QIAquick PCR Purification kit (Qiagen). The respective digested PCR products (45 fmol) were ligated with the digested pIRES2-EGFP vector (15 fmol) using T4 DNA ligase according to the manufacturer's protocol (Invitrogen). The ligation reactions were then used to transform *Escherichia coli* TOP10 cells as per manufacturer's instructions (Invitrogen). These were then grown overnight at 37°C on Luria-Bertani (LB) agar plates containing 50 µg/ml kanamycin (Sigma-Aldrich). Positive colonies were found by PCR as indicated above but using primers that spanned the pIRES2-EGFP multiple cloning site: GGTGGGAGGTCTATATAAGCAGAG and ACATATAGACAAACGCACACC GGC, and using *Taq* DNA polymerase (Invitrogen). The positive clones were used to inoculate 5 ml of LB broth containing 50 µg/ml kanamycin and were grown overnight at 37°C with shaking. Plasmids were harvested with a Qiaprep Spin Miniprep kit (Qiagen). The inserted sequences within each of the expression vectors were sequenced using the above primers at the University of Victoria sequencing facility. After the constructs were verified to be free of mutations the proper clones were grown up in 150 ml of LB broth containing 50 µg/ml kanamycin overnight at 37°C with shaking. Plasmids were harvested with a QIAfilter Plasmid Maxi Kit (Qiagen). The appropriate constructs were again verified by restriction digestions. For use in transfections the plasmid DNA was precipitated in 95% ethanol, 0.12 M sodium acetate, thus sterilizing it, then washed in 80% ethanol, and finally resuspended in sterile water. Each of the above steps was checked by agarose gel electrophoresis: agarose gels (1 to 1.5%) were prepared with OmniPur molecular grade agarose powder (EM Science) in 1X TAE buffer (40 mM Tris-acetic acid pH 8.0, 1 mM EDTA) containing 0.0015% ethidium bromide (Invitrogen). DNA samples were loaded in STOP buffer (7.0 M Urea, 50% sucrose, 50 mM EDTA, 0.1% bromophenol blue). Gels were run at 88 V for 45 min. DNA was visualized and photographed with an AlphaImager 2000 Documentation and Analysis System (Alpha Innotech Corporation, San Leandro CA USA).

### *4.2.6 XLT-15 cell line, transfections and treatments*

*X. laevis* XLT-15 cells were propagated at 25ºC in air on 10 cm diameter culture dishes (Primaria, BD Biosciences) by plating 1.6 x $10^6$ cells/plate in 10 ml of 70% strength Leibovitz's L15 medium (Gibco, Invitrogen) supplemented with 10 mM HEPES pH 7.5, with 10% TH-stripped

heat-inactivated fetal bovine serum (HI-FBS) (HyClone, Logan UT USA), and 100 μg/ml gentamicin (Gibco, Invitrogen). TH-stripped serum was prepared by mixing FBS serum with AG-1X-8 resin (Bio-Rad) (50 mg/ml) for 5 h at room temperature and then with fresh resin overnight at 4ºC. The FBS was then filter-sterilized and heat-inactivated at 56ºC for 10 min. For splitting before confluency or other manipulation, cells were washed in magnesium-free medium solution (MFM: 7.5 mM Tris-HCl pH 7.6, 88 mM NaCl, 1mM KCl, 2.4 mM $NaHCO_3$, 0.88 mM $CaCl_2$), detached by 0.05% trypsin with 0.5 mM EDTA and 0.1% glucose in MFM, quenched in 10 volumes of above serum-containing medium, centrifuged at 1500 x g, re-suspended in fresh medium and subsequently plated. For experiments cells were plated at 0.3 x $10^6$ cells/well in a 6-well plate (Primaria, BD Biosciences) in 2 ml of medium as above but without gentamicin. Cells were allowed to attach for 24 h and were then transfected with 2.5 μg of expression construct DNA per well using 5 μl of the *Trans*IT-LT1 transfection reagent as per manufacturer's protocol (Mirus Bio Corporation, Madison WI USA). After another 24 h the cells were rinsed with MFM and exposed to media containing the vehicle control or 10 nM $T_3$. $T_3$ was initially dissolved in 2.5 mM NaOH at $10^{-3}$ M, filter sterilized and stored as stock at -20ºC. For exposures it was diluted in media to $10^{-5}$ M and was then applied at 1 μl/ml of media to the cells, giving a final concentration of 10 nM $T_3$ with NaOH at 25 nM. The vehicle control was prepared in the same manner giving a final concentration of 25 nM NaOH. For non-transfected cells $T_3$/control-treatment began 24 h after plating. Cells were treated for 24, 48 or 72 h, without any media changes at 25ºC in air. All experiments were performed independently three times.

### *4.2.7 Flow cytometry*

At the end of the treatment period adherent XLT-15 cells were removed from the plate by trypsinization as indicated above, while the detached cells were collected from the medium. Cells were collected by centrifugation at 1500 x g, rinsed once in MFM, re-suspended in 200 μl for adherent cells or 100 μl for detached cells in annexin V binding buffer: 10 mM HEPES pH 7.4, 140 mM NaCl, 2.5 mM $CaCl_2$. 100 μl of each cell suspension was mixed with 5 μl of annexin V-PE and 5 μl of 7AAD (BD Biosciences), and incubated at room temperature for 15 min., subsequently 400 μl of annexin V binding buffer was added and the cells were analyzed by flow cytometry. Cells were analyzed on a FACSCalibur flow cytometry system (BD Biosciences) using a 488 nm argon-ion laser for excitation and three channels for detection of fluorophores: FL1 for EGFP (530/30 nm), FL2 for annexin V-PE (585/42 nm), FL3 for 7AAD (661/16 nm). Forward scatter (FSC) and side scatter (SSC) data were also collected. Voltage settings for

detectors were set as following: FSC at E-1V with amplification gain of 6.40, SSC at 400V with amp. gain of 1.0, FL1 at 430V, FL2 at 550V, and FL3 at 615V. Compensation settings were as follows: for annexin V-PE at FL3-%FL2 of 8.5%, and for EGFP at FL2-%FL1 of 17.5%. 10,000 events were collected per sample, with each sample being measured three times, and the data averaged. Data was analyzed using WinMDI 2.9 software (Joseph Trotter, Scripps Research Institute, La Jolla CA USA).

### *4.2.8 Microscopy*

Transfected XLT-15 cells were also analyzed by epifluorescence microscopy on a Carl Zeiss Axioskop 2 Plus fluorescent microscope (Carl Zeiss Canada, Toronto ON Canada) with a digital camera (DVC Company, Austin TX USA) and Northern Eclipse v5.0 imaging software (Empix Imaging Inc, Mississauga ON Canada). Cells were grown as indicated above but on sterilized glass cover-slips in 6-well plates (Primaria, BD Biosciences), and stained in a volume of 100 µl as indicated above for the flow cytometry analysis except that annexin V was conjugated to Alexa Fluor-350 (Invitrogen) and PI (Invitrogen) was used instead of 7AAD.

### *4.2.9 Immunoblotting*

Cells were washed once in MFM, scraped with a cell scraper if adherent cells and collected by centrifugation at 1500 x g. Protein samples were extracted by first solubilizing the cells in 50 µl of 20 mM HEPES pH 7.5, 8 M urea, 0.2% SDS and 100 mM DTT by trituration, then 150 µl of 20 mM HEPES pH 8.0, 2.67 M urea and 2.67 mM $MgCl_2$ was added giving a final concentration of 20 mM HEPES pH 8.0, 4 M urea, 2 mM $MgCl_2$, 0.05% SDS and 25 mM DTT to which benzonase (Sigma-Aldrich) could be added (10 U/ml) to digest DNA, and incubated at 4ºC for 20 min. The extract was centrifuged at 12,000 x g for 10 min. at 4ºC and the supernatant was stored at -70ºC. Protein concentrations were determined as indicated before except BSA standards were made up in the above buffer. SDS-PAGE analysis and immunoblotting were performed as indicated before with the following modifications. Protein samples (8-10 µg protein depending on experiment) in addition to containing the loading buffer were adjusted to contain equal amounts of salts with above extraction buffer and were heated at 60ºC for 10 min. Proteins were electrophoretically transferred onto a nitrocellulose membrane using tank blotting (Bio-Rad) in 25 mM Tris-base pH 8.3, 192 mM glycine and 20% methanol at 90 V for 30 min. After the transfer, blots were dried overnight. The primary antibody was a pan-cytokeratin rabbit polyclonal IgG antibody raised against amino acids 181-420 of human keratin 10 (H-240; Santa Cruz

Biotechnology Inc., Santa Cruz CA USA) diluted at 1/500 and exposed to blot for 1.5 h at room temperature.

*4.2.10 Caspase-3 cleavage of Full RLKI*

Protein extracts from adherent XLT-15 cells transfected with the Full RLKI expression construct or empty pIRES2-EGFP vector were obtained by lysing the cells in 25 µl of 50 mM HEPES pH 7.4, 100 mM NaCl, 0.5% CHAPS, 1 mM EDTA, 10% glycerol, and 10 mM DTT for 20 min. on ice, and then centrifuging at 12,000 x g for 10 min. at 4ºC. The supernatant was stored at -70ºC. Protein concentrations were determined as indicated before except BSA standards were made up in the above buffer. The samples consisted of empty vector transfected cells 72 h post transfection and Full RLKI construct containing cells 24, 48 and 72 h post transfection. 10 µg protein amounts in 8 µl of buffer (as above) were incubated with 50 U of recombinant human caspase-3 (MP Biomedicals, Aurora OH USA) or equivalent amount of buffer as control, for 1 h at 30ºC. Samples were then analyzed by immunoblotting as indicated above with loading a 10 µg protein amount.

## 4.3 RESULTS

*4.3.1 Transfection of RLKI expression vectors into the X. laevis cell line, XLT-15*

Two expression plasmids were built, one expressing the gene for the full length RLK I (Full RLKI) protein and another expressing part of the gene, producing the N-terminal fragment of RLK I (N-term RLKI) that is the product of caspase cleavage. This was achieved by performing PCR on a cDNA library of *R. catesbeiana* tadpole tail using a high fidelity Pfu DNA polymerase with the combination of primers as shown in Figure 4.2A. Primers P1 and P2 were used to generate the product for the N-term RLKI fragment. Both primers introduced restriction endonucleases cut sites and additionally the P2 primer introduced a stop codon in place of the alanine codon in the consensus caspase cleavage site VEMDA, resulting in a truncated RLK I protein ending with the aspartate as is the case for the caspase cleaved product. Primers P1 and P3 were used to generate the product for the full length RLK I. The introduced restriction sites allowed for the insertion of the PCR products in the correct orientation into the multiple cloning site (MCS) in the pIRES2-EGFP vector (Figure 4.2B). The pIRES2-EGFP vector allows for the expression of the cloned gene and the enhanced green fluorescent protein (EGFP) gene in a single message. The internal ribosomal entry site (IRES) within the message between the gene of interest and the EGFP gene allows for separate translation of each gene. Thus transfected cells

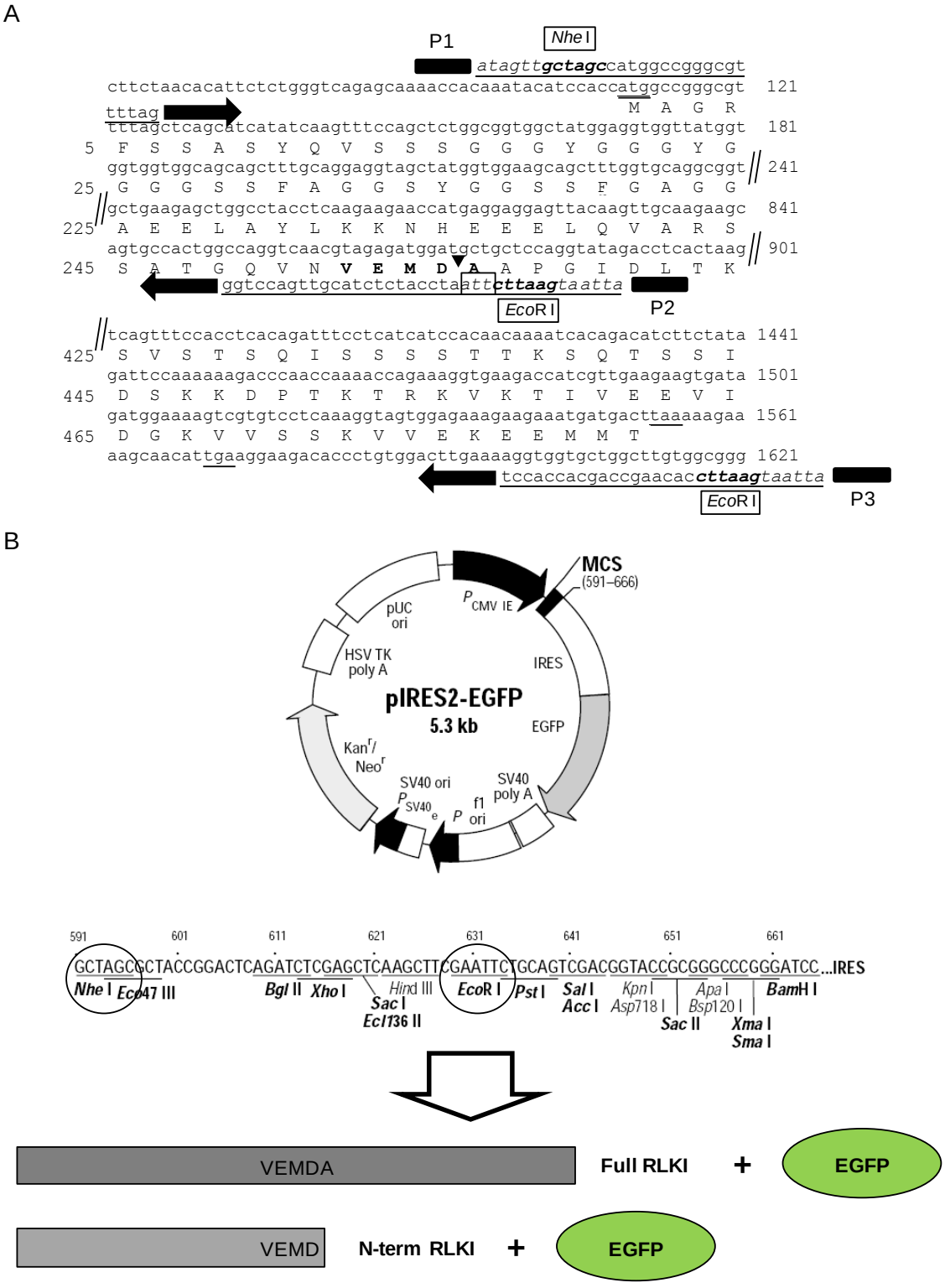


**Figure 4.2. Construction of expression vectors for Full-RLKI and N-term RLKI proteins.** (A) Primers used to generate the proper gene fragments to be inserted into the expression vector are indicated as P1, P2 and P3 (black arrows with sequence underlined), overlaid on the partial

RLK I cDNA and derived amino acid sequence. The consensus caspase cleavage site is indicated in bold (VEMDA) with the black inverted-triangle indicating the cleavage point. Omitted RLK I sequence for the purpose of presentation is indicated by two vertical dashes on the sides. Numbers on the left indicate amino acid position and numbers on the right indicate nucleotide position. P1 and P2 were used to generate the product for the N-term RLKI construct, and P1 and P3 were used to generate the product for the Full RLKI construct. Non-priming sequence within the primers is shown in italics and was used to introduce endonuclease restriction sites (bold sequence and enzyme name indicated in box above or below), and in the case of P2 a stop codon (boxed sequence). Short underlined sequences in the cDNA sequence indicate the initiating methionine codon and stop codons. (B) Annotated map (adapted from BD Biosciences Clontech) of the expression vector pIRES2-EGFP indicating the multiple cloning site (MCS) position and sequence below with the restriction sites (circled) used to generate the two expression constructs that produced the full length protein (Full RLKI) and the truncated N-terminal fragment (N-term RLKI).

---

producing EGFP are also likely producing the protein of interest, both as separate proteins. In this case, two expression plasmids were made to produce either the Full RLKI or the N-term RLKI in combination with EGFP (Figure 4.2B). The inserted genes were sequenced in both plasmids to ensure correct placement within the vector and that no mutations were introduced during the cloning process guaranteeing that the expressed proteins have the same amino acid sequence as was originally found (See chapter 3; Domanski and Helbing, 2007).

The objective was to test the effect of N-term RLKI on apoptosis of cells in the context of TH. This would be compared to the effect of Full RLKI to see if the effect is due to the presence of the N-terminal fragment of the protein and not the full length protein. We chose to use the *X. laevis* myoblastic cell line, XLT-15, derived from the tadpole tail (Yaoita and Nakajima, 1997). This cell line has been reported to be responsive to $T_3$ by undergoing apoptosis. Yaoita and Nakajima reported that a 10 nM $T_3$ treatment decreased the number of normal nuclei from around 80% to 50% to 40% when compared to control, after 24, 48 and 72 h, of treatment respectively. Apoptosis was also demonstrated by TUNEL (terminal deoxynucleotidyltransferase-mediated dUTP-X nick end labeling) and electrophoresis of genomic DNA (Yaoita and Nakajima, 1997). Cells had to be exposed to $T_3$ for at least 24 h for it to have this effect. We speculated that this TH-responsiveness and the origin of the cells would place the RLKI proteins in a context as closely as possible to that of the regressing tadpole tail. The sensitivity of these cells to $T_3$ was examined as shown in Figure 4.3A and B. The XLT-15 cells were exposed to 10 nM $T_3$ for 24, 48 and 72 hours. Cells were analyzed by flow cytometry with staining for cells in early apoptosis with annexin V conjugated to phycoerythrin (PE) and distinguished from late apoptotic cells or necrotic cells by staining with the 7-Amino-actinomycin D (7AAD) DNA binding dye. Figure

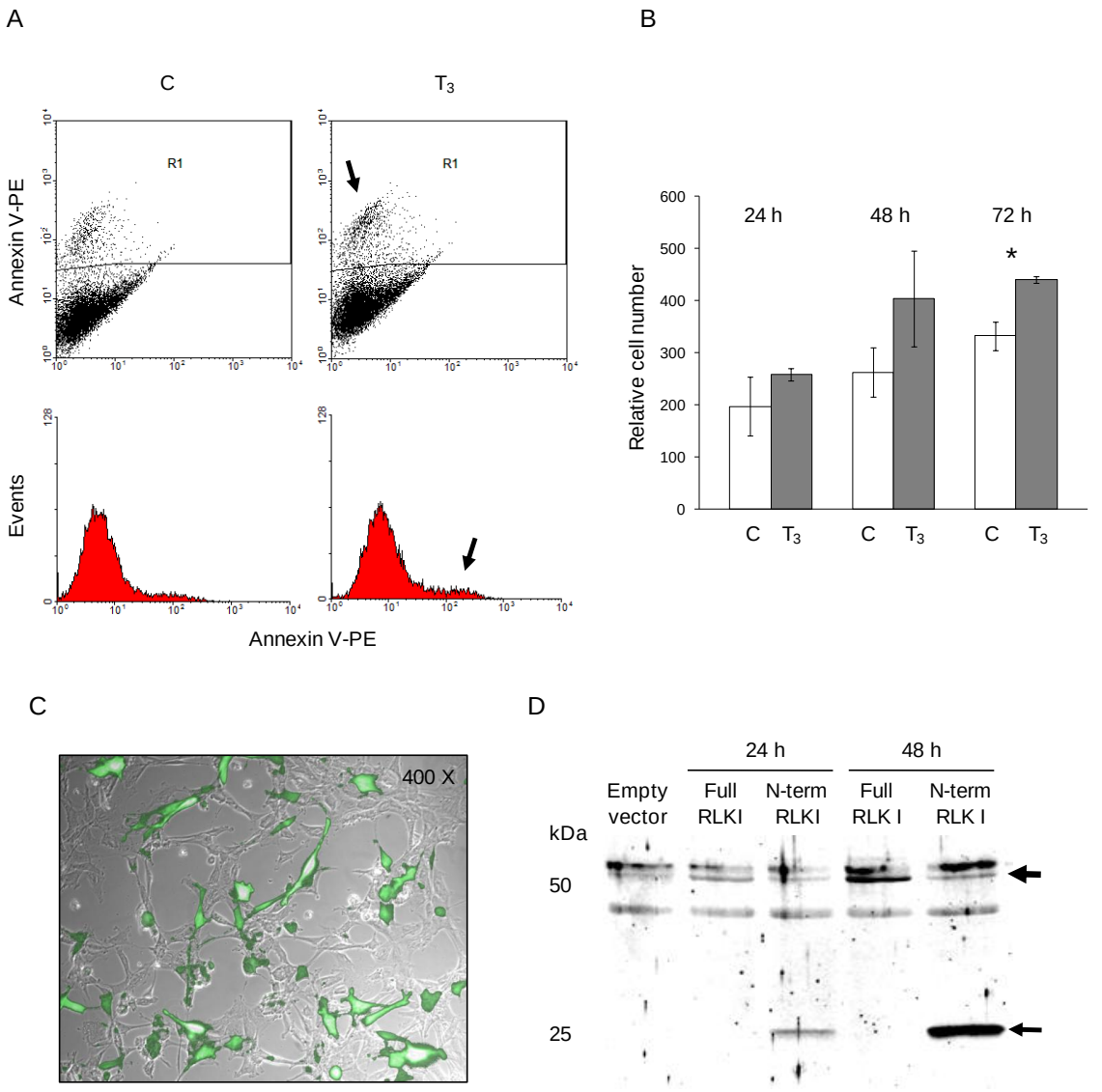


**Figure 4.3. XLT-15 cells respond to $T_3$ by undergoing apoptosis and express proteins from the expression constructs.** (A) Flow cytometry analysis of XLT-15 cells exposed to vehicle control (C) or 10 nM $T_3$ ($T_3$) for 72 h, stained with annexin V-PE. Dot plots show fluorescence of annexin V-PE on the y-axis against the FL1 channel on the x-axis (blank in this analysis) with each dot representing a separate cell for a total of 10,000 events. Histograms show number of events (cells) at different intensity levels of annexin V-PE fluorescence. An increase in the number of annexin V-PE positive cells due to $T_3$ is indicated by arrows. 7AAD positive cells are gated out. (B) Flow cytometry results from three independent experiments representing number of cells in early apoptosis (annexin V-PE positive and 7AAD negative) due to a 10 nM $T_3$ ($T_3$) exposure for the indicated amount of time, compared to vehicle control (C) at each time point. Error bars represent the standard error of the mean, and significance is indicated by an asterisk for $p < 0.05$ (Mann-Whitney U). Looking at early and late apoptotic cells (annexin V-PE positive with or without 7AAD) in combination provided the same profile but the data is not presented as these can also include necrotic cells. (C) XLT-15 cells transfected with the Full-RLKI construct

48 h post transfection observed at 400X with epifluorescence microscopy. Shown is visible light image overlaid with EGFP fluorescence image revealing EGFP-expressing transfected cells (green). (D) Immunoblot of protein extracts (8.4 μg per sample) from XLT-15 cells transfected with the empty vector (48 h post transfection), and the Full RLKI and N-term RLKI expressing constructs, 24 and 48 h post transfection, probed with a pan-cytokeratin antibody. Arrows indicate the expected N-term RLKI fragment (small arrow) and the Full RLKI protein (larger arrow). Relative molecular weights of protein standards are indicated in kDa.

4.3A shows representative dot plots and corresponding histograms showing annexin V-PE staining, without 7AAD staining (i.e. early apoptosis) in the control and $T_3$ samples at 72 h, indicating a slight increase in the amount of early apoptotic cells due to $T_3$. Figure 4.3B shows the averaged data for three replicate experiments, indicating a slight increase in early apoptotic cells due to $T_3$ at each of the three time points, with only the 72 h time point being statistically significant ($p<0.05$). In addition, late apoptotic/necrotic cells gave the same profile, and very few cells were observed to detach throughout the $T_3$ treatment (data not shown). Although the degree to which the cells underwent apoptosis due to $T_3$ appeared to be lower to that reported in the literature, the cells were used in further experiments as a modulation to apoptosis would still be observed.

The XLT-15 cells were transfected with the Full RLKI or the N-term RLKI expression constructs yielding around a 20% transfection efficiency based on EGFP expression (Figure 4.3C). Protein expression was verified by immunoblot analysis using a pan-cytokeratin antibody (Figure 4.3D). Expression of the N-term RLKI and the Full RLKI proteins was detected at 24 h after transfection and became higher at 48 h. The size of the N-term RLKI and Full RLKI proteins was as expected at 25 kDa and 52 kDa, respectively. The immunoblot analysis additionally revealed that the XLT-15 cell line, although of myoblastic and not epithelial origin, may contain three native keratins in the range of around 50 kDa, although this was not unequivocally confirmed.

### *4.3.2 Modulation of apoptosis by N-term RLKI*

The effects of N-term RLKI on apoptosis in the XLT-15 cells were initially assessed by epifluorescence microscopy (Figure 4.4A). EGFP-expressing cells (green) indicated cells expressing the Full RLKI or N-term RLKI proteins. Cells in early apoptosis were detected by staining with annexin V conjugated to a fluorophore (blue) which binds to phosphatidylserine (PS) that is exposed on the outer cell membrane in the early stages of apoptosis (van den Eijnde 1998, van Engeland 1996, Vermes 1995). A membrane impermeant nucleic acid binding dye (propidium iodide (PI) or 7AAD) (red) was used to indicate cells that lost membrane integrity

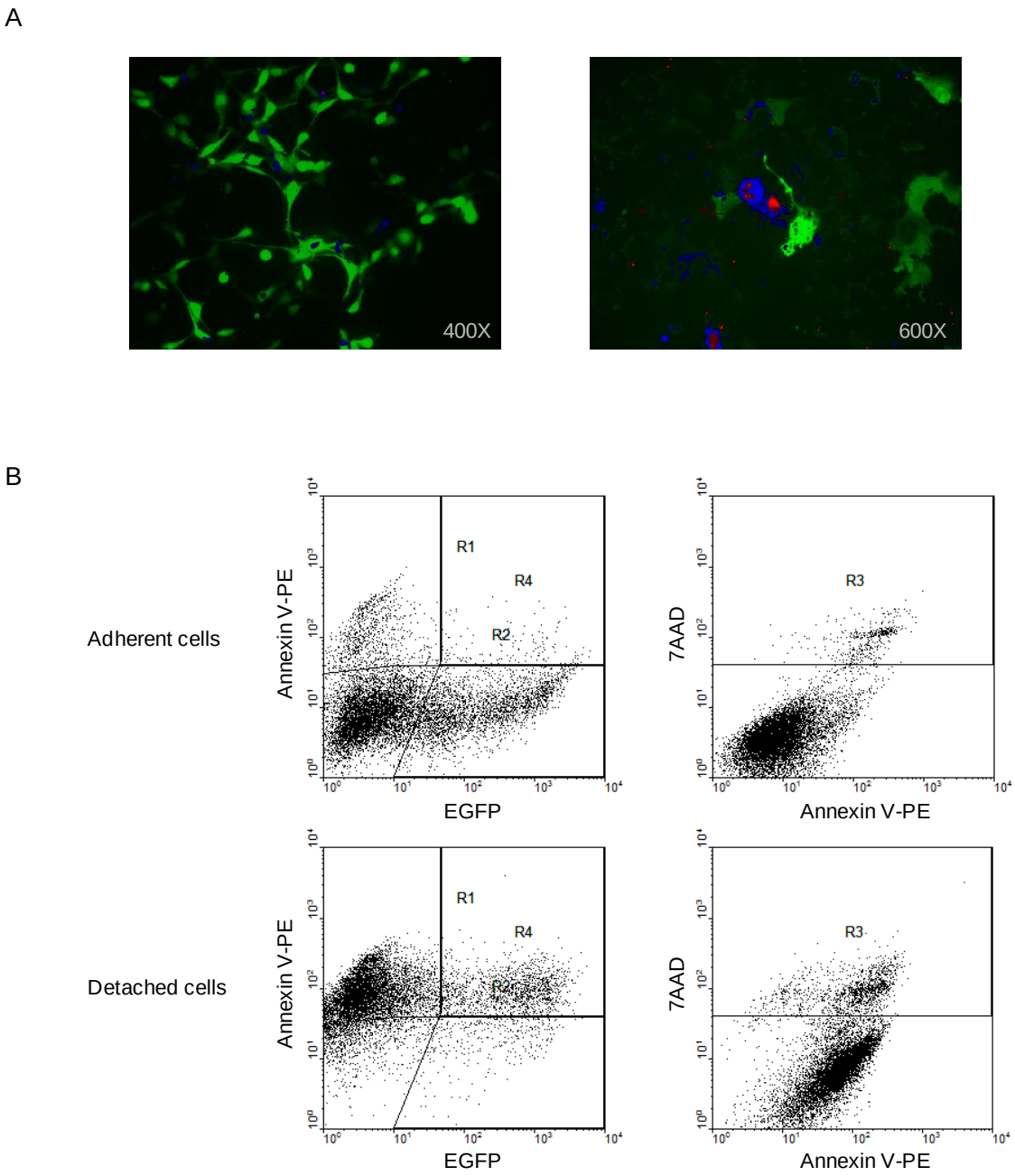


**Figure 4.4. Analyzing apoptosis in XLT-15 cells by epifluorescence microscopy and flow cytometry.** (A) Epifluorescence microscopy images of XLT-15 cells transfected with the Full RLKI construct revealing the expression of EGFP (green) and staining of early apoptotic cells (annexin V-350; blue only) and late apoptotic or necrotic cells (annexin V-350 and PI; blue and red). Magnification is indicated in bottom right-hand corner. (B) Flow cytometry dot plots of fluorescence (log scale) for different channels used to capture signal for EGFP, annexin V-PE and 7AAD. Each dot represents a single cell for a total of 10,000 events measured. Regions used to calculate the number of cells in different states for the adherent and detached cells are indicated. Region 1 (R1) consists of top two quadrants (in EGFP vs. annexin V-PE dot plot) measuring all

annexin V-PE positive cells. Region 2 (R2) consists of two right-hand quadrants measuring all EGFP-expressing cells. Region 4 (R4) consists of top right-hand quadrant measuring all EGFP-expressing cells that are annexin V-PE positive. Region 3 (R3) (in annexin V-PE vs. 7AAD dot plot) measures all 7AAD positive cells.

---

either due to necrosis or the late stages of apoptosis. In combination, these fluorescent dyes allowed to distinguish between apoptotic (annexin V positive only) and necrotic or late apoptotic cells (annexin V and PI/7AAD positive). Fluorescence microscopy, although revealing that it was possible to use the above methods to detect EGFP expression and apoptotic cells in the amphibian XLT-15 cells, proved inadequate for the analysis of many cells that would be required to acquire meaningful data as only a few hundred cells could be realistically measured per sample. Flow cytometry, where 10,000 cells are analyzed per sample, was therefore used to detect the effects of N-term RLKI on apoptosis. For flow cytometry annexin V-PE was used with 7AAD. The fluorescent dyes were chosen to have distinct emission wavelengths from each other and from EGFP, and could be detected on separate channels by the flow cytometer as indicated in Appendix 4.1. XLT-15 cells transfected with the vector and stained with annexin V-PE and 7AAD are shown in Figure 4.4B. In the experiments to assess the effects on apoptosis, both, adherent cells that remained attached to the plate, and cells that detached from the bottom of the plate and were found in the medium, were analyzed separately. The regions that were used to quantify the different states of the cells are indicated in Figure 4.4B. Region 1 (R1) represented by the top two quadrants measured all of the annexin V-PE positive cells. Region 2 (R2) represented by the right-hand two quadrants measured all the EGFP positive and therefore protein (N-term RLKI or Full RLKI) expressing cells. Region 4 (R4) represented by the top right-hand quadrant measured all the EGFP positive cells that are also annexin V-PE positive, and therefore represent the cells that are expressing the respective proteins of interest and are undergoing apoptosis. To ensure that those measured annexin V-PE positive cells, represented cells in early apoptosis and not necrotic or late apoptotic cells, the cells indicated by region 3 (R3) which are 7AAD positive, were gated out (i.e. removed) in the calculations. The same regions were used to measure the separate adherent and detached cell populations (Figure 4.4B).

***Analysis of adherent cells***

The effect that N-term RLKI has on apoptosis in XLT-15 cells was measured in the presence and absence of 10 nM $T_3$, with cells being exposed for 24, 48 and 72 hours, and is compared to cells expressing the full length protein (Full RLKI). This comparison is made to the full length protein and not to an empty vector since the hypothesis is that it is the characteristic of the N-terminal

fragment and not the full length protein that modulates apoptosis. Figure 4.5 shows the results for the adherent cells (washed free of detached cells) which remained attached to the plate throughout the respective time-point after $T_3$ treatment. Although apoptosis is eventually likely to induce detachment of the cells, any change in the number of apoptotic cells between the treatments should be reflected in the number of cells in early apoptosis attached to the plate. Figure 4.5A shows representative dot plots for EGFP and annexin V-PE fluorescence for the N-term RLKI and Full RLKI transfected cells. As shown in Figure 4.5B, based on three independent replicates, EGFP and therefore protein expression peaks at 48 h for both N-term RLKI and Full RLKI, and there is a higher proportion of cells expressing the N-term RLKI construct at each time point, indicating a slightly higher transfection efficiency for that construct. The presence of $T_3$ appears to have no effect on EGFP expression at any of the time points. When the EGFP-expressing cells are analyzed for early apoptosis (Figure 4.5C) it appears that there are more N-term RLKI expressing cells in early apoptosis compared to Full RLKI, however, if the total number of EGFP-expressing cells by each construct is taken into account (i.e. expressed as percent), no differences are found between the two constructs (Figure 4.5D). The fact that the same proportion of EGFP-expressing cells are undergoing apoptosis for both constructs, indicates that the expression of N-term RLKI does not increase or decrease early apoptosis. When all the cells (EGFP-expressing and non-EGFP-expressing) are analyzed for signs of early apoptosis (Appendix 4.2A) or late apoptosis (Appendix 4.2B), no significant differences are found between any of the treatments, except for a slight increase in death by 72 h for both constructs as is also seen in figure 4.5D. The only suggested treatment difference that is observed in Figure 4.5D is a slight increase in early apoptotic cells due to $T_3$ at the 72 h time point for both constructs, however, this difference is not statistically significant. This inability to observe a significant increase in apoptosis at 72 h, as was observed for the untransfected XLT-15 cells (Figure 4.3B), does not indicate a protection from apoptosis due to transfection with either construct. This is indicated by a comparison of early apoptosis in EGFP-expressing cells to non-EGFP-expressing cells at 72 h, where the expression of either protein (N-term RLKI or Full RLKI) does not indicate any protection (Figure 4.5E). An interesting observation from this comparison was at the 24 h time point where the expression of either construct appears to provide less apoptotic cells, as compared to the non-EGFP-expressing cells, which is independent of $T_3$ exposure (Figure 4.5E). This might imply that the expression of either keratin protein, N-term RLKI or the Full RLKI, could provide protection against general cell apoptosis, at least at the 24 h time point. Although this observation would be more definite if it was made to an empty vector control instead, as this decrease in apoptosis could be an effect of taking up a plasmid or just EGFP expression.

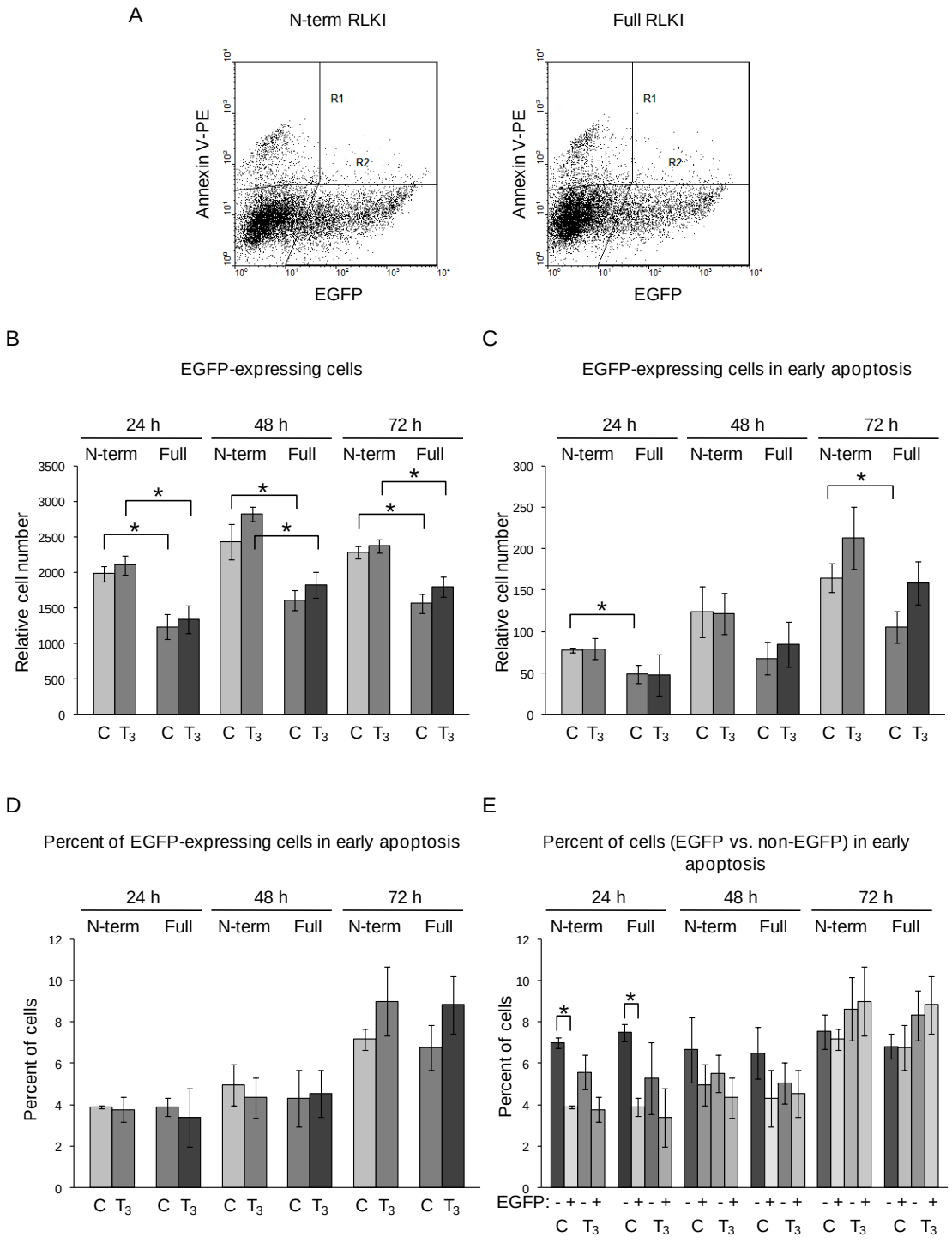


**Figure 4.5. Flow cytometry analysis of apoptosis in adherent XLT-15 cells transfected with N-term RLKI and Full RLKI expression constructs in the presence and absence of $T_3$.** (A) Representative dot plots of EGFP and annexin V-PE fluorescence for control XLT-15 cells transfected with N-term RLKI and Full RLKI constructs at 48 h. Fluorescence is on log scale, with each dot representing a single event (cell) out of 10,000 events. Regions used are also

indicated (as in Figure 4.4B). (B to E) Bar graph representation of flow cytometry data based on three independent replicate experiments. XLT-15 cells were transfected with the N-term RLKI or Full RLKI expression construct and exposed to vehicle control (C) or 10 nM $T_3$ ($T_3$) for the indicated period of time. Relative cell number indicates number of events per 10,000 cells analyzed. Error bars represent the standard error of the mean, and significance is indicated by an asterisk for $p < 0.05$ (Mann-Whitney U). (B) Number of all EGFP-expressing cells (Region 2). (C) Number of EGFP-expressing cells that are also in early apoptosis (Region 4 minus region 3). (D) Percentage of EGFP-expressing cells that are in early apoptosis (Region 4 minus region 3, as percentage of region 2). (E) Comparison of percent of cells that are in early apoptosis, for cells that are EGFP-expressing (+) or non-EGFP-expressing (-) (Percent of EGFP-expressing determined as for D. Percent of non-EGFP-expressing is: region 1 (minus region 3 and 4) as percentage of 10,000 minus region 4.

***Analysis of detached cells***

A population of cells appeared to detach during the course of our experiments and the reason was associated with the transfection procedure, and occurred equally for the empty vector as well as the two expression constructs (data not shown). For this reason and for the fact that modulations to apoptosis may be observed in the detached cells, this population was also analyzed by flow cytometry (Figure 4.6). Figure 4.6A shows representative dot plots for EGFP and annexin V-PE fluorescence for the N-term RLKI and Full RLKI transfected cells. As is observed, the majority of the detached cells are annexin V-PE positive, and there is a larger fraction of EGFP-expressing cells for N-term RLKI (circled) construct than for the Full RLKI construct. This is represented in Figure 4.6B by the bar graphs, indicating a significant difference between the two constructs in EGFP-expressing cells. Looking at the number of EGFP-expressing cells in early apoptosis (Figure 4.6C) indicates that there are more dying cells expressing N-term RLKI, however, when the number of EGFP-expressing cells is taken into account, no differences in early apoptosis are observed between the two constructs (Figure 4.6D). These graphs also indicate that the majority of the cells are in the early stages of apoptosis, versus necrosis or late apoptosis, even at the 72 h time point. As for the adherent cells, $T_3$ does not appear to have any effects. When all the cells (EGFP-expressing and non-EGFP-expressing) are analyzed for signs of early apoptosis (Appendix 4.2C) or late apoptosis (Appendix 4.2D), no significant differences are found between any of the treatments.

Flow cytometry measures the number of cells labelled with a specific fluorophore within a sample of 10,000 cells analyzed, therefore reporting relative and not absolute cell numbers for the treatment. However, if cell proliferation of the transfected cells is assumed to be equal between the two constructs, based on equal cell plating and equal treatments, an additional observation

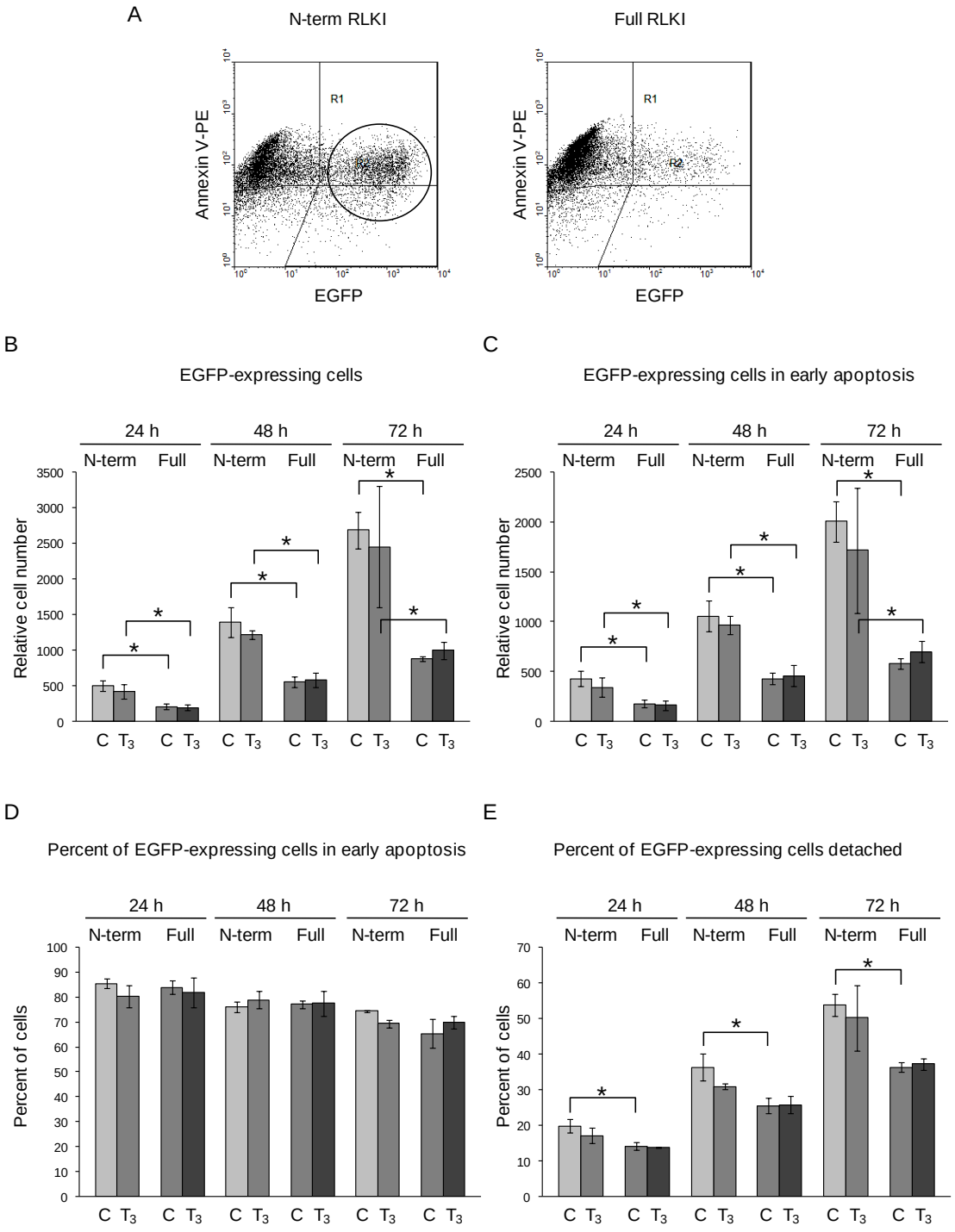


**Figure 4.6. Flow cytometry analysis of apoptosis in detached XLT-15 cells transfected with N-term RLKI and Full RLKI expression constructs in the presence and absence of $T_3$.** (A) Representative dot plots of EGFP and annexin V-PE fluorescence for control XLT-15 cells transfected with N-term RLKI and Full RLKI constructs at 48 h. Fluorescence is on a log scale, with each dot representing a single event (cell) out of 10,000 events. Regions used are also indicated (as in Figure 4.4B). (B to E) Bar graph representation of flow cytometry data based on

three independent replicate experiments. XLT-15 cells were transfected with the N-term RLKI or Full RLKI expression construct and exposed to vehicle control (C) or 10 nM $T_3$ ($T_3$) for the indicated period of time. Relative cell number indicates number of events per 10,000. Error bars represent the standard error of the mean, and significance is indicated by an asterisk for $p < 0.05$ (Mann-Whitney U). (B) Number of all EGFP-expressing cells (Region 2). (C) Number of EGFP-expressing cells that are also in early apoptosis (Region 4 minus region 3). (D) Percentage of EGFP-expressing cells that are in early apoptosis (Region 4 minus region 3 as percentage of region 2). (E) Number of detached EGFP-expressing cells (from B) expressed as percentage of all EGFP-expressing cells measured (detached EGFP-expressing cells plus adherent EGFP-expressing cells (Figure 4.5B)).

about the proportion of detached cells between the two constructs could be made. This is shown in Figure 4.6E where the percentage of EGFP-expressing cells that detached is presented, revealing that the N-term RLKI expressing cells are detaching at a higher proportion than the Full-RLKI expressing cells. This number is derived from the amount of EGFP-expressing cells that detached compared to the total number of EGFP-expressing cells measured in both the adherent and the detached cell populations. Therefore, although no obvious differences were observed in the amounts of apoptotic cells between the constructs within the 72 h tested, there appears to be an increase in cell detachment caused by N-term RLKI, even after compensating for differences in transfection efficiency between the two constructs. The possibility that N-term RLKI is increasing cell detachment is a plausible scenario but due to the stated assumptions it is presented here as a suggestion. The above results would be more substantial if absolute cell numbers could be measured or if cell proliferation was taken into account for each construct and verified to be the same.

### *4.3.3 Caspase cleavage of RLKI*

The evidence that RLK I is cleaved by caspase activity has only come from the indirect observations that it possesses the consensus caspase cleavage site VEMDA and that a 25 kDa N-terminal fragment is produced in the tail after $T_3$-induced metamorphosis. The apoptotic death of the detached XLT-15 cell population, due to the transfection procedure, provided an environment where the cleavage of Full RLKI could be detected. Figure 4.7A shows the progression of apoptosis over a 72 h period of XLT-15 cells transfected with the Full RLKI construct. Cells that are adherent reveal few annexin V-PE positive cells indicating that there is a small amount of apoptosis occurring. In contrast, the detached cells undergo apoptosis, progressively moving from early apoptosis (annexin V-PE positive and 7AAD negative) at 24 h to late apoptosis (annexin V-PE and 7AAD positive) at 72 h. XLT-15 cells have been shown to increase caspase mRNA expression (caspase-3) and activity (caspases-3,-6, and -7) upon apoptosis (Yaoita and Nakajima,

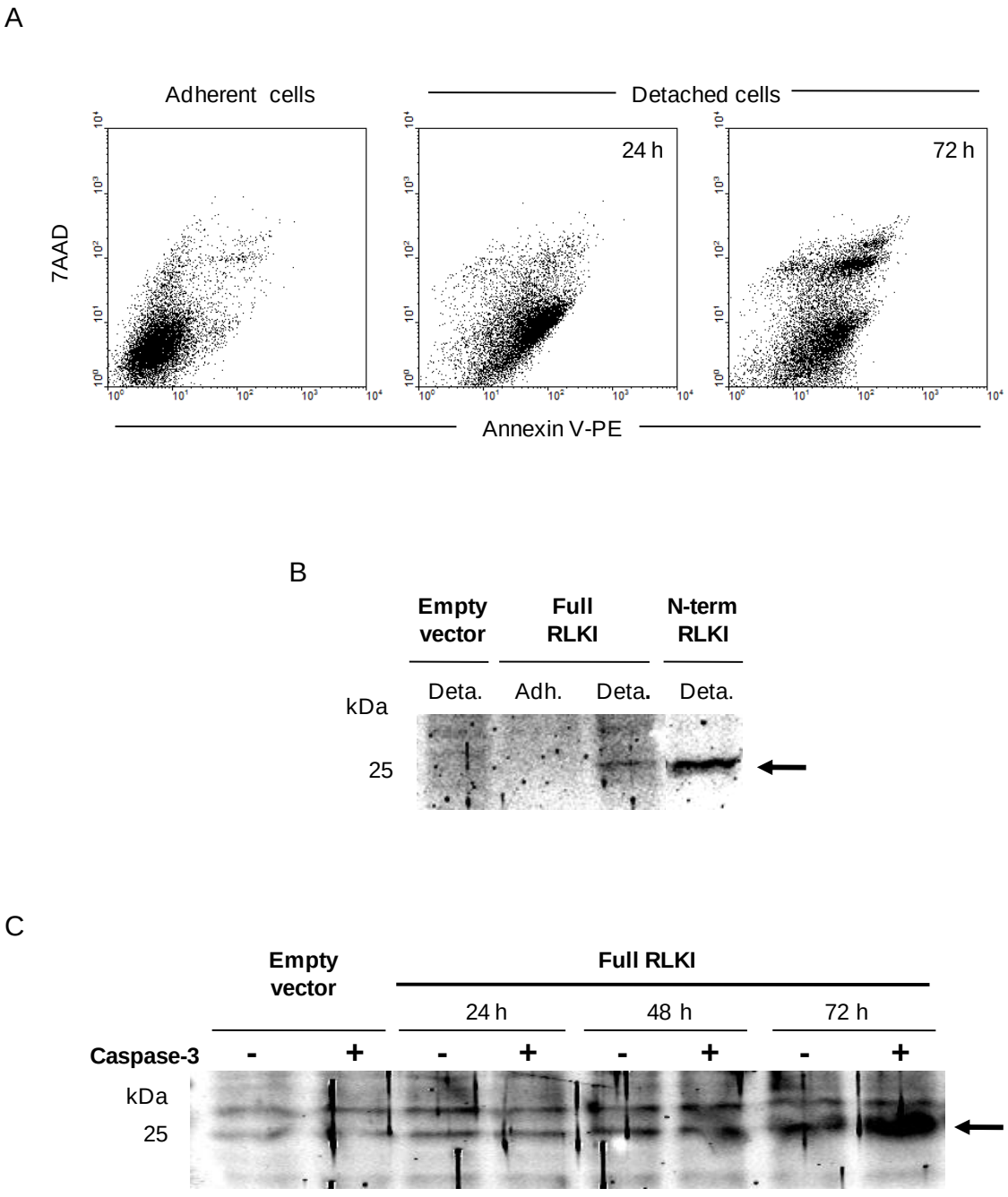


**Figure 4.7. Cleavage of Full RLKI in apoptotic XLT-15 cells and by caspase-3.** (A) Flow cytometry dot plots with annexin V-PE fluorescence on the x-axis and 7AAD fluorescence on the y-axis showing the progression in apoptosis of XLT-15 cells transfected with the Full RLKI construct, going from attached cells (48 h) to detached cells at 24 and 72 h post transfection. Fluorescence is on a log scale, with each dot representing a single event (cell) out of 10,000 events. (B) Immunoblot of protein extracts (10 μg) from detached (Deta.) and adherent (Adh.) XLT-15 cells transfected with empty vector, Full RLKI construct or N-term RLKI construct 48 h post transfection, probed with a pan-cytokeratin antibody. Arrow indicates the expected N-term

RLKI fragment. Relative molecular weights of protein standards are indicated in kDa. (C) Immunoblot of protein extracts (10 μg) from XLT-15 cells transfected with empty vector or Full RLKI construct incubated in the presence (+) or absence (-) of active recombinant human caspase-3, probed with a pan-cytokeratin antibody. Empty vector extract is 72 h post transfection and Full RLKI extracts are as indicated. Arrow indicates the expected N-term RLKI fragment.

1997; Nakajima et al., 2000) and we therefore tested if apoptotic cells transfected with Full RLKI would cleave this full length protein. Figure 4.7B shows that indeed detached apoptotic cells expressing Full RLKI produce a fragment at 25 kDa, in the exact position as the N-term RLKI protein, in contrast to attached cells or empty vector-transfected detached cells. This supports the notion that RLK I is cleaved by caspase activity during apoptosis. We further tested whether Full RLKI could be specifically cleaved by caspase-3 *in vitro.* The optimal cleavage site for caspase-3 has been determined to be DEMD or DEVD, based on *in vitro* tests, and out of a number of caspases tested caspase-3 appears to be the most likely candidate for cleaving the VEMD sequence in RLK I (Talanian et al., 1997; Thornberry et al., 1997). Cell extracts from adherent XLT-15 cells transfected with the Full RLKI construct were obtained at different time points after transfection and incubated in the presence or absence of active recombinant human caspase-3 (Figure 4.7C). In comparison to the empty vector transfected cells, incubation with caspase-3 does increase the intensity of a band at 25 kDa, at the 48 and 72 h time points in the Full RLKI transfected cells. Although the empty vector and control samples show a weaker band at 25 kDa, possibly due to a native keratin being cleaved by the cells own caspases, the increase of the N-terminal RLKI fragment is concomitant with the expected increase in Full-RLKI protein expression at 48 and 72 h post transfection. These findings indicate that caspase-3 can be one of the caspases acting upon RLK I in the tadpole tail.

## 4.4 DISCUSSION

Based on the results for the XLT-15 cells it appears that N-term RLKI does not modulate apoptosis in any way, in the presence or absence of $T_3$. Therefore, the appearance of N-term RLKI in the tadpole tail due to $T_3$ is probably a product of initiation of the apoptotic events rather than it being a modulator or contributor to apoptosis. However, in these experiments only the N-terminal fragment was expressed without there being a C-terminal end, and therefore additional experiments with both fragments might generate different results. In addition, the context of the cell model is slightly different, as RLKI is likely to be expressed by an epithelial cell and not a myoblastic cell as is the case for XLT-15 cells. Byun et al. (2001) observed that transfecting cells with the N-terminal fragment of vimentin (amino acids 1-85), which was a caspase-cleavage

product, interfered with intermediate filament (IF) assembly and induced caspase-dependent apoptotic death. Although this happened in HeLa and MCF-7 cells, that contained and lacked native vimentin IFs, respectively, it is possible that in our case the N-term RLKI could also induce IF collapse in an epithelial cell line leading to apoptosis. Future experiments could be performed where N-term RLKI is expressed in an epithelial cell line such as the *X. laevis* XLA cell line, although this cell line does not undergo apoptosis due to TH (Kanamori and Brown, 1993).

In the early stages of metamorphosis, tail muscle cells have been shown to die mostly by TH-direct processes, however, indirect processes such as changes in the ECM have also been observed to contribute to tail muscle cell apoptosis in the later stages of metamorphosis (Das et al., 2002; Nakajima and Yaoita, 2003). During tail metamorphosis the detachment of cells from the ECM would lead to eventual apoptosis, through the process known as anoikis (Gomperts et al., 2002). It is therefore possible that the TH signal causes caspase-mediated cleavage of RLK I, and as our results with the detached cells suggest, this contributes to cell detachment and thus eventually amplifies the apoptotic process in the tail. Although XLT-15 cells are not epithelial and we are not sure if they have a keratin intermediate filament network, based on the anti-pan-cytokeratin immunoblots (Figure 4.3D) they may possess one, and as observed for N-terminal vimentin, which induced cell rounding and death, (Byun et al., 2001), N-term RLKI may be inducing the collapse of it leading to cell detachment. In fact, keratin IF networks through the linker protein plectin associate with integrins and the ECM, and may have a great effect on cell attachment (Marceau et al., 2001). Mouse hepatocytes which have been devoid of K8/K18 IFs due to a K8-knockout had altered cell adhesion properties such as reduced spreading, had increased integrin β1 density at the surface and the target of integrin signaling, focal adhesion kinase (FAK) had decreased activity, suggesting that keratin IF loss hamperes integrin functional activities at focal adhesions, in turn modulating FAK signaling (Galarneau et al., 2007). FAK has been shown to integrate signals for cell survival and proliferation coming from the integrins which bind the cytoskeleton and ECM, and its decreased activity can lead to decreased cell survival (Gomperts et al., 2002). In the future it would be interesting to visualize the effects of N-term RLKI and Full RLKI on keratin IF networks using the pan-cytokeratin antibody and fluorescence microscopy, and to see if these have any effect on signaling cascades such as that of FAK. If in fact N-term RLKI is found to disrupt keratin IFs it would be additionally interesting to test if this leads to “inside-out” signaling through the integrins leading to their detachment from the substrate.

Contrary to our hypothesis, the overexpression of the N-terminus (aa 1-270) of K18 in a human cell line inhibited TNFα-induced apoptosis (Inada et al. 2001). This was also observed with the overexpression of full K8/K18 and was shown to occur by K18 sequestering TRADD away from the TNF receptor-1 and preventing caspase-8 activation. This mechanism also protected cells only from TNF-induced apoptosis, being unable to save cells from other apoptotic stimuli. Based on research on tadpole tail muscle cell death, the most likely implicated apoptotic path is the mitochondrial/apoptosome apoptotic pathway which is dependent on a functional TR, rather than a cell-surface activation of a death receptor such as the TNF family path (Das et al., 2002; Sachs et al., 1997, 2004; Rowe et al., 2002, 2005). However, in the current studies' comparison of EGFP-expressing adherent cells to non-EGFP-expressing cells, a protection from apoptosis due to the expression of both constructs appeared possible, although not definite. It is possible that the expression of either construct sequesters TRADD or a similar protein, providing protection from a cell-surface activated apoptotic pathway. Death receptors (DR), such as xDR-M1 and xDR-M2 with intracellular death-domains, belonging to the DR family, and death-domain interacting proteins such as FADD (Fas-associated death-domain) have been identified in *X. laevis* and shown to function in apoptosis in cell culture (Tamura et al., 2004; Ishizawa et al., 2006). Furthermore, recent observations have indicated that proteins implicated in a DR-activated apoptotic pathway such as BID and caspase-8 may be contributing to TH-induced tail muscle death in *X. laevis* (Du Pasquier et al., 2006). How TH could activate such a DR-apoptotic pathway is unknown. To determine if a DR-apoptotic pathway is involved in this apoptotic-modulation in the XLT-15 cells it would be interesting to test whether the expression of Full RLKI or N-term RLKI reduces the activation of caspase-8.

Our findings indicate that RLK I can be cleaved in cells undergoing apoptosis and that caspase-3 can be one of the caspases acting upon RLK I. Other caspases that might act on RLK I are caspase-6 and -7 which have been shown to optimally cleave at VEHD and DEVD sequences, respectively (Thornberry et al., 1997). These caspases have also been shown to increase in activity in apoptotic XLT-15 cells (Nakajima et al., 2000). All three caspases (3,6 and 7) have been demonstrated to cleave the type I human keratin consensus sequences of VEMD/A or VEVD/A (Oshima, 2002; Marceau et al., 2007). No caspase-3 has been cloned in *R. catesbeiana* but caspase-3-like activity has been observed (Veldhoen et al., 2006) in the TH-induced tadpole tails. The catalytic protease domains of caspase-3, -6, and -7 share >58% identity at the amino acid level between *X. laevis* and human, and activating aspartate cleavage sites are also conserved, indicating a conserved mechanism between humans and anurans (Nakajima et al.,

2000). The activation of caspase-3 in the larval epidermal cells of *X. laevis* and their eventual apoptotic death has been shown to require a functional TR (Schreiber and Brown, 2003). Thus, the $T_3$-induced cleavage of RLKI likely occurs by the transduction of the TH signal via the nuclear TRs, leading to the activation of caspases. In addition to the requirement for a TR, in studies based on tadpole muscle cells, a functional caspase-9 was shown to be required for TH-induced cell death to occur, indicating that caspase-3, the main caspase to be induced in these cells, is activated through the mitochondrial/apoptosome path (Rowe et al., 2005). Phosphorylation of human keratin K18 within the N-terminal head domain has been shown to inhibit its susceptibility to caspase cleavage within the VEVD sequence and may lead to filament reorganization (Ku and Omary, 2001). In the future it would therefore be interesting to study the mechanisms involved between ligand-activated TRs and caspase activation, as well as the effects of phosphorylation on RLKI cleavage and filament organization.

For human keratins it has only been definitely proven that K14, K15, K17, K18 and K19 are cleaved by caspases (Marceau et al. 2007), although all type I keratins except for K9 and K10 possess the caspase consensus site, making our finding that RLKI is caspase cleaved a significant find. Additionally, RLKI is the first anuran keratin that has been demonstrated to be cleaved by caspase action, and temporally it shows the earliest evidence for caspase activity during TH-induced metamorphosis that has been demonstrated to date.

# Chapter 5: Development of a cultured tail fin biopsy ("C-fin") assay, with RLKI as biomarker, for determining effects of disruptors of thyroid hormone action

## 5.1 INTRODUCTION

The world's development and industrial progress is increasingly adding anthropogenic chemicals into the environment. The number of chemicals currently released into the environment has been estimated at over 30,000 (Commission of the European Communities REACH report, 2006). Some of these chemicals are released into the environment intentionally, such as through agricultural processes, and some are released inadvertently through waste and from products in use. Beyond their toxic effects on organisms when present in high amounts, a number of these chemicals act as endocrine disrupting compounds (EDCs) at sublethal concentrations. The focus of research thus far has been mainly on EDCs of gonadal steroids with (anti-)estrogenic and (anti-)androgenic capabilities with relatively limited information regarding disruptors of TH action (Zoeller, 2005). Nevertheless, close to a hundred compounds have been classified as endocrine disruptors of the TH axis and many new chemicals are hypothesized to act as EDCs of TH action based on their structural resemblance to TH (Brucker-Davis, 1998; Boas et al., 2006). EDCs of TH action can act at a number of points within the TH system. These include, the hypothalamus-pituitary-thyroid (HPT)-axis, TH synthesis at the thyroid gland, TH transport within the blood on carrier proteins such as TTR, metabolism and excretion of THs, transport of TH into and within the cell by dedicated proteins, deiodinase activity within gland and peripheral tissues, and binding to TRs and effects on co-factor association (Boas et al., 2006). The majority of the chemicals that are well known to be TH disruptors are the goitrogens that act on the thyroid gland, preventing thyroid hormone synthesis through the inhibition of iodine import or thyroid peroxidase activity (Leatherland, 2000). A second class of chemicals, the polyhalogenated aromatic hydrocarbon (PHAH) compounds, such as polychlorinated biphenyls (PCBs) and brominated flame retardants (BFRs) which resemble THs in structure, are theorized to disrupt TH action by binding to carrier proteins and receptors instead of the designated hormones (Zoeller, 2005). The evidence for these actions is not as definite and is a current area of intense research (Boas et al., 2006).

The growing concern that polluting anthropogenic chemicals are potential disruptors of the TH system has prompted organizations such as the U.S. Environmental Protection Agency (EPA), Environment Canada, and the Organisation for Economic Co-operation and Development (OECD) to look at screening assays to assess the safety of newly created chemicals and those already present in the environment. The total dependence of amphibian metamorphosis on TH and the high degree of conservation of the TH signalling pathway in vertebrates (Tata, 2006) has led to the suggestion that metamorphosis can be used as a model for the detection of chemicals affecting the TH axis in vertebrates. Indeed, several metamorphosis-based assays using whole animal exposures are currently in the validation phase such as the amphibian metamorphosis assay (AMA) (EPA, 2007) and the *Xenopus* metamorphosis assay (XEMA) (Fort et al., 2007) that are based upon developmental rate and thyroid histology of exposed premetamorphic tadpoles, and the native species-based *R. catesbeiana* metamorphosis assay (Environment Canada, 2001) that is based upon morphological and molecular endpoints (Veldhoen et al, 2006a). The OECD in their report on the AMA for the detection of thyroid active substances expresses the need for additional *in vivo/in vitro* assays to expand the battery of screening assays (OECD, 2006). Moreover, there is a substantial drive through the Interagency Coordinating Committee on the Validation of Alternative Methods (ICCVAM) to develop methods to reduce the use of animals in screening assays (ICCVAM, 2008). Therefore, in addition to the whole-animal morphological assays, a number of research groups have proposed different *molecular* methods of assessing disruption of TH action. These molecular assays although in their infancy promise to be more cost effective, more sensitive, higher throughput, less time consuming, and due to their molecular level may provide additional information on the modes of action of the chemical. Most of these assay methods are based on assessing specific gene expression levels of known TH-responsive genes such as TRβ or TSHβ or on changes of multiple genes revealing specific profiles via cDNA arrays, in each case in live tadpoles challenged with the test chemicals alone or in combination with TH (Veldhoen and Helbing, 2001; Opitz et al., 2006a, 2006b; Helbing et al., 2007a, 2007b; Zhang et al., 2006). Other assays rely on the assessment of artificial gene construct expression where reporter genes are driven by TRE containing promoters as has been done *in vivo* in transgenic tadpoles or *in vitro* in transfected cells (Fini et al., 2007; Jugan et al., 2007; Sugiyama et al., 2005a, 2005b). In each case, the end goal is to link these gene expression changes to actual effects at the organism level and possibly reveal the modes of action of the chemical.

Our laboratory has developed a tail fin biopsy assay using *R. catesbeiana* tadpoles which enables non-lethal tissue sampling from live animals and the assessment of exposure to thyroid active

agents by examining mRNA transcript levels of known TH-responsive genes such as TRβ (Veldhoen and Helbing, 2001, 2005). This method enables a repeated measures experimental design where a tail fin biopsy can be obtained from the same tadpole at multiple time points, however, only a single chemical treatment can be tested per animal which is not conducive to a high throughput screening approach. The current study builds on the tail fin biopsy approach on a native amphibian tadpole by combining this concept with the fact that tadpole tissues can be successfully cultured (Veldhoen et al., 2006; Ji et al., 2007) to develop a cultured tail fin biopsy or "C-fin" assay. By taking multiple tail fin biopsies per animal and then exposing each biopsy to a different treatment condition, the C-fin assay enables the screening of multiple chemical conditions simultaneously with minimal animal use while maintaining complex tissue structure and enabling the determination of biological variation of a response. Additionally, the current study proposes that the detectable caspase cleavage product of RLKI, N-term RLKI, as a result of the TH signal, can be used as a protein biomarker that can indicate perturbations on TH action by potential EDCs in this *ex vivo* system (Domanski and Helbing, 2007). The validity of N-term RLKI as a biomarker of TH-action disruption will be compared with the well studied direct early response gene TRβ which has been used as a candidate biomarker for this purpose in a number of studies in *X. laevis* and *R. catesbeiana* (Zhang et al., 2006; Helbing et al., 2006; Opitz et al., 2006a, 2002; Veldhoen and Helbing, 2001). The C-fin assay is therefore designed to determine direct effects on target tissue TH signalling through the characterization of changes in the proteome and by examining TH-responsive gene transcript levels. Herein, three chemicals were examined that have recently been shown to be potential EDCs of TH action: the bactericidal agent triclosan, the brominated flame retardant tetrabromobisphenol A, and the herbicide acetochlor (Veldhoen et al., 2006a, 2006b; Helbing et al., 2006) to determine the direct tissue effects of these chemicals using the C-fin assay. TH-dependent N-term RLKI protein levels were determined by immunoblotting with the concurrent assessment of TRβ transcript levels using QPCR, in each biopsy. The C-fin assay, using the N-term RLKI protein, was able to detect perturbations in TH-signalling within 48h of exposure demonstrating that this method has utility as a novel screen for TH disrupting chemicals.

## 5.2 MATERIALS AND METHODS

### *5.2.1 Experimental animals*

Care and treatment of animals was as described before (Chapter 3).

### *5.2.2 Organ culture of tail fin biopsies*

Preparation of the organ cultures was adapted from Veldhoen et al, 2006; Ji et al, 2007, and Skirrow and Helbing, 2007. Premetamorphic (TK stage VI-VIII) *R. catesbeiana* tadpoles were euthanized as before (Chapter 3) and subsequently washed three times in 100 ml per tadpole of sterile saline (MFM solution; as described in chapter 4). For the "EtOH wash" samples in figure 5.2B tadpoles were instead washed once in sterile $dH_2O$ (10 sec.) then in 70% ethanol (5 sec.) and two more times in sterile $dH_2O$ (10 sec.), according to Skirrow and Helbing, 2007. These steps were replaced as indicated above with MFM washes as it was discovered that the ethanol wash adversely affected the N-term RLKI response. Six mm biopsies were taken from the dorsal and ventral tail fins using a dermal biopsy punch (Miltex Inc., York PA USA). Biopsies were organ cultured in individual wells at 25ºC in air in 24-well multi-well culture plates (Primaria, BD Biosciences) in 1 ml per biopsy of 70% strength Leibovitz's L15 medium (Gibco, Invitrogen) supplemented with 10 mM HEPES pH 7.5, 50 units/ml penicillin G sodium, 50 μg/ml streptomycin sulfate (Gibco, Invitrogen) and 50 μg/ml neomycin (Sigma-Aldrich). For EDC-assay treatments the media additionally contained the vehicle control, 10 nM $T_3$, or 10 nM $T_3$ in combination with the test chemicals at three different concentrations. $T_3$ was prepared as described previously (Chapter 4). For treatments it was diluted in media to $10^{-5}$ M and was then applied at 1 μl/ml of media, giving a final concentration of 10 nM $T_3$ with NaOH at 25 nM as vehicle. The vehicle control was prepared in the same manner giving a final concentration of 25 nM NaOH. For the dose-response test $T_3$ was applied to a final concentration of 1, 10 or 100 nM and all, including the vehicle control, were adjusted to 250 nM NaOH. Triclosan (5-chloro-2-[2,4-dichloro-phenoxy]-phenol; TCS; CAS 3380-34-5, over 97% pure, Sigma-Aldrich) stock was prepared at 3 mg/ml in 40 mM NaOH and stored at -20ºC. For treatments it was diluted in media to 30 μg/ml and was then applied at 1 μl/ml of media to give a final nominal concentration of 100 nM with NaOH at 400 nM. This was further diluted ten fold twice in media with 400 nM NaOH to give final nominal concentrations of 10 and 1 nM triclosan. For the triclosan assay all treatments including the vehicle control were adjusted to 425 nM NaOH. Tetrabromobisphenol A (2,2',6,6'-Tetrabromo-4,4'-isopropylidendiphenol; TBBPA; CAS 79-94-7; 99.8% purity; AccuStandard, New Haven CT USA) was made as a $10^{-2}$ M, $10^{-3}$ M and $10^{-4}$ M stock in dimethyl sulfoxide (DMSO; CAS 67-68-5; 99.9% purity (0.1% $H_2O$); ACP Chemicals Inc.) and stored at -20ºC. For treatments each was diluted 100-fold in media and then applied at 10 μl/ml of media, giving a final nominal concentration of 10, 100 and 1000 nM TBBPA with DMSO at 0.1 μl/ml. For the TBBPA assay all treatments including the vehicle control were adjusted to 25 nM NaOH and 0.1 μl/ml DMSO. Acetochlor (2-chloro-*N*-(ethoxy-methyl)-*N*-(2-ethyl-6-methylphenyl) acetamide; CAS 34256-82-1; 99.8% purity; AccuStandard) was made as a $10^{-3}$ M, $10^{-4}$ M and $10^{-5}$

M stock in methanol (CAS 67-56-1; 99.8% purity (0.05% $H_2O$); Caledon, Edmonton AB Canada) and stored at -20ºC. For treatments, each stock was diluted 100-fold in media and then applied at 10 µl/ml media, giving a final nominal concentration of 1, 10 and 100 nM acetochlor with methanol at 0.1 µl/ml. For the acetochlor assay all treatments including the vehicle control were adjusted to 25 nM NaOH and 0.1 µl/ml methanol. Tail fin biopsies were treated for 24, or 48 h, without any media changes at 25ºC in air. All experiments used five or six animals to test eight treatment conditions from the eight biopsies obtained per animal. This translates to an eight fold reduction in animal use (5-6 animals rather than 40-48 animals).

### *5.2.3 Protein extraction and immunoblotting*

Proteins were extracted from the 6 mm biopsies (after a 2 mm biopsy was removed for RNA extraction) in 70 µl of extraction buffer (50 mM HEPES pH 7.4, 100 mM NaCl, 0.5% CHAPS, 1 mM EDTA, 10 mM DTT, 4 µg/ml aprotinin, 1 µg/ml leupeptin, 2 µg/ml antipain, 300 µg/ml benzamidine and 100 µM PMSF) on ice using a polypropylene micropestle (Fisher Scientific), and then centrifuging at 12,000 x g for 10 min. at 4ºC. The supernatant was stored at -70ºC. Protein concentrations were determined as indicated before (Chapter 2) except BSA standards were made up in the above buffer. SDS-PAGE analysis and immunoblotting were performed as indicated before (Chapter 4) with the following modifications. Thirty µg protein samples in addition to containing the loading buffer were adjusted to contain equal amounts of salts with above extraction buffer and were heated at 90ºC for 5 min. Immunoblotting was performed as before (Chapter 4), with the pan-cytokeratin rabbit polyclonal IgG antibody as primary antibody (H-240; Santa Cruz Biotechnology Inc). Images were obtained as before using a Li-Cor Odyssey scanner and band density was analyzed using the Li-Cor Odyssey Ver. 2.0.5 software. Band intensity was measured from integrated intensity within equal rectangles drawn around the N-term RLKI protein bands and with subtracted background obtained from the top and bottom border (set at 3 pixels). To further normalize for protein loading, blots were stained with amido black stain after immunoblotting as follows. The immunoblots were stained for 2 min. in 0.1% amido black (Sigma-Aldrich), 25% isopropanol (EM Science) and 10% acetic acid (EM Science), destained for 10 min. in 25% isopropanol and 10% acetic acid, and rinsed in $dH_2O$. Stained blots were scanned and analyzed as before and the integrated intensity of the cytoplasmic β-actin band was used to normalize for protein loading. Levels of N-term RLKI are presented as fold change relative to vehicle control.

*5.2.4 Isolation of RNA and quantitation of gene expression*

At the end of the incubation period for each treatment a 2 mm biopsy was removed from the 6 mm biopsy using a dermal biopsy punch (Miltex Inc.) and stored in 100 μl of RNA*later* (Ambion Inc., Austin TX USA) at -70ºC. RNA was isolated using TRIzol reagent as described by the manufacturer (Invitrogen). Mechanical disruption utilized 200 μl TRIzol reagent, a 1 mm diameter tungsten-carbide bead, and safe-lock Eppendorf 0.5 ml microcentrifuge tubes in a Retsch MM301 Mixer Mill (Fisher Scientific) at 24 Hz three times for 6 min. with the chambers being rotated in between the cycles. 20 μg of glycogen (Roche Diagnostics, Laval PQ Canada) was added prior to isopropanol precipitation to maximize RNA yield. Isolated RNA was subsequently resuspended in 10 μl diethyl pyrocarbonate (DEPC)-treated (Sigma-Aldrich) RNase-free water and stored at -70ºC. cDNA was synthesized from around 1 μg total RNA as per manufacturer's protocol using the RevertAid H Minus First Strand cDNA Synthesis Kit (Fermentas) with minor modifications: RNA was first annealed with 200 ng random hexamer primer and then cDNA was synthesized by adding the mixture of reaction buffer, ribonuclease inhibitor, dNTPs and RevertAid H Minus M-MuLV reverse transcriptase and incubating at 25ºC for 10 min. and then at 42ºC for 1.5 h. The cDNA products were diluted five fold prior to PCR amplification and stored at -20ºC. The steady-state levels of the TRβ transcript and ribosomal protein L8 transcript were analyzed using a MX3005P real-time quantitative PCR system (Stratagene, La Jolla CA USA). Each 15 μl amplification reaction contained 10 mM Tris-HCl (pH 8.3 at 20ºC), 50 mM KCl, 3 mM $MgCl_2$, 0.01% Tween 20, 0.8% glycerol, 40,000-fold dilution of SYBR Green I (Molecular Probes Inc., Eugene OR USA), 200 μM dNTPs, 69.4 nM ROX reference dye (Invitrogen), 5 pmol of each primer (For TRβ: up 5'-AGCAGCAT GTCAGGGTAC-3' and down 5'-TGAAGGCTTCTA AGTCCA-3' and for ribosomal protein L8: up 5'-CAGGGGACAGAGAAAAGGTG-3' and down 5'-TGAGCTTTCTTGCCACAG-3'), 2 μl of diluted cDNA, and one unit of Hot Start Taq DNA polymerase (Fermentas). The thermocycle program for both gene targets included an initial enzyme activation step at 95ºC (4 min.) followed by 40 cycles of 95ºC denaturation (15 sec.), 55ºC annealing (30 sec.), and 72ºC elongation (45 sec.). Controls lacking cDNA template or Taq DNA polymerase were included to determine the specificity of target cDNA amplification. Quadruplicate reactions were performed for each sample and data were averaged and normalized to the expression of the control gene encoding the ribosomal protein L8 using the comparative Ct method (Livak and Schmittgen, 2001). The integrity of amplification reactions was confirmed by the presence of a single DNA product following gel electrophoresis and by amplicon sequencing. Additionally, the efficiency of

the target amplification (TRβ) and the efficiency of the reference amplification (L8) were validated to be approximately equal allowing the use of the Ct method. TRβ expression data are presented as fold change relative to vehicle control.

### *5.2.5 Statistics*

Statistical analyses were performed using SPSS Ver. 12.0 (Chicago IL USA) software using the Mann-Whitney U non-parametric two-tailed test. The Pearson Correlation two-tailed test was performed on the data in figure 5.4.

## 5.3 RESULTS AND DISCUSSION

### *5.3.1 The C-fin assay*

Previous studies have indicated that the tail tissue is a more robust indicator of TH action than other tissues such as the brain and hind-limb, and that premetamorphic tadpoles are more sensitive than prometamorphic tadpoles to TH disruption (Zhang et al., 2006; Opitz et al., 2006a). The C-fin assay thus uses tail fin tissue from premetamorphic (TK stage VI-VIII) *R. catesbeiana* tadpoles which is competent to respond to $T_3$ but has not yet been exposed to the high levels of the endogenous TH that would occur in prometamorphosis. This allows to test for agonistic activity in a test chemical which would induce RLKI cleavage or TRβ expression, and with the addition of exogenous $T_3$ in combination with the test chemical, allows for antagonistic assessment, where the chemical would reduce the levels of the $T_3$-induced RLKI fragment or TRβ mRNA. In addition, the treatment of test chemical in combination with $T_3$ may increase sensitivity revealing weak agonists, where the $T_3$ will work synergistically to raise the level of TRs upon which the test chemical may act. An agonistic compound in this situation will have a potentiating effect on $T_3$, further elevating the levels of N-term RLKI or TRβ. The addition of exogenous $T_3$ also mimics the scenario of exposure to the chemical at metamorphosis, where endogenous THs are present at similar concentrations (~10 nM) to those used in this assay (Regard et al., 1978; Leloup and Buscaglia, 1977). These types of responses have already been well demonstrated with the transcript levels of TRβ in live *X. laevis* tadpoles (Zhang et al., 2006; Opitz et al., 2006a).

Multiple 6 mm biopsies (usually 8) were taken from the dorsal and ventral tail fins of each tadpole and incubated in serum-free media in individual wells in a multiwell-plate (Figure 5.1). This in effect allowed for the tissue from an individual animal to be exposed to multiple

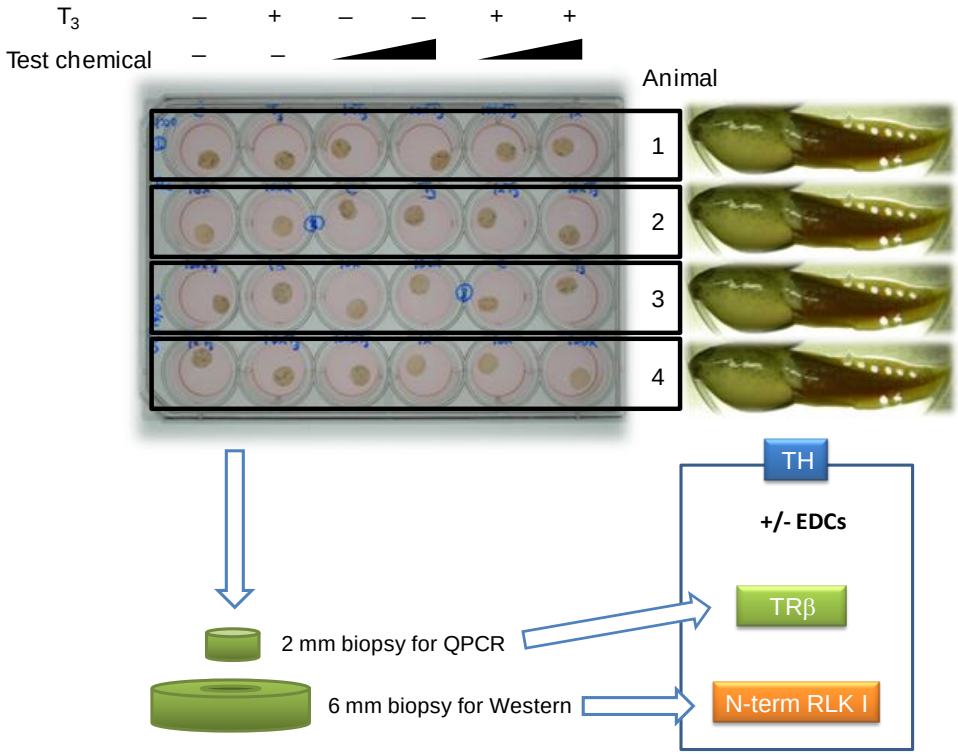


**Figure 5.1. The C-fin assay.** The C-fin assay consists of premetamorphic *R. catesbeiana* tadpole tail fin biopsies (6 mm) exposed individually to test chemicals in the presence or absence of $T_3$ in 24-well multi-well plates in a serum-free medium. At the end of the incubation period a 2 mm biopsy is taken from the 6 mm biopsy and used for the analysis of gene transcript levels (e.g. QPCR analysis of TRβ transcript levels) while the remainder is used for analysis of proteins (e.g. immunoblot analysis for N-term RLKI fragment protein levels).

treatments. For example, eight biopsies from one animal enabled the testing of vehicle control, $T_3$ alone, three concentrations of the test chemical, and $T_3$ in combination with the test chemical at the three concentrations (See figures 5.1 and 5.5-5.7).

At the end of the incubation period an additional 2 mm biopsy was taken out of the original 6 mm biopsy and the tissue was used to analyze for TRβ gene transcript levels by QPCR, while the remainder was used to assess the level of N-term RLKI protein by immunoblot analysis (Figure 5.1). This allowed for the analysis of the two biomarkers in exactly the same tissue treated under identical conditions. Additionally, samples from the C-fin assay could be analyzed for other proteins or gene transcripts through immunoblotting or mass spectrometry, and QPCR or cDNA array analyses, respectively.

### *5.3.2 Characterization of the appearance of the N-term RLKI fragment*

As shown in Figure 5.2A, the N-term RLKI fragment appeared as early as 12 h with a 10 nM $T_3$ dose in this organ-culture setting. The amount of fragment increased with time, with the 48 h time point having a substantially high level. This timing is consistent with what has been observed for a $T_3$-induced response in a time course of TRβ mRNA expression in *X. laevis* tadpole tail (Opitz et al., 2006a) and is sooner than the earliest detection of TRβ protein reported to be observed at 20 h (Eliceiri and Brown, 1994). Additional experiments revealed that the N-term RLKI fragment was either produced in the outer epidermal layers of the tail fin or that these cells are required in the TH signalling process for the fragment to be produced. This was discovered when initial tadpole sterilization techniques, based upon previous organ culture studies which used a brief 70% ethanol wash step (described in Veldhoen et al., 2006) visually removed some of the outer layers of the fin, and failed to produce the expected N-term RLKI fragment, while a gentler wash step in sterile saline that avoided this cell loss produced the expected fragment (Figure 5.2B).

### *5.3.3 The $T_3$-induced response of N-term RLKI and TRβ in the C-fin assay: Proof of concept*

The C-fin assay maximizes the use of the tail fin from an individual animal by taking multiple biopsies from a single tail. However it was necessary to evaluate whether there were any differences in TH-dependent responses between biopsies taken from these different locations. As shown in Figure 5.3A seven different locations, that covered the usual sampling region, were assessed for N-term RLKI and TRβ levels after the biopsies were exposed to 10 nM $T_3$ for 48 h. An eighth biopsy was exposed to vehicle solution only. Figure 5.3B shows a sample immunoblot result and averaged data from six animals (eight biopsies per animal) indicating the level of N-term RLKI in the different regions. All of the regions responded uniformly to $T_3$, without any significant differences, with an average increase of 3-fold over the control. Figure 5.3C shows the TRβ transcript levels for the same samples which also showed no statistical difference in expression between the different regions. The variability in the QPCR data was observed to be larger than for the N-term RLKI levels. The uniformity in TRβ expression throughout the *R. catesbeiana* tail fin after TH induction has been shown before in biopsies taken from live tadpoles (Veldhoen and Helbing, 2001). The next step was to assess the sensitivity of the assay to different concentrations of hormone at different time points. As shown in Figure 5.3D, N-term RLKI is significantly induced over the control at both 24 and 48 hours, at $T_3$ concentrations ranging from 1 to 100 nM. However, at the 24 h time point the different concentrations of $T_3$ (1, 10 and 100 nM) were not distinguishable from each other. In contrast, at the 48 h time point, N-term RLKI

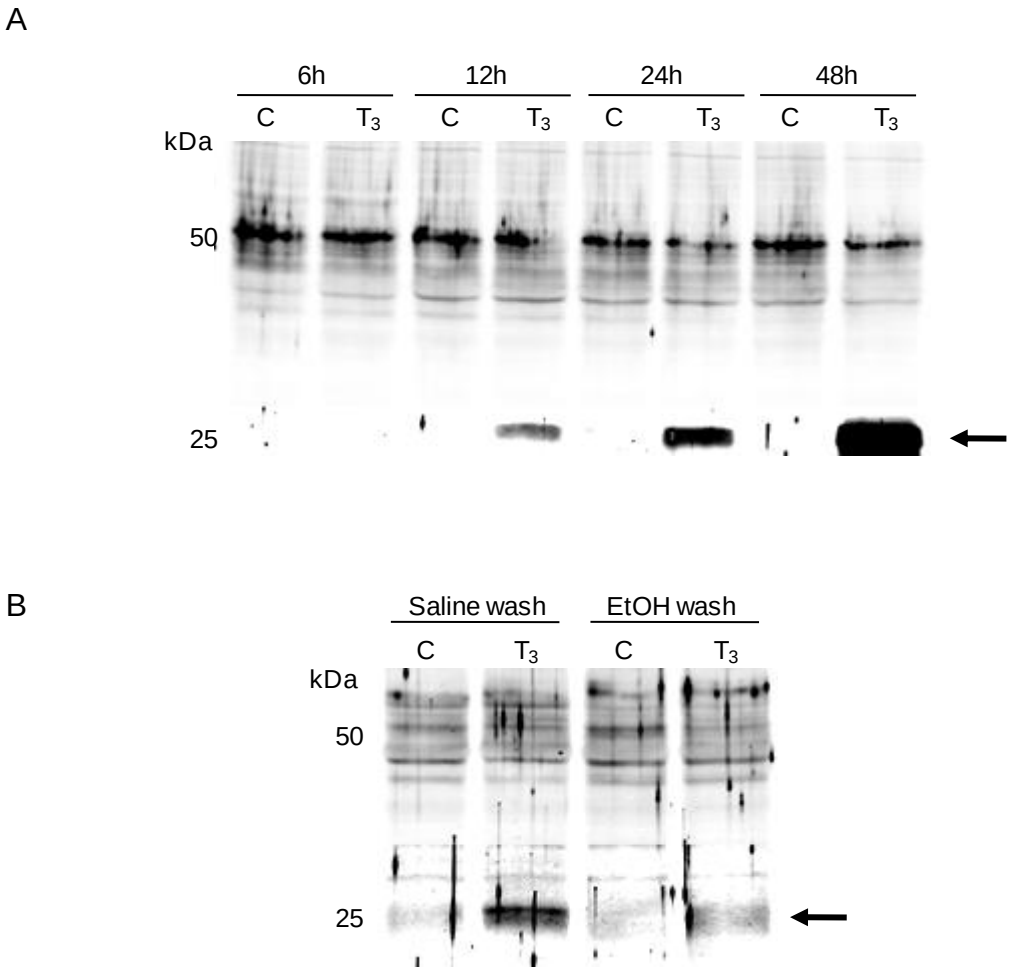


**Figure 5.2. Characterization of N-term RLKI.** (A) Time-course expression of N-term RLKI in premetamorphic *R. catesbeiana* tadpole tail fin tissue biopsies exposed to vehicle control (C) or 10 nM $T_3$ ($T_3$) for the indicated amount of time and analyzed by immunoblotting using a pan-cytokeratin antibody. The N-term RLKI protein fragment is indicated by arrow. Relative molecular weights of protein standards are indicated in kDa. (B) Immunoblot of N-term RLKI as indicated above from tadpoles that were cleaned in sterile saline (Saline wash) or 70% ethanol (EtOH wash) before being sampled for tail fin tissue.

levels were significantly higher in each of the successive increases in $T_3$ concentration (Figure 5.3D). Similar results were obtained with the TRβ transcript levels as seen in Figure 5.3E. A significant response compared to control was detectable for 10 and 100 nM $T_3$ at 24 h with a significantly distinguishable response for the different $T_3$ concentrations occurring only by 48 h (Figure 5.3E). At 48 h the TRβ measurements appeared to be better at distinguishing between the 10 and 100 nM $T_3$ levels than were the N-term RLKI levels (significance levels of $p<0.01$ vs. $p<0.05$), but once again the variability in the levels appeared to be greater for the QPCR analysis. The TRβ response in this assay format is consistent with what has been previously observed to

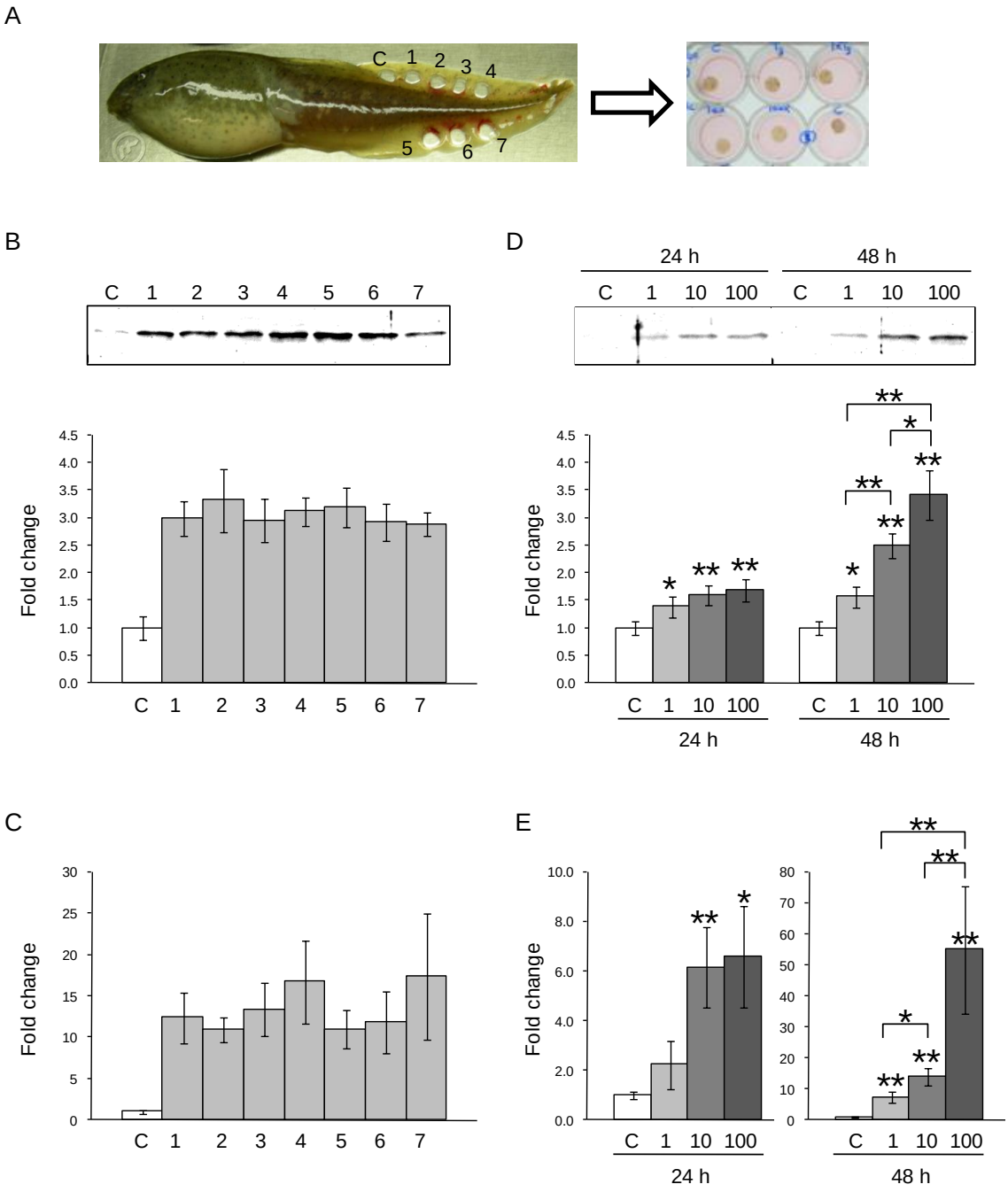


**Figure 5.3. A uniform and dose dependent response to $T_3$ across the tail fin tissue as analyzed by N-term RLKI protein and TRβ transcript levels.** (A) Sampled locations within the tail fin used to indicate a uniform response to $T_3$. Biopsies (6 mm) 1 to 7 were exposed to 10 nM $T_3$ for 48 h and compared to biopsy C exposed to vehicle control. Biopsies were exposed individually in serum-free organ culture medium in multi-well plates as shown to the right. (B) Levels of N-term RLKI protein in the above biopsy samples as measured by immunoblotting with anti-cytokeratin antibody. Sample immunoblot shows the N-term RLKI fragment at 25 kDa. Graph of averaged data from six experiments showing the fold change in the levels of N-term RLKI in the $T_3$ exposed biopsies (1 to 7; gray bars) compared to vehicle control (C; white bar).

Error bars represent the standard error of the mean. (C) As in B but indicating fold change in steady-state levels of the TRβ transcript relative to vehicle control as determined by QPCR. (D) Dose dependent response of N-term RLKI levels in tail biopsies exposed to 1, 10 or 100 nM $T_3$ for 24 or 48 h as indicated by immunoblotting with anti-cytokeratin antibody. Sample immunoblot shows the N-term RLKI fragment at 25 kDa. Graph of averaged data from six experiments showing the fold change in the levels of N-term RLKI relative to vehicle control. Error bars represent the standard error of the mean. Significance is indicated by one asterisk (*) for $p < 0.05$ and by two asterisks (**) for $p < 0.01$ (Mann-Whitney U). Significance compared to controls is indicated above the bar and significances between treatments are indicated by brackets. (E) As for D but indicating fold change in steady-state levels of the TRβ transcript relative to vehicle control as determined by QPCR.

---

occur in live exposed tadpoles (Zhang et al., 2006; Opitz et al. 2006a). Based on N-term RLKI and TRβ, the dose-response of the C-fin assay appears to be more sensitive and discerning than one in an assay proposed by Turque et al. (2005) that consists of somatic gene transfer of a TH/bZIP promoter-luciferase construct into the dorsal caudal muscle of premetamorphic *X. laevis* tadpoles. After an exposure of 48 h the assay could not detect an effect by 0.5 nM $T_3$, but detected an increase of 3- and 5-fold for 5 and 50 nM $T_3$, respectively. A high variability in the response, however, made the two highest concentrations of $T_3$ statistically non-significantly different from each other (Turque et al., 2005). The dose-dependent response of the C-fin assay is also more discerning than the one in an *in vivo*-multiwell-based assay recently published by Fini et al. (2007) where a transgenic *X. laevis* embryonic stage tadpole is used, expressing a EGFP reporter gene driven by a TRE-containing TH/bZIP promoter. In this assay 0.5 nM $T_3$ could be distinguished from 5 and 50 nM $T_3$, but the latter two concentrations were non-distinguishable. Furthermore, 0.5 nM $T_3$ was not significantly different from control at 48 h and the assay was performed with 5 nM $T_3$ for 72 h. In a very sensitive assay, termed the T-screen, based on the rat pituitary tumour cell line, $GH_3$, which responds to $T_3$ by proliferating and producing growth hormone, Schriks et al. (2006) observed that the assay was sensitive and progressively responsive to $T_3$ in the lower range of 0.01 to 1 nM. For the detection of antagonism and potentiating effects it was used with 0.25 nM $T_3$ with an incubation period of 96 h, after which metabolic activity was measured. This high sensitivity to $T_3$ was also observed in an assay based on a lentivirus transfected *X. laevis* cell line with a TRE-luciferase construct (Sugiyama et al., 2005a). A response was observed as low as 0.02 nM $T_3$, however, as similarly observed in the study by Schriks et al., the response reached a plateau at 0.08 nM $T_3$ and was level till the highest concentration tested of 10 nM $T_3$. Intriguingly, chemicals to be tested were included in the absence or presence of 2 nM $T_3$ (Sugiyama et al., 2005a, 2005b). The high sensitivity of such a test may reveal agonists in the absence of $T_3$, but it is less likely to reveal antagonists and unlikely

to reveal potentiating action in the presence of 2 nM $T_3$, as was observed for a number of compounds (Sugiyama et al., 2005a, 2005b).

Figure 5.4 shows the higher variability in the response of TRβ compared to N-term RLKI and reveals the variation within this animal population. This is indicated with relative levels of N-term RLKI (white bars) and TRβ (gray bars) as shown for 12 individual animals that were exposed to 10 nM $T_3$ for 48 h. The range in the TRβ levels is much greater than the range for N-term RLKI in the exact same samples. The negative effect of this variation was mostly avoided by normalizing all the samples to the control treatment within the animal and reporting the data as fold changes from control, and by removing outlier animals that appeared to respond unusually high (e.g. animal #12 Figure 5.4) or ones that did not show a response to $T_3$. Figure 5.4 shows an additional piece of information, which indicates that there is a correlation between TRβ expression and levels of N-term RLKI (Pearson correlation: 0.78, $p<0.003$). Animal #12 has the highest TRβ levels and it also has the highest level of N-term RLKI, and the animal with the lowest N-term RLKI has the second lowest TRβ levels. This indicates that there is some biological factor connecting the control of the levels of both of these biomarkers. This common link might be TRα or even 5-deiodinases, whose level and activity might differ within the animal population.

In conclusion, TRβ assessment appears to be more sensitive to TH, but measurements of the N-term RLKI protein offer a lower variability in the data. The results further indicate that at the 48 h time point the C-fin assay should be able to distinguish antagonistic and agonistic effects of a test chemical if challenged with 10 nM $T_3$, and therefore further analyses focused on that time point and TH concentration.

### *5.3.4 Detection of disruption of TH action using the C-fin assay*

Ideally, to examine the utility of the C-fin assay, and in particular the novel N-term RLKI protein as biomarker, for the detection of agonistic and antagonistic effects on $T_3$ action, the study would have employed well proven and studied compounds such as the synthetic agonist, GC-1 (Furlow et al., 2004) and the synthetic antagonist NH-3 (Lim et al., 2002). Unfortunately both of these compounds are in clinical trials to be used as therapeutics and could not be acquired for the current research (personal communication with Thomas S. Scanlan and J. David Furlow). Instead, the C-fin assay was tested with three chemicals that have been shown to be potential EDCs of TH action: triclosan, tetrabromobisphenol A, and acetochlor. The modes of action of these chemicals

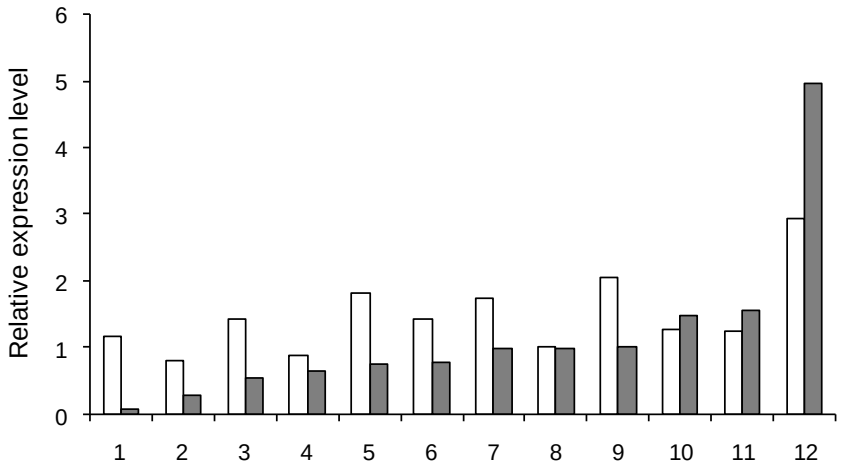


**Figure 5.4. Variability in the expression of $T_3$-induced N-term RLKI protein and TRβ transcript in the tadpole population.** Relative expression levels of N-term RLKI protein (white bars) and TRβ transcript (gray bars) are indicated for twelve individual tadpoles after their tail fin biopsies were exposed to 10 nM $T_3$ for 48 h. N-term RLKI protein levels were determined by immunoblot with anti-cytokeratin antibody and TRβ transcript levels were determined with QPCR. Values were expressed as relative expression by normalizing the N-term RLKI and TRβ expression values to one animal (#8) and presenting the data in increasing order of TRβ expression. A Pearson Correlation test found a correlation of 0.78 between N-term RLKI and TRβ values with a significance level of $p < 0.003$.

are still disputed as are their effects on TH action, however, each has been shown to be disruptive to TH signaling in at least a single system.

***Triclosan***

There is a growing concern regarding the presence of pharmaceuticals and personal care products in the environment and their possible deleterious effects on wildlife and humans. One such compound of potential interest is the antimicrobial agent triclosan (TCS; 5-chloro-2-[2,4-dichloro-phenoxy]-phenol) which is used in a number of consumer products such as toothpaste, deodorants, soaps, polymers and fibres. At the concentrations used (0.15-0.3%), TCS exhibits a broad-spectrum bacteriostatic activity while remaining non-toxic to mammals (Campbell and Zirwas, 2006). However, due to its structural similarity to THs (See figure 5.5A) it has sparked a concern over its potential as an EDC of TH-action at low concentrations, and has recently been shown to have such effects on anuran development and TH-associated gene expression at environmentally relevant concentrations (Veldhoen et al., 2006a). TCS has been detected in wastewater treatment plant effluents in North America, Europe and Australia at concentrations ranging from 0.12 to 9.3 nM, with the highest mean concentration of 4.0 nM in the US (Ying and

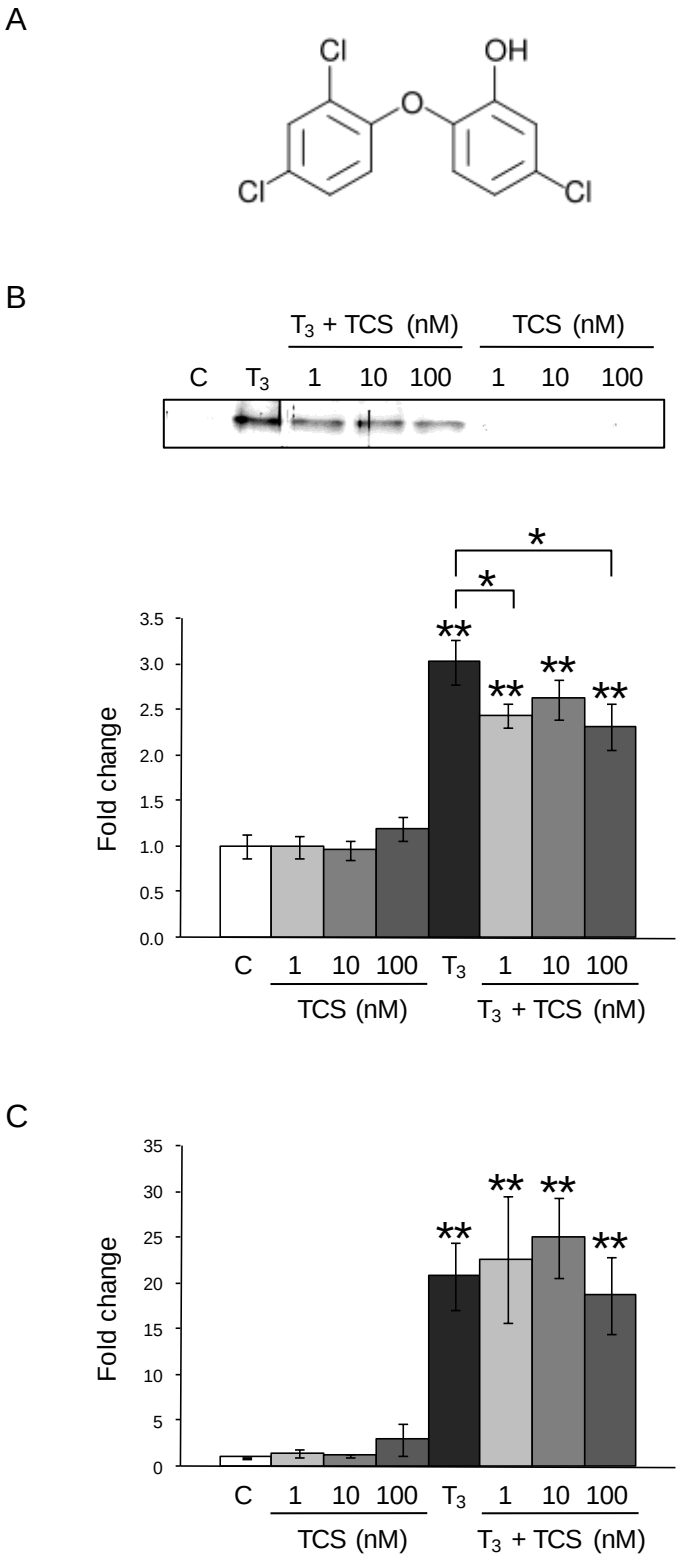


**Figure 5.5. Analysis of triclosan for TH disrupting activity with the N-term RLKI assay and through assessment of TRβ transcript levels.** (A) Structure of triclosan. (B) Levels of N-term RLKI protein in tail fin biopsy samples exposed to vehicle control (C), 10 nM $T_3$ ($T_3$), 1, 10, or

100 nM triclosan (TCS) alone or in combination with 10 nM $T_3$ ($T_3$ + TCS) for 48 h as measured by immunoblotting with anti-cytokeratin antibody. Sample immunoblot shows the N-term RLKI fragment at 25 kDa. Graph of averaged data from five experiments showing the fold change in the levels of N-term RLKI relative to vehicle control. Error bars represent the standard error of the mean. Significance is indicated by one asterisk (*) for $p < 0.05$ and by two asterisks (**) for $p < 0.01$ (Mann-Whitney U). Significance compared to controls is indicated above the bar and significances between treatments are indicated by brackets. (C) As in B but indicating fold change in steady-state levels of the TRβ transcript relative to vehicle control as determined by QPCR.

Kookana, 2007). In a survey of 139 streams across the United States, TCS was detected in over 55% of sites examined with a median concentration of 0.5 nM (Kolpin et al., 2002). TCS and its metabolites have also been found in human plasma and milk with median concentrations of 0.24 nM and 0.06 nM or 55 nM and 1.9 nM, respectively, depending on if the persons were non-users or users of TCS-containing personal products (Allmyr et al., 2006). This and other studies indicate that the direct use of TCS-containing products can expose our tissues to significantly high levels of this compound, highlighting the need for more research on the effects of TCS especially at the TH level (Allmyr et al., 2008).

The effects of TCS (Figure 5.5) were tested at three concentrations of 1, 10, and 100 nM, which were relevant to those found in the environment and human serum. TCS was tested alone or in combination with 10 nM $T_3$ for 48 hours, and the effects were compared to a vehicle control and $T_3$ alone. TCS alone had no statistically significant agonistic effects at any of the concentrations tested as shown by both N-term RLKI (Figure 5.5B) and TRβ (Figure 5.5C). $T_3$ alone increased the levels of N-term RLKI up by 3-fold as expected and of TRβ by around 20-fold. In combination with $T_3$, TCS showed a significant antagonistic effect on the levels of N-term RLKI at the 1 and 100 nM concentrations. Although, the 10 nM TCS-$T_3$ combination showed the same trend, the change was not statistically significant ($p = 0.25$). In comparison to $T_3$ alone, no significant changes in TRβ levels were observed at any of the concentrations of TCS in combination with $T_3$, although the variation in TRβ expression was high once induced by $T_3$, possibly masking any subtle effects that TCS might have. Based on the levels of N-term RLKI it appears that TCS may interfere with $T_3$ signaling reducing the production of this fragment. Veldhoen et al. (2006a) observed a similar antagonistic effect on $T_3$ based on TRβ transcript levels in the tail fin of *R. catesbeiana* tadpoles exposed to 1 and 10 nM TCS. Although in the current study the N-term RLKI levels follow this pattern, this is not observed in the TRβ transcript levels. The observations by Veldhoen et al. were made in live tadpoles that were pre-exposed to TCS for 4 days before being injected with $T_3$ and subsequently tested at 48 h. It is

possible that the N-term RLKI marker is more sensitive to TCS than TRβ in this biopsy assay format, and it would therefore be interesting to test if pre-exposing the biopsies to TCS would alter the levels of TRβ. Additionally, Veldhoen et al. observed that TCS had an effect on the rate of development, based on hindlimb morphology, which in this case showed an agonistic effect for TCS, accelerating $T_3$-induced metamorphosis. In the same study, the effect of TCS was shown to occur at the cellular level as demonstrated on a *X. laevis* XTC-2 cell line, and indicated that the metabolism of the whole animal is not required. In this case, TCS co-applied with $T_3$ was shown to have a potentiating effect on TRβ, TRα, and BTEB gene expression. As in the current study, TCS was never observed to have any effects alone. The discrepancy between TCS being agonistic or antagonistic in combination with $T_3$ can be attributed to the use of animal tissue versus a cell line, as well as pre-exposure regiments or the presence or absence of serum in the medium. Other studies on the effects of TCS on amphibians have shown altered tadpole behaviour and survivorship, however, they did not address any molecular mechanisms and were not performed in the context of TH (Fraker and Smith, 2004; Smith and Burgett, 2005). Considering the high levels of TCS found in humans, the fact that comparable concentrations had an effect on TH-action, and the lack of research on the molecular mechanisms of TCS action in TH disruption warrants further research into this compound.

***Tetrabromobisphenol A***

Brominated flame retardants (BFRs) are compounds that are widely used within consumer products for the suppression of fire (Alaee et al., 2003). With an estimated global consumption of 170,000 tonnes/year in 2004, tetrabromobisphenol A (TBBPA; 2,2',6,6'-Tetrabromo-4,4'-isopropylidendiphenol) is the most widely used BFR in the world, making up 59% of total world BFR usage (BSEF 2008; Law et al., 2006). TBBPA is used in the manufacturing of epoxy resins used in printed circuit boards where it is mostly incorporated in the polymer, but it is also used as an additive in plastics used in numerous consumer products from which it can easily leach out (Alaee et al., 2003; Watanabe and Sakai, 2003). TBBPA has been found as a contaminant in the environment, wildlife and humans (Watanabe and Sakai, 2003; Law et al., 2006). Concentrations in the range of 4-180 μg/kg dry weight (dw) in sewage sludge, 0.5-9800 μg/kg dw in river sediment and levels of 1.14 nM in landfill leachates have been detected at locations in Europe, North America and Japan (Watanabe and Sakai, 2003; Law et al., 2006; Osako et al., 2004). In wildlife, TBBPA has been found in cormorants, fish, and harbour porpoise blubber at concentrations ranging from 2.5 to 14, 0.2 to 245, and from 0.1 to 418 μg/kg lipid weight, respectively (Law et al., 2006). And in humans it has been found in serum at a median

concentration of 0.147 nM (Dirtu et al., 2008). TBBPA appears not to interfere with the estrogenic, progestagenic, androgenic or arylhydrocarbon receptor-mediated pathways (Hamers et al., 2006; Legler and Brouwer, 2003; Darnerud, 2003). The chemical structure of TBBPA is similar to that of THs (Figure 5.6A), and in a number of studies TBBPA has been observed to act as an agonist or antagonist of TH action possibly through binding to carriers such as TTR and/or the TRs (Hamers et al., 2006; Meerts et al., 2000; Kitamura et al., 2005a, 2005b; Veldhoen et al., 2006b). Due to TBBPA's yet uncertain mode of action it was interesting to test this compound with the N-term RLKI and TRβ markers in the C-fin assay.

The effects of TBBPA (Figure 5.6) on TH action were tested at three concentrations: 10, 100 and 1000 nM, which in a number of studies have shown agonistic and antagonistic effects (Hamers et al., 2006; Meerts et al., 2000; Kitamura et al., 2005a, 2005b; Veldhoen et al., 2006b). TBBPA was tested alone or in combination with 10 nM $T_3$ for 48 hours, and the effects were compared to a vehicle control and $T_3$ alone. TBBPA had no effect alone at any of the concentrations tested as shown by both N-term RLKI (Figure 5.6B) and TRβ (Figure 5.6C). $T_3$ alone increased the levels of N-term RLKI up by 2.5-fold as expected and of TRβ by around 15-fold. In combination with $T_3$, TBBPA showed a tendency towards a potentiating effect on N-term RLKI levels at the 10 nM concentration tested ($p = 0.08$), however, this did not pass the requirement of $p < 0.05$ to be considered significant. At the 100 nM dose a similar trend was observed but it was not statistically significant and no significant change was observed at the 1000 nM concentration. Compared to $T_3$ alone, no changes in TRβ levels could be observed at any of the concentrations of TBBPA in combination with $T_3$, although the variation in TRβ expression was high once induced by $T_3$, possibly masking any subtle effects of TBBPA. Based on the levels of N-term RLKI these results indicate that TBBPA might be increasing the effectiveness of $T_3$ or that TBBPA may have a weak agonistic activity and can act at the cellular level, directly at the TRs. Additional replicates and a possible optimization to the C-fin assay could clarify this trend. Previous findings made by Veldhoen et al. (2006b) in the Pacific tree frog premetamorphic tadpole, *Pseudacris regilla*, showed that 10 nM TBBPA, but not 100 nM TBBPA, acted agonistically with 10 nM $T_3$, potentiating tail regression based on muscle area and gelatinase B gene expression. In addition, neither TRα nor TRβ transcript levels, also tested at 48 h, were affected. Furthermore, using the sensitive T-screen assay based on TH responsive $GH_3$ rat pituitary cells, and measuring metabolic rate, Hamers et al. (2006) observed that TBBPA (at 500 nM) had no agonistic effect by itself but had a potentiating effect with $T_3$ (at 0.25 nM). In contrast, other studies using the T-screen method, observed that TBBPA had no potentiating

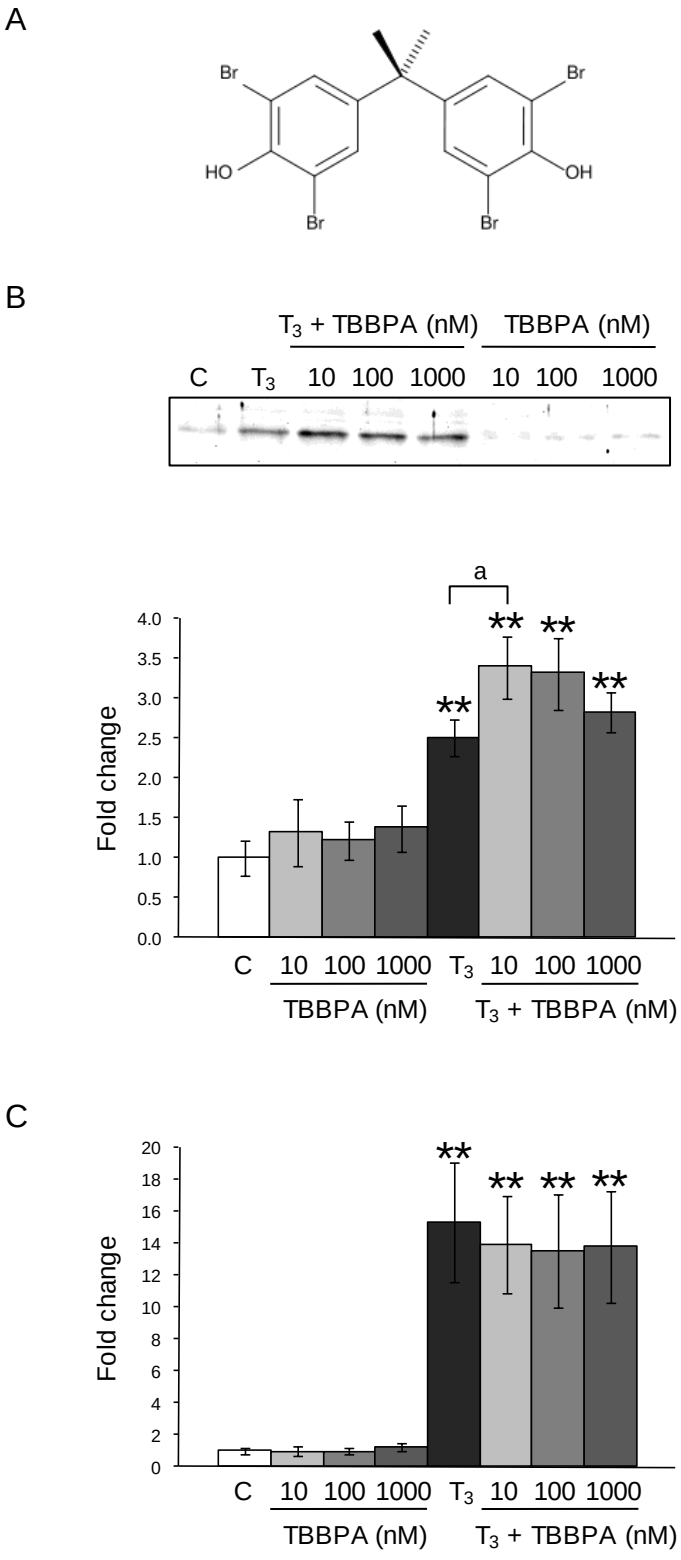


**Figure 5.6. Analysis of TBBPA for TH disrupting activity with the N-term RLKI assay and through assessment of TRβ transcript levels.** (A) Structure of TBBPA. (B) Levels of N-term RLKI protein in tail fin biopsy samples exposed to vehicle control (C), 10 nM $T_3$ ($T_3$), 10, 100, or

1000 nM TBBPA (TBBPA) alone or in combination with 10 nM $T_3$ ($T_3$ + TBBPA) for 48 h as measured by immunoblotting with anti-cytokeratin antibody. Sample immunoblot shows the N-term RLKI fragment at 25 kDa. Graph of averaged data from five experiments showing the fold change in the levels of N-term RLKI relative to vehicle control. Error bars represent the standard error of the mean. Significance is indicated by two asterisks (**) for $p < 0.01$ with (a) indicating a confidence level of $p = 0.08$ (considered not significant in this study) (Mann-Whitney U). Significance compared to controls is indicated above the bar and significances between treatments are indicated by brackets. (C) As in B but indicating fold change in steady-state levels of the TRβ transcript relative to vehicle control as determined by QPCR.

---

effects, although the concentrations of TBBPA used were higher, often in the μM range (Schriks et al., 2006; Kitamura et al., 2005a, 2002). The majority of the literature, however, appears to indicate that TBBPA has antagonistic effects on TH action. Fini et al. (2007), testing TBBPA at 100, 500 and 1000 nM concentrations, found that 1000 nM TBBPA was antagonistic to 5 nM $T_3$ using a transgenic *X. laevis* embryonic stage tadpole expressing an EGFP reporter gene driven by a TRE-containing TH/bZIP promoter in an *in vivo* multiwell-based assay. Similarly, Kitamura et al (2005b) also found antagonistic effects at concentrations between 3.1 to 25 μM on 10 nM $T_3$ using a gene reporter assay consisting of a TRE-luciferase construct in a hamster ovary cell line (CHO-K1) expressing human TRα1 or TRβ1. The same study showed that TBBPA's antagonisitic effect was more pronounced *in vivo* using *Rana rugosa* tadpoles where a 1000 nM concentration slowed $T_3$-induced (50 nM) tail shortening. Kitamura's group also showed that TBBPA was able to weakly displace $T_3$ from human TRs with an $IC_{50}$ of 3.5 μM, based on the use of crude nuclei preps and $^{125}$I-$T_3$. While $T_3$ was a thousand times more effective with an $IC_{50}$ of 3.3 nM. Furthermore, Meerts et al. (2000) found that *in vitro* TBBPA bound to human TTR 10.6-fold stronger ($IC_{50}$ of 7.7 nM) than the natural ligand $T_4$ ($IC_{50}$ of 80.7 nM). These findings indicate that TBBPA at high concentrations can probably bind to TRs acting as an antagonist but other factor(s) such as serum carrier proteins like TTR, the HPT-axis, or deiodinases, present in the whole animal might be more important in its effect. This further supports the use of an *in vivo* or an *ex vivo* assay system that is closer to the actual biology of the organism. The reason for TBBPA acting as an antagonist *in vivo* might be due to its displacement of the natural or submitted TH from the serum carrier TTR, increasing metabolism and excretion of THs thus lowering their effect.

Jugan et al. (2007), using a reporter gene assay with a TRE-luciferase reporter construct in PC12 mammalian cells expressing avian TRα1, found a similar dose-response to ours where TBBPA was agonistic between 10 and 60 μM, but lost any effect above 60 μM, although this was observed with TBBPA alone at concentrations 1,000-60,000 times higher to ours. In addition,

when $T_3$ was added at 0.3 nM, TBBPA acted as an antagonist, with an $IC_{50}$ of 50 μM. Similarly, Jagnytsch et al. (2006) testing TBBPA at concentrations from 5 to 920 nM on premetamorphic *X. laevis* tadpoles observed an agonistic effect at 920 nM TBBPA based on TRβ and TH/bZIP gene expression in the head region, and an antagonistic effect at concentrations from 180-920 nM when given in combination with 0.1 or 1.0 nM $T_3$. The effectiveness of TBBPA to act as an antagonist of TH action appears to be enhanced at higher concentrations and is more pronounced with lower levels of competing $T_3$ (Jagnytsch et al., 2006). It is possible that the 10 nM $T_3$ concentration used in the current experiment was too high to see an antagonistic effect of TBBPA which would be effectively outcompeted by $T_3$ from binding the TRs due to its lower affinity. Future experiments using the C-fin assay could be performed using 1 nM $T_3$ as this concentration was still significantly different from the control for both endpoints (Figure 5.3D and E).

The discrepancies between TBBPA being an agonist or an antagonist might come from the usage of different $T_3$ concentrations in the TH-inductions of each assay, as well as from different starting concentrations of THs which may differ from assay to assay depending if serum-free conditions were used or not. And finally the assays themselves differ in the cellular and biological context, as is the case for the tail biopsies which are a tissue destined to die versus the $GH_3$ cells which proliferate due to the same signal. What is important is that perturbations to the TH pathway are observed.

***Acetochlor***

Acetochlor (2-chloro-*N*-(ethoxy-methyl)-*N*-(2-ethyl-6-methylphenyl) acetamide) (Figure 5.7A) is a pre-emergent herbicide that is widely applied to planted corn to prevent competition from emerging grasses and broadleaf weeds, in turn increasing crop yields. Since its introduction in 1994 acetochlor concentrations in the environment have been increasing, and streams in the Midwestern United States have been observed to have a median concentration of 2.7 nM with concentrations of up to 10 nM (Scribner et al., 2000). Although this compound does not resemble THs in its structure, it has been found to act as an EDC of TH action. Cheek et al. (1999a) have shown that 10 nM acetochlor accelerated $T_3$-induced precocious metamorphosis, based on forelimb emergence, in the northern leopard frog tadpole, *Rana pipiens*. At the molecular level, 10 nM acetochlor was observed to potentiate $T_3$-induced TRβ transcript levels in the tail tissues of *R. catesbeiana* (Veldhoen and Helbing, 2001) and *X. laevis* (Crump et al., 2002). In the *X. laevis* study, which assessed changes in gene expression through the use of an amphibian 420 gene cDNA array, acetochlor was additionally shown to potentiate expression levels of other

previously discovered $T_3$-responsive genes such as TH/bZIP, collagenase-3 and BTEB, as well as attenuate the decrease of $T_3$-downregulated genes such as gene-17,-18, -19 (Crump et al., 2002). These studies suggested that acetochlor might be acting at a pivotal factor in the TH pathway. However, acetochlor did not affect all TH-responsive genes, precluding an effect on deiodinases. Additionally Cheek et al. (1999a) have shown that the acceleration of metamorphosis is unlikely to be modulated through TRs due to a lack of response to acetochlor alone when tadpoles were pre-exposed to $T_3$ and due to the lack of binding of acetochlor to recombinant human TRβ (Cheek at al. 1999b). Furthermore, acetochlor in combination with $T_3$ had no effect on other metamorphic features such as hindlimb development or tadpole growth, and 0.1 or 1000 nM acetochlor concentrations did not have an effect on forelimb emergence as did the 10 nM concentration (Cheek at al. 1999a). These findings suggest that the mode of action of acetochlor is more complex than it simply acting upon TRs or deiodinases and it was therefore of interest to apply the C-fin assay to test whether acetochlor had any effects at the level of the TH pathway represented by the N-term RLKI marker.

The effects of acetochlor (Ac) were tested at three concentrations of 1, 10, and 100 nM which spans median and maximum concentrations measured in streams in the Midwestern United States (Scribner et al., 2000). Acetochlor was tested alone or in combination with 10 nM $T_3$ for 48 hours, and the effects were compared to a vehicle control and $T_3$ alone. $T_3$ alone increased the levels of N-term RLKI (Figure 5.7B) up by around 2.5-fold as expected and of TRβ (Figure 5.7C) by around 25-fold. Based on the levels of N-term RLKI (Figure 5.7B), acetochlor in combination with $T_3$, had no observable potentiating or antagonistic effects at any of the concentrations tested. Additionally, no significant changes in TRβ levels (Figure 5.7C) could be observed at any of the concentrations of acetochlor in combination with $T_3$ when compared with $T_3$ alone. This observation was contrary to the observations in the literature that showed acetochlor potentiating the $T_3$-induced expression of TRβ (Veldhoen and Helbing, 2001; Crump et al., 2002) However, in support of the current results, in a study by Turque et al. (2005) where an assay consisting of a transgenic premetamorphic *X. laevis* tadpole carrying a TRE-containing TH/bZIP-EGFP construct was used to test acetochlor (10 nM) in combination with $T_3$, no significant potentiating effect was observed as revealed by expression in the brain.

Acetochlor alone at the highest concentration showed a trend towards an agonistic effect based on the levels of N-term RLKI (Figure 5.7B), however this was not considered significant ($p=0.10$). This trend was not observed for acetochlor alone at any of the concentrations tested as shown by TRβ transcript levels (Figure 5.7C). The lack of any effects by acetochlor with high statistical

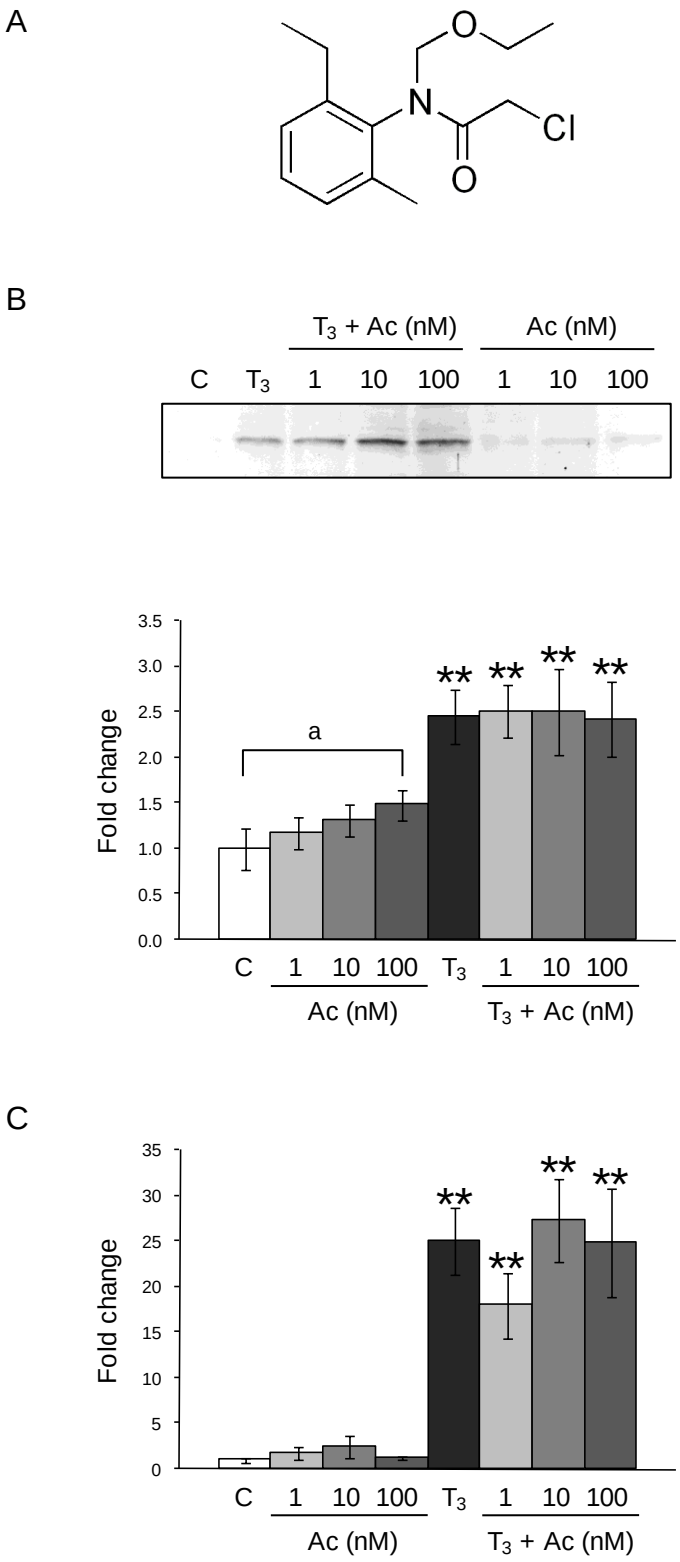


**Figure 5.7. Analysis of acetochlor for TH disrupting activity with the N-term RLKI assay and through assessment of TRβ transcript levels.** (A) Structure of acetochlor. (B) Levels of N-term RLKI protein in tail fin biopsy samples exposed to vehicle control (C), 10 nM $T_3$ ($T_3$), 1, 10,

or 100 nM acetochlor (Ac) alone or in combination with 10 nM $T_3$ ($T_3$ + Ac) for 48 h as measured by immunoblotting with anti-cytokeratin antibody. Sample immunoblot shows the N-term RLKI fragment at 25 kDa. Graph of averaged data from six experiments showing the fold change in the levels of N-term RLKI relative to vehicle control. Error bars represent the standard error of the mean. Significance is indicated by two asterisks (**) for $p < 0.01$ with (a) indicating a confidence level of $p = 0.10$ (considered not significant in this study) (Mann-Whitney U). Significance compared to controls is indicated above the bar and significances between treatments are indicated by brackets. (C) As in B but indicating fold change in steady-state levels of the TRβ transcript relative to vehicle control as determined by QPCR.

significance suggests that acetochlor might only exhibit agonistic potential in the whole organism as was the case with all of the previous studies where exposures were done on live tadpoles. All of the previous studies have also used $T_3$ at a higher concentration of 100 nM, making this an additional possible reason for the discrepancy. In support of the observation of a possible slight agonistic effect with acetochlor alone in the current study, Helbing et al. (2006) observed that acetochlor alone was able to elevate transcript levels of TRα and TRβ within the brain tissue of premetamorphic *R. catesbeiana* tadpoles in addition to potentiating the expression of the receptors in combination with $T_3$. Additionally, Helbing et al. (2006) observed that prometamorphic *R. catesbeiana* tadpoles exposed to acetochlor alone at 1 and 10 nM showed an increase in the transcript levels of TRα and TRβ in the tail fin. Prometamorphic tadpoles will have rising endogenous $T_3$ levels. According to this, if the effect of acetochlor occurs at the level of the cell in the tail fin, the C-fin assay with its $T_3$-induction should have revealed an effect. However, Helbing et al. (2006) measured the effects in the tail fin at 6 days post exposure, and therefore it would be interesting to see if a longer exposure period or a higher 100 nM $T_3$-induction would give different results in the C-fin assay. In conclusion, these findings suggest that the agonistic actions of acetochlor occur only at the whole animal level.

## 5.4 CONCLUSIONS

A central goal of this study included establishing a rapid, sensitive and amenable to high-throughput method for assaying TH agonists and antagonists based on the protein marker N-term RLKI. The assay fulfilled a number of important criteria such as low background with no interference from endogenous hormone, robust and statistically significant responses, dose dependence, and low threshold. Its sensitivity and dose response has been shown to be comparable to transcript and TRE-reporter based assays, and it surpassed some assays in these criteria. The use of a single tadpole for multiple exposures reduces animal use, and the multi-well format reduces reagent costs and makes the assay amenable to high-throughput where large

numbers of chemicals at different concentrations can be tested. Furthermore, having multiple animals, and all exposed to the same set of different treatments will provide information on variability in response to the individual treatments within the animal population. This is in contrast to most metamorphic assays such as the XEMA and the AMA where treatments consist of a number of pooled animals (Fort et al., 2007).The C-fin assay also requires a much shorter time frame than the suggested morphological assays.

In this assay format the detection of N-term RLKI protein was more robust than the TRβ transcript. This was due to the fact that the TRβ transcript levels appeared to be highly variable within the treatments once induced with $T_3$. This high variability in transcript response due to $T_3$ has previously been reported in premetamorphic tadpoles by Turque et al. (2005). The solution, which could be employed in this case as well, was to prime or pretreat the tadpoles for 24 h with a very low dose (0.001 nM) of $T_3$. This weak pulse of $T_3$ was shown to synchronize the $T_3$ transcriptional response and reduce intragroup variability by inducing a low TRβ expression (Turque et al., 2005). The observed lower variability with N-term RLKI compared to TRβ transcript can also be attributed to the fact that the detected N-term RLKI fragment is derived from a very abundant structural protein while the lower abundance TRβ transcript is detected through the process of exponential amplification by QPCR, which is more prone to influences that increase variability.

The C-fin assay based solely on the tail fin tissue is unable to determine TH disrupting effects that occur strictly at the thyroid gland or the HPT-axis, or ones that affect TH metabolism and excretion by the liver, however the assay can still encompass a large range of potential interferences. These include interferences with TH transport across the cell membrane, with TH degradation by deiodinases, with binding to cellular proteins, and interferences with binding to the receptors or coregulator associations and subsequent effects on gene expression and downstream molecular events. Additionally, this *ex vivo* system is removed from other hormonal influences that are present in the whole animal system such as PRL, potential gonadal steroids and effects of the HPT-axis that could potentially mask an EDC's action. The limitation of this assay to certain levels of the TH pathway can also be helpful at suggesting possible modes of action as was seen with the tested chemicals. The results with N-term RLKI corroborated the results previously observed for TCS, that concentrations as low as 1 nM have an effect on $T_3$-action, and that this effect can occur directly at the cellular level without the need for a whole organism which, for example, may modify the parent compound by enzymatic conversion in the liver. This suggests that TCS may act on cellular proteins that bind THs such as transporters,

CTHBPs or TRs. The results with TBBPA, suggest that this compound might have agonistic potential on tadpole tail metamorphosis in combination with $T_3$, without affecting TRβ, as has been observed previously in *Pseudacris regilla* (Veldhoen et al., 2006b), and that this might be through a tissue direct process. The results with acetochlor compared to previous observations of acetochlor having a potentiating effect on $T_3$-induced tadpole metamorphosis and TR transcript levels in live tadpoles, suggest that the mode of action of acetochlor is at a higher level than the tissue/cell level provided in this assay.

A number of research groups have used the dependence of anuran metamorphosis on TH to develop assays for the detection of TH-modulating compounds ranging from whole-animal morphological assays to assays based on germinal transgenic tadpoles with TRE-driven reporters. Unlike any previous TH disruption assays, which usually depend on a genomic response, the C-fin assay incorporates a novel N-term RLKI protein cleavage endpoint. This biomarker, which is an indicator of the initiation steps of apoptosis in the tail, could be used in combination with other genomic markers, increasing the span of investigation on the TH path, thus providing more clues for the determination of the mode of action of a chemical.

The C-fin assay shows great promise for use in detecting disruptors of TH action on a target tissue. With further refinements and the potential for expanding the transcript and protein endpoints, this will prove to be a significant addition to the battery of EDC tests needed to handle the ever-increasing challenge of chemical risk assessment and monitoring.

# Chapter 6: Discussion and future directions

This thesis presents the first mass spectrometry-based proteomic study of anuran metamorphosis. The success of this approach is demonstrated by the discovery and cloning of the novel keratin RLKI, in light of the fact that keratins have been extensively studied during metamorphosis in *R. catesbeiana* for two decades (Yoshizato, 2007). The study also identified other proteins whose levels and/or phosphorylation states are altered within 48 h of the induction of tadpole tail regression prior to overt remodeling of the tail. We have demonstrated the ability to derive this proteomics-based information from a model species for postembryonic development for which limited genome information is currently available. The discovery that RLKI is posttranslationally modified by the action of caspases early in the initiating steps of $T_3$-induced apoptosis underlines the importance of a proteomics-based approach in addition to the currently used genomic approaches.

## *6.1 Proteomic analysis of differential protein expression*

Our extensive fractionation methodology combined with multiple 2D gel analysis and the iTRAQ study identified differentially expressed proteins that are mostly present in high abundance within the cell. This fact does not indicate a short coming of the fractionation method, as mass spectrometric analysis of random protein spots on the 2D gels was able to identify with high confidence a low abundance protein spot as the phosphoprotein mitogen activated protein kinase kinase (MAPKK), considered a low abundance signaling protein. The analysis revealed that this phosphoprotein was not altered in expression level or phosphorylation state under the conditions tested. The ability of 2D gel analysis to reveal subtle changes in protein expression could be improved through the use two color fluorescent labeling methods that can differentially label two protein samples and concurrently analyze them within a single 2D gel avoiding the drawbacks of reproducibility between gels (Gharbi et al., 2002).

Alternative methods to iTRAQ or PhIAT to quantify changes in differential protein expression or alterations in the phosphoproteome can be used. The first method of stable-isotope tagging of proteins was performed by metabolic labelling of *Saccharomyces cerevisiae* for quantitative protein profiling to determine differences in protein expression (Oda et al., 1999). Two yeast cultures grown in growth medium enriched for $^{14}N$ or $^{15}N$ were mixed after treatment and growth, and the extracted proteins separated on a single 2D gel. Differences in protein expression were revealed by MALDI-MS analysis where two peaks for each protein/peptide (one for $^{14}N$ and one

for $^{15}N$) differed in intensity if the original protein/peptide was expressed differentially in the two cultures. The application of this methodology has been limited to biological specimens that can be grown in culture, however, tadpole tail biopsies cultured in normal nutrient medium and in nutrient medium enriched for a stable isotope could possibly be used with MS analysis to indicate expression differences in proteins due to a treatment such as TH. The proteins from two different treatments could first be separated by individual 2D gels to indicate differences in expression levels based on protein spot intensities. A subsequent, single 2D gel could be run on which both samples are separated concurrently, the proteins of interest extracted and analyzed by MS to determine relative expression differences and protein identity, thus improving quantitation. This method can also be used to look at differential expression of phosphoproteins between two treatments through the use of tandem MS and identification of phosphopeptides from metastable losses.

The analysis of phosphoproteins is inherently difficult due to the fact that phosphorylation is stoichiometrically low and that it can be heterogenous for a given protein. Furthermore, phosphoproteins such as signal transduction proteins or cell-cycle regulators are present in low abundance in a cell. This might explain why the current study could only identify GILT, which was actually phosphorylated on its glycan chain rather then the classic amino acid residues. The proteomic analysis of *R. catesbeiana* (Chapter 3) did not employ any enrichment steps targeted at phosphoproteins and only used a phosphoprotein specific stain. Future experiments could employ phosphoprotein enrichment methods such as immobilized metal affinity chromatography (IMAC) (Stensballe et al.,2001) or the more recently developed titanium oxide (TiO) chromatography (Olsen et al., 2006). Olsen et al. through the use of cell fractionation, TiO chromatography, and high performance Fourier Transform Ion Cyclotron Resonance MS analysis could extensively define the sequence of phosphorylation events in the EGF signaling path, revealing thousands of phosphorylation events on proteins with specific temporal profiles and differences between the nucleus and cytoplasm. This global analysis of the phosphoproteome revealed that the majority of the phosphoproteins at the end of the signaling path were transcription factors and coregulators located in the nucleus, most likely low abundance proteins, underlining the challenge of this type of analysis.

2D gel and iTRAQ type of analysis show steady-state levels of proteins at a specific point in time. The steady-state level of a protein is dependent on the rate of its synthesis and its rate of degradation. The latter two processes are currently a missing dimension in proteomic analysis. Information on the rate of these two processes can be obtained by applying a variation of the

metabolic stable-isotope labelling method discussed above (Pratt et al., 2002). To achieve this, a tissue is grown in medium enriched for a stable isotope such as nitrogen to ensure that all the proteins contain the isotope. The culture is then chased with medium containing the normal abundance of nitrogen isotope and samples of the culture are taken out at different time points and proteins are analyzed by MS. Changes in the peak intensities over time for the two different forms of nitrogen for a specific protein or peptide indicate the changes in the synthesis or degradation rates of that protein.

### *6.2 RLKI and apoptosis*

The findings in chapter 4 allow us to speculate that the formation of N-term RLKI as a possible caspase-3 cleavage product due to the TH signal may lead to keratin intermediate filament reorganization, which was observed here as a possible increase in cell detachment, thereby creating a positive feedback loop leading to an eventual increase in apoptosis. Byun et al. (2001) observed that transfecting cells with the N-terminal fragment of the type III intermediate filament protein vimentin, which was a caspase-cleavage product, interfered with intermediate filament (IF) assembly and induced caspase-dependent apoptotic death. Likewise, the N-terminal caspase cleavage product of desmin, also a type III IF protein, disrupted intermediate filament assembly in transfected cells in a dominant-negative fashion, supporting the idea that caspase cleavage products of IF proteins affect the cytoskeleton (Chen et al., 2003). This could possibly be occurring in the N-term RLKI-transfected XLT-15 cells used in our experiments, which are of myoblastic origin and may therefore contain desmin IF networks. Intact keratin IF networks could also be keeping apoptosis at bay as has been shown by Inada et al. (2001) where IFs of K8/K18 sequestered TRADD, preventing TNF-induced apoptosis. And, the release of type I keratins from the IFs due to caspase cleavage could further amplify apoptosis by releasing such pro-apoptotic factors as TRADD. It has been observed *in vitro* and *in vivo* that cells deficient or defective in K8/K18 are more susceptible to stress induced apoptosis (Marceau et al., 2001). Considering that cDNAs encoding caspase-8, TNFR-like death receptors, and FADD have been cloned in *X. laevis* implies a conservation in the mechanisms (Nakajima et al., 2000; Tamura et al., 2004; Ishizawa et al., 2006) and suggests that similar pathways could be at work during metamorphosis. Another method by which intact cytokeratins could protect against apoptosis is through the sequestration of activated caspases reducing their availability to other normal substrates. The observed cytoplasmic inclusions formed after the collapse of the IF network are insoluble aggregates of cleaved keratins, active caspases and other agents involved in the development of apoptosis, and

may therefore also protect healthy neighbouring cells (MacFarlane et al., 2000; Dinsdale et al., 2004).

The early appearance of N-term RLKI after the TH signal could be due to a physical association of RLKI with the activating caspases. This has been observed for K8/K18 filaments which at the onset of an apoptotic signal have been observed to act as scaffolds that sequester pro-caspase-9 and pro-caspase-3 and lead to autoactivation through the association and action of ubiquitinated death-effector-domain containing DNA-binding protein (DEDD) (Dinsdale et al., 2004). Active caspases and cleaved K18 are observed within these complexes early in the apoptotic process. This is thought to create an amplification loop by which caspases are increasingly activated through mutual cleavage, and in addition they disrupt the cytoskeleton leading to the hallmarks of apoptosis.

The transition of larval skin into adult skin has been studied extensively in *R. catesbeiana* (Ishida et al., 2003; Suzuki et al., 2001, 2002). Even in the tail epidermis which is eventually destined to die, epidermal cells differentiate with a transition of basal skein cells to basal cells. In this transition, through a yet undefined process, keratin bundles called figures of Eberth disassemble in the presence of low TH (Suzuki et al., 2002). The figures of Eberth are thought to be composed of RLK II, and this transition also involves the downregulation of RLK II in these cells and the expression of RAK (Suzuki et al., 2001). It would be interesting to test if the disassembly process involves the caspase cleavage of RLK I, and if RLK I interacts with RLK II, as would be expected of keratins which in mammals have been shown to form obligate heterodimers of acidic and basic keratins. Interestingly, as is the case with the RLK II transcript, we observed a decrease in the transcript levels of RLK I in the tadpole tail at metamorphic climax and in $T_3$-induced tadpole tail (Chapter 3; Domanski and Helbing, 2007), suggesting that these two keratins could be co-regulated.

### *6.3 RLKI in the C-fin assay*

The total dependence of amphibian metamorphosis on TH has led to the suggestion that metamorphosis can be used to assess TH disruption. A number of research groups have used this premise to develop assays for the detection of TH-modulating compounds ranging from whole-animal morphological assays to assays based on germinal transgenic tadpoles with TRE-driven reporters. A number of these studies have shown effects of potential EDCs of TH action at sublethal concentrations on the transcriptome level, however, very few of these have associated these changes with significant morphological or developmental alterations, and none have shown

that these transcript alterations have deleterious consequences for reproduction or survival under natural conditions. The use of a protein-based marker such as N-term RLKI brings the analysis one level closer to the consequential morphologic and eventually survival-related endpoints. Previous studies have suggested numerous transcript-based biomarkers, derived from extensive DNA-array and QPCR analyses of tail, hindlimb and brain tissues of exposed *X. laevis* tadpoles, which could be used for determining EDCs of TH-action (Helbing et al. 2007a, 2007b). Interestingly, a 51-kDa cytokeratin type I transcript, similar to RLKI, was suggested as a biomarker in the hindlimb for exposure to goitrogens (Helbing et al. 2007b). These transcript-based biomarkers still need to be extensively validated and no studies have suggested a protein-based biomarker or used one in an assay format. Although assays based on TRE-reporter constructs use the protein levels of luciferase or GFP as endpoints, the current study is the first one to employ a natural protein event in the amphibian as the endpoint in an assay to indicate possible perturbations to TH action.

In addition to observing a posttranslational modification to RLKI, we observed that transcript levels of RLKI are significantly decreased by 48 h of $T_3$ exposure (Chapter 3; Domanski and Helbing, 2007). The RLKI transcript could provide an additional marker that could be used in the TH-disruption assays, and is an example of a TH-responsive gene that is repressed, providing an additional level of assessment to that provided by upregulated genes such as TRβ.

The detection of caspase-cleaved human keratin K18 has already been proven to be of value in the clinic. The specific detection of a neo-epitope, exposed after caspase cleavage in the early stages of apoptosis, by the monoclonal antibody M30 has been used in an ELISA assay (Apoptosense) in the clinic for diagnostic and prognostic assessment of cancer and other pathologies (Roth et al., 2004; Ueno et al., 2003; Olofsson et al., 2007). In addition the assay has been used for screening drugs with potential anti-tumor activity (Olofsson et al. 2007). The N-term RLKI endpoint determination could be improved by the development of an antibody that would specifically detect a neo-epitope on N-term RLKI allowing the use of an ELISA format. This would likely improve the sensitivity of the assay and the linear range of detection. Another way of improving the current assay in terms of sensitivity and linear range could be done by performing the detection step of N-term RLKI using mass spectrometry instead of the current Western. This could be performed using a method termed SISCAPA for Stable Isotope Standards and Capture by Anti-Peptide Antibodies (Anderson et al., 2004). Protein samples extracted from the biopsies would be cleaved into peptides using trypsin. The digests would then be spiked with stable-isotope-labeled internal peptide standards representing the peptides of interest within the

RLKI protein. This mixture would then be enriched for the peptides of interest, including the internal peptide standards, using a column with immobilized anti-peptide antibodies. The eluent would finally be analyzed using either electrospray or MALDI mass spectrometry to quantitate the peptides. Because the caspase cleavage site VEMDA in RLKI is flanked by trypsin cleavage sites the native RLKI protein could be distinguished from the caspase cleaved RLKI and each could be quantitated based on two different stable-isotope-labeled peptide standards: one representing the native peptide and the other representing the peptide product due to caspase cleavage. The antibody enrichment would improve sensitivity and the signal detection through mass spectrometry would increase the dynamic range.

An additional approach, to improve the reproducibility and decrease the variability of the current assay and to omit the use of animals, was tested with the *X. laevis* XLT-15 cells transfected with the full RLKI expression construct. The rational being that the homogenous XLT-15 cells with a lower variability in response would substitute tail fin biopsies in the assay. As previously shown, the XLT-15 cells respond to $T_3$ by a slight increase in apoptosis. With the idea that this increase in apoptosis could be detected by observing the N-term RLKI fragment from the caspase-cleaved full RLKI protein, transfected cells were analyzed for N-term RLKI at 48, 72 and 96 h after being exposed to 10 or 50 nM $T_3$. Due to the very low induction of apoptosis due to $T_3$, however, no N-term RLKI fragment could be detected in the attached cells, although the full protein was clearly cleaved in apoptotic detached cells (data not shown). Since no robust $T_3$ response with a concurrent RLKI cleavage could be established this approach was abandoned. If a XLT-15 cell line stably expressing Full RLKI that was also more responsive to $T_3$ could be cloned it has the potential of precluding the use of animals.

### *6.4 From TH signal to RLKI cleavage*

During tadpole development TRα is present within the tail tissue after hatching while TRβ only becomes detectable at prometamorphosis and rises with the increase in endogenous TH levels (Eliceiri and Brown, 1994). While both TRα and TRβ transcript levels rise in the tail with the progression of metamorphosis and TH-induction, only TRβ protein levels increase, eventually being higher then that of TRα at climax (Opitz et al., 2006a; Eliceiri and Brown, 1994). Considering that N-term RLKI appears very early (12 h) after the TH signal, at about the same time as TRβ transcript levels begin to rise (Opitz et al., 2006a), but before the reported detection of TRβ protein (20 h) (Eliceiri and Brown, 1994), implies that the caspase cleavage of RLKI is most likely under the control of TRα rather than TRβ. We have shown that N-term RLKI and

TRβ appear to be controlled by a common factor by revealing a correlation between $T_3$-induced levels of TRβ transcript and N-term RLKI levels. This common factor is likely to be TRα, but could also be something central to the control of TH levels such as deactivating 5-deiodinase activity. To prove that the TH signal that results in RLKI cleavage is most likely conducted through TRα and not TRβ, the synthetic agonist GC-1 could be used. GC-1 is a TH analog that binds and activates both TRs but with higher specificity for TRβ, allowing this analog to target TRβ expressing tissues and inducing their respective metamorphic responses (Furlow et al., 2004). Furthermore, inhibition of protein synthesis within the tail fin in the first 12 h of the $T_3$ induction could reveal if new proteins such as TRβ need to be produced to result in the formation of N-term RLKI. Additionally, we have shown that cleavage of RLKI may be occurring in the epidermal cells of the tadpole tail as a result of caspase-3 activity. In support of this, Schreiber and Brown (2003) have shown that in *X. laevis* the $T_3$-induced apoptotic death of the larval epidermal cells requires a functional TR. A dominant-negative TRα directed to express only in the larval epidermis was able to prevent the $T_3$-induced appearance of active caspase-3, the down-regulation of larval keratin and the eventual apoptotic death. The molecular events of how a ligand-bound TR activates caspases in apoptotic tissues are largely unknown and are an area that should be investigated in the future.

## BIBLIOGRAPHY

Aebersold R, Mann M. Mass spectrometry-based proteomics. Nature. 2003 Mar 13;422(6928):198-207.

Alaee M, Arias P, Sjödin A, Bergman A. An overview of commercially used brominated flame retardants, their applications, their use patterns in different countries/regions and possible modes of release. Environ Int. 2003 Sep;29(6):683-9.

Allmyr M, Adolfsson-Erici M, McLachlan MS, Sandborgh-Englund G. Triclosan in plasma and milk from Swedish nursing mothers and their exposure via personal care products. Sci Total Environ. 2006 Dec 15;372(1):87-93.

Allmyr M, Harden F, Toms LM, Mueller JF, McLachlan MS, Adolfsson-Erici M, Sandborgh-Englund G. The influence of age and gender on triclosan concentrations in Australian human blood serum. Sci Total Environ. 2008 Jan 18; [Epub ahead of print]

Altschul SF, Madden TL, Schaffer AA, Zhang J, Zhang Z, Miller W, Lipman DJ. Gapped BLAST and PSI-BLAST: a new generation of protein database search programs. Nucleic Acids Research. 1997,25;3389-3402.

Anderson NL, Anderson NG, Haines LR, Hardie DB, Olafson RW, Pearson TW. Mass spectrometric quantitation of peptides and proteins using Stable Isotope Standards and Capture by Anti-Peptide Antibodies (SISCAPA). J Proteome Res. 2004 Mar-Apr;3(2):235-44.

Arunachalam B, Phan UT, Geuze HJ, Cresswell P. Enzymatic reduction of disulfide bonds in lysosomes: characterization of a gamma-interferon-inducible lysosomal thiol reductase (GILT). Proc Natl Acad Sci U S A. 2000 Jan 18;97(2):745-50.

Asahina K, Oofusa K, Obara M, Yoshizato K. Cloning and characterization of the full length cDNA encoding alpha2 type I collagen of bullfrog Rana catesbeiana. Gene. 1997 Jul 31;194(2):283-9.

Asahina K, Utoh R, Obara M, Yoshizato K. Cell-type specific and thyroid hormone-dependent expression of genes of alpha1(I) and alpha2(I) collagen in intestine during amphibian metamorphosis. Matrix Biol. 1999 Feb;18(1):89-103.

Atkinson BG, Helbing CC, Chen Y. Reprogramming of genes expressed in amphibian liver during metamorphosis. In *Metamorphosis: Postembryonic Reprogramming of Gene Expression in Amphibian and Insect Cells.* (Gilbert LI, Tata JR, Atkinson BG, eds.), Academic Press, New York, 1996, p539-566.

Baker BS, Tata JR. Prolactin prevents the autoinduction of thyroid hormone receptor mRNAs during amphibian metamorphosis. Dev Biol. 1992 Feb;149(2):463-7.

Bassett JH, Harvey CB, Williams GR. Mechanisms of thyroid hormone receptor-specific nuclear and extra nuclear actions. Mol Cell Endocrinol. 2003 Dec 31;213(1):1-11.

Becker KB, Stephens KC, Davey JC, Schneider MJ, Galton VA. The type 2 and type 3 iodothyronine deiodinases play important roles in coordinating development in *Rana catesbeiana* tadpoles. Endocrinology. 1997 Jul;138(7):2989-97.

Bergh JJ, Lin HY, Lansing L, Mohamed SN, Davis FB, Mousa S, Davis PJ. Integrin alphaVbeta3 contains a cell surface receptor site for thyroid hormone that is linked to activation of mitogen-activated protein kinase and induction of angiogenesis. Endocrinology. 2005 Jul;146(7):2864-71.

Berry DL, Schwartzman RA, Brown DD. The expression pattern of thyroid hormone response genes in the tadpole tail identifies multiple resorption programs. Dev Biol. 1998a Nov 1;203(1):12-23.

Berry DL, Rose CS, Remo BF, Brown DD. The expression pattern of thyroid hormone response genes in remodeling tadpole tissues defines distinct growth and resorption gene expression programs. Dev Biol. 1998b Nov 1;203(1):24-35.

Bethune J, Wieland F, Moelleken J. COPI-mediated Transport. J Membr Biol. 2006 May;211(2):65-79.

Birkelund S, Bini L, Pallini V, Sanchez-Campillo M, Liberatori S, Clausen JD, Ostergaard S, Holm A, Christiansen G. Characterization of Chlamydia trachomatis l2-induced tyrosine-phosphorylated HeLa cell proteins by two-dimensional gel electrophoresis. Electrophoresis. 1997 Mar-Apr;18(3-4):563-7.

Boardman M, Cross GS, Jones EA, Woodland HR. Regulation of expression of a Xenopus borealis embryonic/larval alpha 3 skeletal-actin gene. Eur J Biochem. 1992 Sep 1;208(2):241-9.

Boas M, Feldt-Rasmussen U, Skakkebaek NE, Main KM. Environmental chemicals and thyroid function. Eur J Endocrinol. 2006 May;154(5):599-611.

Borisov OV, Goshe MB, Conrads TP, Rakov VS, Veenstra TD, Smith RD. Low-energy collision-induced dissociation fragmentation analysis of cysteinyl-modified peptides. Anal Chem. 2002 May 15;74(10):2284-92.

Borth W. Alpha 2-macroglobulin, a multifunctional binding protein with targeting characteristics. Faseb J. 1992 Dec;6(15):3345-53.

Bregman DB, Pestell RG, Kidd VJ. Cell cycle regulation and RNA polymerase II. Front Biosci. 2000 Feb 1;5:D244-57.

Brown DD, Wang Z, Furlow JD, Kanamori A, Schwartzman RA, Remo BF, Pinder A. The thyroid hormone-induced tail resorption program during Xenopus laevis metamorphosis. Proc Natl Acad Sci U S A. 1996 Mar 5;93(5):1924-9.

Brucker-Davis F. Effects of environmental synthetic chemicals on thyroid function. Thyroid. 1998 Sep;8(9):827-56.

BSEF, Bromine Science and Environmental Forum; 2008; http://www.bsef.com

Buchholz DR, Paul BD, Fu L, Shi YB. Molecular and developmental analyses of thyroid hormone receptor function in *Xenopus laevis*, the African clawed frog. Gen Comp Endocrinol. 2006 Jan 1;145(1):1-19.

Buchholz DR, Tomita A, Fu L, Paul BD, Shi YB. Transgenic analysis reveals that thyroid hormone receptor is sufficient to mediate the thyroid hormone signal in frog metamorphosis. Mol Cell Biol. 2004 Oct;24(20):9026-37.

Byun Y, Chen F, Chang R, Trivedi M, Green KJ, Cryns VL. Caspase cleavage of vimentin disrupts intermediate filaments and promotes apoptosis. Cell Death Differ. 2001 May;8(5):443-50.

Campbell L, Zirwas MJ. Triclosan. Dermatitis. 2006 Dec;17(4):204-7.

Cheek AO, Ide CF, Bollinger JE, Rider CV, McLachlan JA. Alteration of leopard frog (Rana pipiens) metamorphosis by the herbicide acetochlor. Arch Environ Contam Toxicol. 1999a Jul;37(1):70-7.

Cheek AO, Kow K, Chen J, McLachlan JA. Potential mechanisms of thyroid disruption in humans: interaction of organochlorine compounds with thyroid receptor, transthyretin, and thyroid-binding globulin. Environ Health Perspect. 1999b Apr;107(4):273-8.

Chen F, Chang R, Trivedi M, Capetanaki Y, Cryns VL. Caspase proteolysis of desmin produces a dominant-negative inhibitor of intermediate filaments and promotes apoptosis. J Biol Chem. 2003 Feb 28;278(9):6848-53.

Chen WJ, Lin KH, Lee YS. Molecular characterization of myocardial fibrosis during hypothyroidism: evidence for negative regulation of the pro-alpha1(I) collagen gene expression by thyroid hormone receptor. Mol Cell Endocrinol. 2000 Apr 25;162(1-2):45-55.

Chong PK, Gan CS, Pham TK, Wright PC. Isobaric tags for relative and absolute quantitation (iTRAQ) reproducibility: Implication of multiple injections. J Proteome Res. 2006 May;5(5):1232-40.

Cimino JA, Jhangiani S, Schwartz E, Cooperman JM. Riboflavin metabolism in the hypothyroid human adult. Proc Soc Exp Biol Med. 1987 Feb;184(2):151-3.

Collie ES, Muscat GE. The human skeletal alpha-actin promoter is regulated by thyroid hormone: identification of a thyroid hormone response element. Cell Growth Differ. 1992 Jan;3(1):31-42.

Commission of the European Communities report to the European Parliament concerning the Registration, Evaluation, Authorisation and Restriction of Chemicals (REACH). The New EU Chemicals Legislation, 2006. http://eur-lex.europa.eu/LexUriServ/site/en/com/2006/com2006_0375en01.pdf.

Crump D, Werry K, Veldhoen N, Van Aggelen G, Helbing CC. Exposure to the herbicide acetochlor alters thyroid hormone-dependent gene expression and metamorphosis in *Xenopus laevis*. Environ Health Perspect. 2002 Dec;110(12):1199-205.

Daly RJ. Cortactin signalling and dynamic actin networks. Biochem J. 2004 Aug 15;382(Pt 1):13-25.

Darnerud PO. Toxic effects of brominated flame retardants in man and in wildlife. Environ Int. 2003 Sep;29(6):841-53.

Das B, Schreiber AM, Huang H, Brown DD. Multiple thyroid hormone-induced muscle growth and death programs during metamorphosis in *Xenopus laevis*. Proc Natl Acad Sci U S A. 2002 Sep 17;99(19):12230-5.

Das B, Cai L, Carter MG, Piao YL, Sharov AA, Ko MS, Brown DD. Gene expression changes at metamorphosis induced by thyroid hormone in Xenopus laevis tadpoles. Dev Biol. 2006 Mar 15;291(2):342-55.

Davey JC, Becker KB, Schneider MJ, St Germain DL, Galton VA. Cloning of a cDNA for the type II iodothyronine deiodinase. J Biol Chem. 1995 Nov 10;270(45):26786-9.

Davey JC, Schneider MJ, Galton VA. Cloning of a thyroid hormone-responsive *Rana catesbeiana* c-erbA-beta gene. Dev Genet. 1994;15(4):339-46.

Davis PJ, Davis FB, Cody V. Membrane receptors mediating thyroid hormone action. Trends Endocrinol Metab. 2005 Nov;16(9):429-35.

Davis PJ, Shih A, Lin HY, Martino LJ, Davis FB. Thyroxine promotes association of mitogen-activated protein kinase and nuclear thyroid hormone receptor (TR) and causes serine phosphorylation of TR. J Biol Chem. 2000 Dec 1;275(48):38032-9.

Denver RJ. Neuroendocrine control of amphibian metamorphosis. In *Metamorphosis: Postembryonic Reprogramming of Gene Expression in Amphibian and Insect Cells.* New York, Academic Press. 1996.

Denver RJ, Pavgi S, Shi YB. Thyroid hormone-dependent gene expression program for *Xenopus* neural development. J Biol Chem. 1997 Mar 28;272(13):8179-88.

DeVito M, Biegel L, Brouwer A, Brown S, Brucker-Davis F, Cheek AO, Christensen R, Colborn T, Cooke P, Crissman J, Crofton K, Doerge D, Gray E, Hauser P, Hurley P, Kohn M, Lazar J, McMaster S, McClain M, McConnell E, Meier C, Miller R, Tietge J, Tyl R. Screening methods for thyroid hormone disruptors. Environ Health Perspect. 1999 May;107(5):407-15.

Dinsdale D, Lee JC, Dewson G, Cohen GM, Peter ME. Intermediate filaments control the intracellular distribution of caspases during apoptosis. Am J Pathol. 2004 Feb;164(2):395-407.

Dirtu AC, Roosens L, Geens T, Gheorghe A, Neels H, Covaci A. Simultaneous determination of bisphenol A, triclosan, and tetrabromobisphenol A in human serum using solid-phase extraction and gas chromatography-electron capture negative-ionization mass spectrometry.Anal Bioanal Chem. 2008 Jan 11; [Epub ahead of print]

Dodd, M.H.I., Dodd, J. M., *In physiology of the Amphibia*, ed. B. Lofts. 1976, NewYork: Academic Press.

Dodds AW, Law SK. The phylogeny and evolution of the thioester bond-containing proteins C3, C4 and alpha 2-macroglobulin. Immunol Rev. 1998 Dec;166,15-26.

Du Pasquier D, Rincheval V, Sinzelle L, Chesneau A, Ballagny C, Sachs LM, Demeneix B, Mazabraud A. Developmental cell death during Xenopus metamorphosis involves BID cleavage and caspase 2 and 8 activation. Dev Dyn. 2006 Aug;235(8):2083-94.

Eberle D, Hegarty B, Bossard P, Ferre P, Foufelle F. SREBP transcription factors: master regulators of lipid homeostasis. Biochimie. 2004 Nov;86(11):839-48.

Eckey M, Moehren U, Baniahmad A. Gene silencing by the thyroid hormone receptor. Mol Cell Endocrinol. 2003 Dec 31;213(1):13-22.

Eliceiri BP, Brown DD. Quantitation of endogenous thyroid hormone receptors alpha and beta during embryogenesis and metamorphosis in *Xenopus laevis*. J Biol Chem. 1994 Sep 30;269(39):24459-65.

Environment Canada: Toxicity Testing Using Premetamorphic Bullfrog Tadpoles (*Rana catesbeiana*) Pacific Environmental Sciences Centre, Environment Canada, Standard operating procedure ID: BULLFROG10.SOP, Issue Date February, 2001.

EPA: Final report for the multi-chemical study performed by a contractor for the amphibian metamorphosis assay validation (2007) http://www.epa.gov/endo/pubs/attachment_h_appendices_all_battelle_multi-chem_report.pdf

Fenn JB, Mann M, Meng CK, Wong SF, Whitehouse CM. Electrospray ionization for mass spectrometry of large biomolecules. Science. 1989 Oct 6;246(4926):64-71.

Fini JB, Le Mevel S, Turque N, Palmier K, Zalko D, Cravedi JP, Demeneix BA. An in vivo multiwell-based fluorescent screen for monitoring vertebrate thyroid hormone disruption. Environ Sci Technol. 2007 Aug 15;41(16):5908-14.

Forman LJ, Just JJ. Cellular quantitation of hemoglobin transition during natural and thyroid-hormone-induced metamorphosis of the bullfrog, Rana catesbeiana. Gen Comp Endocrinol. 1981 May;44(1):1-12.

Fort DJ, Degitz S, Tietge J, Touart LW. The hypothalamic-pituitary-thyroid (HPT) axis in frogs and its role in frog development and reproduction. Crit Rev Toxicol. 2007 Jan-Feb;37(1-2):117-61.

Fraker SL, Smith GR. Direct and interactive effects of ecologically relevant concentrations of organic wastewater contaminants on Rana pipiens tadpoles. Environ Toxicol. 2004 Jun;19(3):250-6.

Fries E, Kaczmarczyk A. Inter-alpha-inhibitor, hyaluronan and inflammation. Acta Biochim Pol. 2003 50(3):735-42.

Friesema EC, Ganguly S, Abdalla A, Manning Fox JE, Halestrap AP, Visser TJ. Identification of monocarboxylate transporter 8 as a specific thyroid hormone transporter. J Biol Chem. 2003 Oct 10;278(41):40128-35.

Furlow JD, Yang HY, Hsu M, Lim W, Ermio DJ, Chiellini G, Scanlan TS. Induction of larval tissue resorption in Xenopus laevis tadpoles by the thyroid hormone receptor agonist GC-1. J Biol Chem. 2004 Jun 18;279(25):26555-62.

Furlow JD, Neff ES. A developmental switch induced by thyroid hormone: *Xenopus laevis* metamorphosis. Trends Endocrinol Metab. 2006 Mar;17(2):40-7.

Gafken PR, Lampe PD. Methodologies for characterizing phosphoproteins by mass spectrometry. Cell Commun Adhes. 2006 Sep-Dec;13(5-6):249-62.

Galarneau L, Loranger A, Gilbert S, Marceau N. Keratins modulate hepatic cell adhesion, size and G1/S transition. Exp Cell Res. 2007 Jan 1;313(1):179-94.

Gerner C, Holzmann K, Grimm R, Sauermann G. Similarity between nuclear matrix proteins of various cells revealed by an improved isolation method. J Cell Biochem. 1998 Dec 1;71(3):363-74.

Gharbi S, Gaffney P, Yang A, Zvelebil MJ, Cramer R, Waterfield MD, Timms JF. Evaluation of two-dimensional differential gel electrophoresis for proteomic expression analysis of a model breast cancer cell system. Mol Cell Proteomics. 2002 Feb;1(2):91-8.

Gilbert LI, Tata JR, Atkinson BG. Metamorphosis: postembryonic reprogramming of gene expression in amphibian and insect cells. San Diego, Academic Press, 1996.

Gomperts BD, Kramer IM, Tatham PER. *Signal Transduction*. San Diego, Academic Press. 2002.

Goshe MB, Conrads TP, Panisko EA, Angell NH, Veenstra TD, Smith RD. Phosphoprotein isotope-coded affinity tag approach for isolating and quantitating phosphopeptides in proteome-wide analyses. Anal Chem. 2001 Jun 1;73(11):2578-86.

Goshe MB, Veenstra TD, Panisko EA, Conrads TP, Angell NH, Smith RD. Phosphoprotein isotope-coded affinity tags: application to the enrichment and identification of low-abundance phosphoproteins. Anal Chem. 2002 Feb 1;74(3):607-16.

Goshe MB, Smith RD. Stable isotope-coded proteomic mass spectrometry. Curr Opin Biotechnol. 2003 Feb;14(1):101-9.

Gray LE Jr, Ostby J, Wilson V, Lambright C, Bobseine K, Hartig P, Hotchkiss A, Wolf C, Furr J, Price M, Parks L, Cooper RL, Stoker TE, Laws SC, Degitz SJ, Jensen KM, Kahl MD, Korte JJ, Makynen EA, Tietge JE, Ankley GT. Xenoendocrine disrupters-tiered screening and testing: filling key data gaps. Toxicology. 2002 Dec 27;181-182:371-82.

Gray KM, Janssens PA. Gonadal hormones inhibit the induction of metamorphosis by thyroid hormones in *Xenopus laevis* tadpoles in vivo, but not in vitro. Gen Comp Endocrinol. 1990 Feb;77(2):202-11.

Griffin JE, Ojeda SR. *Textbook of endocrine physiology.* Fourth Edition. 2000: Oxford University Press.

Grossmann J, Fischer B, Baerenfaller K, Owiti J, Buhmann JM, Gruissem W, Baginsky S. A workflow to increase the detection rate of proteins from unsequenced organisms in high-throughput proteomics experiments. Proteomics. 2007 Dec;7(23):4245-54.

Gustafson TA, Bahl JJ, Markham BE, Roeske WR, Morkin E. Hormonal regulation of myosin heavy chain and alpha-actin gene expression in cultured fetal rat heart myocytes. J Biol Chem. 1987 Sep 25;262(27):13316-22.

Gygi SP, Rist B, Gerber SA, Turecek F, Gelb MH, Aebersold R. Quantitative analysis of complex protein mixtures using isotope-coded affinity tags. Nat Biotechnol. 1999 Oct;17(10):994-9.

Hajdúch M, Havlíèek L, Veselý J, Novotný R, Mihál V, Strnad M. Synthetic cyclin dependent kinase inhibitors. New generation of potent anti-cancer drugs. Adv Exp Med Biol. 1999;457:341-53.

Hale RC, Alaee M, Manchester-Neesvig JB, Stapleton HM, Ikonomou MG. Polybrominated diphenyl ether flame retardants in the North American environment. Environ Int. 2003 Sep;29(6):771-9.

Hamers T, Kamstra JH, Sonneveld E, Murk AJ, Kester MH, Andersson PL, Legler J, Brouwer A. *In vitro* profiling of the endocrine-disrupting potency of brominated flame retardants. Toxicol Sci. 2006 Jul;92(1):157-73.

Han Y, Ma B, Zhang K. SPIDER: software for protein identification from sequence tags with de novo sequencing error. J Bioinform Comput Biol. 2005 Jun;3(3):697-716.

Hanada H, Katsu K, Kanno T, Sato EF, Kashiwagi A, Sasaki J, Inoue M, Utsumi K. Cyclosporin A inhibits thyroid hormone-induced shortening of the tadpole tail through membrane permeability transition. Comp Biochem Physiol B Biochem Mol Biol. 2003 Jul;135(3):473-83.

Harraghy N, Mitchell TJ. Isolation and characterization of the promoter and partial enhancer region of the porcine inter-alpha-trypsin inhibitor heavy chain 4 gene. Clin Diagn Lab Immunol. 2005 Nov;12(11):1336-9.

Hasebe T, Oshima H, Kawamura K, Kikuyama S. Rapid and selective removal of larval erythrocytes from systemic circulation during metamorphosis of the bullfrog, Rana catesbeiana. Dev Growth Differ. 1999 Oct;41(5):639-43.

Hashimoto K, Yamada M, Matsumoto S, Monden T, Satoh T, Mori M. Mouse sterol response element binding protein-1c gene expression is negatively regulated by thyroid hormone. Endocrinology. 2006 Sep;147(9):4292-302.

Hasunuma I, Yamamoto K, Kikuyama S. Molecular cloning of bullfrog prolactin receptor cDNA: changes in prolactin receptor mRNA level during metamorphosis. Gen Comp Endocrinol. 2004 Sep 15;138(3):200-10.

Hayes T, Chan R, Licht P. Interactions of temperature and steroids on larval growth, development, and metamorphosis in a toad (*Bufo boreas*). J Exp Zool. 1993 Jul 1;266(3):206-15.

Helbing C, Gergely G, Atkinson BG. Sequential up-regulation of thyroid hormone b receptor, ornithine transcarbamylase, and carbamyl phosphate synthetase mRNAs in the liver of *Rana catesbeiana* tadpoles during spontaneous and thyroid hormone-induced metamorphosis. Dev. Genet, 1992, 13, 289-301.

Helbing CC, Atkinson BG. 3,5,3'-Triiodothyronine-induced carbamyl-phosphate synthetase gene expression is stabilized in the liver of *Rana catesbeiana* tadpoles during heat shock. J Biol Chem. 1994 Apr 22;269(16):11743-50.

Helbing CC, Werry K, Crump D, Domanski D, Veldhoen N, Bailey CM. Expression profiles of novel thyroid hormone-responsive genes and proteins in the tail of *Xenopus laevis* tadpoles undergoing precocious metamorphosis. Mol Endocrinol. 2003 Jul;17(7):1395-409.

Helbing CC, Ovaska K, Ji L. Evaluation of the effect of acetochlor on thyroid hormone receptor gene expression in the brain and behavior of *Rana catesbeiana* tadpoles. Aquat Toxicol. 2006 Oct 25;80(1):42-51.

Helbing CC, Bailey CM, Ji L, Gunderson MP, Zhang F, Veldhoen N, Skirrow RC, Mu R, Lesperance M, Holcombe GW, Kosian PA, Tietge J, Korte JJ, Degitz SJ. Identification of gene

expression indicators for thyroid axis disruption in a *Xenopus laevis* metamorphosis screening assay. Part 1. Effects on the brain. Aquat Toxicol. 2007a May 31;82(4):227-41.

Helbing CC, Ji L, Bailey CM, Veldhoen N, Zhang F, Holcombe GW, Kosian PA, Tietge J, Korte JJ, Degitz SJ. Identification of gene expression indicators for thyroid axis disruption in a *Xenopus laevis* metamorphosis screening assay. Part 2. Effects on the tail and hindlimb. Aquat Toxicol. 2007b May 31;82(4):215-26.

Heller M, Mattou H, Menzel C, Yao X. Trypsin catalyzed 16O-to-18O exchange for comparative proteomics: tandem mass spectrometry comparison using MALDI-TOF, ESI-QTOF, and ESI-ion trap mass spectrometers. J Am Soc Mass Spectrom. 2003 Jul;14(7):704-18.

Herrmann H, Fouquet B, Franke WW. Expression of intermediate filament proteins during development of *Xenopus laevis*. II. Identification and molecular characterization of desmin. Development. 1989 Feb;105(2):299-307.

Honey K, Duff M, Beers C, Brissette WH, Elliott EA, Peters C, Maric M, Cresswell P, Rudensky A. Cathepsin S regulates the expression of cathepsin L and the turnover of gamma-interferon-inducible lysosomal thiol reductase in B lymphocytes. J Biol Chem. 2001 Jun 22;276(25):22573-8.

Hu H, Merrifield P, Atkinson BG. Expression of the myosin heavy chain genes in the tail muscle of thyroid hormone-induced metamorphosing Rana catesbeiana tadpoles. Dev Genet. 1999 24(1-2):151-64.

Huang H, Brown DD. Prolactin is not a juvenile hormone in *Xenopus laevis* metamorphosis. Proc Natl Acad Sci U S A. 2000 Jan 4;97(1):195-9.

Huang ZQ, Li J, Sachs LM, Cole PA, Wong J. A role for cofactor-cofactor and cofactor-histone interactions in targeting p300, SWI/SNF and Mediator for transcription. EMBO J. 2003 May 1;22(9):2146-55.

Hunter T, Sefton BM. Transforming gene product of Rous sarcoma virus phosphorylates tyrosine. Proc Natl Acad Sci U S A. 1980 Mar;77(3):1311-5.

Inada H, Izawa I, Nishizawa M, Fujita E, Kiyono T, Takahashi T, Momoi T, Inagaki M. Keratin attenuates tumor necrosis factor-induced cytotoxicity through association with TRADD. J Cell Biol. 2001 Oct 29;155(3):415-26.

Inoshita H, Masuyama H, Hiramatsu Y. The different effects of endocrine-disrupting chemicals on estrogen receptor-mediated transcription through interaction with coactivator TRAP220 in uterine tissue. J Mol Endocrinol. 2003 Dec;31(3):551-61.

Interagency Coordinating Committee on the Validation of Alternative Methods (ICCVAM): The NICEATM-ICCVAM Five Year Plan (2008-2012) January 2008 NIH Publication No. 08-6410; http://iccvam.niehs.nih.gov/docs/5yearplan.htm

Ishida Y, Suzuki K, Utoh R, Obara M, Yoshizato K. Molecular identification of the skin transformation center of anuran larval skin using genes of Rana adult keratin (RAK) and SPARC as probes. Dev Growth Differ. 2003 Oct-Dec;45(5-6):515-26.

Ishizawa YH, Tamura K, Yamaguchi T, Matsumoto K, Komiyama M, Takamatsu N, Shiba T, Ito M. *Xenopus* death-domain-containing proteins FADD and RIP1 synergistically activate JNK and NF-kappaB. Biol Cell. 2006 Aug;98(8):465-78.

Izutsu Y, Tochinai S, Iwabuchi K, Onoe K. Larval antigen molecules recognized by adult immune cells of inbred Xenopus laevis: two pathways for recognition by adult splenic T cells. Dev Biol. 2000 May 15;221(2):365-74.

Izutsu Y, Tochinai S, Maeno M, Iwabuchi K, Onoe K. Larval antigen molecules recognized by adult immune cells of inbred Xenopus laevis: partial characterization and implication in metamorphosis. Dev Growth Differ. 2002 Dec;44(6):477-88.

Jagnytsch O, Opitz R, Lutz I, Kloas W. Effects of tetrabromobisphenol A on larval development and thyroid hormone-regulated biomarkers of the amphibian *Xenopus laevis*. Environ Res. 2006 Jul;101(3):340-8.

Jansen MS, Nagel SC, Miranda PJ, Lobenhofer EK, Afshari CA, McDonnell DP. Short-chain fatty acids enhance nuclear receptor activity through mitogen-activated protein kinase activation and histone deacetylase inhibition. Proc Natl Acad Sci U S A. 2004 May 4;101(18):7199-204.

Jelaso AM, DeLong C, Means J, Ide CF. Dietary exposure to Aroclor 1254 alters gene expression in *Xenopus laevis* frogs. Environ Res. 2005 May;98(1):64-72.

Jensen ON, Podtelejnikov A, Mann M. Delayed extraction improves specificity in database searches by matrix-assisted laser desorption/ionization peptide maps. Rapid Commun Mass Spectrom. 1996;10(11):1371-8.

Ji L. The effect of genistein on thyroid hormone-dependent tail regression in the *Rana catesbeiana* tadpole. Master's Thesis, University of Victoria, 2005.

Ji L, Domanski D, Skirrow RC, Helbing CC. Genistein prevents thyroid hormone-dependent tail regression of *Rana catesbeiana* tadpoles by targetting protein kinase C and thyroid hormone receptor alpha. Dev Dyn. 2007 Mar;236(3):777-90.

Josic D, Brown MK, Huang F, Lim YP, Rucevic M, Clifton JG, Hixson DC. Proteomic characterization of inter-alpha inhibitor proteins from human plasma. Proteomics. 2006 May;6(9):2874-85.

Jugan ML, Lévy-Bimbot M, Pomérance M, Tamisier-Karolak S, Blondeau JP, Lévi Y. A new bioluminescent cellular assay to measure the transcriptional effects of chemicals that modulate the alpha-1 thyroid hormone receptor. Toxicol In Vitro. 2007 Sep;21(6):1197-205.

Just JJ, Atkinson BG. Hemoglobin transitions in the bullfrog, *Rana catesbeiana*, during spontaneous and induced metamorphosis. Journal of Experimental Zoology. 1972 182(271-280.

Kaltenbach JA. Endocrinology of amphibian metamorphosis. In *Metamorphosis: Postembryonic Reprogramming of Gene Expression in Amphibian and Insect Cells.* New York, Academic Press. 1996.

Kanamori A, Brown DD. Cultured cells as a model for amphibian metamorphosis. Proc Natl Acad Sci U S A. 1993 Jul 1;90(13):6013-7.

Karas M, Hillenkamp F. Laser desorption ionization of proteins with molecular masses exceeding 10,000 daltons. Anal Chem. 1988 Oct 15;60(20):2299-301.

Kashiwagi A, Hanada H, Yabuki M, Kanno T, Ishisaka R, Sasaki J, Inoue M, Utsumi K. Thyroxine enhancement and the role of reactive oxygen species in tadpole tail apoptosis. Free Radic Biol Med. 1999 Apr;26(7-8):1001-9.

Kaufmann H, Bailey JE, Fussenegger M. Use of antibodies for detection of phosphorylated proteins separated by two-dimensional gel electrophoresis. Proteomics. 2001 Feb;1(2):194-9.

Kavok NS, Krasilnikova OA, Babenko NA. Thyroxine signal transduction in liver cells involves phospholipase C and phospholipase D activation. Genomic independent action of thyroid hormone. BMC Cell Biol. 2001;2:5. Epub 2001 Apr 2.

Kawai A, Ikeya J, Kinoshita T, Yoshizato K. A three-step mechanism of action of thyroid hormone and mesenchyme in metamorphic changes in anuran larval skin. Dev Biol. 1994 Dec;166(2):477-88.

Kikuyama S, Kawamura K, Tanaka S, Yamamoto K. Aspects of amphibian metamorphosis: hormonal control. Int Rev Cytol. 1993;145:105-48.

Kinter M, Sherman NE. Protein sequencing and identification using tandem mass spectrometry. (Desiderio DM, Nibbering NMM, eds.) New York, Wiley-Interscience. 2000.

Kitamura S, Jinno N, Ohta S, Kuroki H, Fujimoto N. Thyroid hormonal activity of the flame retardants tetrabromobisphenol A and tetrachlorobisphenol A. Biochem Biophys Res Commun. 2002 Apr 26;293(1):554-9.

Kitamura S, Suzuki T, Sanoh S, Kohta R, Jinno N, Sugihara K, Yoshihara S, Fujimoto N, Watanabe H, Ohta S. Comparative study of the endocrine-disrupting activity of bisphenol A and 19 related compounds. Toxicol Sci. 2005a Apr;84(2):249-59.

Kitamura S, Kato T, Iida M, Jinno N, Suzuki T, Ohta S, Fujimoto N, Hanada H, Kashiwagi K, Kashiwagi A. Anti-thyroid hormonal activity of tetrabromobisphenol A, a flame retardant, and related compounds: Affinity to the mammalian thyroid hormone receptor, and effect on tadpole metamorphosis. Life Sci. 2005b Feb 18;76(14):1589-601.

Klose J, Kobalz U. Two-dimensional electrophoresis of proteins: an updated protocol and implications for a functional analysis of the genome. Electrophoresis. 1995 Jun;16(6):1034-59.

Kobayashi H, Sato H, Yoshizato K. Regionally regulated conversion of protein expression in the skin during anuran metamorphosis. J Exp Zool. 1996 Feb 15;274(3):187-92.

Kolpin DW, Furlong ET, Meyer MT, Thurman EM, Zaugg SD, Barber LB, Buxton HT. Pharmaceuticals, hormones, and other organic wastewater contaminants in U.S. streams, 1999-2000: a national reconnaissance. Environ Sci Technol. 2002 Mar 15;36(6):1202-11.

Kornfeld S, Mellman I. The biogenesis of lysosomes. Annu Rev Cell Biol. 1989, 5;483-525.

Kovtoun SV, English RD, Cotter RJ. Mass correlated acceleration in a reflectron MALDI TOF mass spectrometer: an approach for enhanced resolution over a broad mass range. J Am Soc Mass Spectrom. 2002 Feb;13(2):135-43.

Krain LP, Denver RJ. Developmental expression and hormonal regulation of glucocorticoid and thyroid hormone receptors during metamorphosis in Xenopus laevis. J Endocrinol. 2004 Apr;181(1):91-104.

Ku NO, Omary MB. Effect of mutation and phosphorylation of type I keratins on their caspase-mediated degradation. J Biol Chem. 2001 Jul 20;276(29):26792-8.

Larsen MR, Sørensen GL, Fey SJ, Larsen PM, Roepstorff P. Phospho-proteomics: evaluation of the use of enzymatic de-phosphorylation and differential mass spectrometric peptide mass mapping for site specific phosphorylation assignment in proteins separated by gel electrophoresis. Proteomics. 2001 Feb;1(2):223-38.

Law RJ, Allchin CR, de Boer J, Covaci A, Herzke D, Lepom P, Morris S, Tronczynski J, de Wit CA. Levels and trends of brominated flame retardants in the European environment. Chemosphere. 2006 Jun;64(2):187-208.

Leatherland JF. Contaminant-altered thyroid function in wildlife. In Environmental Endocrine Disruptors. New York, Taylor & Francis. 2000.

Lee KY, Helbing CC, Choi KS, Johnston RN, Wang JH. Neuronal Cdc2-like kinase (Nclk) binds and phosphorylates the retinoblastoma protein. J Biol Chem. 1997 Feb 28;272(9):5622-6.

Legler J, Brouwer A. Are brominated flame retardants endocrine disruptors? Environ Int. 2003 Sep;29(6):879-85.

Leloup J and Buscaglia M. La triiodothyronine: hormone de la metamorphose des amphibiens. C. R. Acad. Sci. 1977, 284, 2261-2263

Levy O, Dai G, Riedel C, Ginter CS, Paul EM, Lebowitz AN, Carrasco N. Characterization of the thyroid Na+/I- symporter with an anti-COOH terminus antibody. Proc Natl Acad Sci U S A. 1997 May 27;94(11):5568-73.

Lim W, Nguyen NH, Yang HY, Scanlan TS, Furlow JD. A thyroid hormone antagonist that inhibits thyroid hormone action in vivo. J Biol Chem. 2002 Sep 20;277(38):35664-70.

Lin HY, Davis FB, Gordinier JK, Martino LJ, Davis PJ. Thyroid hormone induces activation of mitogen-activated protein kinase in cultured cells. Am J Physiol. 1999a May;276(5 Pt 1):C1014-24.

Lin HY, Shih A, Davis FB, Davis PJ. Thyroid hormone promotes the phosphorylation of STAT3 and potentiates the action of epidermal growth factor in cultured cells. Biochem J. 1999b Mar 1;338 ( Pt 2):427-32.

Lin KH, Lee HY, Shih CH, Yen CC, Chen SL, Yang RC, Wang CS. Plasma protein regulation by thyroid hormone. J Endocrinol. 2003 Dec;179(3):367-77.

Linder S, Havelka AM, Ueno T, Shoshan MC. Determining tumor apoptosis and necrosis in patient serum using cytokeratin 18 as a biomarker. Cancer Lett. 2004 Oct 8;214(1):1-9.

Livak KJ, Schmittgen TD. Analysis of relative gene expression data using real-time quantitative PCR and the 2(-Delta Delta C(T)) Method. Methods. 2001 Dec;25(4):402-8.

Luster AD, Weinshank RL, Feinman R, Ravetch JV. Molecular and biochemical characterization of a novel gamma-interferon-inducible protein. J Biol Chem. 1988 Aug 25;263(24):12036-43.

Lutz GJ, Lieber RL. Myosin isoforms in anuran skeletal muscle: their influence on contractile properties and in vivo muscle function. Microsc Res Tech. 2000 Sep 15;50(6):443-57.

Ma B, Zhang K, Hendrie C, Liang C, Li M, Doherty-Kirby A, Lajoie G. PEAKS: powerful software for peptide de novo sequencing by tandem mass spectrometry. Rapid Commun Mass Spectrom. 2003 17(20):2337-42.

MacFarlane M, Merrison W, Dinsdale D, Cohen GM. Active caspases and cleaved cytokeratins are sequestered into cytoplasmic inclusions in TRAIL-induced apoptosis. J Cell Biol. 2000 Mar 20;148(6):1239-54.

Makino E, Sakaguchi M, Iwatsuki K, Huh NH. Introduction of an N-terminal peptide of S100C/A11 into human cells induces apoptotic cell death. J Mol Med. 2004 Sep;82(9):612-20.

Manning G, Whyte DB, Martinez R, Hunter T, Sudarsanam S. The protein kinase complement of the human genome. Science. 2002 Dec 6;298(5600):1912-34.

Marceau N, Loranger A, Gilbert S, Daigle N, Champetier S. Keratin-mediated resistance to stress and apoptosis in simple epithelial cells in relation to health and disease. Biochem Cell Biol. 2001 79(5):543-55.

Marceau N, Schutte B, Gilbert S, Loranger A, Henfling ME, Broers JL, Mathew J, Ramaekers FC. Dual roles of intermediate filaments in apoptosis. Exp Cell Res. 2007 Jun 10;313(10):2265-81.

Maric M, Arunachalam B, Phan UT, Dong C, Garrett WS, Cannon KS, Alfonso C, Karlsson L, Flavell RA, Cresswell P. Defective antigen processing in GILT-free mice. Science. 2001 Nov 9;294(5545):1361-5.

Maruyama T, Watt KW, Riggs A. Hemoglobins of the tadpole of the bullfrog, Rana catesbeiana. Amino acid sequence of the alpha chain of a major component. J Biol Chem. 1980 Apr 25;255(8):3285-93.

Masuyama H, Hiramatsu Y. Involvement of suppressor for Gal 1 in the ubiquitin/proteasome-mediated degradation of estrogen receptors. J Biol Chem. 2004 Mar 26;279(13):12020-6.

McCormack AL, Somogyi A, Dongré AR, Wysocki VH. Fragmentation of protonated peptides: surface-induced dissociation in conjunction with a quantum mechanical approach. Anal Chem. 1993 Oct 15;65(20):2859-72.

Medzihradszky KF, Campbell JM, Baldwin MA, Falick AM, Juhasz P, Vestal ML, Burlingame AL. The characteristics of peptide collision-induced dissociation using a high-performance MALDI-TOF/TOF tandem mass spectrometer. Anal Chem. 2000 Feb 1;72(3):552-8.

Meerts IA, van Zanden JJ, Luijks EA, van Leeuwen-Bol I, Marsh G, Jakobsson E, Bergman A, Brouwer A. Potent competitive interactions of some brominated flame retardants and related compounds with human transthyretin in vitro. Toxicol Sci. 2000 Jul;56(1):95-104.

Min G, Kim H, Bae Y, Petz L, Kemper JK. Inhibitory cross-talk between estrogen receptor (ER) and constitutively activated androstane receptor (CAR). CAR inhibits ER-mediated signaling pathway by squelching p160 coactivators. J Biol Chem. 2002 Sep 13;277(37):34626-33.

Miwa N, Kawamura S. Frog p26olf, a molecule with two S100-like regions in a single peptide. Microsc Res Tech. 2003 Apr 15;60(6):593-9.

Miyatani S, Winkles JA, Sargent TD, Dawid IB. Stage-specific keratins in Xenopus laevis embryos and tadpoles: the XK81 gene family. J Cell Biol. 1986 Nov;103(5):1957-65.

Morris HR, Paxton T, Dell A, Langhorne J, Berg M, Bordoli RS, Hoyes J, Bateman RH. High sensitivity collisionally-activated decomposition tandem mass spectrometry on a novel quadrupole/orthogonal-acceleration time-of-flight mass spectrometer. Rapid Commun Mass Spectrom. 1996;10(8):889-96.

Moskaitis JE, Sargent TD, Smith LH Jr, Pastori RL, Schoenberg DR. *Xenopus laevis* serum albumin: sequence of the complementary deoxyribonucleic acids encoding the 68- and 74-kilodalton peptides and the regulation of albumin gene expression by thyroid hormone during development. Mol Endocrinol. 1989 Mar;3(3):464-73.

Mukai M, Obara M, Yoshizato K. Characterization of gene of anuran cathepsin D as a metamorphosis-associated enzyme. Development, Growth and Differentiation. 1995 37):463-477.

Muscat GE, Griggs R, Downes M, Emery J. Characterization of the thyroid hormone response element in the skeletal alpha-actin gene: negative regulation of T3 receptor binding by the retinoid X receptor. Cell Growth Differ. 1993 Apr;4(4):269-79.

Nakajima K, Yaoita Y. Dual mechanisms governing muscle cell death in tadpole tail during amphibian metamorphosis. Dev Dyn. 2003 Jun;227(2):246-55.

Nakajima K, Takahashi A, Yaoita Y. Structure, expression, and function of the *Xenopus laevis* caspase family. J Biol Chem. 2000 Apr 7;275(14):10484-91.

Nesvizhskii AI, Aebersold R. Interpretation of shotgun proteomic data: the protein inference problem. Mol Cell Proteomics. 2005 Oct;4(10):1419-40.

Nieuwkoop, P.D. and J. Faber, Normal table of *Xenopus laevis*. 1956, Garland, New York.

Nishikawa A, Murata E, Akita M, Kaneko K, Moriya O, Tomita M, Hayashi H. Roles of macrophages in programmed cell death and remodeling of tail and body muscle of *Xenopus laevis* during metamorphosis. Histochem Cell Biol. 1998 Jan;109(1):11-7.

Norris, D., O., *Vertebrate Endocrinology*. Third edition ed. 1996: Academic Press.

Oda Y, Huang K, Cross FR, Cowburn D, Chait BT. Accurate quantitation of protein expression and site-specific phosphorylation. Proc Natl Acad Sci U S A. 1999 Jun 8;96(12):6591-6.

OECD, Environment, Health and Safety Publications, Series on Testing and Assessment, No. 57 Detailed review paper on thyroid hormone disruption assays (2006) http://www.oecd.org/dataoecd/49/35/37235405.pdf

O'Farrell PH. High resolution two-dimensional electrophoresis of proteins. J Biol Chem. 1975 May 25;250(10):4007-21.

Okada R, Iwata T, Kato T, Kikuchi M, Yamamoto K, Kikuyama S. Cloning of bullfrog thyroid-stimulating hormone (TSH) beta subunit cDNA: expression of TSHbeta mRNA during metamorphosis. Gen Comp Endocrinol. 2000 Aug;119(2):224-31.

Olofsson MH, Ueno T, Pan Y, Xu R, Cai F, van der Kuip H, Muerdter TE, Sonnenberg M, Aulitzky WE, Schwarz S, Andersson E, Shoshan MC, Havelka AM, Toi M, Linder S. Cytokeratin-18 is a useful serum biomarker for early determination of response of breast carcinomas to chemotherapy. Clin Cancer Res. 2007 Jun 1;13(11):3198-206.

Olsen JV, Blagoev B, Gnad F, Macek B, Kumar C, Mortensen P, Mann M. Global, in vivo, and site-specific phosphorylation dynamics in signaling networks. Cell. 2006 Nov 3;127(3):635-48.

Omary MB, Ku NO, Liao J, Price D. Keratin modifications and solubility properties in epithelial cells and in vitro. Subcell Biochem. 1998 (31),105-40.

Ong SE, Blagoev B, Kratchmarova I, Kristensen DB, Steen H, Pandey A, Mann M. Stable isotope labeling by amino acids in cell culture, SILAC, as a simple and accurate approach to expression proteomics. Mol Cell Proteomics. 2002 May;1(5):376-86.

Oofusa K, Yomori S, Yoshizato K. Regionally and hormonally regulated expression of genes of collagen and collagenase in the anuran larval skin. Int J Dev Biol. 1994 Jun;38(2):345-50.

Opitz, R., Levy, G., Bo¨gi, C., Lutz, I., and Kloas, W. Endocrine disruption in fish and amphibians. Rec. Res. Dev. Endocrinol. 2002, 3, 127–170.

Opitz R, Lutz I, Nguyen NH, Scanlan TS, Kloas W. Analysis of thyroid hormone receptor betaA mRNA expression in Xenopus laevis tadpoles as a means to detect agonism and antagonism of thyroid hormone action. Toxicol Appl Pharmacol. 2006a Apr 1;212(1):1-13.

Opitz R, Hartmann S, Blank T, Braunbeck T, Lutz I, Kloas W. Evaluation of histological and molecular endpoints for enhanced detection of thyroid system disruption in Xenopus laevis tadpoles. Toxicol Sci. 2006b Apr;90(2):337-48.

Osako M, Kim YJ, Sakai S. Leaching of brominated flame retardants in leachate from landfills in Japan. Chemosphere. 2004 Dec;57(10):1571-9.

Oshima RG. Apoptosis and keratin intermediate filaments. Cell Death Differ. 2002 May;9(5):486-92.

Patton WF, Schulenberg B, Steinberg TH. Two-dimensional gel electrophoresis; better than a poke in the ICAT? Curr Opin Biotechnol. 2002 Aug;13(4):321-8.

Paul BD, Shi YB. Distinct expression profiles of transcriptional coactivators for thyroid hormone receptors during *Xenopus laevis* metamorphosis. Cell Res. 2003 Dec;13(6):459-64.

Pennati M, Folini M, Zaffaroni N. Targeting survivin in cancer therapy: fulfilled promises and open questions. Carcinogenesis. 2007 Jun;28(6):1133-9.

Pereira PJ, Macedo-Ribeiro S, Parraga A, Perez-Luque R, Cunningham O, Darcy K, Mantle TJ, Coll M. Structure of human biliverdin IXbeta reductase, an early fetal bilirubin IXbeta producing enzyme. Nat Struct Biol. 2001 Mar;8(3):215-20.

Perkins DN, Pappin DJ, Creasy DM, Cottrell JS. Probability-based protein identification by searching sequence databases using mass spectrometry data. Electrophoresis. 1999 Dec;20(18):3551-67.

Phan UT, Arunachalam B, Cresswell P. Gamma-interferon-inducible lysosomal thiol reductase (GILT). Maturation, activity, and mechanism of action. J Biol Chem. 2000 Aug 25;275(34):25907-14.

Pineiro M, Alava MA, Gonzalez-Ramon N, Osada J, Lasierra P, Larrad L, Pineiro A, Lampreave F. ITIH4 serum concentration increases during acute-phase processes in human patients and is up-regulated by interleukin-6 in hepatocarcinoma HepG2 cells. Biochem Biophys Res Commun. 1999 Sep 16;263(1):224-9.

Pineiro M, Andres M, Iturralde M, Carmona S, Hirvonen J, Pyorala S, Heegaard PM, Tjornehoj K, Lampreave F, Pineiro A, Alava MA. ITIH4 (inter-alpha-trypsin inhibitor heavy chain 4) is a new acute-phase protein isolated from cattle during experimental infection. Infect Immun. 2004 Jul;72(7):3777-82.

Pratt JM, Petty J, Riba-Garcia I, Robertson DH, Gaskell SJ, Oliver SG, Beynon RJ. Dynamics of protein turnover, a missing dimension in proteomics. Mol Cell Proteomics. 2002 Aug;1(8):579-91.

Puzianowska-Kuznicka M, Damjanovski S, Shi YB. Both thyroid hormone and 9-cis retinoic acid receptors are required to efficiently mediate the effects of thyroid hormone on embryonic development and specific gene regulation in *Xenopus laevis*. Mol Cell Biol. 1997 Aug;17(8):4738-49.

Ramsby ML, Makowski GS. Differential detergent fractionation of eukaryotic cells. Analysis by two-dimensional gel electrophoresis. Methods Mol Biol. 1999;112:53-66.

Ray LB, Dent JN. An analysis of the influence of thyroid hormone on the synthesis of proteins in the tail fin of bullfrog tadpoles. J Exp Zool. 1986 Nov;240(2):191-201.

Regard E, Taurog A, Nakashima T. Plasma thyroxine and triiodothyronine levels in spontaneously metamorphosing *Rana catesbeiana* tadpoles and in adult anuran amphibia. Endocrinology. 1978 Mar;102(3):674-84.

Ricard-Blum S, Ruggiero F. The collagen superfamily: from the extracellular matrix to the cell membrane. Pathol Biol (Paris). 2005 Sep;53(7):430-42.

Ritchie JW, Shi YB, Hayashi Y, Baird FE, Muchekehu RW, Christie GR, Taylor PM. A role for thyroid hormone transporters in transcriptional regulation by thyroid hormone receptors. Mol Endocrinol. 2003 Apr;17(4):653-61.

Robert J, Wolff J, Jijakli H, Graf JD, Karch F, Kobel HR. Developmental expression of the creatine kinase isozyme system of *Xenopus*: maternally derived CK-IV isoform persists far beyond the degradation of its maternal mRNA and into the zygotic expression period. Development. 1990 Mar;108(3):507-14.

Robert J, Du Pasquier L, Kobel HR. Differential expression of creatine kinase isozymes during development of *Xenopus laevis*: an unusual heterodimeric isozyme appears at metamorphosis. Differentiation. 1991 Feb;46(1):23-34.

Rollerová E, Gáspárová Z, Wsólová L, Urbancíková M. Interaction of acetochlor with estrogen receptor in the rat uterus. Acetochlor--possible endocrine modulator? Gen Physiol Biophys. 2000 Mar;19(1):73-84.

Rollins-Smith LA. Metamorphosis and the amphibian immune system. Immunol Rev. 1998 Dec;166(221-30.

Ross PL, Huang YN, Marchese JN, Williamson B, Parker K, Hattan S, Khainovski N, Pillai S, Dey S, Daniels S, Purkayastha S, Juhasz P, Martin S, Bartlet-Jones M, He F, Jacobson A, Pappin DJ. Multiplexed protein quantitation in Saccharomyces cerevisiae using amine-reactive isobaric tagging reagents. Mol Cell Proteomics. 2004 Dec;3(12):1154-69.

Roth GA, Krenn C, Brunner M, Moser B, Ploder M, Spittler A, Pelinka L, Sautner T, Wolner E, Boltz-Nitulescu G, Ankersmit HJ. Elevated serum levels of epithelial cell apoptosis-specific cytokeratin 18 neoepitope m30 in critically ill patients. Shock. 2004 Sep;22(3):218-20.

Rowe I, Coen L, Le Blay K, Le Mével S, Demeneix BA. Autonomous regulation of muscle fibre fate during metamorphosis in *Xenopus tropicalis*. Dev Dyn. 2002 Aug;224(4):381-90.

Rowe I, Le Blay K, Du Pasquier D, Palmier K, Levi G, Demeneix B, Coen L. Apoptosis of tail muscle during amphibian metamorphosis involves a caspase 9-dependent mechanism. Dev Dyn. 2005 May;233(1):76-87.

Sachs LM, Jones PL, Havis E, Rouse N, Demeneix BA, Shi YB. Nuclear receptor corepressor recruitment by unliganded thyroid hormone receptor in gene repression during *Xenopus laevis* development. Mol Cell Biol. 2002 Dec;22(24):8527-38.

Sachs LM, Abdallah B, Hassan A, Levi G, De Luze A, Reed JC, Demeneix BA. Apoptosis in *Xenopus* tadpole tail muscles involves Bax-dependent pathways. FASEB J. 1997 Aug;11(10):801-8.

Sachs LM, Le Mevel S, Demeneix BA. Implication of bax in *Xenopus laevis* tail regression at metamorphosis. Dev Dyn. 2004 Dec;231(4):671-82.

Sakaguchi M, Miyazaki M, Takaishi M, Sakaguchi Y, Makino E, Kataoka N, Yamada H, Namba M, Huh NH. S100C/A11 is a key mediator of Ca(2+)-induced growth inhibition of human epidermal keratinocytes. J Cell Biol. 2003 Nov 24;163(4):825-35.

Sato Y, Buchholz DR, Paul BD, Shi YB. A role of unliganded thyroid hormone receptor in postembryonic development in *Xenopus laevis*. Mech Dev. 2007 Jul;124(6):476-88.

Sawada T, Oofusa K, Yoshizato K. Thyroid hormone response element-like sequence in anuran matrix metalloproteinase 1 gene is responsive to in vivo thyroid hormone administration. J Endocrinol. 2001 Jun;169(3):477-86.

Schantz SL, Widholm JJ, Rice DC. Effects of PCB exposure on neuropsychological function in children. Environ Health Perspect. 2003 Mar;111(3):357-576.

Schneider MJ, Davey JC, Galton VA. *Rana catesbeiana* tadpole red blood cells express an alpha, but not a beta, c-erbA gene. Endocrinology. 1993 Dec;133(6):2488-95.

Schreiber AM, Das B, Huang H, Marsh-Armstrong N, Brown DD. Diverse developmental programs of Xenopus laevis metamorphosis are inhibited by a dominant negative thyroid hormone receptor. Proc Natl Acad Sci U S A. 2001 Sep 11;98(19):10739-44.

Schreiber AM, Brown DD. Tadpole skin dies autonomously in response to thyroid hormone at metamorphosis. Proc Natl Acad Sci U S A. 2003 Feb 18;100(4):1769-74.

Schriks M, Vrabie CM, Gutleb AC, Faassen EJ, Rietjens IM, Murk AJ. T-screen to quantify functional potentiating, antagonistic and thyroid hormone-like activities of poly halogenated aromatic hydrocarbons (PHAHs). Toxicol In Vitro. 2006 Jun;20(4):490-8.

Scribner EA, Battaglin WA, Goolsby DA, Thurman EM. Changes in herbicide concentrations in Midwestern streams in relation to changes in use, 1989-1998. Sci Total Environ. 2000 Apr 5;248(2-3):255-63.

Seshimo H, Ryuzaki M, Yoshizato K. Specific inhibition of Triiodothyronine-induced tadpole tail-fin regression by cathepsin D-inhibitor pepstatin. Dev Biol. 1977 Aug;59(1):96-100.

Shchemelinin I, Sefc L, Necas E. Protein kinase inhibitors. Folia Biol (Praha). 2006;52(4):137-48.

Shi YB. Amphibian Metamorphosis: from morphology to molecular biology. New York, Wiley-Liss. 2000.

Shi YB, Liang VC, Parkison C, Cheng SY. Tissue-dependent developmental expression of a cytosolic thyroid hormone protein gene in *Xenopus*: its role in the regulation of amphibian metamorphosis. FEBS Lett. 1994 Nov 21;355(1):61-4.

Shi YB, Fu L, Hsia SC, Tomita A, Buchholz D. Thyroid hormone regulation of apoptotic tissue remodeling during anuran metamorphosis. Cell Res. 2001 Dec;11(4):245-52.

Shibusawa N, Hollenberg AN, Wondisford FE. Thyroid hormone receptor DNA binding is required for both positive and negative gene regulation. J Biol Chem. 2003 Jan 10;278(2):732-8.

Shimada N, Yamauchi K. Characteristics of 3,5,3'-triiodothyronine (T3)-uptake system of tadpole red blood cells: effect of endocrine-disrupting chemicals on cellular T3 response. J Endocrinol. 2004 Dec;183(3):627-37.

Shin DJ, Osborne TF. Thyroid hormone regulation and cholesterol metabolism are connected through Sterol Regulatory Element-Binding Protein-2 (SREBP-2). J Biol Chem. 2003 Sep 5;278(36):34114-8.

Skirrow RC. Cyclin dependent activity is necessary for thyroid hormone induced tail regression in the *Rana catesbeiania* tadpole. Master's Thesis, University of Victoria. 2003.

Skirrow RC, Helbing CC. Decreased cyclin-dependent kinase activity promotes thyroid hormone-dependent tail regression in Rana catesbeiana. Cell Tissue Res. 2007 May;328(2):281-9.

Skirrow RC, Veldhoen N, Domanski D, Helbing CC. Roscovitine inhibits thyroid hormone-induced tail regression of the frog tadpole and reveals a role for cyclin C/Cdk8 in the establishment of the gene expression program (under review, 2008).

Smith DJ, Zhu H, Kolatkar PR, Tam LT, Baldwin TO, Roe BA, Broyles RH, Riggs AF. The hemoglobins of the bullfrog, Rana catesbeiana. The cDNA-derived amino acid sequences of the

alpha chains of adult hemoglobins B and C: their roles in deoxygenation-induced aggregation. J Biol Chem. 1993 Dec 25;268(36):26961-71.

Smith-Gill S, Carver V. Biochemical characterization of organ differentiation and maturation. Metamorphosis: A problem in developmental biology 2nd Edition. L Gilbert,Frieden E. New York, Plenum Press, 1981**:** 491-544.

Smith GR, Burgett AA. Effects of three organic wastewater contaminants on American toad, Bufo americanus, tadpoles. Ecotoxicology. 2005 May;14(4):477-82.

Song K, Kim TM, Kim HJ, Kim JW, Kim HH, Kwon HB, Kim WS, Choi HS. Molecular cloning and characterization of a novel inhibitor of apoptosis protein from Xenopus laevis. Biochem Biophys Res Commun. 2003 Jan 31;301(1):236-42.

Soskic V, Görlach M, Poznanovic S, Boehmer FD, Godovac-Zimmermann J. Functional proteomics analysis of signal transduction pathways of the platelet-derived growth factor beta receptor. Biochemistry. 1999 Feb 9;38(6):1757-64.

Steinberg TH, Agnew BJ, Gee KR, Leung WY, Goodman T, Schulenberg B, Hendrickson J, Beechem JM, Haugland RP, Patton WF. Global quantitative phosphoprotein analysis using Multiplexed Proteomics technology. Proteomics. 2003 Jul;3(7):1128-44.

Stensballe A, Andersen S, Jensen ON. Characterization of phosphoproteins from electrophoretic gels by nanoscale Fe(III) affinity chromatography with off-line mass spectrometry analysis. Proteomics. 2001 Feb;1(2):207-22.

St Germain DL, Galton VA. The deiodinase family of selenoproteins. Thyroid. 1997 Aug;7(4):655-68.

St Germain DL, Schwartzman RA, Croteau W, Kanamori A, Wang Z, Brown DD, Galton VA. A thyroid hormone-regulated gene in Xenopus laevis encodes a type III iodothyronine 5-deiodinase. Proc Natl Acad Sci U S A. 1994 Aug 2;91(16):7767-71.

Sugiyama S, Miyoshi H, Yamauchi K. Characteristics of a thyroid hormone responsive reporter gene transduced into a Xenopus laevis cell line using lentivirus vector. Gen Comp Endocrinol. 2005a Dec;144(3):270-9.

Sugiyama S, Shimada N, Miyoshi H, Yamauchi K. Detection of thyroid system-disrupting chemicals using in vitro and in vivo screening assays in Xenopus laevis. Toxicol Sci. 2005b Dec;88(2):367-74.

Sui L, Wang J, Li BM. Administration of Triiodo-L: -thyronine into Dorsal Hippocampus Alters Phosphorylation of Akt, Mammalian Target of Rapamycin, p70S6 Kinase and 4E-BP1 in Rats. Neurochem Res. 2007 Dec 20; [Epub ahead of print]

Sullivan DT, MacIntyre R, Fuda N, Fiori J, Barrilla J, Ramizel L. Analysis of glycolytic enzyme co-localization in Drosophila flight muscle. J Exp Biol. 2003 Jun;206(Pt 12):2031-8.

Suzuki K, Sato K, Katsu K, Hayashita H, Kristensen DB, Yoshizato K. Novel Rana keratin genes and their expression during larval to adult epidermal conversion in bullfrog tadpoles. Differentiation. 2001 Aug;68(1):44-54.

Suzuki K, Utoh R, Kotani K, Obara M, Yoshizato K. Lineage of anuran epidermal basal cells and their differentiation potential in relation to metamorphic skin remodeling. Dev Growth Differ. 2002 Jun;44(3):225-38.

Tabb MM, Blumberg B. New modes of action for endocrine-disrupting chemicals. Mol Endocrinol. 2006 Mar;20(3):475-82.

Takada S, Shibata T, Hiraoka Y, Masuda H. Identification of ribonucleotide reductase protein R1 as an activator of microtubule nucleation in Xenopus egg mitotic extracts. Mol Biol Cell. 2000 Dec;11(12):4173-87.

Talanian RV, Quinlan C, Trautz S, Hackett MC, Mankovich JA, Banach D, Ghayur T, Brady KD, Wong WW. Substrate specificities of caspase family proteases. J Biol Chem. 1997 Apr 11;272(15):9677-82.

Tamura K, Noyama T, Ishizawa YH, Takamatsu N, Shiba T, Ito M. *Xenopus* death receptor-M1 and -M2, new members of the tumor necrosis factor receptor superfamily, trigger apoptotic signaling by differential mechanisms. J Biol Chem. 2004 Feb 27;279(9):7629-35.

Tata J. Requirement for RNA and protein synthesis for induced regression of the tadpole tail in organ culture. Dev Biol. 1966 13(1):77-94.

Tata JR. Gene expression during metamorphosis: an ideal model for post-embryonic development. Bioessays. 1993 Apr;15(4):239-48.

Tata JR. Amphibian metamorphosis as a model for the developmental actions of thyroid hormone. Mol Cell Endocrinol. 2006 Feb 26;246(1-2):10-20.

Tata JR. Early metamorphic competence of *Xenopus* larvae. Dev Biol. 1968 Nov;18(5):415-40.

Tata JR, Kawahara A, Baker BS. Prolactin inhibits both thyroid hormone-induced morphogenesis and cell death in cultured amphibian larval tissues. Dev Biol. 1991 Jul;146(1):72-80.

Taylor AC, Kollros JJ. Stages in the normal development of *Rana pipiens* larvae. Anatomical Record, 1946. 94:7-24.

Thompson JD, Higgins DG, Gibson TJ. CLUSTAL W: improving the sensitivity of progressive multiple sequence alignment through sequence weighting, positions-specific gap penalties and weight matrix choice. Nucleic Acids Research. 1994 22(4673-4680.

Thornberry NA, Rano TA, Peterson EP, Rasper DM, Timkey T, Garcia-Calvo M, Houtzager VM, Nordstrom PA, Roy S, Vaillancourt JP, Chapman KT, Nicholson DW. A combinatorial approach defines specificities of members of the caspase family and granzyme B. Functional relationships established for key mediators of apoptosis. J Biol Chem. 1997 Jul 18;272(29):17907-11.

Tomita A, Buchholz DR, Shi YB. Recruitment of N-CoR/SMRT-TBLR1 corepressor complex by unliganded thyroid hormone receptor for gene repression during frog development. Mol Cell Biol. 2004 Apr;24(8):3337-46.

Turque N, Palmier K, Le Mével S, Alliot C, Demeneix BA. A rapid, physiologic protocol for testing transcriptional effects of thyroid-disrupting agents in premetamorphic Xenopus tadpoles. Environ Health Perspect. 2005 Nov;113(11):1588-93.

Ueno T, Toi M, Bivén K, Bando H, Ogawa T, Linder S. Measurement of an apoptotic product in the sera of breast cancer patients. Eur J Cancer. 2003 Apr;39(6):769-74.

Ueno T, Toi M, Linder S. Detection of epithelial cell death in the body by cytokeratin 18 measurement. Biomed Pharmacother. 2005 Oct;59 Suppl 2;S359-62.

Utoh R, Asahina K, Suzuki K, Kotani K, Obara M, Yoshizato K. Developmentally and regionally regulated participation of epidermal cells in the formation of collagen lamella of anuran tadpole skin. Dev Growth Differ. 2000 Dec;42(6):571-80.

van Beeren HC, Bakker O, Wiersinga WM. Desethylamiodarone interferes with the binding of co-activator GRIP-1 to the beta 1-thyroid hormone receptor. FEBS Lett. 2000 Sep 22;481(3):213-6.

Van den Bergh G, Arckens L. Recent advances in 2D electrophoresis: an array of possibilities. Expert Rev Proteomics. 2005 Apr;2(2):243-52.

van den Eijnde SM, Boshart L, Baehrecke EH, De Zeeuw CI, Reutelingsperger CP, Vermeij-Keers C. Cell surface exposure of phosphatidylserine during apoptosis is phylogenetically conserved. Apoptosis. 1998;3(1):9-16.

van Engeland M, Ramaekers FC, Schutte B, Reutelingsperger CP. A novel assay to measure loss of plasma membrane asymmetry during apoptosis of adherent cells in culture. Cytometry. 1996 Jun 1;24(2):131-9.

Vasudevan N, Koibuchi N, Chin WW, Pfaff DW. Differential crosstalk between estrogen receptor (ER)alpha and ERbeta and the thyroid hormone receptor isoforms results in flexible regulation of the consensus ERE. Brain Res Mol Brain Res. 2001 Nov 1;95(1-2):9-17.

Veldhoen N, Helbing CC. Detection of environmental endocrine-disruptor effects on gene expression in live *Rana catesbeiana* tadpoles using a tail fin biopsy technique. Environ Toxicol Chem. 2001 Dec;20(12):2704-8.

Veldhoen N, Crump D, Werry K, Helbing CC. Distinctive gene profiles occur at key points during natural metamorphosis in the Xenopus laevis tadpole tail. Dev Dyn. 2002 Dec;225(4):457-68.

Veldhoen, N, Helbing, C. Monitoring gene expression on *Rana catesbeiana* tadpoles using a tail fin biopsy technique and its application to the detection of environmental endocrine disruptor effects, *in:* Techniques in Aquatic Toxicology – Vol. 2 (G. Ostrander, ed.), 2005. pp. 315-327, Taylor & Francis, Boca Raton, FL.

Veldhoen N, Skirrow RC, Ji L, Domanski D, Bonfield RE, Bailey CM, Helbing CC. Use of heterologous cDNA arrays and organ culture in the detection of thyroid hormone-dependent responses in a sentinel frog, *Rana catesbeiana*. Comparative Biochemistry and Physiology Part D: Genomics and Proteomics, Volume 1, Issue 2, June 2006, Pages 187-199.

Veldhoen N, Skirrow RC, Osachoff H, Wigmore H, Clapson DJ, Gunderson MP, Van Aggelen G, Helbing CC. The bactericidal agent triclosan modulates thyroid hormone-associated gene expression and disrupts postembryonic anuran development. Aquat Toxicol. 2006a Dec 1;80(3):217-27.

Veldhoen N, Boggs A, Walzak K, Helbing CC. Exposure to tetrabromobisphenol-A alters TH-associated gene expression and tadpole metamorphosis in the Pacific tree frog *Pseudacris regilla*. Aquat Toxicol. 2006b Jun 30;78(3):292-302.

Vermes I, Haanen C, Steffens-Nakken H, Reutelingsperger C. A novel assay for apoptosis. Flow cytometric detection of phosphatidylserine expression on early apoptotic cells using fluorescein labelled Annexin V. J Immunol Methods. 1995 Jul 17;184(1):39-51.

Wagner M, Helbing C. Multiple variants of the ING1 and ING2 tumor suppressors are differentially expressed and thyroid hormone-responsive in *Xenopus laevis*. General and Comparative Endocrinology. 2005 144,38-50

Wagner RL, Apriletti JW, McGrath ME, West BL, Baxter JD, Fletterick RJ. A structural role for hormone in the thyroid hormone receptor. Nature. 1995 Dec 14;378(6558):690-7.

Wang D, de la Fuente C, Deng L, Wang L, Zilberman I, Eadie C, Healey M, Stein D, Denny T, Harrison LE, Meijer L, Kashanchi F. Inhibition of human immunodeficiency virus type 1 transcription by chemical cyclin-dependent kinase inhibitors. J Virol. 2001 Aug;75(16):7266-79.

Wang Z, Brown DD. Thyroid hormone-induced gene expression program for amphibian tail resorption. J Biol Chem. 1993 Aug 5;268(22):16270-8.

Watanabe I, Sakai S. Environmental release and behavior of brominated flame retardants. Environ Int. 2003 Sep;29(6):665-82.

Watanabe M, Ohshima M, Morohashi M, Maeno M, Izutsu Y. Ontogenic emergence and localization of larval skin antigen molecule recognized by adult T cells of Xenopus laevis: Regulation by thyroid hormone during metamorphosis. Dev Growth Differ. 2003 Feb;45(1):77-84.

Watanabe Y, Kobayashi H, Suzuki K, Kotani K, Yoshizato K. New epidermal keratin genes from Xenopus laevis: hormonal and regional regulation of their expression during anuran skin metamorphosis. Biochim Biophys Acta. 2001 Feb 16;1517(3):339-50.

Watanabe Y, Tanaka R, Kobayashi H, Utoh R, Suzuki K, Obara M, Yoshizato K. Metamorphosis-dependent transcriptional regulation of xak-c, a novel Xenopus type I keratin gene. Dev Dyn. 2002 Dec;225(4):561-70.

Watt KW, Maruyama T, Riggs A. Hemoglobins of the tadpole of the bullfrog, Rana catesbeiana. Amino acid sequence of the beta chain of a major component. J Biol Chem. 1980 Apr 25;255(8):3294-301.

Wells L, Vosseller K, Cole RN, Cronshaw JM, Matunis MJ, Hart GW. Mapping sites of O-GlcNAc modification using affinity tags for serine and threonine post-translational modifications. Mol Cell Proteomics. 2002 Oct;1(10):791-804.

White BA, Nicoll CS. Hormonal control of amphibian metamorphosis. In *Metamorphosis A Problem in Developmental Biology 2nd Ed.* (Gilbert LI, Frieden E, eds.), Plenum Press, New York and London, 1981, p363-396.

Wong J, Shi YB. Coordinated regulation of and transcriptional activation by Xenopus thyroid hormone and retinoid X receptors. J Biol Chem. 1995 Aug 4;270(31):18479-83.

Yamaguchi T, Komoda Y, Nakajima H. Biliverdin-IX alpha reductase and biliverdin-IX beta reductase from human liver. Purification and characterization. J Biol Chem. 1994 Sep 30;269(39):24343-8.

Yamaguchi T, Nakajima H. Changes in the composition of bilirubin-IX isomers during human prenatal development. Eur J Biochem. 1995 Oct 15;233(2):467-72.

Yamauchi K, Kasahara T, Hayashi H, Horiuchi R. Purification and characterization of a 3,5,3'-L-triiodothyronine-specific binding protein from bullfrog tadpole plasma: a homolog of mammalian transthyretin. Endocrinology. 1993 May;132(5):2254-61.

Yaoita Y, Nakajima K. Induction of apoptosis and CPP32 expression by thyroid hormone in a myoblastic cell line derived from tadpole tail. J Biol Chem. 1997 Feb 21;272(8):5122-7.

Yen PM. Physiological and molecular basis of thyroid hormone action. Physiol Rev. 2001 Jul;81(3):1097-142.

Yen PM, Ando S, Feng X, Liu Y, Maruvada P, Xia X. Thyroid hormone action at the cellular, genomic and target gene levels. Mol Cell Endocrinol. 2006 Feb 26;246(1-2):121-7.

Ying GG, Kookana RS. Triclosan in wastewaters and biosolids from Australian wastewater treatment plants. Environ Int. 2007 Feb;33(2):199-205.

Yoshizato K. Molecular mechanism and evolutional significance of epithelial-mesenchymal interactions in the body- and tail-dependent metamorphic transformation of anuran larval skin. Int Rev Cytol. 2007;260:213-60.

Zhang F, Degitz SJ, Holcombe GW, Kosian PA, Tietge J, Veldhoen N, Helbing CC. Evaluation of gene expression endpoints in the context of a *Xenopus laevis* metamorphosis-based bioassay to detect thyroid hormone disruptors. Aquat Toxicol. 2006 Jan 5;76(1):24-36.

Zhang J, Lazar MA. The mechanism of action of thyroid hormones. Annu Rev Physiol. 2000;62:439-66.

Zhang Y, Yin L, Hillgartner FB. SREBP-1 integrates the actions of thyroid hormone, insulin, cAMP, and medium-chain fatty acids on ACCalpha transcription in hepatocytes. J Lipid Res. 2003 Feb;44(2):356-68.

Zhao X, Lorenc H, Stephenson H, Wang YJ, Witherspoon D, Katzenellenbogen B, Pfaff D, Vasudevan N. Thyroid hormone can increase estrogen-mediated transcription from a consensus estrogen response element in neuroblastoma cells. Proc Natl Acad Sci U S A. 2005 Mar 29;102(13):4890-5.

Zhou H, Watts JD, Aebersold R. A systematic approach to the analysis of protein phosphorylation. Nat Biotechnol. 2001 Apr;19(4):375-8.

Zoeller RT, Rovet J. Timing of thyroid hormone action in the developing brain: clinical observations and experimental findings. J Neuroendocrinol. 2004 Oct;16(10):809-18.

Zoeller RT. Environmental chemicals as thyroid hormone analogues: new studies indicate that thyroid hormone receptors are targets of industrial chemicals? Mol Cell Endocrinol. 2005 Oct 20;242(1-2):10-5.

# **Appendix 1** Abbreviations

| | |
|---|---|
| **2D-SDS-PAGE** | Two-dimensional sodium dodecyl sulfate-polyacrylamide gel electrophoresis |
| **7AAD** | 7-Amino-actinomycin D |
| **°C** | Degree Celsius |
| **µ** | micro |
| **µl** | microlitre |
| **A2M** | alpha-2-macroglobulin |
| **aa** | Amino acid |
| **Ac** | Acetochlor |
| **ACTH** | Adrenocorticotropin releasing hormone |
| **AF-1** | Activation function 1 domain |
| **AMA** | Amphibian metamorphosis assay |
| **Amp** | Ampicillin |
| **APCs** | Antigen presenting cells |
| **APS** | Ammonium persulphate |
| **AR** | Androgen receptor |
| **Bax** | Bcl-2-associated X protein |
| **BCA** | Bicinchoninic acid assay |
| **Bcl-$X_L$** | B-Cell lymphoma protein 2 homolog |
| **BID** | BH3-Interacting Death agonist protein |
| **BFR** | Brominated flame retardants |
| **bp** | Base pair |
| **BTEB** | Basic transcription element binding protein |
| **BVR-A** | Biliverdin reductase A |
| **$CaCl_2$** | Calcium chloride |
| **cAMP** | Cyclic adenosine monophosphate |
| **CAR** | Constitutive androstane receptor |
| **CBP** | CREB-binding protein |
| **Cdk** | Cyclin-dependent kinase |
| **cDNA** | Complementary deoxyribonucleic acid |
| **CHAPS** | 3-[(3-cholamidopropyl)dimethylammonio]-1-propanesulfonate |
| **CID** | Collision-induced dissociation |
| **COPI** | Coatomer protein complex |
| **CREB** | cAMP-response element-binding protein |
| **CRF** | Corticotropin releasing factor |
| **CTD** | C-terminal domain |
| **CTHBP** | Cytoplasmic TH binding proteins |
| **CTL** | Cytotoxic T lymphocytes |
| **D2** | Type II 5'-deiodinase |
| **D3** | Type III 5-deiodinase |
| **DAPI** | 4'-6-Diamidino-2-phenylindole |
| **Da** | Dalton |
| **DBD** | DNA binding domain |
| **DEPC** | Diethylpyrocarbonate |
| **DIT** | 3-5-diiodinated tyrosine |
| **DMSO** | Dimethylsulfoxide |
| **DNA** | Deoxyribonucleic acid |
| **dNTP** | Deoxynucleotidetriphosphate |
| **DRIPs** | Vitamin D receptor interacting proteins |

| | |
|---|---|
| **DR** | Death receptor |
| **DTT** | Dithiothreitol |
| **ECL** | Enhanced chemiluminescence |
| **EDC** | Endocrine-disrupting compound |
| **EDTA** | Ethylenedinitrilo-tetraacetic acid |
| **ECM** | Extracellular matrix |
| **EGF** | Epidermal growth factor |
| **EGFP** | Enhanced green fluorescent protein |
| **EGTA** | O,O'-bis(2-aminoethyl)ethyleneglycol-N,N,N',N'-tetraacetic acid |
| **EPA** | U.S. Environmental Protection Agency |
| **ERE** | Estrogen response elements |
| **ER** | Endoplasmic reticulum |
| **ERα** | Estrogen receptor alpha |
| **ERβ** | Estrogen receptor beta |
| **ESI** | Electrospray ionization |
| **EtBr** | Ethidium bromide |
| **EtOH** | Ethanol |
| **FADD** | Fas-associated death-domain |
| **FAK** | Focal adhesion kinase |
| **fmol** | Femtomole |
| **GH** | Growth hormone |
| **GILT** | Gamma-interferon-inducible lysosomal thiol reductase |
| **GR** | Glucocorticoid receptor |
| **GRE** | Glucocorticoid response element |
| **GSP** | Gene specific primers |
| **h** | hour |
| **HAT** | Histone acetyltransferase |
| **HDAC** | Histone deacetylase |
| **HEPES** | 4-(2-hydroxyethyl)-1-piperazineethanesulfonic acid |
| **HPLC** | High performance liquid chromatography |
| **HPT** | Hypothalamus-pituitary-thyroid axis |
| **HRE** | Hormone response element |
| **HRP** | Horse radish peroxidase |
| **IaI** | Inter-alpha inhibitor |
| **ICAT** | Isotope-coded affinity tagging |
| **ICCVAM** | Interagency Coordinating Committee on the Validation of Alternative Methods |
| **IEF** | Isoelectric focusing |
| **IFNγ** | Iinterferon-gamma |
| **IF** | Intermediate filament |
| **Ig** | Immunoglobulin |
| **IMAC** | Immobilized metal affinity chromatography |
| **IRES** | Internal ribosomal entry site |
| **iTRAQ** | Isobaric tags for relative and absolute quantitation |
| **$I^-$** | Inorganic iodide |
| **k** | kilo |
| **KCl** | Potassium chloride |
| **$K_d$** | Dissociation constant |
| **kDa** | kiloDalton |
| **LBD** | Ligand binding domain |
| **LB medium** | Luria-Bertani medium |

| | |
|---|---|
| **M6P** | Mannose-6-phosphate |
| **m** | milli |
| **M** | molarity |
| **MALDI** | Matrix-assisted laser desorption/ionization |
| **MAPK** | Mitogen-activated protein kinase |
| **MAPKK** | Mitogen-activated protein kinase kinase |
| **MCT8** | Monocarboxylate transporter 8 |
| **mg** | milligram |
| **$MgCl_2$** | Magnesium chloride |
| **MHCII** | Major histocompatability complex II |
| **MHC** | Myosin heavy chain |
| **min** | minute |
| **MIT** | 3-monoiodinated tyrosine |
| **MLC** | Myosin light chain |
| **ml** | millitre |
| **MMP1** | Matrix metalloproteinase 1 |
| **mM** | millimolar |
| **mRNA** | Messenger RNA |
| **MS** | Mass spectrometry |
| **MS/MS** | Tandem MS |
| **m/z** | Mass-to-charge ratio |
| **NaCl** | Sodium chloride |
| **$NaH_2PO_4H_2O$** | Sodium phosphate |
| **$NaHCO_3$** | Sodium bicarbonate |
| **NaOH** | Sodium hydroxide |
| **N-CoR** | Nuclear receptor co-repressor |
| **NF** | Nieuwkoop and Faber |
| **NK** | Natural killer cells |
| **NLS** | Nuclear localization signal |
| **nm** | nanometre |
| **NR** | Nuclear receptor |
| **nTRE** | Negative TRE |
| **NTS** | Nucleolar translocation sequence |
| **OECD** | Organisation for Economic Co-operation and Development |
| **ORF** | Open reading frame |
| **P/CAF** | p300/CBP-associated factor |
| **p160/SRCs** | Steroid receptor co-activators |
| **PAGE** | Polyacrylamide gel electrophoresis |
| **PBDE** | Polybrominated diphenyl ether |
| **PCB** | Polychlorinated biphenyls |
| **PCNA** | Proliferating cell nuclear antigen |
| **PCR** | Polymerase chain reaction |
| **PI3K** | Phosphatidylinositol 3-kinase |
| **PI** | Propidium iodide |
| **pI** | Isoelectric point |
| **PHAH** | Polyhalogenated aromatic hydrocarbon |
| **PhIAT** | Phosphoprotein isotope-coded affinity tag |
| **PKC** | Protein kinase C |
| **PMF** | Peptide-mass fingerprinting |
| **PMSF** | Phenylmethylsulphonylfluoride |
| **PRL** | Prolactin |

| | |
|---|---|
| **PS** | Phosphatidylserine |
| **pSer** | Phosphorylated serine |
| **pThr** | Phosphorylated threonine |
| **PTM** | Posttranslational modifications |
| **pTRE** | Positive TRE |
| **pTyr** | Phosphorylated tyrosine |
| **QPCR** | Quantitative real-time polymerase chain reaction |
| **Q** | Quadrupole |
| **RACE** | 5'- and 3'-rapid amplification of cDNA ends |
| **RAK** | *Rana catesbeiana* adult type I keratin |
| **RAR** | Retinoic acid receptor |
| **RBCs** | Red blood cells |
| **RLKI** | *Rana catesbeiana* larval type I keratin |
| **RLKII** | *Rana catesbeiana* larval type II keratin |
| **RNA** | Ribonucleic acid |
| **RNA Pol II** | RNA Polymerase II |
| **$rT_3$** | Reverse $T_3$ |
| **RT-PCR** | Reverse transcription-PCR |
| **RXR** | 9-*cis*-retinoic acid receptor |
| **s** | second |
| **SDS** | Sodium dodecyl sulfate |
| **SDS-PAGE** | Sodium dodecyl sulfate-polyacrylamide gel electrophoresis |
| **SH3** | Src homology 3 domain |
| **SMRT** | Silencing mediators of retinoid and thyroid hormone receptors |
| **SRC** | Steroid receptor coactivator |
| **SREBP-2** | Sterol regulatory element binding protein-2 |
| **STAT** | Signal transducer and activator of transcription |
| **$T_2$** | Diiodothyronine |
| **$T_3$** | 3,5,3'-Triiodothyronine |
| **$T_4$** | 3,5,3',5'-tetraiodo-L-thyronine; Thyroxine |
| **Taq** | *Thermus aquaticus* |
| **TBBPA** | Tetrabromobisphenol A |
| **TBG** | Thyronine binding globulin |
| **TBP** | TATA box binding protein |
| **TBS** | Tris-buffered saline |
| **TBST** | TBS with 0.1% Tween |
| **TCS** | Triclosan |
| **TEMED** | *N,N,N',N'*-tetramethylethylenediamine |
| **TFIIB** | Transcription factor IIB |
| **TH** | Thyroid hormone |
| **TH/bZIP** | TH-Responsive basic leucine zipper transcription factor |
| **TIM** | Triose phosphate isomerase |
| **TiO** | Titanium oxide |
| **TK** | Taylor and Kollros |
| **TNF** | Tumour necrosis factor |
| **TOF** | Time-of-flight |
| **TRADD** | TNF receptor 1-associated death domain |
| **TRAP220** | TR-associated protein 220 |
| **TRAP** | Thyroid hormone receptor associated protein |
| **TRDN** | Dominant negative mutant of TR$\alpha$ |
| **TRE** | Thryoid hormone response element |

| | |
|---|---|
| **TRH** | Thyrotropin releasing hormone |
| **Tris-HCl** | Tris(hydroxymethyl)aminomethane hydrochloride |
| **TR** | Thyroid hormone receptor |
| **TSH** | Thyroid stimulating hormone |
| **TTR** | Transthyretin |
| **TUNEL** | Terminal deoxynucleotidyltransferase-mediated dUTP-X nick end labeling |
| **UDP-GT** | Uridine disphosphate glucuronyltransferase |
| **UV** | Ultraviolet |
| **VRC** | Vanadyl ribonucleoside complexes |
| **XEMA** | *Xenopus* metamorphosis assay |

## **Appendix 3.1** 2D gel analysis of *R. catesbeiana* tail fin fractions showing phosphoprotein images overlayed with total protein spots

2D gel analysis of the nuclear, mitochondrial and microsomal subcellular fractions, and of the anion-exchange HPLC cytosolic fractions. Total proteins are shown in black and white, with the phosphoprotein stain image shown in red overlayed on top. Relative molecular weights of protein standards are indicated in kDa.

Arrow in 190 mM cytosolic fraction shows protein spot identified as *X. tropicalis* Mitogen-activated protein kinase kinase (MAPKK; NCBI#Q66JE6_XENTR, expected size of 43.6 kDa) by MALDI-TOF-TOF tandem-MS analysis, based on 8 peptides, resulting in 100% identification confidence level.

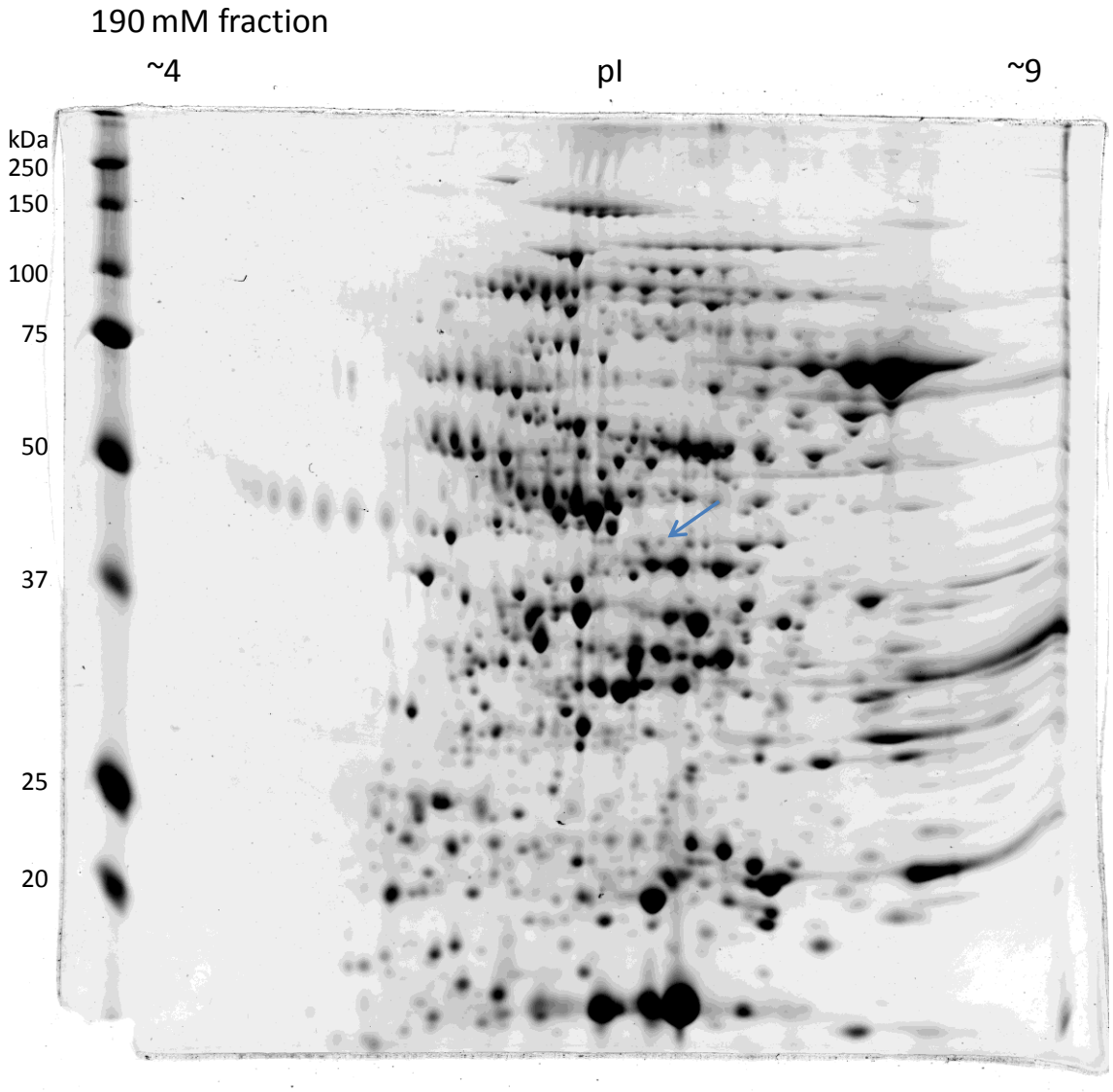

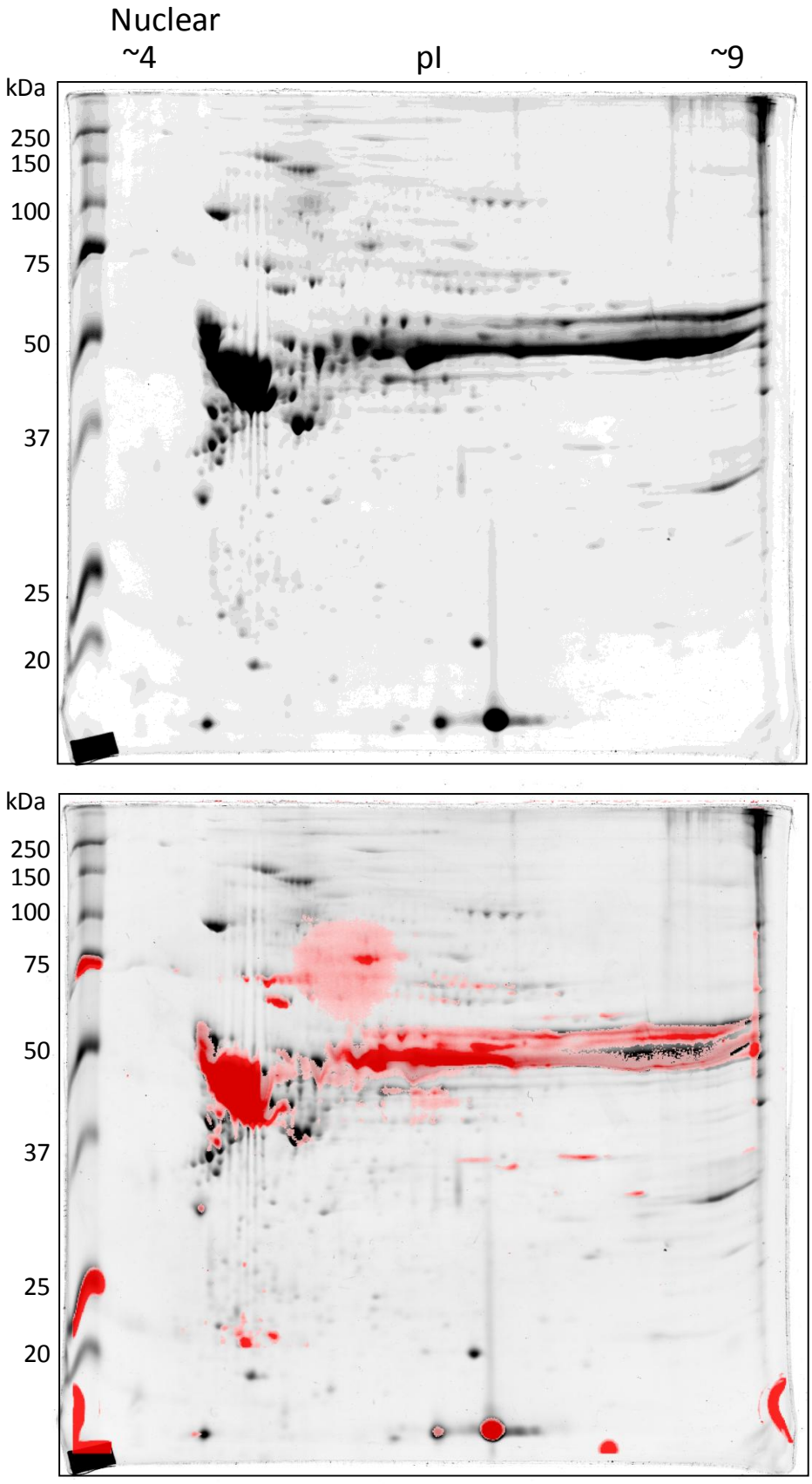
Nuclear
~4
pI
~9
kDa
250
150
100
75
50
37
25
20
kDa
250
150
100
75
50
37
25
20

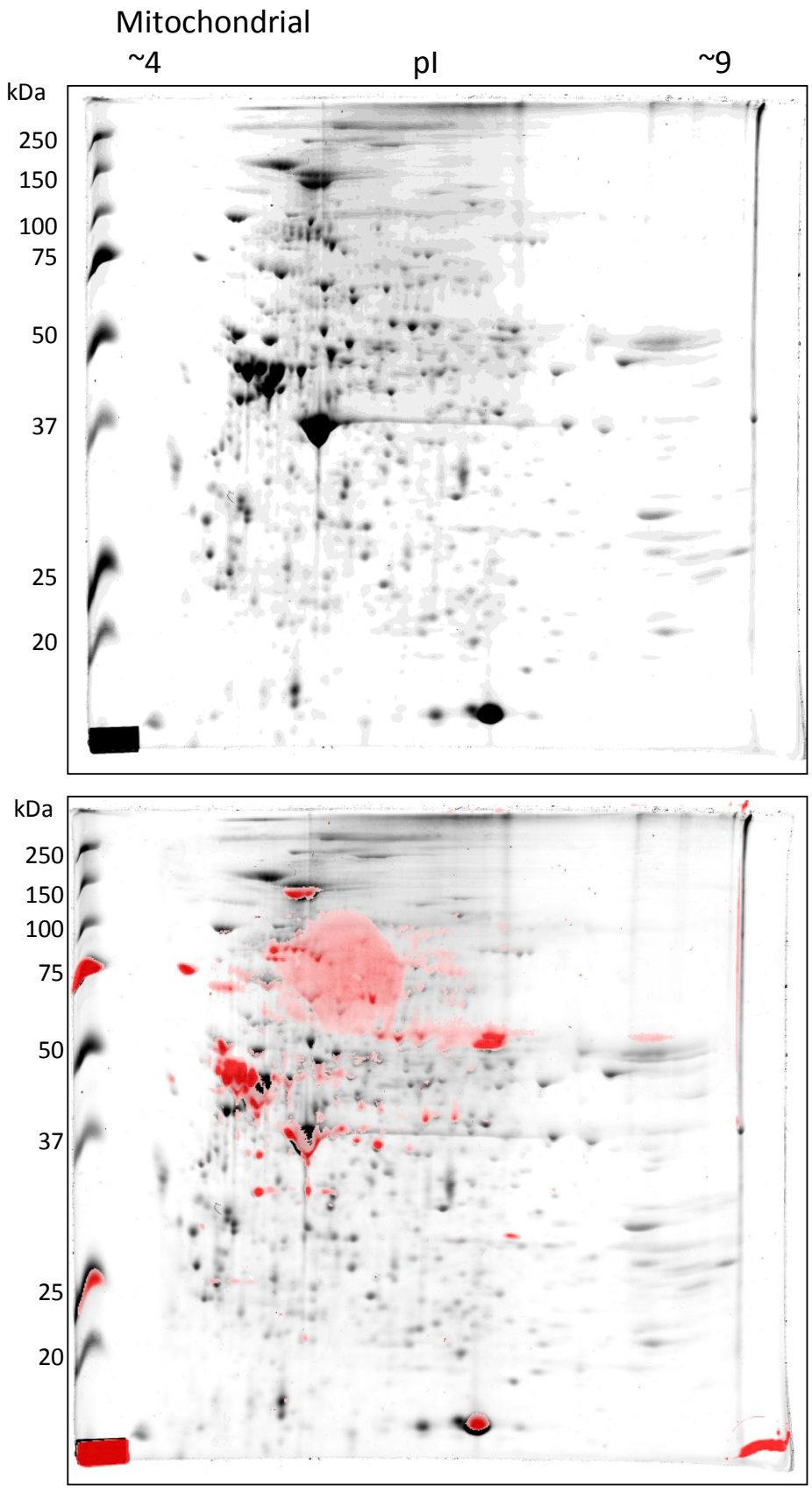
Mitochondrial
~4
pI
~9
kDa
250
150
100
75
50
37
25
20
kDa
250
150
100
75
50
37
25
20

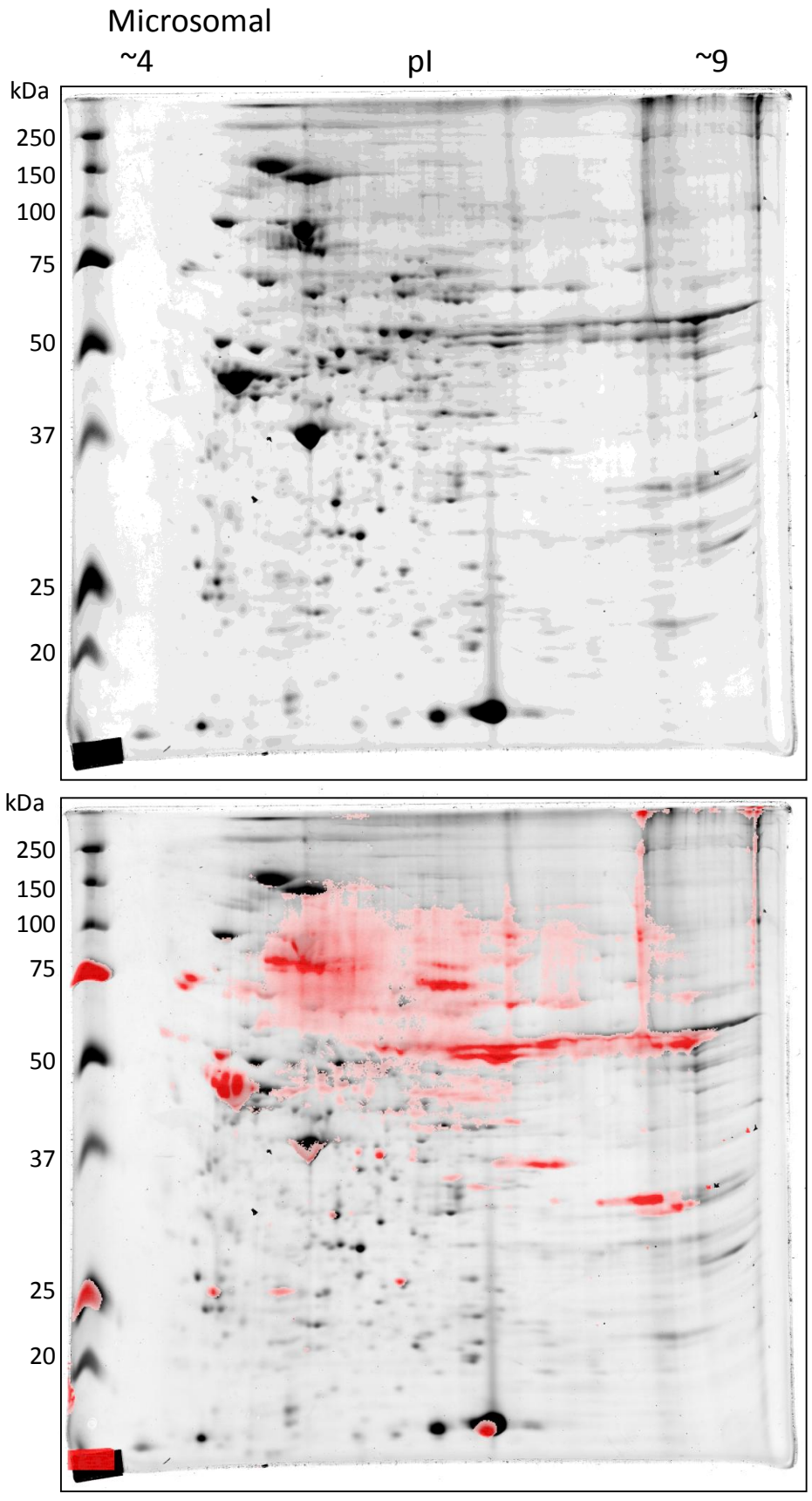
Microsomal
~4
pI
~9
kDa
250
150
100
75
50
37
25
20
kDa
250
150
100
75
50
37
25
20

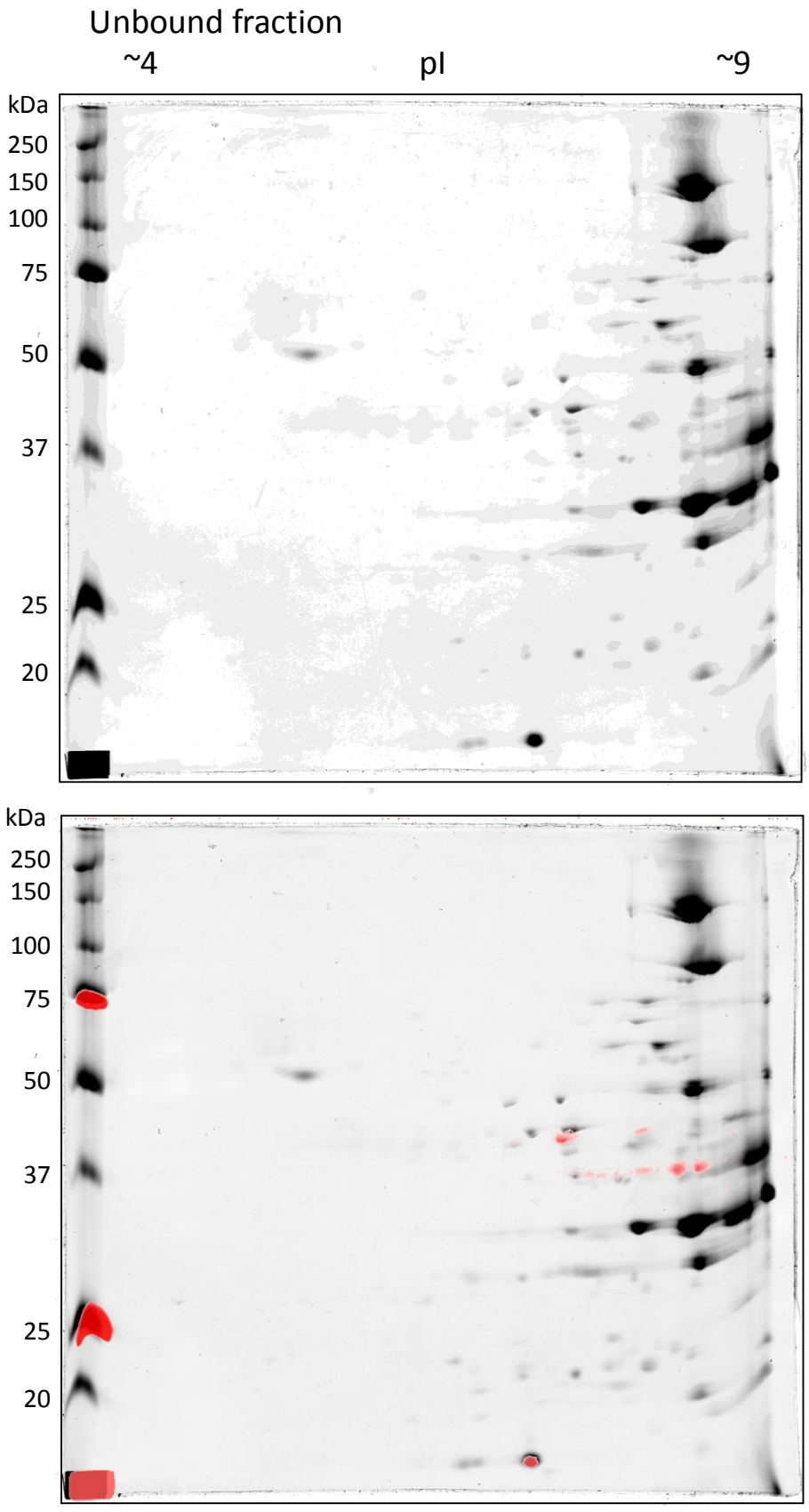
Unbound fraction
~4
pI
~9
kDa
250
150
100
75
50
37
25
20
kDa
250
150
100
75
50
37
25
20

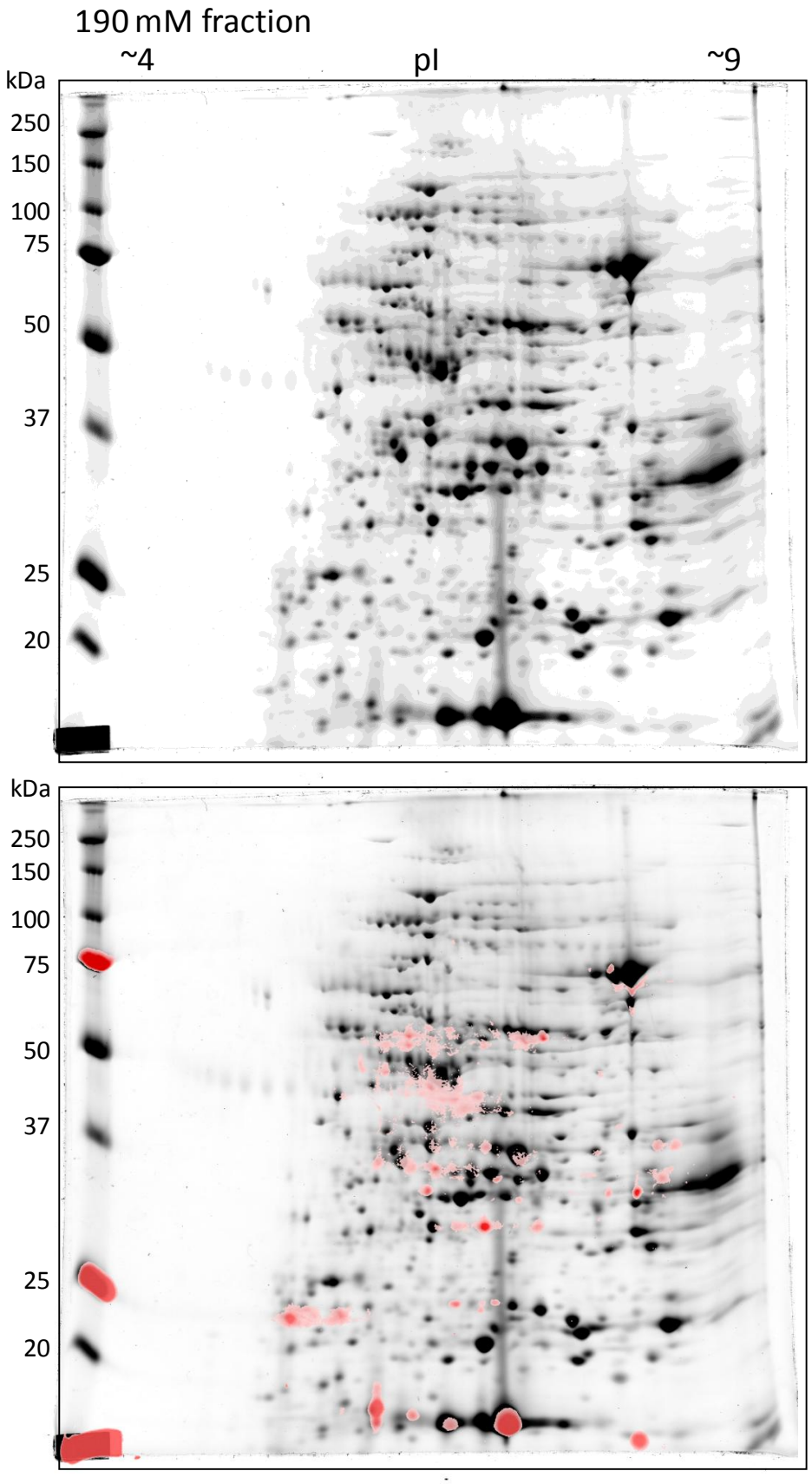
190 mM fraction
~4
pI
~9
kDa
250
150
100
75
50
37
25
20
kDa
250
150
100
75
50
37
25
20

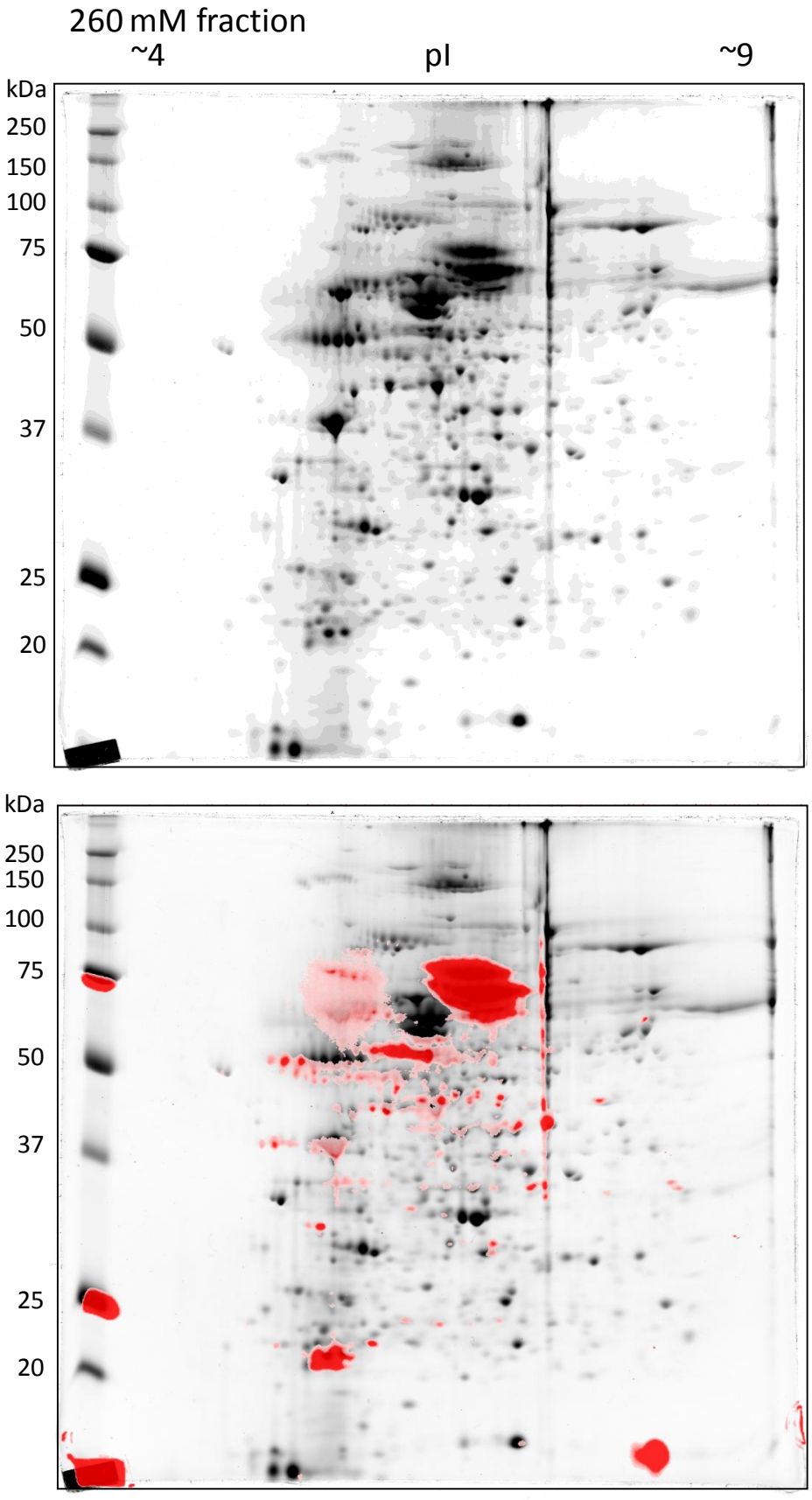
260 mM fraction
~4
pI
~9
kDa
250
150
100
75
50
37
25
20
kDa
250
150
100
75
50
37
25
20

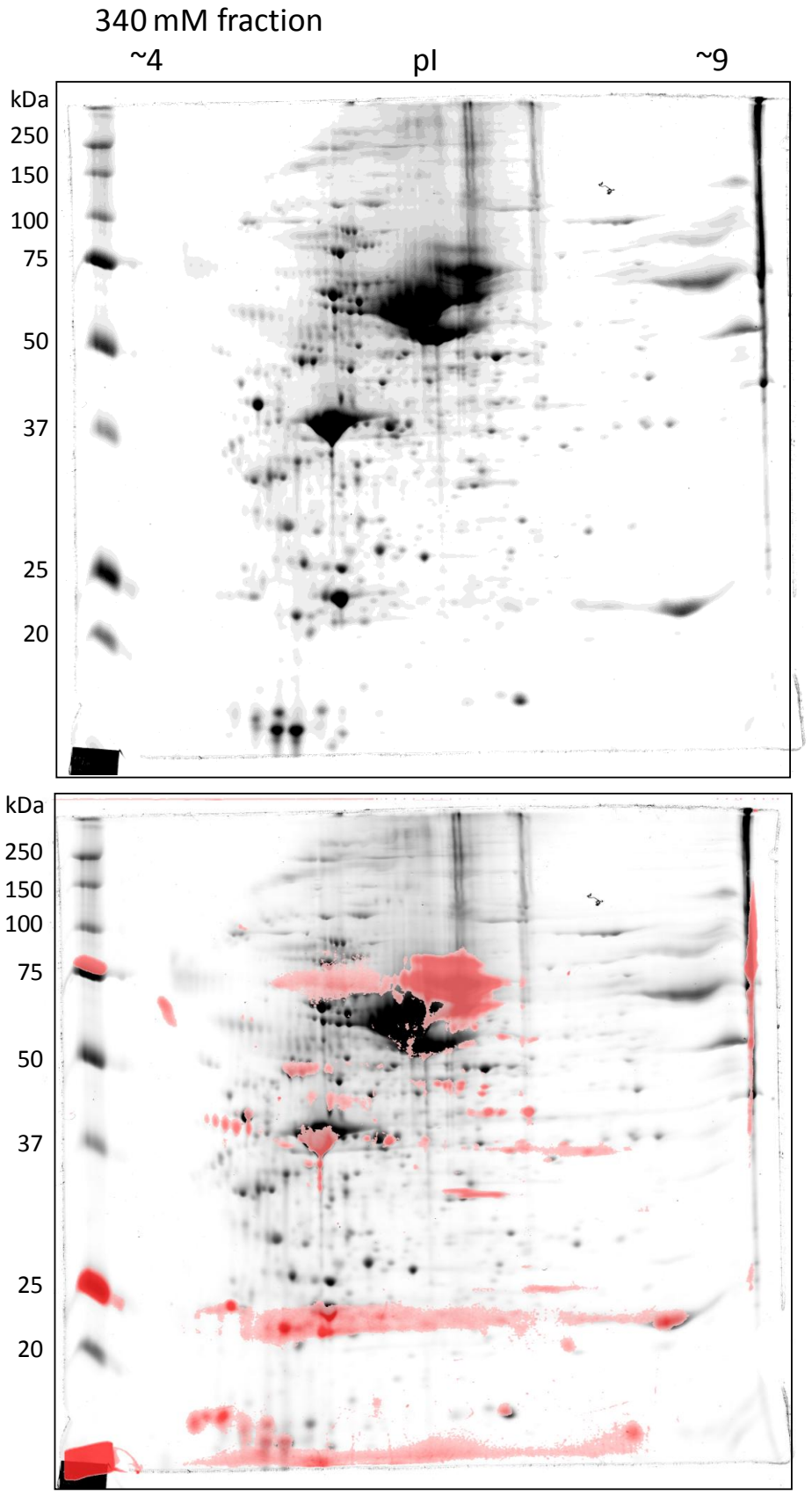
340 mM fraction
~4
pI
~9
kDa
250
150
100
75
50
37
25
20
kDa
250
150
100
75
50
37
25
20

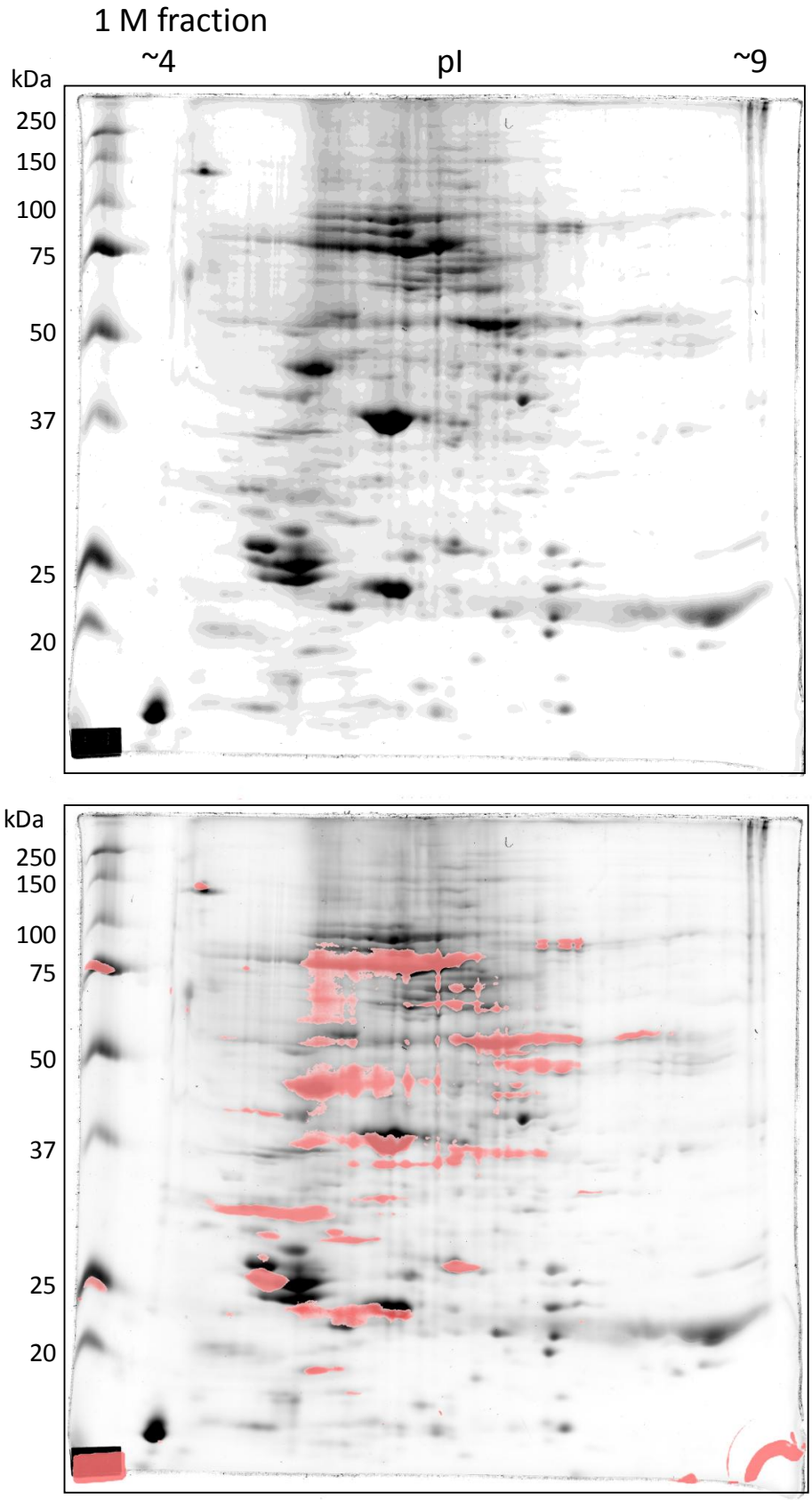
1 M fraction
~4
pI
~9
kDa
250
150
100
75
50
37
25
20
kDa
250
150
100
75
50
37
25
20

## **Appendix 3.2** Sample interpretation of tandem-MS spectrum

Tandem-MS (MS/MS) spectrum of iTRAQ labeled peptide identified as Immunoglobulin heavy chain constant region [AAC12914/*Hydrolagus colliei*], that was increased by 4.6 fold in $T_3$-treated *R. catesbeiana* tail fin samples (See Table 3.6).

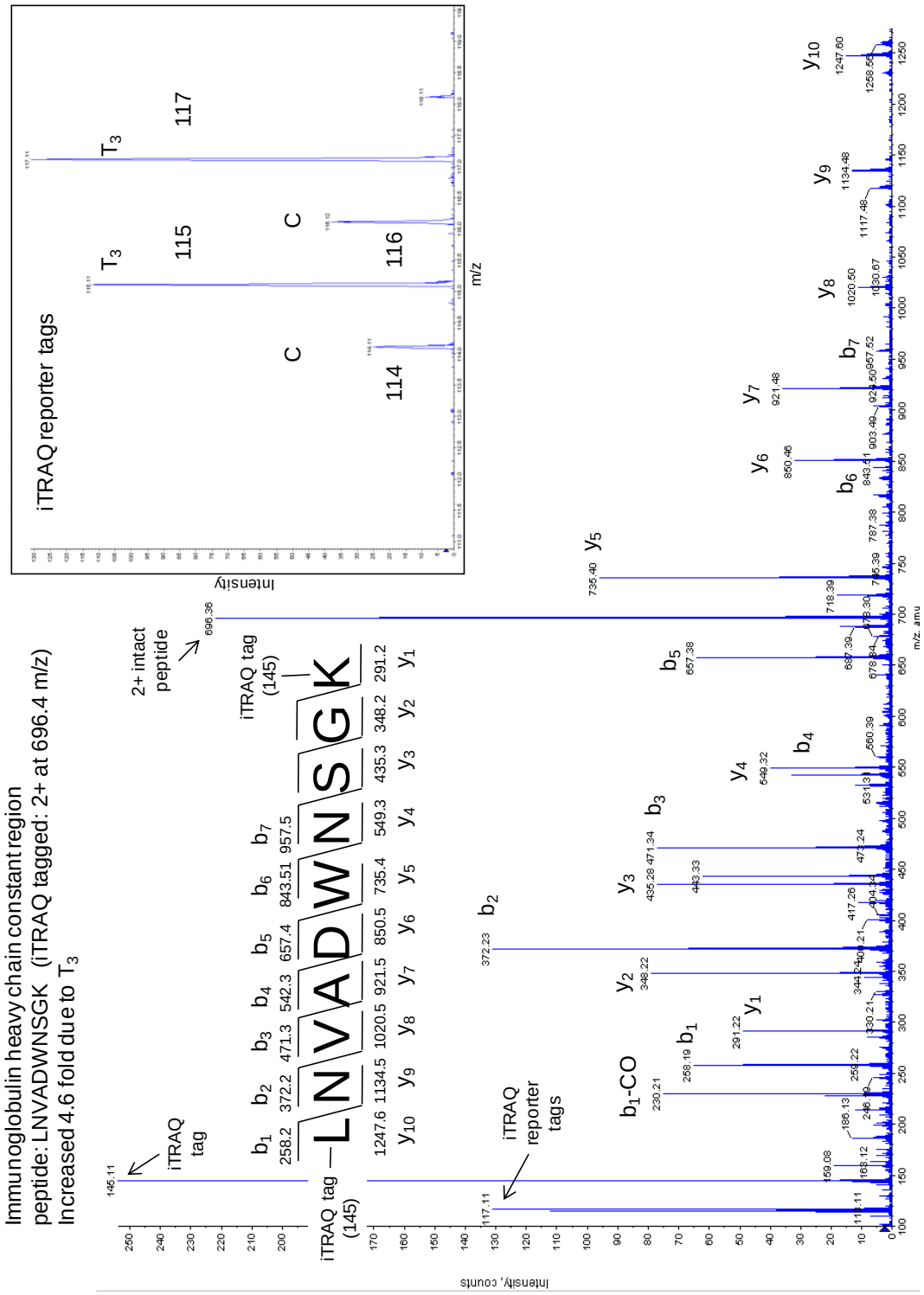

## **Appendix 3.3** List of *de novo* sequenced non-identified peptides altered in the iTRAQ analysis

| Fold change[1] | Observed peptide mass (Da, iTRAQ $[M+H]^+$)[2] | Observed peptide sequence[3] | % Confidence[4] |
|---|---|---|---|
| 4.3 | 1278.7 | LTSTDSLELR | 100 |
| 1.6 | 1930.3 | (frag)VESGGLALLK | 100 |
| 2 | 1714.2 | CAVHVVLGEK | 99 |
| 1.6 | 939.6 | YLDLK | 99 |
| 0.66 | 2145.1 | LDAPSNDQDTHCLELQR | 99 |
| 1.6 | 1869.6 | (frag)PQSPGMPR | 100 |
| 0.56 | 1032.6 | TFYWK | manual |
| 0.65 | 994.6 | LLFWK | 100 |
| 0.66 | 2732.2 | (frag)GELVDLNHTPAR | 99 |

Non-identified peptides with high quality sequence information that were found to change in abundance in the *R. catesbeiana* tail fin due to $T_3$ treatment as found by iTRAQ analysis. [1]Fold change ratios greater than 1.0 indicate an increase, and those below 1.0 indicate the reciprocal of the decrease. The number is the average change of two replicate experiments, which consisted of two treatment samples and two control samples. [2]Observed mass of the peptide in the MS analysis, modified with the iTRAQ reagent, reported as singly charged. [3]Amino acid sequence determined for the observed peptide by manual *de novo* or automatic *de novo* by PEAKS software sequencing. (frag.) indicates that only a partial peptide sequence could be determined. The masses of isoleucine are indistinguishable from leucine in MS and therefore L can be I and *vice versa*. [4]Percent confidence for the peptide sequence as reported by the PEAKS software. "manual" indicates that the peptide sequence was obtained manually and no percent confidence can be reported.

# Appendix 4.1

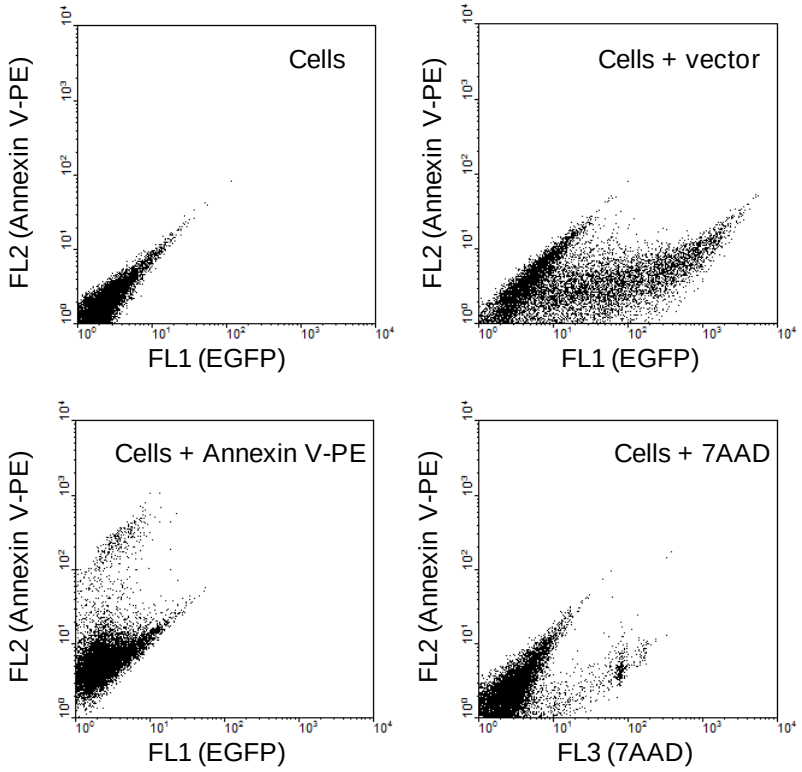


**Appendix 4.1. Distinction of signals for EGFP-expressing cells from apoptotic and necrotic cells in flow cytometry.** The fluorescent dyes used in flow cytometry were chosen to have distinct emission wavelengths from each other and from EGFP, and could be detected on separate channels by the flow cytometer. Any overlap between the emission spectra of the fluorophores was taken into account and removed by adjusting compensation, causing each to only contribute signal to the appropriate channel as shown by the dot plots of fluorescence (log scale) for different channels used to capture signal for EGFP (FL1), annexin V-PE (FL2) and 7AAD (FL3). Each dot represents a single cell for a total of 10,000 events measured. Shown are unstained non-transfected XLT-15 cells (Cells: background fluorescence only), unstained transfected cells expressing EGFP (Cells + vector: FL1 fluorescence only), non-transfected cells stained only with annexin V-PE (Cells + Annexin V-PE: FL2 fluorescence only), and non-transfected cells stained only with 7AAD (Cells + 7AAD: FL3 fluorescence only).

# Appendix 4.2

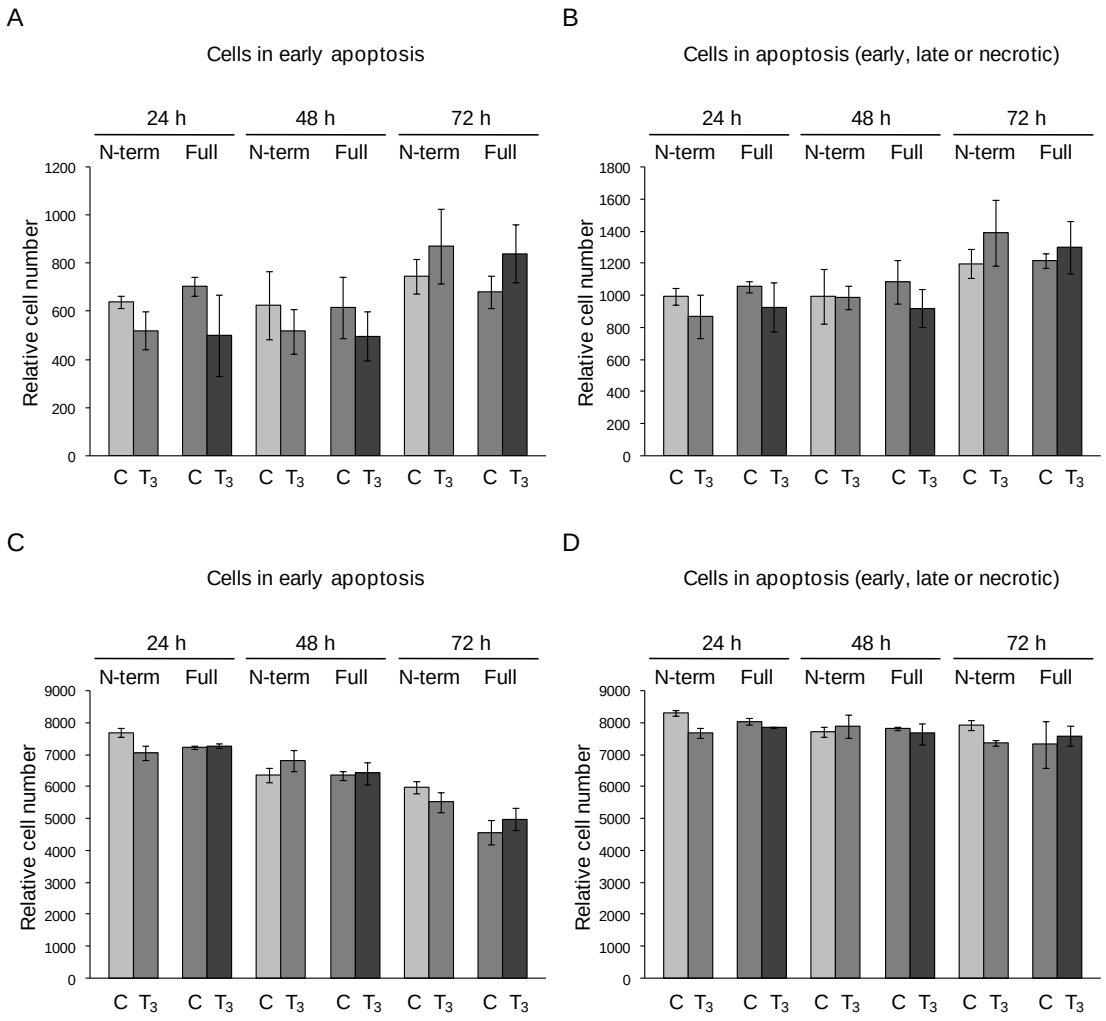


**Appendix 4.2. Flow cytometry analysis of apoptosis in adherent and detached XLT-15 cells transfected with N-term RLKI and Full RLKI expression constructs in the presence and absence of $T_3$.** Bar graph representation of flow cytometry data based on three independent replicate experiments. XLT-15 cells were transfected with the N-term RLKI or Full RLKI expression construct and exposed to vehicle control (C) or 10 nM $T_3$ ($T_3$) for the indicated period of time. Relative cell number indicates number of events per 10,000 cells analyzed. Error bars represent the standard error of the mean, and significance is indicated by an asterisk for $p < 0.05$ (Mann-Whitney U). (A) Number of all adherent cells (with or without EGFP expression) in early apoptosis (Region 1 minus region 3). (B) Number of all adherent cells in early or late apoptosis (with or without EGFP expression and may also include necrotic cells) (Region 1). (C) as for A but for the detached cell population. (D) as for B but for the detached cell population.